The fate and behaviour of diluted bitumen and its chemical constituents in freshwater systems following simulated spills

Sawyer Stoyanovich

Thesis submitted to the University of Ottawa in partial fulfillment of the requirements for the

PhD of Science

In

Biology

Specializing in Chemical and Environmental Toxicology

Department of Biology

Faculty of Science

University of Ottawa

Ontario, Canada

ABSTRACT

As conventional oil reserves deplete and more efficient refining technologies emerge, the use and transportation of heavy fuel oils such as dilbit is rising. Despite the risk of accidental dilbit spills, the fate and behaviour in aquatic systems is largely unknown. The objective of this thesis was to develop new approaches and insights to directly address knowledge gaps surrounding the fate and behaviour of diluted bitumen (dilbit) in freshwater systems.

During the summers of 2017 and 2018, a large-scale collaborative field study was conducted at the International Institute for sustainable Development's – Experimental Lakes Area (IISD-ELA), a world-renowned freshwater research station located in Northwestern Ontario, Canada. First, two tank-based dilbit spill simulations were carried out at oil:water ratios of 1:8000 and 1:800 v/v (Chapter 2). Here I examined the physical fate and behaviour of dilbit spilled onto the water's surface for 11 days. In this chapter I provide, for the first time, experimental evidence of dilbit physically sinking after 8 days of environmental weathering in land-based tanks containing natural lake water. Building on the findings of chapter 2, the remaining four chapters focus on a series of 70-d long experimental dilbit spills carried out in limnocorrals (10 m diameter x 1.5 m depth) installed directly in a freshwater lake. Chapter 3 provides, to our knowledge, the most detailed temporal account to date of dilbit submergence in freshwater at multiple oil:water ratios. In Chapter 4 I provide the rates at which over 100 individual hydrocarbons are depleted over time from the dilbit slicks and apply diagnostic ratios to postulate which weathering processes are responsible for the observed depletions. As predicted, evaporation, dissolution, and photooxidation are

prominent weathering processes whereas biodegradation is not. I then describe both the short- and long-term behaviour of these compounds as they partition from the dilbit slick to the air, water, and sediments of the limnocorrals in Chapter 5. While the concentrations of polycyclic aromatic hydrocarbons (PAHs) were elevated in the water columns of each treatment, they were orders of magnitude lower than concentrations that pose a toxicological risk. The same was true for all sediment samples except those that were in direct contact with sunken dilbit. This suggests that the major threat of dilbit spills from an ecotoxicological point of view is the dilbit-laden sediments produced by submergence. Finally, I demonstrated the successful application of a mass transfer model to predict the dissolution trends of the highly toxic benzene, toluene, ethylbenzene, and *o,m,p*-xylene (BTEX) compounds following the dilbit spills. In Chapter 7 I detail the implications and conclusions for each chapter and the thesis as a whole. I also describe areas where future research is needed. In the end, the conclusions of this thesis were: 1) dilbit has the propensity to sink following spills in freshwater, 2) prominent weathering processes include evaporation, dissolution, and photooxidation, 3) our regression design allowed for important relationships between contamination and spill size to be realized, 4) sunken dilbit poses a toxicological threat to aquatic biota, and 5) mass transfer models can accurately predict BTEX dynamics in the water column following a dilbit spill.

TABLE OF CONTENTS

ABSTRACT ii
TABLE OF CONTENTS iv
DEDICATION ix
ACKNOWLEDGEMENTS x
LIST OF ABBREVIATIONS xii
LIST OF TABLES xiv
LIST OF FIGURES xvii
PREFACE xxv
CHAPTER 1: GENERAL INTRODUCTION 1
1 OIL PRODUCTION IN CANADA 1
1.1. Canadian Oil Production 1
1.2. Chemical Composition of Dilbit 2
1.2.1. Saturates 3
1.2.2. Aromatics 4
1.2.3. Resins and Asphaltenes 5
1.3. Physical Properties of Dilbit 6
2 DILBIT WEATHERING 8
2.1. Evaporation 9
2.2. Dissolution 10
2.3. Photooxidation 10
2.4. Biodegradation 11
2.5. Emulsification 12
3 TRANSPORT, SPILLS, AND RECOVERY 12
4 KNOWLEDGE GAPS 14
5 PREVIOUS DILBIT STUDIES 16
6 THE USE OF LIMNOCORRALS TO SIMULATE LAKES 17
7 IN SUMMARY 19
REFERENCES 21
CHAPTER 2: SIMULATING A SPILL OF DILUTED BITUMEN: ENVIRONMENTAL WEATHERING AND SUBMERGENCE IN A MODEL FRESHWATER SYSTEM 27
STATEMENT OF CONTRIBUTIONS 27
ABSTRACT 28
1 INTRODUCTION 29

2 MATERIALS AND METHODS 32
2.1. Experimental Set Up 32
2.2. Dilbit Slick Samples 33
2.3. Water Column Samples 34
3 RESULTS AND DICUSSION 34
3.1. Dilbit Physical Properties 36
3.2. Dilbit Chemistry 40
3.3. Water Column Chemistry 41
4 CONCLUSION 45
ACKNOWLEDGEMENTS 46
SUPPORTING INFORMATION 47
REFERENCES 61
CHAPTER 3: SIMULATING DILUTED BITUMEN SPILLS IN BOREAL LAKE LIMNOCORRALS- PART 2: FACTORS AFFECTING THE PHYSICAL CHARACTERISTICS AND SUBMERGENCE OF DILUTED BITUMEN 65
STATEMENT OF CONTRIBUTIONS 65
ABSTRACT 66
1 INTRODUCTION 67
2 MATERIALS AND METHODS 70
2.1. Study Site 70
2.2. Experimental Design 71
2.3. Environmental and Water Quality Monitoring 74
2.4. Dilbit Slick Behavioural Monitoring 74
2.5. Dilbit Slick Samples 75
2.6. Chemical Weathering 76
2.7. Physical Property Models 76
3 RESULTS AND DISCUSSION 77
3.1. Physical Behaviour 77
3.2. Temporal Changes in Physical and Chemical Properties 82
3.2.1. Volatile Loss 82
3.2.2. Density and Viscosity 87
4 CONCLUSION 91
ACKNOWLEDGEMENTS 92
SUPPORTING INFORMATION 93
REFERENCES 113

CHAPTER 4: CHEMICAL WEATHERING PATTERNS OF DILUTED BITUMEN SPILLED INTO FRESHWATER LIMNOCORRALS 118
STATEMENT OF CONTRIBUTIONS 118
ABSTRACT 119
1 INTRODUCTION 120
2 MATERIALS AND METHODS 122
2.1. Experimental Set Up 122
2.2. Sample Collection 124
2.3. Analytical 125
2.4. Interpretation and Calculations 126
2.5. Statistical Analyses 127
2.6. Weathering Ratio Analysis 128
3 RESULTS AND DISCUSSION 129
3.1. Depletion of n-alkanes 129
3.2. Depletion of PAHs 132
3.3. Comparison among hydrocarbon groups 136
3.4. Weathering Ratios 138
4 CONCLUSION 143
ACKNOWLEDGEMENTS 144
SUPPORTING INFORMATION 144
REFERENCES 173
CHAPTER 5: FATE OF POLYCYCLIC AROMATIC HYDROCARBONS (PAHS) FROM DILUTED BITUMEN SPILLED INTO FRESHWATER LIMNOCORRALS 178
STATEMENT OF CONTRIBUTIONS 178
ABSTRACT 179
1 INTRODUCTION 180
2 MATERIALS AND METHODS 182
2.1. Experimental Spills and Sampling 182
2.2. Water Column Sampling 184
Due to rigorous sampling schedules and intensive analytical demands, ... 185
2.3. Sediment Sampling 185
2.4. Air Sampling 186
2.5. Sample Analyses 187
2.6. Data Modelling and Analyses 188
3 RESULTS AND DICUSSION 189

3.1. Hydrocarbon Contamination of the Water Column 189
3.2. Chemical Source Modelling of the Water Column 194
3.3. Hydrocarbon Contamination of the Sediments 195
3.4. Chemical Source Modelling of the Sediments 200
3.5. Hydrocarbons in the Air 201
3.6. Hydrocarbons in the Water Column and Sediments Predicted by Size of Spill 204
3.7. PAH Mass Balance 207
3.8. Implications for Ecological Exposure Following Dilbit Spills 209
4 CONCLUSION 212
ACKNOWLEDGEMENTS 212
SUPPORTING INFORMATION 213
REFERENCES 237
CHAPTER 6: EARLY MASS TRANSFER OF MONOCYCLICS TO WATER FOLLOWING DILUTED BITUMEN SPILLS IN FRESHWATER LIMNOCORRALS 242
STATEMENT OF CONTRIBUTIONS 242
ABSTRACT 243
1 INTRODUCTION 244
2 MATERIALS AND METHODS 247
2.1. Simulated Dilbit Spills 247
2.2. Analysis of Water Samples 247
2.3. Diluted bitumen-water mass transfer model 248
2.3.1. Loss of BTEX from diluted bitumen 248
2.3.2. Uptake and elimination of BTEX from water 250
2.4. Model Evaluation 251
3 RESULTS AND DISCUSSION 253
3.1. Temporal progression of BTEX in water column 253
3.2. Modelled dissolution and evaporation rates of BTEX 257
3.3. Model Performance 258
3.4. Simulated Mass Balance for BTEX 263
3.5. Sensitivity Analysis 264
3.6. Implications and Limitations 268
ACKNOWLEDGEMENTS 270
SUPPORTING INFORMATION 271
REFERENCES 297

CHAPTER 7: GENERAL CONCLUSIONS AND IMPLICATIONS 301
STUDY OUTCOMES 301
CHAPTER 2 301
CHAPTER 3 302
CHAPTER 4 303
CHAPTER 5 304
CHAPTER 6 305
GENERAL CONCLUSIONS 306
Diluted bitumen has the propensity to sink under calm freshwater conditions 306
Sediments are the ultimate sink for diluted bitumen in a freshwater lake 306
Evaporation, dissolution, and photooxidation are prominent weathering processes in freshwater while biodegradation is not 309
Benefits of a regression design- outcomes linked to spill size 310
Sunken dilbit poses the greatest toxicological threat following dilbit spills in freshwater 311
Mass transfer model can predict monocyclic dynamics following dilbit spill 312
FUTURE DIRECTIONS 312
CLOSING STATEMENT 315
REFERENCES 316
APPENDIX A: DILBIT MASS BALANCE ESTIMATES 318

DEDICATION

In Loving Memory of

Mary Pettypiece
&
Neils Stoyanovich

ACKNOWLEDGEMENTS

First and foremost, I would like to thank my supervisor, Dr. Jules Blais, for affording me the opportunity to work on such a unique and fulfilling project, and for the guidance over the course of my graduate studies. Your effort and dedication towards your students did not go unnoticed. Thank you to Linda Kimpe and Dave Eickmeyer for your constant technical support and expertise over the years. To my committee members, Dr. Alexandre Poulain, Dr. Craig Hebert, and Dr. Ian Clark. Thank you for all your support and direction throughout the last four years.

To Bruce Hollebone, Keval Shah, Zeyu Yang, Robert Faragher, Fatemeh Mirnaghi and the rest of the team at Environment and Climate Change Canada, thank you for all of your technical help and vast knowledge in the field of oil science, this thesis would not have been possible without your support over the last four years.

To Pepe, thank you a hundred times over for all of your help over the years. You've been a role model to me and a true example of what a selfless scientist, expert, and teacher should be! You've taught me so many valuable lessons, perhaps the most important being how to master the art of *R*, without your guidance I would likely still be making plots in Excel!

To Jonathan Séguin, it was awesome having such a great friend alongside me as we both tried to navigate our way through grad school. It wouldn't have been the same without you! I'll always remember those 2-day drives back and forth to the ELA and the places we stopped, whether it was a random Polish restaurant in Wawa, or for a freezing swim in an *E. coli* infested tidal pool on Lake Superior, never a dull moment!

To Leslie Saunders, thank you for all the help and advice with the modelling aspects of my thesis! I was starting to think I would never successfully complete this part of my thesis, but your guidance and expertise really helped me finalize the final and arguably most important chapter, thank you! I would also like to thank the rest of the Blais lab members (current and previous), Lauren Gallant, Kirsten Smythe, M.C. Roy, Cynthia Cheney, Brian Moeun, Jenn Keir, Jennifer Kissinger, Madison Bell, Mija Ažđajić, Alexandre Salat, Braden Gregory, Phil Thomas, and Claudia Tanamel, for all the collaborative support, advice, and friendship!

Thank you to all the BOREAL members, Tyler Black, Lauren Timlick, Jeff Cederwall, Sammy Patterson, Johanna Mason, Hannah Kosichek, Leah Cundall, and Daniel Denton- we put a truly remarkable project together and we should all be very proud! I would also like to thank the FOReST team and the rest of the IISD-ELA crew (yes… even Blake Cooney). I will forever miss the summers of 2017, 2018, and 2019 and all the friendships I made and all the trouble we got ourselves into, a lot of which cannot be listed in a doctorate thesis.

I would like to especially thank my parents, Jill and Matt Stoyanovich, for always providing unconditional love and support, and never having an issue with me being a 26-year-old still in school! I appreciate everything you've done for me; I would have never made it this far without you! Finally, Avery Froome, you've been by my side throughout all the ups and downs as I stressfully tried to put this thesis together. You've always been a positive voice in my ear and have helped out in more ways than you know. Thank You!

Amherstburg, April, 2021

LIST OF ABBREVIATIONS

ANOVA	Analysis of Variance
APAH	Alkylated polycyclic aromatic hydrocarbon
API	American Petroleum Institute
ASTM	American Society for Testing and Materials
AWB	Access Western Blend
Bbl	Billion barrels
BNT	Benzonaphthothiophene
BTEX	Benzene, toluene, ethylbenzene, and xylenes
C0-*PAH*	Specified PAH with no alkyl groups
C1-*PAH*	Specified PAH with 1 alkyl group
C2-*PAH*	Specified PAH with 2 alkyl groups
C3-*PAH*	Specified PAH with 3 alkyl groups
C4-*PAH*	Specified PAH with 4 alkyl groups
CAPP	Canadian Association of Petroleum Producers
CCME	Canadian Council of Ministers of the Environment
CER	Canada Energy Regulator
CHR	Chrysene
CI	Confidence Interval
CLB	Cold Lake Blend
CLWB	Cold Lake Winter Blend
DBT	Dibenzothiophene
DCM	Dichloromethane
Dilbit	Diluted bitumen
d.w.	Dry weight
DWH	*Deepwater Horizon*
FID	Flame ionization detection
FLA	Fluoranthene
FLU	Fluorene
GC	Gas chromatography
GC-FID	Gas chromatography- Flame Ionization Detection
GC-MS	Gas chromatography- Mass Spectrometry
HMW	High molecular weight
IDL	Instrument Detection Limit
IISD-ELA	International Institute for Sustainable Development Experimental Lakes Area
$k_{i,OE}$	Evaporation rate for compound *i*
$k_{i,OT}$	Total oil loss rate for compound *i*
$k_{i,OW}$	Dissolution rate for compound *i*
$k_{i,WE}$	Water evaporation rate for compound *i*

$k_{i,WO}$	Water-oil reabsorption rate for compound *i*
$k_{i,WR}$	Water reaction rate for compound *i*
$k_{i,WS}$	Water-sediment diffusion rate for compound *i*
$k_{i,WT}$	Total water loss rate for compound *i*
K_{OW}	Octanol-water partition coefficient
k_{WL}	Water leakage rate
LMW	Low molecular weight
MDL	Method Detection Limit
mPa S	Millipascal-second
MS	Mass spectrometry
n-alkanes	normal alkanes
NAP	Naphthalene
NASEM	National Academies of Sciences, Engineering, and Medicine
NEB	National Energy Board
NSERC	Natural Sciences and Engineering Research Council
OPA	Oil-particulate aggregates
OSA	Oil-sediment aggregates
PAH	Polycyclic aromatic hydrocarbon
PCA	Principle component analysis
PDMS	Polydimethylsiloxane
PHEN	Phenanthrene
PTFE	Polytetrafluoroethylene
PVC	Polyvinyl chloride
RSC	Royal Society of Canada
SARA	Saturates, aromatics, resins, and asphaltenes
SPME	Solid phase microextraction
TMD	2,6,10-trimethyldodecane
TMP	2,6,10-trimethylpentadecane
TPAH	Total polycyclic aromatic hydrocarbon
TPH	Total petroleum hydrocarbons
TRB	Transport Research Board
TSS	Total suspended sediments
U.S. EPA	Unites States Environmental Protection Agency
WCS	Western Canadian Select
ΣPAH_n	The sum of *n* PAH compounds

LIST OF TABLES

Table 1. 1. Major classes of SARA compounds in commonly transported crude oils presented as percentage by weight (%). 3

Table S2. 1. Limits of detection for selected PAH compounds in a 1L water sample ... 57
Table S2. 2. Daily water quality parameters measured within each of the treatment microcosms over the 11-day period of the simulated dilbit spills. All measurements made between 9:00am – 10:30am unless otherwise indicated. Values for water temperature, pressure, dissolved oxygen (DO), conductivity (Cond) and total suspended sediments (TSS) are shown. 58
Table S2. 3. Physical properties of source oil and samples collected throughout the spill. Values are a single measurement, otherwise represent as the mean of 3 measurements 59
Table S2. 4. Summary of non-linear model fit parameters for density and viscosity over time. TSS represents total sum of squares. 59
Table S2. 5. Summary of the degradation kinetics of CCME fractions present in dilbit samples taken from both the low and high tank 59

Table S3. 1. Physical Properties of fresh, unweathered CLWB 96
Table S3. 2. Identified targets and abbreviations ..... **Error! Bookmark not defined.**
Table S3. 3. Chemical composition of fresh, unweathered 2018 CLWB. Full chemical names provided in Table S3.2. 97

Table S4. 1. Identified targets and abbreviations 148
Table S4. 2. Relative standard deviation (%RSD) for each individual analyte measured in reference oil (13.1% Prudhoe Bay Crude Oil) throughout the analytical period of the experimental samples (n = 13). 149
Table S4. 3. Commonly used weathering ratios to elucidate the role of different weathering processes acting on surface slicks 150
Table S4. 4. Relative standard deviation (%RSD) for each individual weathering ratio measured in the reference oil (13.1% Prudhoe Bay Crude Oil) throughout the analytical period of the experimental samples (n = 13). 151
Table S4. 5. Physical properties of the studied CLWB dilbit 152
Table S4. 6. Total n-alkane and PAH depletion rate constants measured in each of the dilbit amended treatments. Negative values represent depletion rates. SE represents the standard error associated with the rate constant. 154
Table S4. 7. First order rate constants (± standard error) for individual n-alkanes in each of the dilbit amended treatments. Cases when concentrations of the individual compounds in the dilbit slicks were below detection limits were omitted from the computation of rate coefficients. Negative rate constants identify cases of depletion whereas positive rate constants identify cases of no observable depletion..... 158
Table S4. 8. First order rate constants (± standard error) for individual parent and alkylated PAHs in each of the dilbit amended treatments. Cases when concentrations of the individual compounds in the dilbit slicks were below detection limits were omitted

from the computation of rate coefficients. Negative rate constants identify cases of depletion whereas positive rate constants identify cases of no observable depletion. 163
Table S4. 9. Regression outputs from linear regressions performed in Figure S3.15. 168
Table S4. 10. Comparison of rate constants between the present study and others using Cold Lake blend (CLB) dilbit. Rates marked as “0” represent no depletion (i.e., a positive rate constant). 169
Table S4. 11. Comparison of study characteristics between the present study and the tank study of King et al., (2014). Fold changes recorded in green represent values greater than those of King et al. (2014) and fold changes recorded in red represent values lower than those of King et al., (2014). 170

Table 5. 1. Environmental mass balance of PAH groups in the water column and sediments. Percentages are reflective of the maximum concentration observed in the water column and sediments for each compound group. 209

Table S5. 1. Identified targets and abbreviations. Abbreviations s,w,a represent sediment, water, and air samples. 216
Table S5. 2. Mean percent recoveries (± standard deviation) for deuterated compounds in water, sediment, and air samples 217
Table S5. 3. Maximum concentrations of 7 different PAH groups measured in our study compared to other studies using diluted bitumen at similar oil:water ratios. 222
Table S5. 4. Comparison between sediment jar and oiled sediment core data. 228
Table S5. 5. Water column regression coefficients obtained by regressing the $\log_{10}$ transformed concentration of each respective PAH group against the $\log_{10}$ transformed oil:water ratio (alpha = 0.05). Certain compounds remained below detection limit during the earlier timepoints of the study and therefore did not yield sufficient regression coefficients, denoted by “*NA*”. 231
Table S5. 6. Sediment regression coefficients obtained by regressing the $\log_{10}$ transformed concentration of each respective PAH group against the $\log_{10}$ transformed oil:water ratio (alpha = 0.05). Certain compounds remained below detection limit during the earlier timepoints of the study and therefore did not yield sufficient regression coefficients, denoted by “*NA*”. 234
Table S5. 7. CCME guidelines for protection of aquatic life. Only PAHs with available data are presented. 236

Table S6. 1. Physical Properties of fresh, unweathered Cold Lake Winter Blend (CLWB) dilbit 271
Table S6. 2. Method detection limits (MDLs) for each BTEX compounds 274
Table S6. 3. Retention time (RT), identification and confirmation ions of analytes 274
Table S6. 4. Compound specific chemical properties and calculated input parameters included in the mass transfer model 279
Table S6. 5. Treatment/limnocorral specific environmental inputs used in mass transfer model. 280
Table S6. 6. Equations and variables used to calculate rate constants and condition in which ordinary differential equations were integrated 281
Table S6. 7. Oil slick thickness sensitivity analysis parameters 281

Table S6. 8. Raw time series water column concentrations of BTEX compounds. Values of 0 represent occurrences where concentrations were below MDL 282
Table S6. 9. Coefficients and significance of regressions in Figure S6.2. $Log_{10}[C] = m*log_{10}[oil:water] + b$ 285
Table S6. 10. Comparison between the present study and other tank studies using dilbit blends under various conditions and oil:water ratios 286
Table S6. 11. Rate constants for individual BTEX components used in the mass transfer model 287
Table S6. 12. Mean model bias (MB) and 95% confidence intervals for each BTEX compound and ΣBTEX 293
Table S6. 13. Sensitivity (S) of state variables on the maximum ΣBTEX concentration in the water column. 293
Table S6. 14. The resulting change in maximum ΣBTEX concentration in the water column that result from changing the value of the state variables by +/- 10%. 294
Table S6. 15. Sensitivity (S) of oil slick thickness on the maximum ΣBTEX concentration in the water column. 295
Table S6. 16. The resulting change in maximum ΣBTEX concentration in the water column that result from changing the oil slick thickness by +/- 90%. 295

Table 7. 1. Mass balance estimates on the final day of sampling for each individual treatment. 307

LIST OF FIGURES

Figure 1. 1. Classification of petroleum showing the relationship between viscosity density and API gravity over a range of oil types. Adapted from Lee et al (Lee et al., 2015) and Speight (Speight, 2014). 7
Figure 1. 2. Overview of the main weathering processes affecting the fate and behaviour of diluted bitumen spilled in freshwater and marine environments. 9

Figure 2. 1. Visible changes in the appearance of dilbit slicks in the low treatment (0.17 L dilbit) from day 0 (A) to day 11 (B) and high treatment (1.64 L dilbit) from day 0 (C) to day 11 (D). 36
Figure 2. 2. Temporal changes in density (A) and viscosity (B) of dilbit (measured at 15 °C) in the high-treatment microcosm. The solid horizontal line in panel (A) represents the density of freshwater (FW). Line of best fit (dashed) and 95% confidence intervals (p 37
Figure 2. 3. Changes in concentration over time of the four major petroleum fractions of dilbit: F1 (<nC10), F2 (nC10-nC16), F3 (nC16-nC34), and F4 (>nC34). Samples were collected from the surface slick of the low- (A) and high- (B) treatment microcosms. Line of best fit (dashed) and 95% confidence intervals (purple) are indicated. 41
Figure 2. 4. Water column concentrations of 7 major PAH groups in the low-treatment microcosm at 10 cm (A) and 40 cm (B) depths and the high-treatment microcosm at 10 cm (C) and 40 cm (D) depths. Concentrations represent sums of parent compounds and their alkylated homologs for each group. Gaps in data points represent sampling dates where concentrations were <LOD. Standard error is shown for samples that were randomly selected to be collected in triplicate. NAP: naphthalene; PHE: phenanthrene; DBT: dibenzothiophene; FLU: fluorene; FLA: fluoranthene; BNT: benzonaphthothiophene; CHR: chrysene..... 43

Figure S2. 1. Land based tank used in present study (A) and diagram demonstrating the different design aspects of the tank set up (B) 53
Figure S2. 2. Chemical characterization of fresh, unweathered Cold Lake Winter Blend (CLWB) dilbit used in this study. Petroleum hydrocarbons (A), biomarkers (B), n-alkanes (C) and polycyclic aromatic hydrocarbon (D) profiles are shown. TPH: total petroleum hydrocarbons, TSH: total saturate hydrocarbons, TAH: total aromatic hydrocarbons, F1: <n-C9, F2: n-C10 – n-C16, F3: n-C16 – n-C34, F4: >n-C34, T: terpanes, H: hopanes, S: steranes, N: naphthalene, P: phenanthrene, D: dibenzothiophene, F: fluorene, Fl: fluoranthene, B: benzonaphthothiophene, C: chrysene..... 54
Figure S2. 3. Surface slick sample collected from the high-treatment microcosm utilizing a section of polyester absorbent pad..... 55
Figure S2. 4. High volume dilbit sample collected from the high-treatment microcosm for physical property analysis 55
Figure S2. 5. Weather parameters throughout the experimental timeline measured at the meteorological site at IISD-ELA 56

Figure 3. 1. Experimental design of limnocorrals and simulated CLWB dilbit spills. (A) Main aspects of limnocorral and distribution of limnocorrals throughout the NW littoral zone of L260 at the IISD-ELA. (B) The distribution dilbit treatments including two

controls, one near field (NFC) and one far field (FFC). (C) Overview of dilbit slick sampling timepoints and associated analyses. 73
Figure 3. 2. Aerial photographs showing changes in percentage surface area (SA) coverage of the dilbit slick from day 1 to day 6 for the 180L (A,B) and 42L treatment (C,D). North Arrows and average wind speed/direction during the time of the photo are indicated. 78
Figure 3. 3. Submergence patterns observed in the seven dilbit treatments throughout the experiment. The timespan between when dilbit was first noticed on the sediments and when no floating dilbit slick remained (A) and the linear relationship between spill volume and sinking times (B) are shown. 80
Figure 3. 4. The loss of volatile hydrocarbons from surface dilbit slicks. (A) Temporal changes of $\leq C_{16}$ hydrocarbons relative to the source dilbit in samples collected surface of dilbit slicks. (B) Regression coefficients obtained by regressing hopane normalized loss relative to CLWB against spill volume over time (example from day 8 shown in inset). Slope estimates and 95% CI's are from individual regressions, red data points are slopes significantly different from zero (i.e., $p < 0.05$). Regressions are only shown up to sampling day 22 (July 12, 2018) since the majority of slicks had submerged following this day yielding insufficient sample size to perform further regressions for subsequent sampling days. 84
Figure 3. 5. Temporal changes in (A) density (g mL^{-1}; at 15 °C) and (B) viscosity (mPa·S at shear rate between 0.01 – 100 s^{-1}; at 15 °C) of samples collected from the two highest treatments (82 and 180 L) throughout the experimental spills. Monod-type models fitted to each data set are presented. The horizontal dashed line represents the density of freshwater at 15 °C. 88

Figure S3. 1. The addition of 180 L of CLWB (1:590 oil:water, v/v) onto the water surface of the limnocorral. (A) Overview of addition method, (B) View of telescopic arm and pumping system being held at approximately 5 – 10 cm from the water's surface. The oil exited the hose parallel to the waters surface to avoid forcing oil below the water surface and allowing it to spread out during the addition. 99
Figure S3. 2. Examples of colour change and skin formation observed throughout the experiment. 100
Figure S3. 3. Examples of tar balls observed floating on the water surface (A), neutrally buoyant in the water column (B), and submerged on the sediments (C). 100
Figure S3. 4. Changes in thickness of slick and formation of strings, water level represented by red dashed line in (C). 100
Figure S3. 5. Aerial photograph timelines for a low (A), medium (B), and high (C) treatment showing changes in slick coverage and eventual disappearance. 101
Figure S3. 6. Examples of dilbit submergence in selected treatments early on in the experiment. All photographs were taken underwater directly above the sediment layer except for panel (F) which was taken above the water surface, the small white globules are dilbit lying on the sediments. While tarballs appear white in colour, this is an effect of the water column on the lighting, the tarballs appeared light to dark brown when removed from the water. 102
Figure S3. 7. Examples of dilbit submergence in selected treatments later on in the experiment. All photographs were taken underwater directly above the sediment layer.

Panels E) and F) depict the unique behaviour of tarballs that was observed only in the two highest treatments. Sections of the tarballs appear to be extending upward while being held down by the bulk oil suggesting that there may be density differences across the tarballs. While tarballs appear white in colour, this is an effect of the water column on the lighting, the tarballs appeared light to dark brown when removed from the water. 103
Figure S3. 8. Examples of tar mats on the sediment bottom of the two highest treatments towards the end of the experiments. Panels B and C are zoomed in versions of the aerial photographs A and C. Tar mat measurements were made using ImageJ software version 1.50. 104
Figure S3. 9. Detailed submergence timelines for each of the seven dilbit amended treatments during the summer of 2018. 105
Figure S3. 10. Monitoring of daily precipitation (black bars) and total suspended solids (open circles) over time in each of the dilbit treatments. Gray rectangles mark the onset and completion of submergence. 106
Figure S3. 11. Photographs of floating slicks showing examples of sections of slick that are extending down into the water column while still remaining attached to the bulk surface slick. The red dashed lines represent the location of the water's surface for reference. With sufficient precipitation energy, it is possible that these slicks would break up, thus allowing the sinking sections to fully submerge to the sediments. 107
Figure S3. 12. Temporal changes of the four petroleum hydrocarbon fractions separated by GC-FID in dilbit slicks samples. Concentrations were normalized to C_{30} $\alpha\beta$ hopane and presented as percentage loss relative to the source CLWB dilbit. The varying x axis scale reflects when the respective dilbit slick was completely submerged, leaving no residual surface oil to sample. F3 and F4 fractions from panel G on day 8 and 15 were omitted due to analytical issues. 108
Figure S3. 13. Individual regressions performed on slick samples collected at each time point. Data used to generate figure 3.4B in main research article. Each panel represents a sampling timepoint. 109
Figure S3. 14. Temporal changes in physical properties (AB- density, CD- viscosity, EF- water content). Density and viscosity were measured at three different temperatures (0, 15, and 30 ºC), whereas water content was measured at room temperature. 110
Figure S3. 15. The relationship between (A) density measured at 15 ºC, (B) viscosity measured at 15 ºC, and the percentage of volatile hydrocarbon (<C16) loss relative to the source CLWB. (C) The relationship between viscosity measured at 15 ºC and density measured a Lines represent a fitted linear regression model and associated standard error. 111

Figure 4. 1. Depletion of total n-alkanes in each dilbit amended treatments over time (AB) and first order depletion rate constants of individual n-alkanes (CD). Absolute rates are presented, error bars represent standard error of the slope coefficient. Missing data bars represent treatments where the specific analyte did not exhibit any degradation over time (i.e., $k>0$). Timelines of collected surface slick samples due to differences in dilbit submergence times. 130

Figure 4. 2. Individual n-alkane (A) and PAHs (B) absolute rate constants (|k|) as a function of molecular weight in each of the dilbit amended treatments. Compounds that did not show evidence of loss over time (i.e., *k*>0) were omitted from this analysis. ... 132
Figure 4. 3. Depletion of total PAHs in each dilbit amended treatments over time (AB) and first order depletion rate constants of individual PAHs (CD). Absolute rates are presented, error bars represent standard error of the slope coefficient. Missing data bars represent treatments where the specific analyte did not exhibit any degradation over time (i.e., *k*>0). Timelines of collected surface slick samples due to differences in dilbit submergence times. ... 134
Figure 4. 4. Diagnostic weathering ratios of alkanes and PAHs. Solid black horizontal line represents the ratio in the source CLWB dilbit. The gray shaded area marks the ±RSD analytical uncertainty for each diagnostic ratio determined by calculating %RSD on the reference oil (n = 13). ... 139
Figure 4. 5. Percent relative standard deviation (RSD) of selected analyte diagnostic ratios for dilbit samples collected from the water's surface between 6 h – 70 d after the experimental dilbit additions. Sample sizes for each treatment are in the legend. Fresh, unweathered CLB samples were not considered in this analysis. The RSD threshold value of 5% is labelled in the black dashed line. ... 142

Figure S4. 1. Limnocorral design employed in the 2018 in-situ dilbit experiment. ... 144
Figure S4. 2. The addition of 180 L of CLWB (1:590 oil:water, v/v) onto the water surface of the limnocorral. (A) Overview of addition method, (B) View of telescopic arm and pumping system being held at approximately 5 – 10 cm from the water's surface. The oil exited the hose parallel to the waters surface to avoid forcing oil below the water surface and allowing it to spread out during the addition. ... 146
Figure S4. 3. Dilbit slick sampling regime employed throughout this study. Each black circle represents when a sample from each treatment was collected along the pre-determined sampling timeline. Following submergence of the surface slick, there was not sufficient floating dilbit remaining to be collected, and is marked as N.S., no sample. Samples were not collected in the 5.5 and 1.5 L treatments at 6 and 12 hours. ... 147
Figure S4. 4. Chemical composition of CLWB used in this study. A) n-alkanes, B) aromatics, and C) petroleum biomarkers. ... 153
Figure S4. 5. Concentrations of n-alkanes (A) and alkylated PAHs (B) in surface dilbit-slick samples collected during the 70-day study in each of the seven dilbit-amended treatments. Legends presented in panel A are shared with panel B. Temporal trends in sample collection differ in each treatment (ex: 0 – 70 d for 180L, 0 – 15 d for 1.5 L) due to submergence of floating slicks. ... 155
Figure S4. 6. N-Alkane loss in dilbit slick samples during weathering. Concentrations were normalized to $C_{30}\,\alpha\beta$ Hopane. Horizontal red lines represent to the total *n*-alkane loss relative to the CLWB dilbit. Each panel corresponds to the final sampling day of that particular treatment. Final sampling days vary due to submergence of the dilbit slicks which limited surface sample collection. Broken bars represent percentages greater than 150%. ... 156
Figure S4. 7. Principal component analysis of n-alkane profiles normalized Hopane in dilbit slick samples collected throughout the entire study from each treatment. ... 157

Figure S4. 8. Linear regressions of natural logarithm transformed n-alkane normalized concentrations over time during the first 15 days of the study..... 159
Figure S4. 9. Rate constants of isoprenoid alkanes. No significant relationship between spill volume and rate constants was observed for any of the isoprenoid alkanes. Missing data bars represent treatments where the specific analyte did not exhibit any degradation. 160
Figure S4. 10. PAH loss in dilbit slick samples during weathering. Concentrations were normalized to C_{30} $\alpha\beta$ Hopane. Horizontal red lines represent to the total PAH loss relative to the CLWB dilbit. Each panel corresponds to the final sampling day of that particular treatment. Final sampling days vary due to submergence of the dilbit slicks which limited surface sample collection..... 161
Figure S4. 11. Principal component analysis of PAH profiles normalized Hopane in dilbit slick samples collected throughout the entire study from each treatment. 162
Figure S4. 12. Linear regressions of natural logarithm transformed PAH normalized concentrations over time during the first 15 days of the study..... 164
Figure S4. 13. Relationship between individual PAH degradation rate constants and the degree of alkylation in each of the seven dilbit amended treatments. 165
Figure S4. 14. Compound specific regression outputs for n-alkanes (A) and PAHs (B) following linear regression of the standard error associated with each calculated rate constant and spill volume. A negative slope (i.e., below horizontal dashed line) represents an inverse relationship between standard error and spill volume. Relationships that are statistically significant are white. 166
Figure S4. 15. Differences in slick appearance on the same day (day 6) in two higher volume treatments (AB) and two lower treatments (CD). 167

Figure 5. 1. Overview of environmental media sampling timepoints and associated analyses. Panel (A) shows the sampling regime for the dilbit slick (D), water column (W), sediments (S), and Air. Panel (B) shows the number of samples collected at each timepoint for each environmental medium (9 slick samples, 34 water samples, 9 sediment samples, and 4 air samples- at each timepoint)..... 184
Figure 5. 2. PAH group concentrations in the water column over time. The sum of the parent and each alkylated homolog in each group is presented. Error bars represent standard deviation measured over N= 6 (180 L, 18 L, 1.5 L, and NFC) and n = 2 (82 L, 42 L, 5.5 L, 2.9 L, and FFC). Note changing y-axis scale..... 190
Figure 5. 3. Principal component analysis of PAH profiles normalized to ΣPAH46 in water samples collected throughout the entire study from each treatment and control. Principal components 1 and 2 account for 52% of the variability in the data set. Ellipses represent the 95% confidence interval within the 2-D space..... 195
Figure 5. 4. PAH group concentrations over time in the sediments. The sum of the parent and each alkylated homolog in each group is presented. Note changing y-axis scale..... 197
Figure 5. 5. PAH group concentrations in sediment samples in direct contact with sunken dilbit. The sum of the parent and each alkylated homolog in each group is in (A). 14 EPA priority PAHs are in panel (B). Error bars are standard deviations measured over N= 3..... 198

Figure 5. 6. Principal component analysis of the PAH profiles normalized to ΣPAH_{46} in sediment samples collected throughout the entire study from each treatment and control. Principal components 1 and 2 account for 65% of the variability in the data set. Ellipses represent the 95% confidence interval within the 2-D space. 201
Figure 5. 7. PAH group concentrations over time in the air column above the 180 L (A), 18 L (B), and NFC (C) treatments. The sum of the parent and each alkylated homolog in each group is presented. Note changing y-axis scale. 203
Figure 5. 8. Regression slopes obtained by linear regression of log_{10} transformed oil:water ratio against log_{10} transformed concentration in the water column of each PAH group. Regression parameters are presented in Table S5.5. 205
Figure 5. 9. Regression slopes obtained by linear regression of log_{10} transformed oil:water ratio against log_{10} transformed concentration in the sediments of each PAH group. Regression parameters are presented in Table S5.6. 207

Figure S5. 1. Schematic of limnocorral set up showing water and sediment sampling methods. 213
Figure S5. 2. The addition of 180 L of CLWB (1:500 oil:water, v/v) onto the water surface of the limnocorral. (A) Overview of addition method and visible sandbags used to seal the membrane to the sediments, (B) View of telescopic arm and pumping system being held at approximately 5 – 10 cm from the water's surface. The oil exited the hose parallel to the water's surface to avoid forcing oil below the water surface and allowing it to spread out during the addition. 214
Figure S5. 3. Distribution of spill volumes and resulting oil:water ratios 214
Figure S5. 4. Example of a tarball sitting on top of the sediment in a coring tube. The tarball was removed and then the top 1cm of the core was processed for PAH analysis. 215
Figure S5. 5. Temporal progression of mean ΣPAH_{46} concentrations in the water column, error bars represent standard deviation (A) and the resulting proportions of each PAH group during the period of maximum ΣPAH_{46} concentration in each treatment (B). 218
Figure S5. 6. Temporal progression of alkylated PAH concentrations in the water columns of each treatment and control, across each parent PAH group. The error bars represent standard deviation about the mean. 219
Figure S5. 7. Ternary plot showing the proportions of PAH groups by ring number that make up the ΣPAH46 concentrations in both water and sediment samples. 220
Figure S5. 8. The relationship between water column concentration of individual PAHs and logKOW. The dashed lines represent linear regression outputs. Individual compound concentrations were normalized to the ΣPAH_{46} concentration of each respective sample. Compounds whose concentrations were below MDL were omitted from this analysis. 221
Figure S5. 9. Temporal progression of petroleum biomarker compound concentrations(mean ± standard deviation) in the water column. 223
Figure S5. 10. Concentration profiles of petroleum biomarkers in water samples collected on day 8 from each dilbit amended treatment. Error bars represent standard deviation about the mean. 224

Figure S5. 11. The relationship between sediment concentration of individual PAHs and logK_{OW}. The dashed lines represent linear regression outputs. Individual compound concentrations were normalized to the ΣPAH_{46} concentration of each respective sample. Compounds whose concentrations were below MDL were omitted from this analysis. 225
Figure S5. 12. Temporal progression of mean ΣPAH_{46} concentrations in the sediments (A) and the resulting proportions of each PAH group during the period of maximum ΣPAH_{46} concentration in each treatment (B). 226
Figure S5. 13. Temporal progression of alkylated PAH concentrations in sediment samples collected from each treatment and control, across each parent PAH group. 227
Figure S5. 14. Temporal progression of ΣPAH_{40} concentrations in the sediments (A) and the resulting proportions of each PAH group during the period of maximum ΣPAH_{40} concentration in each treatment (B). 228
Figure S5. 15. Alkylated PAH profiles of each air sample collected over time during the first 8 days of the study. 229
Figure S5. 16. Individual linear regressions comparing concentration in the water column and spill volume at each timepoint for each PAH group. Both axes were logarithmically transformed. To account for cases where concentrations were 0, a constant of 1 was added to each measurement prior to transformation. The controls were excluded from the regressions..... 230
Figure S5. 17. Individual linear regressions comparing concentration in the sediments and spill volume at each timepoint for each PAH group. Both axes were logarithmically transformed. To account for cases where concentrations were 0, a constant of 1 was added to each measurement prior to transformation. The controls were excluded from the regressions..... 233

Figure 6. 1. (A) ΣBTEX, (B) benzene, (C) toluene, (D) ethylbenzene, and (E) *o,m,p*-xylenes over time 255
Figure 6. 2. Predicted and observed ΣBTEX concentrations in the water column of each treatment over time. 261
Figure 6. 3. Relationship between the measured and model estimated maximum concentration of individual BTEX compounds and ΣBTEX measured over time in each treatment. The red line represents the overall goodness of fit for all BTEX compounds and treatments. 180 L treatment = black; 82 L treatment = orange; 42 L treatment = blue; 18 L treatment = green; 5.5 L treatment = yellow; 2.9 L treatment = pink; and 1.5 L treatment = gray. 262
Figure 6. 4. Predicted ΣBTEX concentrations in the water column in each treatment at different dilbit slick thickness values, varied at +/- 90% of base model values. Base model values include: 180 L = 0.0034 m; 82 L = 0.0037 m; 42 L = 0.00022 m; 18 L = 0.00023 m; 5.5 L = 0.00042 m; 2.9 L = 0.00048 m; 1.5 L = 0.00075 m..... 267

Figure S6. 1. Example of calibration curves for benzene (a) and toluene (b) used for the 24-hour time interval samples. 273
Figure S6. 2. Example of chromatogram of a water sample collected from the 18 L treatment at the 24 h sampling timepoint. 275

Figure S6. 3. The proportion of each individual BTEX compound that makes up the maximum ΣBTEX concentration observed in each treatment. The y-axis represents each treatment and the timepoint in which the maximum ΣBTEX concentration was observed during the study. 283
Figure S6. 4. Individual linear regressions of log transformed BTEX in the water column against log transformed oil:water (v/v) ratios. 284
Figure S6. 5. Predicted and observed water column concentrations of benzene, toluene, ethylbenzene, and *o,m,p*-xylenes over time in each treatment. Observed ethylbenzene concentrations were below MDL in the 5.5, 2.9, and 1.5 L treatments and were replaced by the respective MDL value divided by 2. 291
Figure S6. 6. Relationship between the measured and model estimated concentrations of individual BTEX compounds and ΣBTEX measured over time in each treatment. 180 L treatment = black; 82 L treatment = orange; 42 L treatment = blue; 18 L treatment = green; 5.5 L treatment = yellow; 2.9 L treatment = pink; and 1.5 L treatment = gray. . 292

Figure 7. 1. Environmental mass balance of spilled dilbit in each treatment demonstrating the percentage of dilbit that evaporated, remained floating, and submerged to the sediments over time. 308

PREFACE

This thesis was written as individual manuscripts in accordance with the guidelines provided by the University of Ottawa's Faculty of Graduate and Postdoctoral Studies. Each chapter represents an individual manuscript prepared for publication under the Boreal Lake Oil Release Experimental by Additions to Limnocorrals (BOREAL) project. Chapter 1 is an introduction to this thesis and provides the necessary information for the manuscripts that follow. Chapter 2 is a manuscript formatted to Elsevier's guidelines for authors provided by the journal *Environmental Toxicology and Chemistry (ET&C)*. Chapter 3 is a manuscript formatted to the American Chemical Society guidelines for authors provided by the journal *Environmental Science and Technology (ES&T)*. Chapter 4 is a manuscript formatted to Elsevier's guidelines for authors provided by the journal *Science of the Total Environment (STOTEN)*. Chapter 5 is a manuscript formatted to Elsevier's guidelines for authors provided by the journal *Science of the Total Environment (STOTEN)*. Chapter 6 is a manuscript formatted to the American Chemical Society guidelines for authors provided by the journal *Environmental Science and Technology (ES&T)*. Chapter 7 summarizes the manuscripts and provides concluding remarks and future directions.

CHAPTER 1: GENERAL INTRODUCTION

1 OIL PRODUCTION IN CANADA

1.1. Canadian Oil Production

The Alberta Oil Sands have become a dominant contributor to the economy of Western Canada. Oil sands are landlocked in three major deposits found in the northern regions of Alberta: the Athabasca-Wabiskaw region, the Cold Lake deposits, and the Peace River deposits. Together, these regions cover a total of 140,000 square kilometers, containing an established reserve of 162 billion barrels (bbl) of oil as of 2019 (AER, 2020), making it the third-largest oil reserve in the world behind Saudi Arabia and Venezuela (Holditch, 2003). The heavy crude found in the oil sands represents roughly 50% of the four million barrels of crude oil produced per day within Canada (CAPP, 2019). The production of Canadian Oil Sand products is forecasted to increase by a million b/d over the next decade in order to meet global demands (CAPP, 2019; NASEM, 2016).

The main economic product extracted in Canada, contributing to over 97% of crude oil reserves, is bitumen (Alberta's Energy Reserves, 2018). Bitumen is a component of "oil sands"; comprised of 10% bitumen, 5% water and 85% solids (Wik et al., 2008; Yang et al., 2011). The bitumen extracted from the oil sands has a density > 1.0 g mL^{-1} and a viscosity of roughly 275 000 to 500 000 mPa·s (millipascal second) and is too dense and viscous to be transported in its crude state, so it is diluted to a density and viscosity range required to meet specifications for transport by rail, pipeline or tankers (Fingas, 2015). These diluents are often natural gas condensates, composed of low molecular weight hydrocarbons ($<C_{12}$) and blended at ratios of 20:80 to 30:70

(diluent:bitumen) depending on the time of year (Crosby et al., 2013; Government of Canada, 2013). The composition of the diluent will have implications on the behaviour of the dilbit if it enters the environment. The diluent is highly volatile and can rapidly evaporate off the oil slick, leaving behind a heavier residual oil similar to the original bitumen (Government of Canada, 2013; Lee et al., 2015; National Academies of Sciences and Medicine, 2016). Oils behave in a variety of ways depending on their composition, the environment to which they are introduced and the way in which their fate is altered over time. It is therefore important to characterize the physical and chemical properties of dilbit in order to understand their interactions with and impact on the environment.

1.2. Chemical Composition of Dilbit

The behaviour of individual chemical constituents found in dilbit is highly variable once exposed to environmental conditions. Certain lighter components are distinguished by their tendency to volatilize, while others prefer to bind to particles and settle into the water column, some oxidize in the presence of sunlight, and others are completely inert. Crude oil's behaviour in the environment is thus largely influenced by its chemical composition, which can be divided into four main chemical classes: saturates, aromatics, resins, and asphaltenes (SARA) (Yang et al., 2011). The contribution of each class of compounds to the overall chemical composition depends on the origin of the petroleum product. For example, highly viscous oils like bitumen contain a greater proportion of heavy resins and asphaltenes compared to a light crude oil (ex: Scotia Light) which is dominated by saturates and aromatics (Table 1.1) (Hollebone, 2015).

Table 1. 1. Major classes of SARA compounds in commonly transported crude oils presented as percentage by weight (%).

Crude Oil Type	Saturates	Aromatics	Resins	Asphaltenes
Light Crude[a]	92	8	1	0
Medium Crude[b]	78	15	6	1
Heavy Crude[c]	38	29	20	13
Diluted Bitumen[d]	25	22	33	20

[a]Scotia Light, [b]West Texas Intermediate, [c]Sockeye Sour, [d]Cold Lake Blend

1.2.1. Saturates

The saturate fraction is considered one of the major chemical classes in dilbit and is made up of hydrocarbon molecules that solely demonstrate carbon-carbon bonding patterns, with all other available bonding points saturated by hydrogen (Speight, 2014). Three subclasses of saturates exist; n-alkanes having straight chain structures, naphthenes having multiple saturated ring structures, and fused-ring aliphatics having large complex structures combining straight chain and naphthenic structures. In general, n-alkanes with less than fifteen carbons, often the main components of diluent, are volatile and therefore do not persist for long periods of time in aquatic systems (Gros et al., 2014; Lee et al., 2015). Waxes (*n*-alkanes >C20) can often represent a substantial proportion of crude oils, they are non-toxic but fairly resistant to biodegradation due to their low bioavailability in water (Hollebone, 2015). Of the four major petroleum fractions, the saturate fraction is considered the least toxic and the most biodegradable with the exception of large fused ring aliphatics (i.e., hopanes, steranes, and terpanes), a group of cyclic alkanes that are highly recalcitrant in the

environment and are thus utilized in the field of environmental forensics as petroleum biomarkers (King et al., 2014; Lee et al., 2015; Venosa et al., 1997).

The term ‘biomarker’, as it relates to oil, describes compounds that are originally produced by living organisms that are considered relatively resistant to biotic and abiotic degradation and are therefore preserved in the environment over geological time (Aeppli et al., 2014). These compounds originate mainly in the lipid membranes of prokaryotic and eukaryotic organisms (Peters et al., n.d.). Biomarker compounds in dilbit consist predominantly of hopanes, terpanes, and steranes that are produced in petroleum reservoirs at various proportions (Bragg et al., 1994; Venosa et al., 1997). These compounds can be used to assess the depositional environment of petroleum and track processes such as maturation and biodegradation (Brooks et al., 1988; Yang et al., 2011).

1.2.2. Aromatics

The aromatic fraction of dilbit contains cyclic, planar, and unsaturated hydrocarbons that have structures of single or multiple fused benzene rings (Lee et al., 2015). They are mainly divided as (a) mono-aromatics (i.e., BTEX; benzene, toluene, ethylbenzene, and xylenes) and polycyclic aromatic compounds (PACs). The mono-aromatics are very abundant in the diluent fraction and are the most water soluble and volatile components of the dilbit (National Academies of Sciences and Medicine, 2016). The BTEX series is on the US-EPA’s list of toxic priority pollutants as they are known to be acutely toxic to aquatic organisms (US-EPA, 2014). Upon entering the aquatic environment, the majority of BTEX evaporates due to its volatility, however these compounds are also polarizable and soluble in water (i.e., low Kow < 4) due to their

ability to form hydrogen bonds with water (Feng et al., 2016). A recent study by Philibert et al., (Philibert et al., 2016) revealed that following spills of condensate bitumen blend, BTEX is a more suitable predictor of lethality and malformation in early life stages of zebra fish compared to PAHs.

Polycyclic aromatic compounds (PAHs) are ubiquitous in the environment and are derived from petrogenic, pyrogenic, and biogenic sources (Stout et al., 2015). PAHs have two or more fused aromatic rings and may also have additional alkyl side groups (alkylated PAHs) and sulfur heteroatoms. The chemical fingerprint of dilbit demonstrates an enrichment in alkylated PAH homologues in comparison to the un-substituted parent compounds due to degradation processes as well as the low geologic heat present during the formation of bitumen deposits (Stout et al., 2015; Yang et al., 2011). PAHs are less volatile than the monoaromatics and commonly more persistent in the environment. These compounds have gained much attention in the scientific community due to their toxicity, carcinogenicity and relative resistance to biodegradation (specific to the larger 3-5 ringed PAHs) (Achten and Andersson, 2015; Lee et al., 2015; Van Hamme et al., 2003). For example, Incardona et al. (2015) found that juvenile pink salmon (*Oncorhynchus gorbuscha*) and herring (*Clupea pallas*) exposed to low levels of PAHs similar to what would be experienced following a crude oil spill (0.2 – 45.5 and 0.04 – 0.23 μg/L, respectively) experienced abnormal heart development and reduced cardiorespiratory function.

1.2.3. Resins and Asphaltenes

Diluted bitumen is often enriched in resins and asphaltenes in comparison to other major classes of crude oil (Table 1.1). Resins are chemically related to

asphaltenes, but are smaller and slightly more polar (Bertoncini et al., 2013; Lee et al., 2015). The chemical structures of resins and asphaltenes include elements other than carbon and hydrogen such as heteroatoms S, N, and low levels of O and are therefore not considered true hydrocarbons. Unlike saturates and aromatics, their true structures have not been determined, and we therefore identify them based on their solubility rather than structure. Resins are soluble in n-pentane but insoluble in propane, whereas asphaltenes are soluble in toluene (Lee et al., 2015). These compounds are poorly resolved by Gas Chromatography, contributing to the unresolved complex mixture (UCM) hump seen in chromatograms. Components of the asphaltene structure have begun to be elucidated using infrared spectroscopy which include an aromatic core connected by cycloalkanes with grafted alkane chains bonded to the aromatic core (Ilyin et al., 2016). The high proportions of resins and asphaltenes are considered the major driver of bitumen's elevated density and viscosity compared to other forms of crude oil due to their high molecular weight (Lee et al., 2015).

1.3. Physical Properties of Dilbit

Density is the mass of a given volume of oil, typically expressed in units of g mL^{-1} or Kg m^{-3}. API (American Petroleum Institute) gravity, measured in degrees; °API, is an inverse measurement of oil density compared to the density of water and is often used in the petroleum industry to compare petroleum types. Freshwater is assigned an API gravity of 10° at 15°C; light crudes have an API gravity of >31.1°, medium crudes have an API gravity of 22.3 – 31.1°, heavy crudes have an API gravity of <22.3° and bitumens have an API gravity between 5 and 10° (Figure 1.1) (Speight, 2014). Most oils are less dense than water and therefore float on it, oils of API>10° will float, whereas

bitumen (<10° API) will sink. Diluents that are added to bitumen to decrease density have API gravities two fold higher than light crude oils (ex: Cold Lake Diluent; 69° API), and therefore when added to bitumen, decrease the overall density of the mixture substantially (e.g. 2018 Cold Lake Blend dilbit; 0.92 g mL-1 at 15° C) (Crude Quality Inc., 2019; Lee et al., 2015).

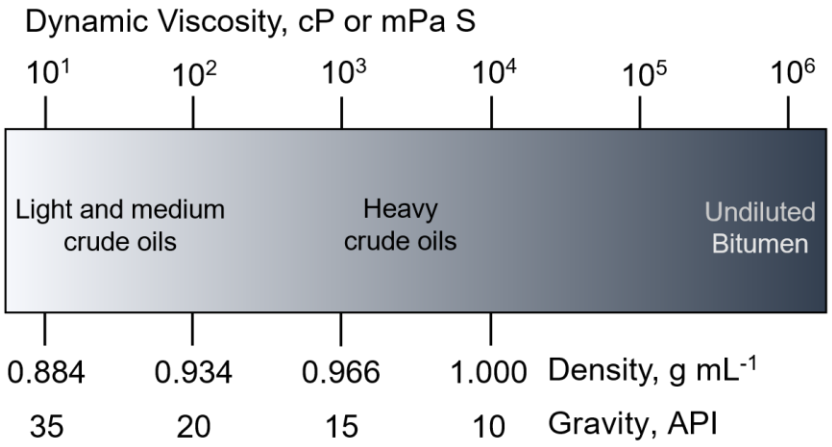

Figure 1. 1. Classification of petroleum showing the relationship between viscosity density and API gravity over a range of oil types. Adapted from Lee et al (Lee et al., 2015) and Speight (Speight, 2014).

Viscosity is defined as the resistance of a liquid to deformation following shear stress or flow, or simply the “thickness” of a liquid, the lower the viscosity the easier it flows (Marty and Potter, 2014). Viscosity, along with density and API gravity, is another property commonly used to classify petroleum types (Figure 1.1). In order to meet pipeline specifications for transport, the material must have a viscosity less than 350 mPa·S (Muñoz et al., 2016), whereas undiluted bitumens typically have a viscosity > 50,000 – 100,000 mPa·S (Speight, 2014). The addition of diluent lowers viscosity considerably (e.g., 2018 Cold Lake Blend dilbit: 181 mPa·S at 15° C).

Weathering of diluted bitumen (discussed further below) can thus have profound effects on the fate of dilbit in the environment, as the diluent is removed by processes

such as evaporation, a residual oil is left behind with similar physical characteristics to crude bitumen (i.e., very dense and viscous). Increased density can result in submergence in freshwater, increased viscosity decreases dilbit's spreading, dispersion, and efficacy of cleanup techniques (Lee et al., 2015).

2 DILBIT WEATHERING

When oil products are released into an aquatic environment, they are immediately subject to a variety of biotic and abiotic processes, collectively termed weathering (Figure 1.2). Weathering processes occur at a variety of different rates, but begin immediately after the oil enters the environment (Fingas, 2015). These processes; evaporation, dissolution, photo-oxidation, biodegradation, and emulsification, encompass changes in petroleum properties brought about by physical, chemical, and biological interactions when exposed to environmental conditions (American Petroleum Institute, 1999; Lee et al., 2015; McGenity et al., 2012; National Academies of Sciences and Medicine, 2016).

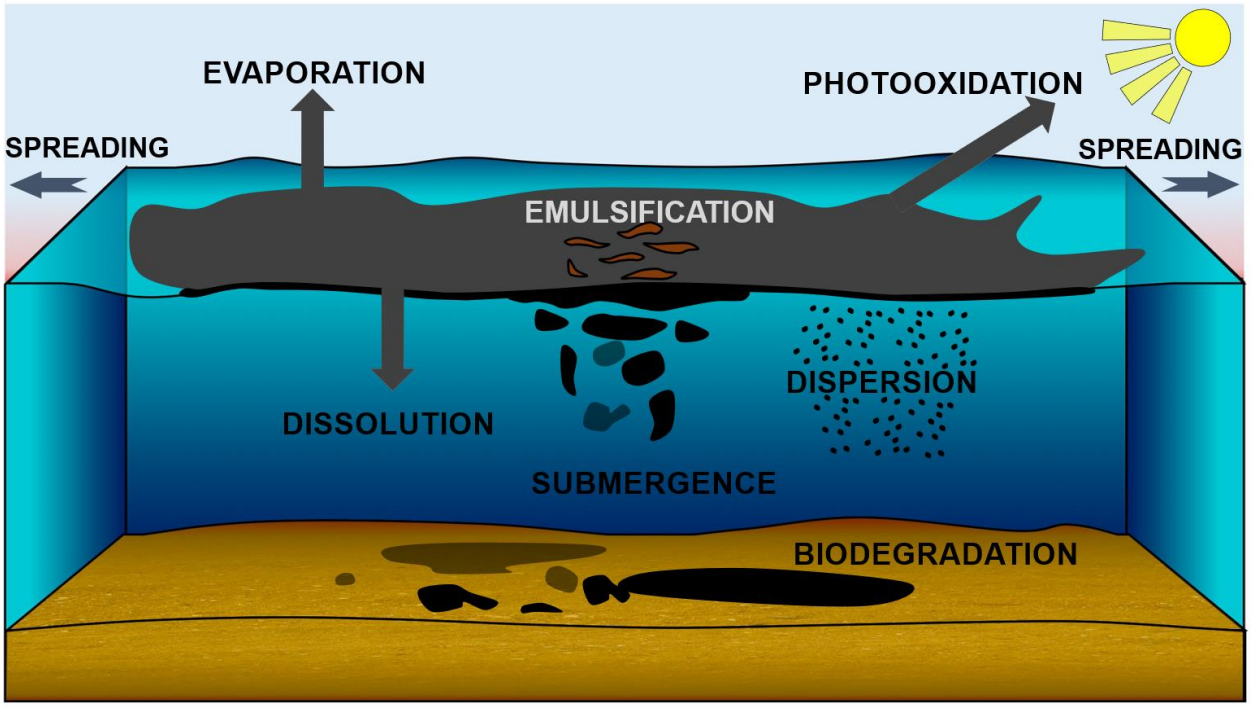

Figure 1. 2. Overview of the main weathering processes affecting the fate and behaviour of diluted bitumen spilled in freshwater and marine environments.

2.1. Evaporation

Evaporation in an oil spill scenario can be defined as the transfer of low molecular weight (LMW) fractions and some medium molecular weight (MMW) fractions from the liquid oil slick phase to the vapor phase (Government of Canada, 2013; Lee et al., 2015; Nazir et al., 2008). This is the primary mechanism of oil mass loss, and thus the most important weathering process occurring in the first hours of a spill (Sebastiao and Soares, 1995). The volatile components will partition to the air, leaving behind the heavier residual compounds. Typically, hydrocarbon components containing more than eighteen carbons in their chemical structure will not evaporate (Lehr et al., 2002; Regnier and Scott, 1975). In the case of dilbit, the diluent is often most prone to evaporation, returning the dilbit to its dense and viscous bituminous state, posing

concerns for submergence in freshwater (King et al., 2014; Lee et al., 2015; National Academies of Sciences and Medicine, 2016). The rate of evaporation is very rapid immediately after a spill and then slows down, following a logarithmic growth curve with time (Fingas, 2015).

2.2. Dissolution

Through dissolution, some of dilbit's water soluble components are lost to the water column below the slick. These include the monoaromatics (i.e., BTEX) and some of the LMW PAHs (i.e., naphthalene, phenanthrene). These soluble components of oil are also quite volatile and therefore the two processes of evaporation and dissolution are often in competition upon oil's entry into the environment (Guo and Wang, 2009; Lee et al., 2015). For some of the LMW compounds, evaporation is a more favorable process, thus only small quantities of compounds actually dissolve in water (Mishra and Kumar, 2015). Only a fraction of a percent of the oil's components actually enter the water and therefore dissolution does not significantly change the mass balance of the oil (Fingas, 2015). Regardless of this, dissolution cannot be considered as a negligible process, as even small amounts of harmful contaminants can have implications for toxicity to the surrounding biota in aquatic systems (Table 2) (Guo and Wang, 2009; Riazi and Roomi, 2008).

2.3. Photooxidation

Photooxidation involves the sunlight-catalyzed oxidation of reduced carbon present in petroleum (Shankar et al., 2015). Chromophores (mainly PAHs) present in the oil absorb sunlight and initiate a series of photochemical reactions. The two principal mechanisms include direct photolysis and indirect photolysis which

requires the presence of a photosensitizer to initiate the reaction (Shankar et al., 2015), ultimately producing a range of oxygenated products, the full suite of which is not yet understood (D'Auria et al., 2008; Lee et al., 2015). Aeppli et al (2012) have shown that oil residues collected over 18 months following the Deep Water Horizon spill show increases in oxygen content up to 60% compared to the original spilled oil. Yang et al (Yang et al., 2016) note that the photo-chemical degradation of hydrocarbons can have an impact on its fate and behaviour in the environment, especially when the oil has a high aromatic fraction, which is most susceptible to photooxidation. The newly formed oxygenated products (i.e., acids, ketones, and esters) may become more water soluble and therefore demonstrate different mobility in the environment compared to the parent compound (Charrié-Duhaut et al., 2000; Lee et al., 2015; Wang and Fingas, 2003).

2.4. Biodegradation

Biodegradation of crude oil is one of the most important processes involved in the long-term weathering and removal of petroleum from the environment (Venosa and Zhu, 2003). Biodegradation is a natural process in which microorganisms utilize their enzymes to break down organic compounds in the environment, and in turn use the carbon for metabolism and growth (Varjani, 2017). This process occurs more rapidly and extensively under aerobic conditions, however it can also occur under anaerobic conditions (Das and Chandran, 2011; Varjani, 2017). Typically, hydrocarbons such as branched and unbranched alkanes and select PAHs are often the target of biodegradation, with the efficiency of biodegradation decreasing with an increasing number of aromatic rings and degree of alkylation (Das and Chandran, 2011). These reactions occur in specific conditions that are largely dependent on the composition of

the hydrocarbons, nutrient availability, physical state of the oil spill, oxygen availability, temperature, pH, and available electron acceptors (Atlas, 1991).

2.5. Emulsification

This process requires highly turbulent waters and wave turbulence in order for emulsions to form. The water turbulence allows for the entrainment of water inside the oil slick, thus increasing the overall volume and viscosity of the slick. If the water content in oil reaches 60-80%, the effective volume of the spilled oil can increase two to five-fold and increase the slick's viscosity by 1000-fold. The presence of asphaltenes plays a role in the stability of these emulsions due to the formation of strong asphaltene films around the water droplets in the oil (Fingas and Fieldhouse, 2004). High oil viscosity has implications for the efficacy of nearly all oil recovery techniques (Lee et al., 2015; Wadsworth, 1995). Conventional devices such as skimmers, weirs, and oleophilic ropes/discs work well on oils with maximum viscosities of 10,000 mPa·s; while belt, screw, and air conveyor devices will function well on oils with viscosities up to 100,000 mPa·s (Federici and Mintz, 2014b; Wadsworth, 1995).

3 TRANSPORT, SPILLS, AND RECOVERY

Pipelines are considered the safest mode of transporting crude oil (Green and Jackson, 2015; Transport Canada, 2013), and when pipelines are operating at capacity, crude oil is transported by rail. From 2010 to 2018, a total 1300 billion L of crude oil was transported out of Canada, by pipeline and railway combined (CER, 2019), of which an estimated 14 million L was spilled in Canada (Oliver Wyman, 2019). It has been speculated that such spills are likely to continue, in part because some estimates

forecast a million barrels per day (b/d) increase in oil sands production in the next decade (CAPP, 2019; CER, 2016).

Inland oil spills, particularly in freshwater lakes, exhibit a variety of behavioural differences compared to marine spills. Nearby shorelines and smaller water bodies can limit spreading and consequently evaporation, which can prolong both air and water quality concerns. Turbulent lakes and rivers with high suspended sediment loads will promote the formation of oil-sediment aggregates (OSAs) which can drastically increase the density of the spilled material (Gustitus and Clement, 2017). The density threshold for submergence is lower in freshwater (~1 g mL^{-1}) compared to seawater (~1.03 g mL^{-1}). The lack of strong tidal action and currents in freshwater lakes can cause stranded oil to persist for longer periods of time on lake shores or riverbanks (API, 2016; Baca and Getter, 1985). Finally, smaller, shallow water bodies have less dilution capabilities than large open marine settings (Lee et al., 2015). Both the receiving environment (i.e., small inland lake vs. large open marine system) and the type of material spilled can have implications on the recovery techniques used during clean up.

In general, the effectiveness of oil spill remediation techniques depends largely on the physical properties of the spilled oil. *In-situ* burning can remove oil from the water surface but it is only efficient when the volatile components are still present and the slick is >2 mm thick (Fingas, 2015). For any heavy oil, including dilbit, the window of opportunity to ignite the oil is within the first 1 to 2 hours of the spill (Federici and Mintz, 2014a). Chemical dispersants can be employed to disperse the oil into the water column (Canevari, 1978), however their effectiveness tends to decrease with increasing oil viscosity, no longer becoming dispersible when viscosity exceeds 10 000 mPa·S

(Federici and Mintz, 2014a; Nordvik, 1995; Zhao et al., 2014). Finally, traditionally employed mechanical techniques, including skimmers and booms, have limited effectiveness on oils with viscosities > 100 000 mPa·S (Federici and Mintz, 2014a; ITOPF, 2012; Wadsworth, 1995).

4 KNOWLEDGE GAPS

Pipelines are one of the safest modes of transporting Canada's diluted bitumen (dilbit) to market (Green and Jackson, 2015; Transport Canada, 2013), however the possibility for spills are still a major public issue. Despite environmental concerns and pipeline expansion, very little is known about the environmental effects of a dilbit spill. Since 2013 a number of oil spill response reviews have been published by government and expert panels in both Canada and the United States. A few examples are listed:

- *A Review of Canada's Ship-Source Oil Spill Preparedness and Response Regime: Setting the Course for the Future (Transport Canada, 2013);*
- *A Review of Canada's Ship-Source Spill Preparedness and Response: Setting the Course for the Future, Phase II, Requirements for the Arctic and for Hazardous and Noxious Substances Nationally (Transport Canada, 2014);*
- *Royal Society of Canada - Expert Panel Report on the Behaviour and Environmental Impacts of Crude Oil Released into Aqueous Environments (Lee et al., 2015);*
- *U.S. National Academies of Science - Spills of Diluted Bitumen from Pipelines: A Comparative Study of Environmental Fate, Effects, and Response (National Academies of Sciences and Medicine, 2016); and,*

- *Transportation Research Board and National Research Council, TRB Special Report 311: Effects of Diluted Bitumen on Crude Oil Transmission Pipelines, (Transportation Research Board and National Research Council, 2014).*

These reviews have, at least in part, identified knowledge gaps related to the collective understanding of the fate and behaviour of spilled dilbit in various environments including freshwater.

A primary concern for the effects of dilbit products on freshwater ecosystems is whether dilbit will sink down to the sediments, as this has major implications for the efficacy of spill cleanup (Lee et al., 2015). Oil slicks on the water's surface can be skimmed using conventional methods, whereas a spill that submerges to the sediment requires recovery methods that are expensive and may cause further damage to the benthic environment (Winter and Haddad, 2014). The consequences of dilbit sinking in freshwater ecosystems were seen first-hand during the 2010 Kalamazoo River spill in Marshall Michigan, where roughly 3.2 million L of dilbit entered the Kalamazoo River following a pipeline rupture (US EPA, 2013). The dilbit sank upon entering the river due to a combination of weathering and interaction with sediment (Crosby et al., 2013; Dew et al., 2015). Remediation of the spill required dewatering, aeration, and sediment dredging in the Kalamazoo River system, extending clean-up for 3 years post-spill (Winter and Haddad, 2014). Understanding the risk of dilbit to submerge is paramount, as the traditional approaches for mitigating and recovering oil that floats on the water's surface cannot be employed (King et al., 2014).

5 PREVIOUS DILBIT STUDIES

While many studies have begun to elucidate the fate and behaviour of dilbit under laboratory settings (Government of Canada, 2013; Hua et al., 2018; Schreiber et al., 2019; Yang et al., 2016; Yarranton et al., 2015), few have performed experiments at larger scales. SL Ross Environmental Research Ltd. (2012) added CLB to a large indoor tank containing freshwater and allowed it to weather for 11 days under controlled conditions while tracking changes in density. Witt O'Briens et al. (2013) tracked changes in physical and chemical properties, as well as hydrocarbon accumulation in the water column for 10 days following experimental spills into large tanks. King et al. (2014; 2019) conducted multiple dilbit weathering studies (8 – 15 days) in outdoor flume tanks, tracking physical and chemical changes as well as the dissolution of monocyclic aromatic compounds into the water column. Finally, Ortmann et al. (2020) reported PAH concentrations in the water column for 14 days following dilbit spills into flume tank enclosures filled with natural seawater.

While the laboratory and tank studies discussed above offer valuable insight into dilbit's behaviour in aquatic systems, considerable knowledge gaps still persist on dilbit's fate, behaviour, and effects in natural freshwater systems (Government of Canada, 2013; Hua et al., 2018; King et al., 2014; Lee et al., 2015; National Academies of Sciences and Medicine, 2016; SL Ross, 2012; Winter and Haddad, 2014; Yang et al., 2018). Currently no work has addressed dilbit's behaviour in outdoor systems comprised of natural (unfiltered) freshwater and sediments under ambient environmental conditions.

The International Institute for Sustainable Development's Experimental Lakes Area (IISD-ELA) was one of the first facilities to be devoted primarily to large, ecosystem scale experiments (Schindler, 1998). Large limnocorrals have been used for over 50 years (Goldman, 1962) as a method to study outcomes following a simulated perturbation such as nutrient limitation and contaminant addition. While laboratory and tank experiments are useful in identifying causal relationships and underlying mechanisms, they often become simplifications of study systems, especially when conducted at small spatial or temporal scales (Stewart et al., 2013). Limnocorrals offer a more sophisticated approach that can support more realistic levels of biocomplexity. Although limnocorrals still afford some drawbacks, such as the lack of catchment interaction and weaker surface wave energy (Schindler, 1998), they still provide invaluable information that would not be attainable without performing a whole lake manipulation which would be a logistical/environmental challenge when it comes to oil spills.

6 THE USE OF LIMNOCORRALS TO SIMULATE LAKES

The International Institute for Sustainable Development's Experimental Lakes Area (IISD-ELA) was one of the first facilities to be devoted primary to large, ecosystem scale experiments (Schindler, 1998). Large limnocorrals have been used for over 50 years (Goldman, 1962) as a method to study outcomes following a simulated perturbation such as nutrient limitation and contaminant addition. Limnocorrals offer a unique opportunity for oil spill studies, as they bridge the gap between lab and tank-based studies, which often lack representable natural characteristics and a full lake study, which would be a logistical/environmental challenge when it comes to oil spills.

While limnocorrals do have shortcomings, such as the inability to replicate whole-lake mixing, leakage from the seams of wall material and lack of catchment influences, they can still provide invaluable results that, when interpreted appropriately, can be scaled to larger systems (Schindler, 1998).

One of the greatest challenges in the large-scale limnocorral approach is deciding how to apply statistical techniques for objective description and verifiable inferences (Gamble, 1990). Two of the most widely used techniques are (1) linear regression and (2) analysis of variance (ANOVA), and while they share the same underlying mathematical model, they differ in many key ways (Cottingham et al., 2005). First, ANOVA-based designs answer the *qualitative* question of "how a response variable differs across different levels of a discrete independent variable". On the other hand, regression-based designs answer the *quantitative* question of "how the response variable changes along a gradient of continuous independent variable levels" (Cottingham et al., 2005). In a traditional sense, ANOVA designs lend themselves better to statistical exploration through the use of replicates. However, at the scale in which these limnocorrals are constructed along the designated littoral zone of a lake, it is not practical nor possible to replicate these systems in sufficient quantity. Previous authors have discussed the replicability of large scale enclosures (Menzel and Case, 1977; Pilson et al., 1979; Takahashi et al., 1975), however, as highlighted by Gamble (1990), the physico-chemical properties of enclosures that are initially set up as replicates often diverge from one another over time. Further, differences in depth, water volume, biological assemblages, and sediment substrate along a littoral zone of a lake would cause each replicate to be slightly different than the next, creating more issues in

applying inferential statistics. These issues can be solved by incorporating a regression approach which removes the need for replicates and instead describes a relationship by linear regression analysis. Cottingham et al. (2005) highlight that regression has more statistical power than ANOVA, provides useful information that can be used to both interpolate/extrapolate the outcome of response variables at different values of the independent variable, and can be used to develop ecological models which is a primary goal of oil-spill related studies.

7 IN SUMMARY

This thesis will focus on tracking the physical and chemical fate of dilbit and its chemical constituents following a series of experimental spills to both land-based tanks and freshwater limnocorrals comprised of natural lake water and sediments. The three primary goals of this research are to use environmental samples (i.e., water, dilbit, and sediment) collected throughout the experimental spills to (i) study the environmental weathering processes acting upon the dilbit slick, (ii) quantify the exchange of chemical compounds among the environmental media, and (iii) develop and test models that can predict such behaviour. The work proposed herein is among the first of its kind and will place diluted bitumen spills in a Canadian context by examining the effects of a series of spill sizes on systems that simulate boreal shield lakes in Northern Ontario. Over the course of the research, the project advances from conducting on-land tank experiments to tracking changes in the physical and chemical properties of dilbit spilled in a lake using a limnocorral approach. The project will then advance further to provide new information to spill responders, forecasting windows of opportunity between the onset of

spill and time of sinking, where conventional spill countermeasures can be effective and at what point alternative measures need to be employed.

REFERENCES

Achten, C., Andersson, J.T., 2015. Overview of Polycyclic Aromatic Compounds (PAC). Polycycl. Aromat. Compd. 35, 177–186. https://doi.org/10.1080/10406638.2014.994071

Aeppli, C., Carmichael, C.A., Nelson, R.K., Lemkau, K.L., Graham, W.M., Redmond, M.C., Valentine, D.L., Reddy, C.M., 2012. Oil weathering after the Deepwater Horizon disaster led to the formation of oxygenated residues. Environ. Sci. Technol. 46, 8799–8807.

Aeppli, C., Nelson, R.K., Radovic, J.R., Carmichael, C.A., Valentine, D.L., Reddy, C.M., 2014. Recalcitrance and degradation of petroleum biomarkers upon abiotic and biotic natural weathering of Deepwater Horizon oil. Environ. Sci. Technol. 48, 6726–6734.

AER, 2020. ST98: Alberta Energy Outlook (AEO),. Alberta Energy Regulator (AER).

Alberta's Energy Reserves, 2018. ST98: Alberta's Energy Reserves and Supply/Demand Outlook - Google Search.

American Petroleum Institute, 1999. Fate of oil spilled in marine waters (No. 4691). Health and Environmental Science Department.

API, 2016. (American Petroleum Institute). Options for Minimizing Environmental Impacts of Inland Spill Response (No. API TECHNICAL REPORT 425).

Atlas, R.M., 1991. Microbial hydrocarbon degradation—bioremediation of oil spills. J. Chem. Technol. Biotechnol. 52, 149–156.

Baca, B.J., Getter, C.D., 1985. Freshwater oil spill considerations: protection and cleanup, in: International Oil Spill Conference. American Petroleum Institute, pp. 385–390. https://doi.org/10.7901/2169-3358-1985-1-385

Bertoncini, F., Courtiade-Tholance, M., Thiébaut, D., 2013. Gas Chromatography and 2D-gas Chromatography for Petroleum Industry: The Race for Selectivity. Editions Technip.

Bragg, J.R., Prince, R.C., Harner, E.J., Atlas, R.M., 1994. Effectiveness of bioremediation for the Exxon Valdez oil spill. Nature 368, 413. https://doi.org/10.1038/368413a0

Brooks, P.W., Fowler, M.G., Macqueen, R.W., 1988. Biological marker and conventional organic geochemistry of oil sands/heavy oils, Western Canada Basin. Org. Geochem. 12, 519–538.

Canevari, G.P., 1978. Some observations on the mechanism and chemistry aspects of chemical dispersion,. ASTM Int. West Conshohocken PA Chemical dispersants for the control of oil spills, 5–17. https://doi.org/10.1520/STP35706S

CAPP, 2019. 2019 Crude Oil Forecast, Markets and Transportation (No. 2019– 0018). Canadian Association of Petroleum Producers (CAPP), Calgary, AB.

CER, 2019. Crude Oil annual Export Summary - 2018 [WWW Document]. URL www.cer-rec.gc.ca/nrg/sttstc/crdlndptrlmprdct/stt/crdlsmmr/crdlsmmr-eng.html (accessed 3.10.19).

CER, 2016. Canada's Energy Future 2016: Energy Supply and Demand Projections to 2040 (No. ISSN 2292-1710). Canada Energy Regulator (CER).

Charrié-Duhaut, A., Lemoine, S., Adam, P., Connan, J., Albrecht, P., 2000. Abiotic oxidation of petroleum bitumens under natural conditions. Org. Geochem. 31, 977–1003.
Cottingham, K.L., Lennon, J.T., Brown, B.L., 2005. Knowing when to draw the line: designing more informative ecological experiments. Front. Ecol. Environ. 3, 145–152.
Crosby, S., Fay, R., Groark, C., Smith, J.R., Sullivan, T., Pavia, R., Shigenaka, G., 2013. Transporting Alberta oil sands products: defining the issues and assessing the risks (No. NOAA Technical Memorandum NOS OR&R 43). U.S. Dept. of Commerce, Seattle, WA: Emergency Response Division, NOAA.
Crude Quality Inc., 2019. crudemonitor.ca.
Das, N., Chandran, P., 2011. Microbial degradation of petroleum hydrocarbon contaminants: an overview. Biotechnol. Res. Int. 2011.
D'Auria, M., Racioppi, R., Velluzzi, V., 2008. Photodegradation of crude oil: liquid injection and headspace solid-phase microextraction for crude oil analysis by gas chromatography with mass spectrometer detector. J. Chromatogr. Sci. 46, 339–344.
Dew, W.A., Hontela, A., Rood, S.B., Pyle, G.G., 2015. Biological effects and toxicity of diluted bitumen and its constituents in freshwater systems. J. Appl. Toxicol. 35, 1219–1227. https://doi.org/10.1002/jat.3196
Federici, C., Mintz, J., 2014a. Oil Properties and Their Impact on Spill Response Options.
Federici, C., Mintz, J., 2014b. Oil properties and their impact on spill response options. CNA Analysis & Solutions.
Feng, Y.-J., Huang, T., Wang, C., Liu, Y.-R., Jiang, S., Miao, S.-K., Chen, J., Huang, W., 2016. π-Hydrogen Bonding of Aromatics on the Surface of Aerosols: Insights from Ab Initio and Molecular Dynamics Simulation. J. Phys. Chem. B 120, 6667–6673.
Fingas, M., 2015. Review of The Properties and Behaviour of Diluted Bitumen, in: Proceeding of the 39th Arctic and Marine Oil-Spill Program Technical Seminar. Environment and Climate Change Canada, Vancouver, B.C., Canada, pp. 470–494.
Fingas, M., Fieldhouse, B., 2004. Formation of water-in-oil emulsions and application to oil spill modelling. J. Hazard. Mater. 107, 37–50. http://dx.doi.org/10.1016/j.jhazmat.2003.11.008
Gamble, J.C., 1990. Mesocosms: statistical and experimental design considerations, in: Enclosed Experimental Marine Ecosystems: A Review and Recommendations. Springer, pp. 188–196.
Goldman, C.R., 1962. A METHOD OF STUDYING NUTRIENT LIMITING FACTORS IN SITU IN WATER COLUMNS ISOLATED BY POLYETHYLENE FILM 1. Limnol. Oceanogr. 7, 99–101.
Government of Canada, 2013. Properties, composition and marine spill behaviour, fate and transport of two diluted bitumen products from the Canadian oil sands (No. ISBN 987-1-100-23004-7), Federal Government Technical Report.
Green, K.P., Jackson, T., 2015. Safety in the transportation of Oil and Gas: pipelines or rail? Fraser Institute Vancouver, BC.

Gros, J., Nabi, D., Würz, B., Wick, L.Y., Brussaard, C.P., Huisman, J., van der Meer, J.R., Reddy, C.M., Arey, J.S., 2014. First day of an oil spill on the open sea: Early mass transfers of hydrocarbons to air and water. Environ. Sci. Technol. 48, 9400–9411. https://doi.org/10.1021/es502437e

Guo, W.J., Wang, Y.X., 2009. A numerical oil spill model based on a hybrid method. Mar. Pollut. Bull. 58, 726–734.

Gustitus, S.A., Clement, T.P., 2017. Formation, Fate, and Impacts of Microscopic and Macroscopic Oil-Sediment Residues in Nearshore Marine Environments: A Critical Review. Rev. Geophys. 55, 1130–1157. https://doi.org/10.1002/2017RG000572

Holditch, S.A., 2003. The increasing role of unconventional reservoirs in the future of the oil and gas business. J. Pet. Technol. 55, 34–79.

Hollebone, B.P., 2015. Appendix A The Oil Properties Data Appendix, in: Handbook of Oil Spill Science and Technology. John Wiley & Sons, Ltd, pp. 575–681. https://doi.org/10.1002/9781118989982.app1

Hua, Y., Mirnaghi, F.S., Yang, Z., Hollebone, B.P., Brown, C.E., 2018. Effect of evaporative weathering and oil-sediment interactions on the fate and behavior of diluted bitumen in marine environments. Part 1. Spill-related properties, oil buoyancy, and oil-particulate aggregates characterization. Chemosphere 191, 1038–1047. https://doi.org/0.1016/j.chemosphere.2017.10.156

Ilyin, S., Arinina, M., Polyakova, M., Bondarenko, G., Konstantinov, I., Kulichikhin, V., Malkin, A., 2016. Asphaltenes in heavy crude oil: Designation, precipitation, solutions, and effects on viscosity. J. Pet. Sci. Eng. 147, 211–217.

Incardona, J.P., Carls, M.G., Holland, L., Linbo, T.L., Baldwin, D.H., Myers, M.S., Peck, K.A., Tagal, M., Rice, S.D., Scholz, N.L., 2015. Very low embryonic crude oil exposures cause lasting cardiac defects in salmon and herring. Sci. Rep. 5, 13499.

ITOPF, 2012. Use of Skimmers in Oil Pollution Response. International Tanker Owners Pollution Federation (ITOPF).

King, T., Toole, P., Robinson, B., Ryan, S., Lee, K., Boufadel, M.C., Li, H., Clyburne, J.A., 2019. Influence of Climatic Parameters on Changes in the Density and Viscosity of Diluted Bitumen after a Spill. J. Rnvion. Sci. Pollut. Res. 5, 373–382. https://doi.org/doi.org/10.30799/jespr.176.19050305

King, T.L., Robinson, B., Boufadel, M., Lee, K., 2014. Flume tank studies to elucidate the fate and behavior of diluted bitumen spilled at sea. Mar. Pollut. Bull. 83, 32–37. https://doi.org/10.1016/j.marpolbul.2014.04.042

King, T.L., Robinson, B., Lee, K., Li, H., Boufadel, M.C., Clyburne, J.A., 2019. Seasonal Effect Data on Monocyclic Aromatics Dissolution from Surface Spills of Bitumen Blends: Implications for Environmental Risk Assessments, in: Proceedings of the Forty-Second AMOP Technical Seminar. Environment and Climate Change Canada, Ottawa, ON, Canada, pp. 773–790.

Lee, K. (chair), Boufadel, M., Chen, B., Foght, J., Hodson, P., Swanson, S., Venosa, A., 2015. Expert Panel Report on the Behaviour and Environmental Impacts of Crude Oil Released into Aqueous Environments (No. ISBN: 978-1-928140-02-3). Royal Society of Canada, Ottawa, ON, Canada.

Lehr, W., Jones, R., Evans, M., Simecek-Beatty, D., Overstreet, R., 2002. Revisions of the ADIOS oil spill model. Environ. Model. Softw. 17, 189–197.
Marty, J., Potter, S., 2014. Risk Assessment for Marine Spills in Canadian Waters, Phase 1: Oil Spills South of the 60th Parallel. WSP Can.
McGenity, T.J., Folwell, B.D., McKew, B.A., Sanni, G.O., 2012. Marine crude-oil biodegradation: a central role for interspecies interactions. Aquat. Biosyst. 8, 10.
Menzel, D.W., Case, J., 1977. Concept and design: controlled ecosystem pollution experiment. Bull. Mar. Sci. 27, 1–7.
Mishra, A.K., Kumar, G.S., 2015. Weathering of oil spill: modeling and analysis. Aquat. Procedia 4, 435–442.
Muñoz, J.A., Ancheyta, J., Castañeda, L.C., 2016. Required viscosity values to ensure proper transportation of crude oil by pipeline. Energy Fuels 30, 8850–8854.
NASEM, 2016. Spills of Diluted Bitumen from Pipelines: A Comparative Study of Environmental Fate, Effects, and Response (No. ISBN: 978-0-309-38010-2). National Academies of Sciences, Engineering and Medicine (NASEM), Washington, DC.
National Academies of Sciences, Medicine, 2016. Spills of Diluted Bitumen from Pipelines: A Comparative Study of Environmental Fate, Effects, and Response. National Academies Press.
National Resources Canada, 2017. Canada has the third-largest proven oil reserve in the world, most of which is in the oil sands. [WWW Document]. URL http://www.nrcan.gc.ca/energy/oil-sands/18085 (accessed 3.25.19).
Nazir, M., Khan, F., Amyotte, P., Sadiq, R., 2008. Multimedia fate of oil spills in a marine environment—An integrated modelling approach. Process Saf. Environ. Prot. 86, 141–148.
Nordvik, A.B., 1995. The technology windows-of-opportunity for marine oil spill response as related to oil weathering and operations. Spill Sci. Technol. Bull. 2, 17–46. https://doi.org/10.1016/1353-2561(95)00013-T
Oliver Wyman, 2019. Canadian Crude Oil Transportation: Comparing the Safety of Pipelines and Railways, Prepared for The Railway Association of Canada. Marsh & McLennan Companies.
Ortmann, A.C., Cobanli, S.E., Wohlgeschaffen, G., MacDonald, J., Gladwell, A., Davis, A., Robinson, B., Mason, J., King, T.L., 2020. Measuring the fate of different diluted bitumen products in coastal surface waters. Mar. Pollut. Bull. 153, 111003.
Peters, K.E., Walters, C.C., Moldowan, J.M., n.d. The Biomarker Guide: Biomarkers and Isotopes in the Environment and Human History 2005. Cambridge University Press: New York.
Philibert, D.A., Philibert, C.P., Lewis, C., Tierney, K.B., 2016. Comparison of diluted bitumen (dilbit) and conventional crude oil toxicity to developing zebrafish. Environ. Sci. Technol. 50, 6091–6098.
Pilson, M.E., Oviatt, C.A., Vargo, G.A., Vargo, S.L., 1979. Replicability of MERL microcosms: initial observations. Adv. Mar. Environ. Res. Ed. Jacoff FS EPA-6009-79-035 361–383.
Regnier, Z.R., Scott, B.F., 1975. Evaporation rates of oil components. Environ. Sci. Technol. 9, 469–472.

Riazi, M.R., Roomi, Y.A., 2008. A model to predict rate of dissolution of toxic compounds into seawater from an oil spill. Int. J. Toxicol. 27, 379–386.
Schindler, D.W., 1998. Whole-ecosystem experiments: replication versus realism: the need for ecosystem-scale experiments. Ecosystems 1, 323–334.
Schreiber, L., Fortin, N., Tremblay, J., Wasserscheid, J., Elias, M., Mason, J., Sanschagrin, S., Cobanli, S., King, T., Lee, K., 2019. Potential for Microbially Mediated Natural Attenuation of Diluted Bitumen on the Coast of British Columbia (Canada). Appl Env. Microbiol 85, e00086-19. https://doi.org/10.1128/AEM.00086-19
Sebastiao, P., Soares, C.G., 1995. Modeling the fate of oil spills at sea. Spill Sci. Technol. Bull. 2, 121–131.
Shankar, R., Shim, W.J., An, J.G., Yim, U.H., 2015. A practical review on photooxidation of crude oil: Laboratory lamp setup and factors affecting it. Water Res. 68, 304–315.
SL Ross, 2012. Meso-scale weathering of Cold Lake bitumen/condensate blend. SL Ross Environ. Res. Ltd 200–1140.
Speight, J.G., 2014. The chemistry and technology of petroleum. CRC press.
Stewart, R.I., Dossena, M., Bohan, D.A., Jeppesen, E., Kordas, R.L., Ledger, M.E., Meerhoff, M., Moss, B., Mulder, C., Shurin, J.B., 2013. Mesocosm experiments as a tool for ecological climate-change research, in: Advances in Ecological Research. Elsevier, pp. 71–181.
Stout, S.A., Emsbo-Mattingly, S.D., Douglas, G.S., Uhler, A.D., McCarthy, K.J., 2015. Beyond 16 priority pollutant PAHs: A review of PACs used in environmental forensic chemistry. Polycycl. Aromat. Compd. 35, 285–315.
Takahashi, M., Thomas, W., Seibert, D., Beers, J., Koeller, P., Parsons, T., 1975. The replication of biological events in enclosed water columns. Arch Hydrobiol 76, 5–23.
Transport Canada, 2014. A Review of Canada's Ship-Source Spill Preparedness and Response: Setting the Course for the Future, Phase II, Requirements for the Arctic and for Hazardous and Noxious Substances Nationally (No. ISBN 978-1-100-24991-9). Tanker Safety Panel Secretariat Ottawa, Canada.
Transport Canada, 2013. Tanker Safety Expert Panel - A review of Canada's Ship-source Oil Spill Preparedness And Response Regime: Setting the course for the future (No. ISBN 978-1-100-54627-8). Tanker Safety Panel Secretariat Ottawa, Canada.
Transportation Research Board and National Research Council, 2014. TRB Special Report 311: Effects of Diluted Bitumen on Crude Oil Transmission Pipelines (No. https://doi.org/10.17226/18381). The National Academies Press, Washington, DC.
US EPA, 2013. Dredging Begins on Kalamazoo River, Enbridge Oil Spill, Marshall, Michigan. U.S. Environmental Protection Agency (US EPA).
US-EPA, 2014. Priority Pollutants List.
Van Hamme, J.D., Singh, A., Ward, O.P., 2003. Recent advances in petroleum microbiology. Microbiol. Mol. Biol. Rev. 67, 503–549.
Varjani, S.J., 2017. Microbial degradation of petroleum hydrocarbons. Bioresour. Technol. 223, 277–286.

Venosa, A.D., Suidan, M.T., King, D., Wrenn, B.A., 1997. Use of hopane as a conservative biomarker for monitoring the bioremediation effectiveness of crude oil contaminating a sandy beach. J. Ind. Microbiol. Biotechnol. 18, 131–139. https://doi.org/10.1038/sj.jim.2900304

Venosa, A.D., Zhu, X., 2003. Biodegradation of crude oil contaminating marine shorelines and freshwater wetlands. Spill Sci. Technol. Bull. 8, 163–178.

Wadsworth, T., 1995. Containment & Recovery of Oil Spills at Sea: Methods and Limitations.

Wang, Z., Fingas, M.F., 2003. Development of oil hydrocarbon fingerprinting and identification techniques. Mar. Pollut. Bull. 47, 423–452.

Wik, S., Sparks, B.D., Ng, S., Tu, Y., Li, Z., Chung, K.H., Kotlyar, L.S., 2008. Effect of bitumen composition and process water chemistry on model oilsands separation using a warm slurry extraction process simulation. Fuel 87, 1413–1421.

Winter, J., Haddad, R., 2014. Ecological impacts of dilbit spills: Considerations for natural resource damage assessment, in: 37th AMOP Technical Seminar on Environmental Contamination and Response, Alberta, Canada, June. pp. 3–5.

Witt O'Briens, Polaris Applied Sciences, Western Canada Marine Response Corporation, 2013. A study of fate and behavior of diluted bitumen oils in marine waters: Dilbit Experiments, Trans Mountain Pipeline ULC.

Yang, C., Wang, Z., Yang, Z., Hollebone, B., Brown, C.E., Landriault, M., Fieldhouse, B., 2011. Chemical fingerprints of Alberta oil sands and related petroleum products. Environ. Forensics 12, 173–188.

Yang, Z., Hollebone, B.P., Brown, C.E., Yang, C., Wang, Z., Zhang, G., Lambert, P., Landriault, M., Shah, K., 2016. The photolytic behavior of diluted bitumen in simulated seawater by exposed to the natural sunlight. Fuel 186, 128–139.

Yang, Z., Hua, Y., Mirnaghi, F., Hollebone, B.P., Jackman, P., Brown, C.E., Yang, C., Shah, K., Landriault, M., Chan, B., 2018. Effect of evaporative weathering and oil-sediment interaction on the fate and behavior of diluted bitumen in marine environments. Part 2. The water accommodated and particle-laden hydrocarbon species and toxicity of the aqueous phase. Chemosphere 191, 145–155. https://doi.org/10.1016/j.chemosphere.2017.10.033

Yarranton, H., Motahhari, H.R., Schoeggl, F., Zhou, J.Z., 2015. Evaporative Weathering of Diluted Bitumen Films. J. Can. Pet. Technol. 54, 223–244. https://doi.org/10.2118/174557-PA

Zhao, L., Torlapati, J., Boufadel, M.C., King, T., Robinson, B., Lee, K., 2014. VDROP: A comprehensive model for droplet formation of oils and gases in liquids-Incorporation of the interfacial tension and droplet viscosity. Chem. Eng. J. 253, 93–106. https://doi.org/10.1016/j.cej.2014.04.082

CHAPTER 2: SIMULATING A SPILL OF DILUTED BITUMEN: ENVIRONMENTAL WEATHERING AND SUBMERGENCE IN A MODEL FRESHWATER SYSTEM

Stoyanovich, S[a]., Yang, Z[b]., Hanson, M[c]., Hollebone, B.P[b]., Orihel, D. M[d]., Palace, V[e]., Rodriguez-Gil, JR[a]., Faragher, R[b]., Mirnaghi, F.S[b]., Shah, K[b]., Blais, J.M[a*].

[a] Department of Biology, University of Ottawa, Ottawa, Ontario, Canada

[b] Emergencies Science and Technology Section, Environment and Climate Change Canada, Ottawa, Ontario, Canada

[c] Department of Environment and Geography, University of Manitoba, Winnipeg, Manitoba, Canada.

[d] Department of Biology and School of Environmental Studies, Queen's University, Kingston, Ontario, Canada

[e] International Institute for Sustainable Development Experimental Lakes Area, Winnipeg, Manitoba, Canada

*Corresponding Author: Jules Blais (jules.blais@uottawa.ca)

STATEMENT OF CONTRIBUTIONS

Stoyanovich, S: conceptualization, writing, formal analysis, analytical, field work
Yang, Z: analytical, reviewing
Hanson, M: reviewing, funding acquisition
Hollebone, B: reviewing, funding acquisition, analytical
Orihel, D: reviewing, funding acquisition
Palace, V: reviewing, funding acquisition
Rodriguez-Gil, J: reviewing
Faragher, R: reviewing, field work, analytical
Mirnaghi, F: reviewing, analytical
Shah, K: field work, analytical
Blais, J: supervision, reviewing, funding acquisition, conceptualization, corresponding author

Environmental Toxicology and Chemistry published this chapter:

Stoyanovich, S.S., Yang, Z., Hanson, M., Hollebone, B.P., Orihel, D.M., Palace, V., Rodriguez-Gil, J.L., Faragher, R., Mirnaghi, F.S., Shah, K. and Blais, J.M., 2019. Simulating a spill of diluted bitumen: environmental weathering and submergence in a model freshwater system. *Environmental toxicology and chemistry*, *38*(12), pp.2621-2628. https://doi.org/10.1002/etc.4600.

ABSTRACT

The main petroleum product transported through pipelines in Canada is diluted bitumen (dilbit), a semiliquid form of heavy crude oil mixed with natural gas condensates to facilitate transport. The weathering, fate, behaviour, and environmental effects of dilbit are crucial to consider when responding to a spill; however, few environmental studies on dilbit have been completed. We report on 11-d-long experimental spills of dilbit (Cold Lake Winter Blend) in outdoor microcosms meant to simulate a low-energy aquatic system containing natural lake water and sediments treated with low (1:8000 oil:water) and high (1:800 oil:water) volumes of dilbit. In the first 24 h of the experiment, volatile hydrocarbons quickly evaporated from the dilbit, resulting in increased dilbit density and viscosity. These changes in dilbit's physical and chemical properties ultimately led to its submergence after 8 d. We also detected rapid accumulation of polycyclic aromatic compounds in the water column of the treated microcosms following the spills. The present study provides new information on the environmental fate and behaviour of dilbit in a freshwater environment that will be critical to environmental risk assessments of proposed pipeline projects. In particular, the study demonstrates the propensity for dilbit to sink under ambient environmental conditions in freshwaters typical of many boreal lakes.

1 INTRODUCTION

Bitumen, a semi-liquid form of landlocked petroleum, is Canada's primary petroleum product, accounting for over 97% of Canada's total crude oil reserves (Alberta's Energy Reserves, 2018). Bitumen products represent an extensively biodegraded form of crude oil and have lost most of the lower molecular weight compounds over geological time (Yang et al., 2011). Bitumen is thus dominated by highly recalcitrant resin and asphaltene compounds as well as higher molecular weight *n*-alkanes, alkylated polycyclic aromatic compounds (APACs), and biomarker compounds including pentacyclic triterpenes (Yang et al., 2011). Crude bitumen's highly dense and viscous state does not allow it to flow easily, requiring the addition of diluents to facilitate transport by pipeline. These diluents are often a by-product of natural gas production, termed condensates, that are composed mainly of lower molecular weight saturates and minor BTEX components (i.e., benzene, toluene, ethylbenzene, xylenes) (Lee et al., 2015; Speight, 2010). Dilbit is typically blended at ratios of 20:80 to 30:70 (diluent:bitumen) depending on the time of year (Crosby et al., 2013; Government of Canada, 2013). The addition of diluent increases the chemical complexity of the bitumen, and can affect how it behaves in aqueous systems (Lee et al., 2015). The behaviour of diluted bitumen (dilbit) is governed by complex physical and chemical weathering processes, including evaporation, photooxidation, emulsification, dispersion, biodegradation and sedimentation (American Petroleum Institute, 1999; Fingas, 2015; Garrett et al., 1998; Lee et al., 2015; McGenity et al., 2012; National Academies of Sciences and Medicine, 2016). These processes encompass changes in petroleum properties brought about by varying environmental conditions. For example, natural

variation in wind and rain energy can contribute to the dilbit's dispersion tendency into the water column, moments of enhanced turbidity in the water column could promote the formation of oil-particle aggregates causing submergence, and exposure to natural sunlight could have an impact on photooxidative processes. All of these potential processes outlined above are challenging to replicate in a laboratory setting.

Recently, a variety of studies exploring dilbit's fate and behaviour in aquatic systems have been carried out at both laboratory and tank scales. Hua et al. (Hua et al., 2018) mixed two types of weathered dilbit, Cold Lake Blend (CLB) and Access Western Blend (AWB), with sediment and seawater in a laboratory and tracked how dilbit's interaction with the sediment affected its sinking behaviour. SL Ross Environmental Research Ltd. (SL Ross, 2012) added CLB to a large indoor tank containing freshwater and allowed it to weather for 11 days under controlled conditions while tracking changes in density. King et al. (King et al., 2014) conducted a 13-day weathering study by adding CLB and AWB to an outdoor flume tank containing filtered seawater and tracking evaporative losses and density increases. Though this work has offered valuable insight into dilbit's behaviour in aquatic systems, considerable knowledge gaps still persist on dilbit's fate, behaviour, and effects in freshwater (Government of Canada, 2013; Lee et al., 2015; National Academies of Sciences and Medicine, 2016; Winter and Haddad, 2014). Currently no work has addressed dilbit's behaviour in outdoor systems comprised of natural (unfiltered) freshwater and sediments under ambient environmental conditions.

One of the most pressing questions is whether and how quickly dilbit sinks in freshwater, as this has major implications for the efficacy of spill cleanup (Lee et al.,

2015). Oil slicks floating on the water's surface can be skimmed using conventional methods, whereas a spill that submerges to the sediment layer may require recovery methods that are expensive and may be detrimental to ecosystem health (Winter and Haddad, 2014). The consequences of dilbit sinking in freshwater ecosystems were seen during the 2010 Kalamazoo River dilbit spill in Michigan, where roughly 3.2 million litres of dilbit entered the Kalamazoo River following a pipeline rupture (US EPA, 2013). The dilbit sank upon entering the river due to a combination of weathering and interaction with sediment (Crosby et al., 2013; Dew et al., 2015). Remediation of the spill required dewatering, aeration, and sediment removal in both Talmadge Creek and the Kalamazoo River system, extending clean-up for 3 years post-spill, with severe impacts on the benthic environment (Winter and Haddad, 2014).

Here we conducted experimental releases of dilbit in open-air freshwater microcosms to simulate a dilbit spill in a low energy littoral zone of a boreal lake. Over 11 days, we tracked changes in the chemical and physical properties of the spilled dilbit, including changes in its density and viscosity, as well as the partitioning of hydrocarbons into the water column. This work offers a novel assessment of dilbit's fate following exposure to natural environmental conditions, allowing us to address important areas of uncertainty, such as the potential for sinking. The findings will inform scientists and environmental managers about the potential risks associated with dilbit's behaviour in a natural freshwater environment.

2 MATERIALS AND METHODS

2.1. Experimental Set Up

The experiment was conducted in land-based, outdoor microcosms at the International Institute for Sustainable Development Experimental Lakes Area (IISD-ELA), a freshwater research center located in Kenora, Ontario, Canada. Each microcosm consisted of an outer low-density polyethylene containment tank (2.7 m diameter x 0.72 m height) and an inner high-density polyethylene bag (designated as the “microcosm wall”) affixed to a hexagonal floating collar (2 m diameter x 0.1 m height) (SI Figure S2.1). A total of 160 L of natural sediment was added to achieve an approximate sediment thickness of 5cm and 1400 L of lake water, collected from IISD-ELA’s Lake 240 (49°40 N, 93°44 W), were added to each bag and the systems were allowed to equilibrate for 2 days. There were no signs of hydrocarbon contamination originating from the polyethylene material since hydrocarbon concentrations in the water of the control microcosm were consistently below respective limits of detection (see SI, s2.3). The final water depth was 0.5 m in each microcosm. The land-based tanks were placed in a flat, open storage yard at the IISD-ELA surrounded by tree cover and were not subject to any form of mechanical or artificial energy throughout the study, therefore simulating a relatively still-water environment.

Two high density polyethylene bottles containing aliquots of Cold Lake Winter Blend dilbit (CLWB) were prepared. On August 13, 2017, the contents of each bottle were poured onto the water surface of the treatment microcosms. The amount of dilbit added to the microcosms was determined by difference of the before and after pour weights (± 0.05g) of the dilbit containers. For the high-treatment, 1501.0 g was added,

corresponding to a volume of 1.64 L and for the low-treatment, 152.3 g of oil was added resulting in a volume of 0.166 L, while no dilbit was added to the control microcosm. This resulted in oil:water ratios of 1:8000 and 1:800 respectively. The three microcosms, referred to as low (0.166L), high (1.64L), and control (0L) treatments respectively, were exposed to natural sunlight, wind, and rain at all times throughout the spill period (SI Figure S2.5).

2.2. Dilbit Slick Samples

We collected high-volume samples (25 mL) of the surface slick in only the high-treatment microcosm after 1, 24 and 264 hours to measure temporal changes in the density, viscosity and water content. An additional sample was also collected 840 hours post-spill during a follow up site visit. We collected wipe samples of the surface slick from all three treatments 6, 24, 48, 96, 168, and 264 hours following the dilbit addition for chemical analysis of total petroleum hydrocarbons (TPH), n-alkanes, 7 alkylated polycyclic aromatic hydrocarbons (PAH) homologs, and petroleum biomarkers (see SI, s1.2). Density measurements were made using an Anton Paar density meter (Anton Paar, Montreal PQ, Canada). We performed dynamic viscosity measurements using an Anton Paar Stabinger SVM 3000 Viscometer (Anton Paar, Montreal PQ, Canada) and HAAK VTiQ Vicotester (Thermo Fisher Scientific, Waltham, MA) following ASTM D7042 (ASTM D7042-16, 2016). Percent water content was determined by Karl Fischer titration using a Metrohm 901 automatic titrator following ASTM E203 (ASTM E203-16, 2016). TPH concentrations of the oil slick were divided into four fractions based on carbon number; F1 (<nC10), F2 (nC10-nC16), F3 (nC16-nC34), and F4 (>nC34) and determined using a gas chromatograph equipped with a flame ionization detector (GC-

FID) following the same procedure as Yang et al. (Canadian Council of Ministers of the Environment, 2001; Yang et al., 2017, 2015).

2.3. Water Column Samples

We collected bulk water samples (i.e., comprising of dissolved and particulates) in 1-L amber glass bottles from two depths below the water surface (10 and 40 cm) in each microcosm at 6, 24, 48, 96, 168 and 264 hours following the dilbit addition (see Supporting Information). All water samples were spiked with surrogates and extracted with 50 mL of dichloromethane (DCM) for 16 hours on a continuous running roller apparatus. Concentration, column fractionation and instrument analysis procedures for the detection of n-alkanes, APAHs and biomarkers used in this study are described by Yang et al (Yang et al., 2018).

3 RESULTS AND DICUSSION

We observed that dilbit rapidly weathered and sank in model freshwater systems under ambient outdoor conditions. The appearance of the dilbit slicks changed considerably over the 11-day experiment, including the formation of a surface crust and changes in colour, from dark black to light brown, likely attributed to sunlight exposure and water entrainment (Figure 2.1) (Bobra and Tennyson, 1989; Lee et al., 2015). The crust formation is typical of oils stranded on land or in low energy aquatic environments that are not subject to substantial agitation, similar to our experimental system. Following sunlight exposure and evaporation, as the smaller compounds are removed, the heavier resins and asphaltenes remain and can migrate to the oil's surface, forming a crust (Fingas, 2015; Hollebone et al., 2011; Lee et al., 2015). Notably, a large portion

of the surface slicks in both low- and high-treatment microcosms sank to the sediments by the end of the 8th day of the experiment. Following the initial submergence observations, the microcosms experienced a rainfall event (4.8 mm of rain in 8 hours, SI Figure S2.5), providing additional turbulence that may have accelerated sinking. One potential mechanism that was not explored is the formation of oil-particle aggregates. It is possible that with increased turbulence following the rain event the sediments may have become suspended in the water column increasing the possibility for the dilbit to adhere to the sediment particles and thus settle out to the sediment bottom (Gustitus and Clement, 2017). However, throughout the study there was no visual sign of increased suspended sediment load and total suspended solid (TSS) measurements made on days 2, 7 and 11 showed very low concentrations in the water column of the treatment microcosms (ranging from 0 - 2mg/L) making it unlikely that this was the major driver of submergence. Ultimately, submergence can be attributed in large part to increases in density due to evaporation of the lighter chemical components and water uptake following prolonged environmental exposure. Other weathering processes including photooxidation could also be contributing to density increases, however given the short duration of this study, it is unlikely that this process would contribute to significant dilbit mass loss, and therefore was not explored in this study (Marty and Potter, 2014). It is important to note that our experimental system did not experience any substantial form of turbulence that would typically be encountered in a lake, river or tributary system (i.e., wind energy, surface currents and internal currents) and is therefore representative of a still-water system. In natural systems, energetic water movements could enhance spreading and evaporative processes, speeding up overall

weathering rates (Lee et al., 2015; Mackay and Matsugu, 1973; Reed et al., 1999; Sebastiao and Soares, 1995).

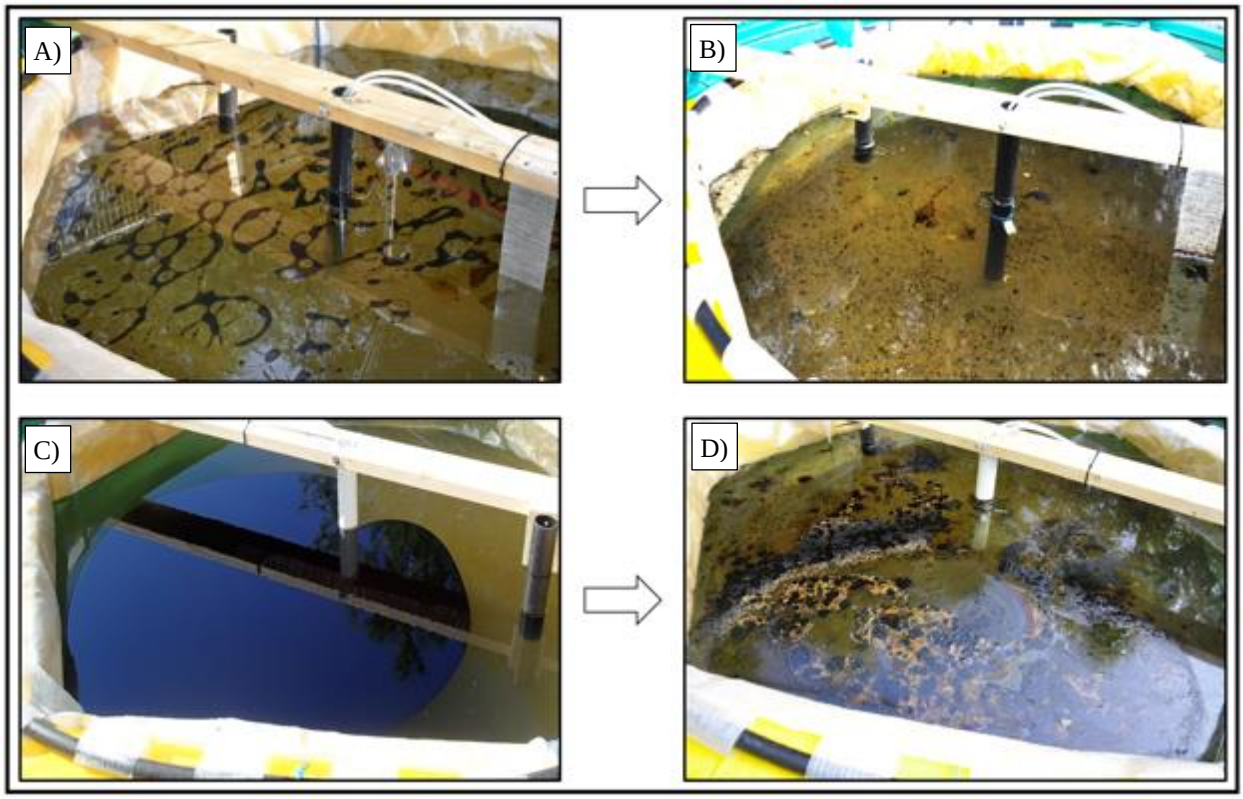

Figure 2. 1. Visible changes in the appearance of dilbit slicks in the low treatment (0.17 L dilbit) from day 0 (A) to day 11 (B) and high treatment (1.64 L dilbit) from day 0 (C) to day 11 (D).

3.1. Dilbit Physical Properties

Commonly-transported dilbit products all have a lower density than freshwater in their fresh, unweathered state (Government of Canada, 2013). In our study, the density (measured at 15°C) of dilbit increased rapidly from 0.9186 to 0.9883 g/mL in the first 24 hours after the spill event. We attribute this rapid increase in density of dilbit to evaporation of lighter constituents and uptake of water into the slick. After 24 hours, increases in density were more gradual, eventually reaching 1.0034 g/mL after 264 hours, and finally, 1.0037 g/mL after 840 hours (Figure 2.2A). Modelled changes in

density over time suggests dilbit's density was greater than 1 g/mL by approximately the 96-hour mark, however the dilbit did not begin to sink until day 8 (192 hours). Assuming that the major driver for submergence was dilbit's density exceeding that of water (i.e., > 0.9991 g/mL), there appears to have been a delay in submergence. This discrepancy could be due to inherent error in model predictions due to low sample numbers and wide confidence intervals (Figure 2.2A). We are also assuming the dilbit does not weather uniformly, and therefore samples collected for density analysis are not necessarily representative of the bulk dilbit. This increase in density led to the submergence of the slick that was observed after 8 days of weathering in both microcosms.

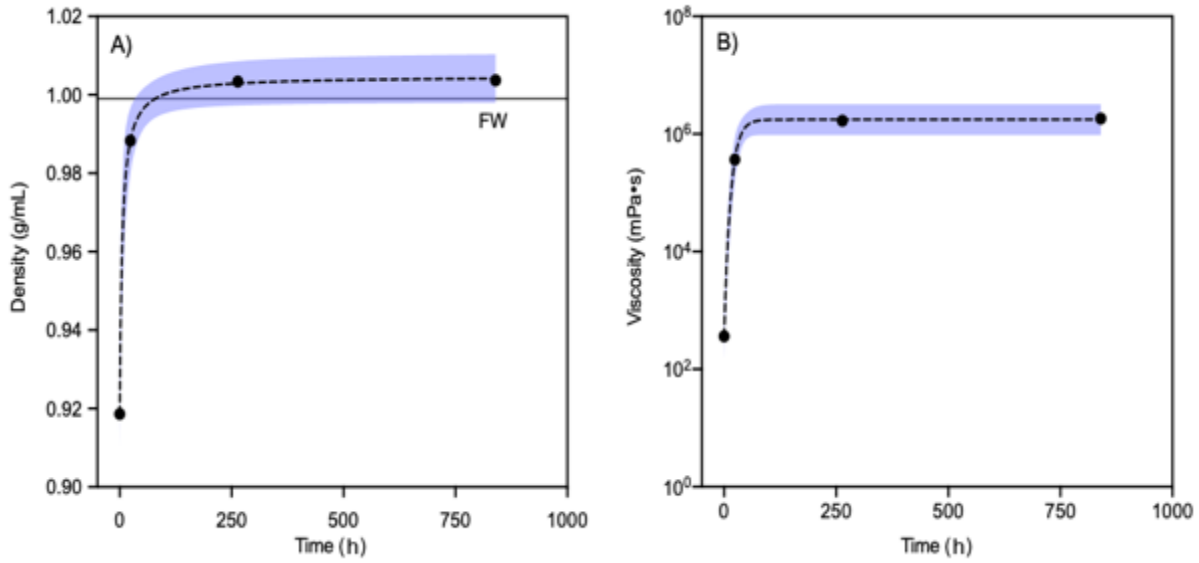

Figure 2. 2. Temporal changes in density (A) and viscosity (B) of dilbit (measured at 15 °C) in the high-treatment microcosm. The solid horizontal line in panel (A) represents the density of freshwater (FW). Line of best fit (dashed) and 95% confidence intervals (purple) are indicated. FW: freshwater.

Changes in dilbit's density in the microcosms were similar to some, but not all, studies that have simulated weathering in both laboratory and large-scale tank conditions. In one study, Cold Lake Blend (CLB) dilbit increased in density following 96

hours of constant evaporative weathering at 80°C in a laboratory setting from 0.9249 to 1.0085 g/mL (Government of Canada, 2013). A study by King et al. (King et al., 2014) found that CLB reached a maximum density of 1.0014 g/mL after 13 days following addition to an outdoor flume tank containing filtered seawater. In another case, SL Ross (SL Ross, 2012) tracked density changes of CLB as it weathered in an indoor flume tank for 13 days. The dilbit was exposed to high intensity ultraviolet (UV) lamps meant to mimic sunlight as well as wind energy from a fan. The dilbit's density rose from an initial value to 0.945 g/mL to a maximum of 0.998 g/mL (measured at 20 °C) after 96 hours, never surpassing the density of freshwater. A possible explanation for the apparent differences in maximum density measurements between the study by SL Ross and our study could be a tank effect. In our study, the dilbit was exposed to natural environmental conditions (i.e., sunlight, rain, wind, biota) which could have lead to greater weathering compared to the artificial conditions experienced by dilbit in an indoor facility.

Dilbit viscosity (measured at 15°C) increased by several orders of magnitude shortly after addition to the microcosms, from 362 to 367,000 mPa·s within the first 24 hours, and then to 1,670,000 and 1,837,000 mPa·s, after 264 and 840 hours, respectively following a similar trend to density increases (Figure 2.2B). Such increases in the viscosity of dilbit are caused by several weathering processes, most notably by evaporation of the low molecular weight (LMW) hydrocarbons and the incorporation of water into the dilbit slick (Fingas, 2014; Lee et al., 2015). Following a spill in a turbulent environment where oil dispersion forces are high, crude oil can often retain water droplets that are stabilized by concentrations of resins and asphaltenes that migrate to

the oil-water interface and form a gel-like coating around the water droplet (Gafonova and Yarranton, 2001; Yan et al., 1999; Yarranton et al., 2000). This process is termed emulsification and can result in viscosity increases 1000 times larger than the original value and can remain stable for long periods of time (Lee et al., 2015). In our study the surface slick increased in water content from 0.41% to 18.66% (w/w) after 24 hours and then remained below 20% for the remainder of the study, thus being classified according to Fingas and Fieldhouse (Fingas and Fieldhouse, 2004) as an unstable water-in-oil entrained state (SI Table S3.3). SL Ross (SL Ross, 2012) had similar findings in their indoor tank study, where dilbit's water content reached a maximum of 34% after 24 hours, and then remained below 20% for the remainder of the 13 day study. Stable water-in-oil emulsions typically form when water content of oils range from 70% to 80% (Fingas and Fieldhouse, 2009), dilbit often becomes too viscous to allow water droplets to further penetrate into the oil mass to a significant extent, which could explain our observation that dilbit's water content reached a maximum of 20% (Fingas, 2015).

High oil viscosity has implications for the efficacy of nearly all oil recovery techniques (Lee et al., 2015; Wadsworth, 1995). Conventional devices such as skimmers, weirs, and oleophilic ropes/discs work well on oils with maximum viscosities of 10,000 mPa·s, while belt, screw, and air conveyor devices will function well on oils with viscosities up to 100,000 mPa·s (Federici and Mintz, 2014; Wadsworth, 1995). Dilbit viscosity in our study surpassed these values after only 24 hours of weathering, and then by an order of magnitude after 264 hours of weathering under ambient

conditions in summer, stressing the importance of responding to dilbit spills as soon as possible.

3.2. Dilbit Chemistry

The chemical composition of the dilbit slick changed considerably over the 11-day experiment (Figure 2.3). Specifically, we saw significant decreases in the lower molecular weight dilbit constituents over time. Smaller hydrocarbons (<nC16) are prone to evaporation in the environment at the onset of a spill and are thus effectively removed from the slick.(Lee et al., 2015) The first-order depletion rate coefficients of the lighter F1 and F2 fractions were 0.32 h^{-1} (95% CI 0.15 – 0.50) and 0.0036 h^{-1} (95% CI 0.00026 - 0.0069), respectively, in the low-treatment microcosm and 0.35 h^{-1} (95% CI 0.24 – 0.47) and 0.0074 h^{-1} (95% CI 0.0018 - 0.013), respectively, in the high-treatment microcosm; all of these rate coefficients were significantly different from 0 ($p < 0.05$). In contrast, the F3 and F4 fractions did not change significantly in composition after 11 days, suggestive of their recalcitrance (Figure 2.3) (Lee et al., 2015). Rate constants in the high-treatment microcosm were slightly higher compared to the low-treatment (SI Table S3.5). These rate constants provide estimates of the persistence of these dilbit constituents in a simulated freshwater system.

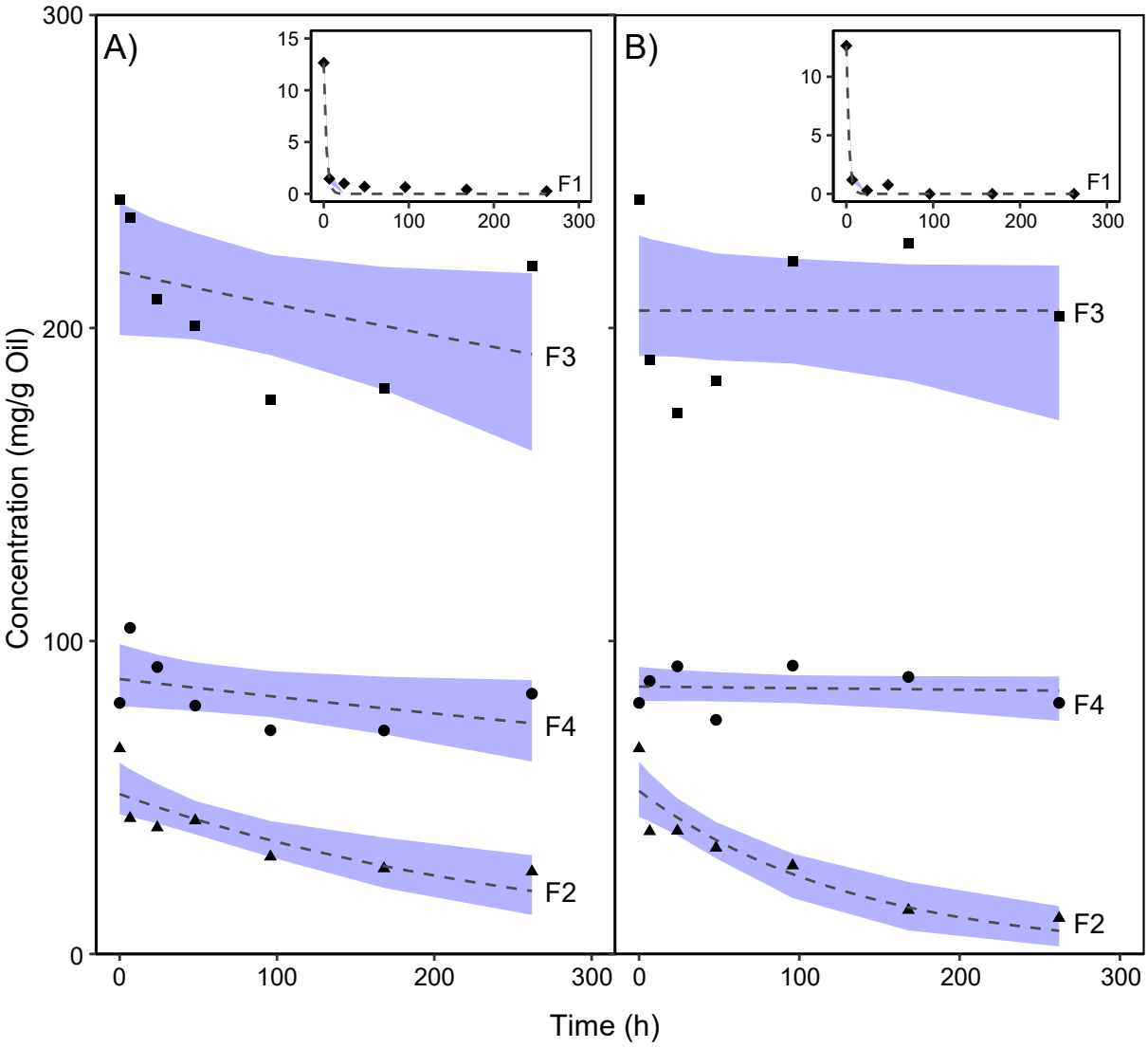

Figure 2. 3. Changes in concentration over time of the four major petroleum fractions of dilbit: F1 (<nC10), F2 (nC10-nC16), F3 (nC16-nC34), and F4 (>nC34). Samples were collected from the surface slick of the low- (A) and high- (B) treatment microcosms. Line of best fit (dashed) and 95% confidence intervals (purple) are indicated.

3.3. Water Column Chemistry

In general, chronic toxicity of crude oil to aquatic species has been commonly associated with 3- to 5- ring PAHs (Madison et al., 2017; Philibert et al., 2016). Here we examined the partitioning behaviour of PAHs (parent and alkylated) from the dilbit slick into the bulk water column phase (dissolved and particulates) to determine potential

concentrations aquatic biota could be exposed to following a spill. Increases in water column concentrations of small 2 - 3-ring phenanthrenes, dibenzothiophenes, and fluorenes were similar in both low- and high-treatment microcosms, with no observable effect of volume of dilbit added (Figure 2.4). The 4-ring PAHs; fluoranthene, chrysene, and benzonaphthothiophene, which are known to cause aryl hydrocarbon receptor (AHR)-dependent toxicity, remained below detection limits in the water column throughout the study (Incardona et al., 2006). With few exceptions, PAH water column concentrations in the control microcosm were consistently below respective limits of detection (see Supporting Information).

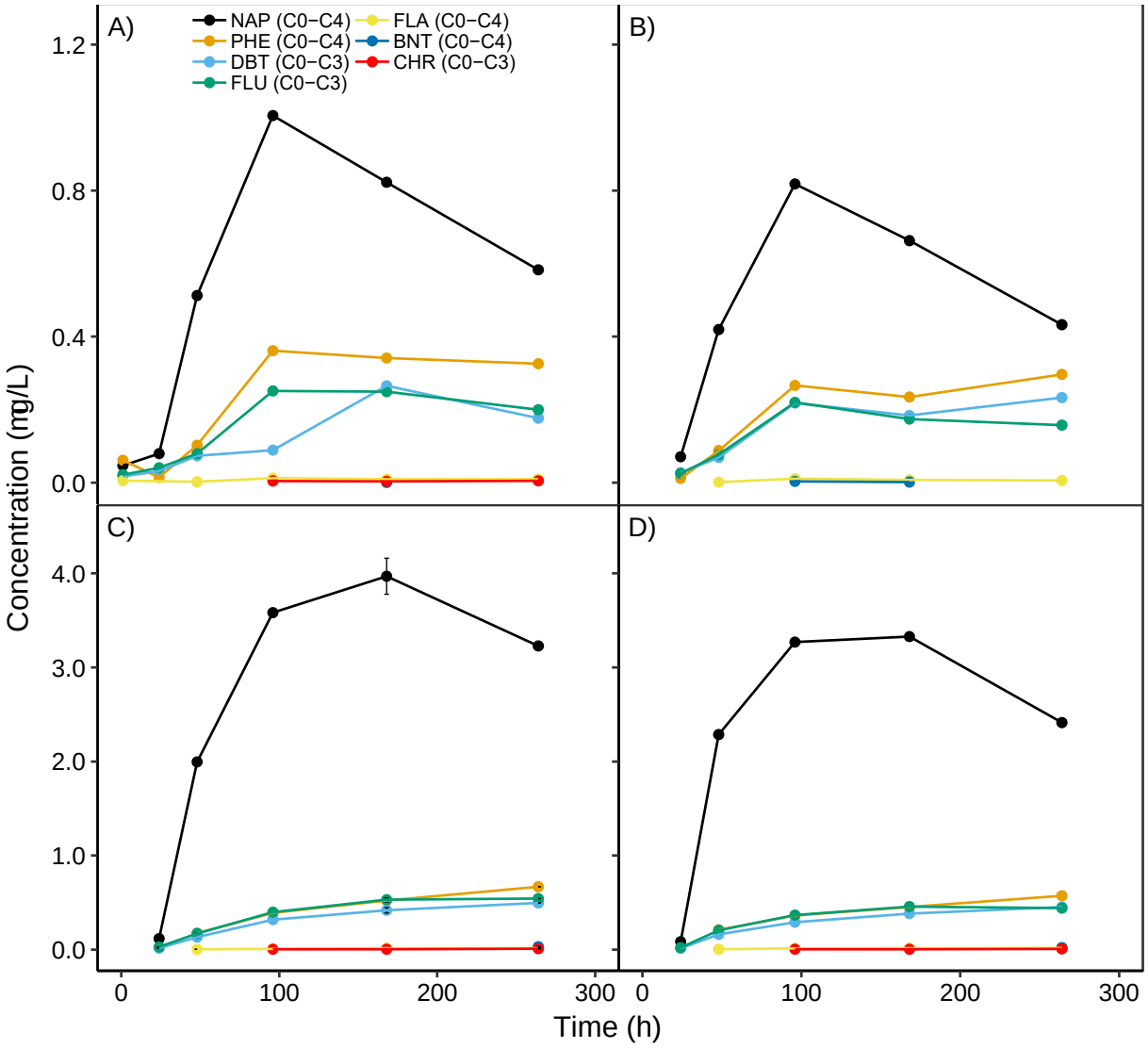

Figure 2. 4. Water column concentrations of 7 major PAH groups in the low-treatment microcosm at 10 cm (A) and 40 cm (B) depths and the high-treatment microcosm at 10 cm (C) and 40 cm (D) depths. Concentrations represent sums of parent compounds and their alkylated homologs for each group. Gaps in data points represent sampling dates where concentrations were <LOD. Standard error is shown for samples that were randomly selected to be collected in triplicate. NAP: naphthalene; PHE: phenanthrene; DBT: dibenzothiophene; FLU: fluorene; FLA: fluoranthene; BNT: benzonaphthothiophene; CHR: chrysene.

PAH concentrations increased within the first 96 hours and then stabilized in all cases except for naphthalene, which subsequently began to decrease until the end of the study (Figure 2.4). The reason for the observed plateaus is difficult to discern since

the PAHs were only reaching a fraction of a percentage of their saturation concentrations in the water column (ex: Phenanthrene reached 0.02% saturation in the high-treatment) (Mackay et al., 2006). It is possible that the increased viscosity and thickness of the weathered dilbit slick paired with the formation of an outer crust sealed off the remaining dilbit, significantly reducing further dissolution of compounds into the water column, thus causing a plateau in water column PAH concentrations (Fingas, 2015). The concentration of naphthalene increased over time in both microcosms and showed evidence of a dose dependence, reaching maximum concentrations after 4 days (1.0 μg/L) in the low-treatment and 7 days (4.0 μg/L) in the high-treatment. The naphthalene concentrations subsequently began to decrease over time, whereas the other PAHs remained stable. It is possible that the observed decrease is due to naphthalene's evaporation across the water – air interface given its relatively high vapour pressure (11 Pa) compared to the rest of the PAHs analyzed in the water column (ranging from 0.02 - 1.4×10^{-6} Pa) (Stogiannidis and Laane, 2015). Additionally, the dilbit layer may have restricted transfer of the semi-volatile naphthalenes between the water and air, especially in the high-treatment which had considerable water surface area coverage early on (Figure 2.1). Submergence of the dilbit slick would have removed this barrier, further allowing the evaporation of the naphthalenes from water and contributing to its gradual decrease in concentration over time. This effect would be more pronounced in the high-treatment microcosm where dilbit spread to cover a much larger surface area compared to the low-treatment (Figure 2.1). This could potentially explain the earlier onset of naphthalene decrease noted in the low-treatment (96 hours), which had more open air-water interface throughout the entire study.

The concentrations of PAHs in water following a dilbit spill appear to be dependent on a compound's alkylation and molecular size. Greater alkylation and an increased number of aromatic rings reduces water solubility (Andersson and Achten, 2015; Lee et al., 2015). In our study, the lesser alkylated PAHs (ex: C1 and C2 forms) reached higher concentrations in the water column in both microcosms compared to the more alkylated homologues (ex: C3 and C4 forms). Parent, unsubstituted PAHs (i.e., C0) concentrations in the water column were low, mirroring their low abundances in the source CLWB-dilbit.

4 CONCLUSION

Following the addition of dilbit to our land-based microcosms under ambient environmental conditions, volatile F1 and F2 dilbit fractions evaporated rapidly, leaving behind the heavier residual F3 and F4 fractions. As the lighter ends evaporated, the physical properties of dilbit began to resemble those of the source crude bitumen, evidenced by density surpassing 1 g/mL and viscosity surpassing 1,000,000 mPa s after 11 days. Though the formation of oil-sediment aggregates has been shown to potentially induce submergence, it was not tested in this study as the concentrations of suspended sediments in the treatment microcosms were very low (0 – 2 mg/L, SI Table S3.2) (Fitzpatrick et al., 2015; Government of Canada, 2013; Lee et al., 2015). Water column concentrations of lower molecular weight APAHs increased over time in both microcosms, but since there are no water quality guidelines for APAHs, we can make no comparisons to thresholds for protecting aquatic life (Andersson and Achten, 2015).

Our study demonstrates how chemical and physical composition of dilbit in fresh water can drastically change in a very short period of time, ultimately affecting its tendency to sink in a freshwater system. Our findings stress the need for rapid spill response, as well as the development of non-invasive techniques to recover sunken dilbit in freshwater sites. Gaining a better understanding of how dilbit and its chemical constituents behave in aquatic environments will aid in informing evidence-based environmental risk assessments and spill management strategies for this unconventional oil product.

ACKNOWLEDGEMENTS

Funding for the present study was provided by a Natural Sciences and Engineering Research Council Strategic Partnership Grant (STPGP 493786-16 awarded to J. Blais, M. Hanson, and D.M. Orihel), a grant under the Oceans Protection Program, in-kind contributions from Environment and Climate Change Canada, and in-kind support from the IISD-Experimental Lakes Area. A special thank you to J. Séguin,T. Black, J. Mason, H. Kosichek, D. Secker, and J. Cederwall for their contributions to the experimental setup. Thank you to the 2 anonymous reviewers for taking their time to review our manuscript and provide helpful comments that contributed to its improvement.

SUPPORTING INFORMATION

1. Experimental Set-Up and Sampling

This study was carried out at the International Institute for Sustainable Development Experimental Lakes Area (IISD-ELA), a unique research station in northwestern Ontario, Canada, dedicated to holistic, interdisciplinary field research and ecosystem manipulation studies. Each microcosm consisted of a circular, flat-bottomed, low-density polyethylene outer containment tank (2.7 m diameter x 0.72 m height) (ACE Rotomolds, Hospers, Iowa, USA) filled with lake water collected from Lake 240 (49°40 N, 93°44 W), one of IISD-ELA's oligotrophic research lakes (Figure S2.1A). In each containment tank, a hexagonal 2 m diameter polystyrene collar (Dow, Midland, Michigan, USA) was floated in the center. Attached to the collar, a 2 m diameter, closed bottom bag constructed from Novathene, a woven high-density polyethylene fabric (Curry Industries, Winnipeg, Manitoba, Canada), was suspended down to the bottom of the containment tank. A total of 160 L of sediment and 1413 L of water were added to each microcosm, with a final water depth of ~0.5m in each enclosure (Figure S2.1B).

1.1 Dilbit Addition

Prior to addition, two high-density polyethylene bottles containing aliquots of identical Cold Lake Winter Blend (CLWB), a form of dilbit commonly transported through pipelines in Canada(Government of Canada, 2013; King et al., 2015), were shaken by hand for 5 minutes at ambient temperature and poured from the bottle over the back of a pre-cleaned stainless steel spoon at the water surface. A chemical profile of the fresh CLWB can be found in Figure S2.2.

1.2 Dilbit Slick Sampling

Sections of polyester absorbent pads (PIG® Thick Liquids Absorbent Mat Pads) were pre-cut and stored in certified 125mL wide mouth amber glass jars with lids lined with a TFE-fluorocarbon polymer film until the time of sampling. Subsamples of oil were collected from the surface slick in each microcosm using the absorbent pad and preserved following ASTM Methods D4489 and D3325.("ASTM D3325-90 Standard Practice for Preservation of Waterborne Oil Samples," 2013; "ASTM D4489-95 Standard Practices for Sampling of Waterborne Oils," 2017) At each time point, we passed a wipe through the oil slick until a sample approximately 15mL had adhered, which we then placed back in the jar and sealed it (Figure S2.3, Figure S2.4). In the case of the control tank, we simply passed the wipe through the water surface. We placed samples immediately in a cooler and stored them away from any potential light sources to prevent further photochemical reactions.

1.3 Water Column Sampling

We collected water samples from the desired depths (10 and 40 cm) via the LDPE tubing sampling set-up described above. A section (approximately 20 cm) of ¼" Masterflex silicone tubing (Cole-Parmer, Montreal, Quebec, Canada) was connected to the LDPE tubing at the edge of the tank and fed through a Waterra Spectra Field Pro peristaltic pump (E-476-field pro pump; Hoskin Scientific Ltd., Burlington, Ontario, Canada) at 500 mL/min. On every sampling event, we discarded the first liter of pumped water (equivalent to approximately 5 times the volume of water contained in the length of LDPE tubing) prior to the collection of any samples to ensure the collected sample

was representative of the water column in the enclosures. Water samples (1 L) for analytical chemistry were collected from the 10 cm and 40 cm ports on pre-weighted, certified-clean amber glass bottles with TFE-fluorocarbon polymer film cap liners at 1h, 6h, 24h, 48h, 96h, 7d and 11d.

2. Analytical Methods

2.1 Sample Preparation

Prior to use, we rinsed all glassware with acetone, dichloromethane (DCM) and hexane. The analysis of the concentrated solvent blank demonstrated the glassware was clean and target-analyte free. We spiked all water samples with appropriate surrogates (o-terphenyl, d_{50}-tetracosane, d_8-naphthalene, d_{10}-acenaphthene, d_{10}-phenanthrene, d_{12}-benz[a]anthracene, and d_{12}-perylene), and then extracted them with 50 mL of DCM for 16 hours on a continuous running roller apparatus on the same day as sample collection. The average time to extraction following sample collection was 20 hours (including the 16-hour rolling phase). We rinsed the remaining water phase twice with 10 mL of DCM to thoroughly extract the sample. We combined extracts and concentrated them to a volume of 1 – 2 mL by rotary evaporation, and then solvent-exchanged to hexane phase, and made up to the final volume of 1.0 mL with hexane. To extract collected oil samples, we dissolved approximately 0.8 g of sample into hexane and made up to a final volume of 10.0 mL. We then spiked a 200 µL aliquot of the oil solution with the same surrogates as stated above. Once both the water and oil samples were in extracted form, the extracts were quantitatively transferred onto a chromatographic column packed with 3 g of silica gel, which was topped with about 1

cm of anhydrous granular sodium sulfate. We then pre-conditioned the column with 20 mL of hexane, for sample cleanup and fractionation. Hexane and a hexane-DCM mixture (1:1, v:v) were used to sequentially elute the saturated and aromatic compounds, respectively. These two fractions were concentrated under a gentle stream of nitrogen to appropriate volumes, spiked with internal standards (IS) (including 5-α-androstane, C_{30} 17β(H),21β(H)-hopane and d_{14}-terphenyl for total (GC-detectable) petroleum hydrocarbons (TPHs) and *n*-alkanes, petroleum biomarker compounds, and polycyclic aromatic compounds (PAHs) analysis, respectively), and then adjusted to a volume of 1.0 mL for GC-MS and GC-FID analyses. The saturated fraction was used for analysis of aliphatics (total saturated hydrocarbons, TSHs), *n*-alkanes, and biomarker terpanes and steranes; the aromatic fraction was used for analysis of aromatic hydrocarbons (TAHs), alkylated homologous PAHs and other unsubstituted PAHs.

2.2 Instrument and Sample Analysis

We determined TPH concentration (largely *n*-C_8 through *n*-C_{50}) on an Agilent 7890A gas chromatograph equipped with a flame ionization detector (FID) using Agilent OpenLAB ChemStation for data collection. We performed chemical separation using a DB-5HT fused silica column (30 m × 0.25 mm i.d., 0.10 μm film thickness) and hydrogen (1.3 mL/min) as a carrier gas. The injector and detector temperatures were 290°C and 300°C, respectively. The temperature program used for TPH determination was: 40°C for 2 min, ramp at 20°C/min to 340°C, and held for 20 min. We analyzed target PAH compounds (including 7 alkylated PAH homologous groups and other unsubstituted PAHs), and biomarker compounds using an Agilent 7890A GC equipped

with an Agilent 5975C mass selective detector (MSD). The GC separation employed a DB-5MS capillary column (30 m × 0.25 mm i.d. × 0.25 µm film thickness). Samples (1.0 µL) injected into the GC in splitless mode (injector temperature at 290°C) with 1.0 mL/min of helium as carrier gas. The MSD operated in select ion monitoring (SIM) mode. For the analysis of alkylated PAHs, n-alkanes and petroleum biomarkers, the column temperature was held at 60°C for 2.0 min, and then programmed 6°C/min to 300 °C and held for 20 min. For the analysis of other unsubstituted PAHs, GC oven temperature started from 60°C for 1.0 min, heated to 160°C at 15 °C/min, then 8°C/min to 300°C and held for 7.0 min. Data was acquired and analyzed with Agilent Enhanced MSD ChemStation.

2.3 Quality Assurance

Recoveries of o-terphenyl and d_{50}-tetracosane, surrogates for GC-FID analysis of TPH, were determined to be 89 ± 11 % and 91 ± 14 % (± standard deviation) for all the water samples, 99 ± 12% and 88 ± 9% for all the oil samples. The recoveries of five deuterated PAH surrogates ranged from 62 ± 11% to 94 ± 7% and from 79 ± 12% to 103 ±14% from d_8-naphthalens to d_{12}-perylene, for GC-MS analysis of PAHs and APAHs for all the water and oil samples, respectively. All the recoveries were considered to be within acceptable limits for analysis. Limits of detection for different PAH compounds in water samples ranged from 0.4 – 3.3 ng/L (Table S3.1). We performed a method blank analysis to monitor the laboratory background at every 10 samples. For quality control, ESTS reference oil Prudhoe Bay crude oil (13% weathered) was used as the reference oil standard.

3. Environmental Parameters

Throughout the 11-day study, the site experienced an average wind speed of 5.7 km/h and total precipitation of 16.4 mm. Rainfall primarily occurred during two rain events, on day 2 (7.6 mm) and day 8 (4.8 mm) (Figure S2.5). The experiment took place in an open area surrounded by large trees and was therefore sheltered from any strong wind events, inhibiting any wave action that would have been imparted by wind.

3.1 Density and Viscosity Modelling

Density measurements were fitted to a non-linear expedient model adapted from King et al., using GraphPad Prism Version 8.0.0. The density model is given by:

$$\rho = \rho_0 + (\rho_f - \rho_0)\frac{t}{T + t}$$

Where ρ_0 is the initial density (g/mL) of the fresh, unweathered source dilbit, ρ_f is the final density (g/mL) of the dilbit sample collected at the end of the study, t is time (h) and T is a time constant representing the time (h) it takes for the density to increase by half of $(\rho_f - \rho_0)$.(King et al., 2014)

The experimental data can then be fit to this model:

15°C $$\rho = 0.9186 + (1.005 - 0.9186)\frac{t}{5.6+t}$$

Viscosity measurements were fitted to a non-linear model exponential plateau model using GraphPad Prism Version 8.0.0. The viscosity model is given by:

$$\nu = \nu_f - (\nu_f - \nu_0)e^{-kt}$$

Where ν_0 is the initial viscosity (mPa·S) of the fresh, unweathered source dilbit, ν_f is the final viscosity (mPa·S) of the dilbit sample collected at the end of the study, t is time (h) and k is a rate constant (h^{-1})

The experimental data can then be fit to this model:

15°C $$\text{Log}(\nu) = 6.243 + (6.243 - 2.560)e^{-0.07047t}$$

Supporting Figures

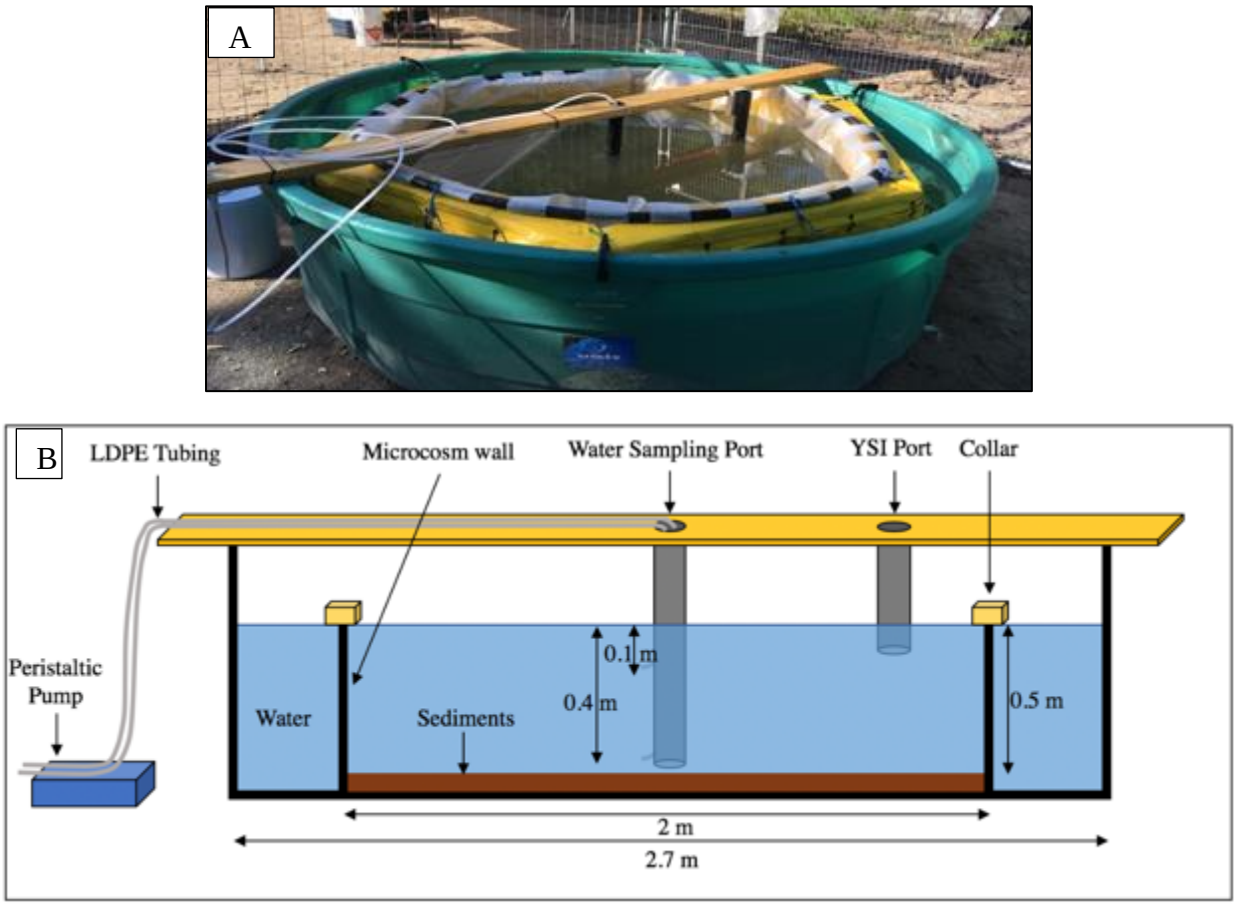

Figure S2. 1. Land based tank used in present study (A) and diagram demonstrating the different design aspects of the tank set up (B)

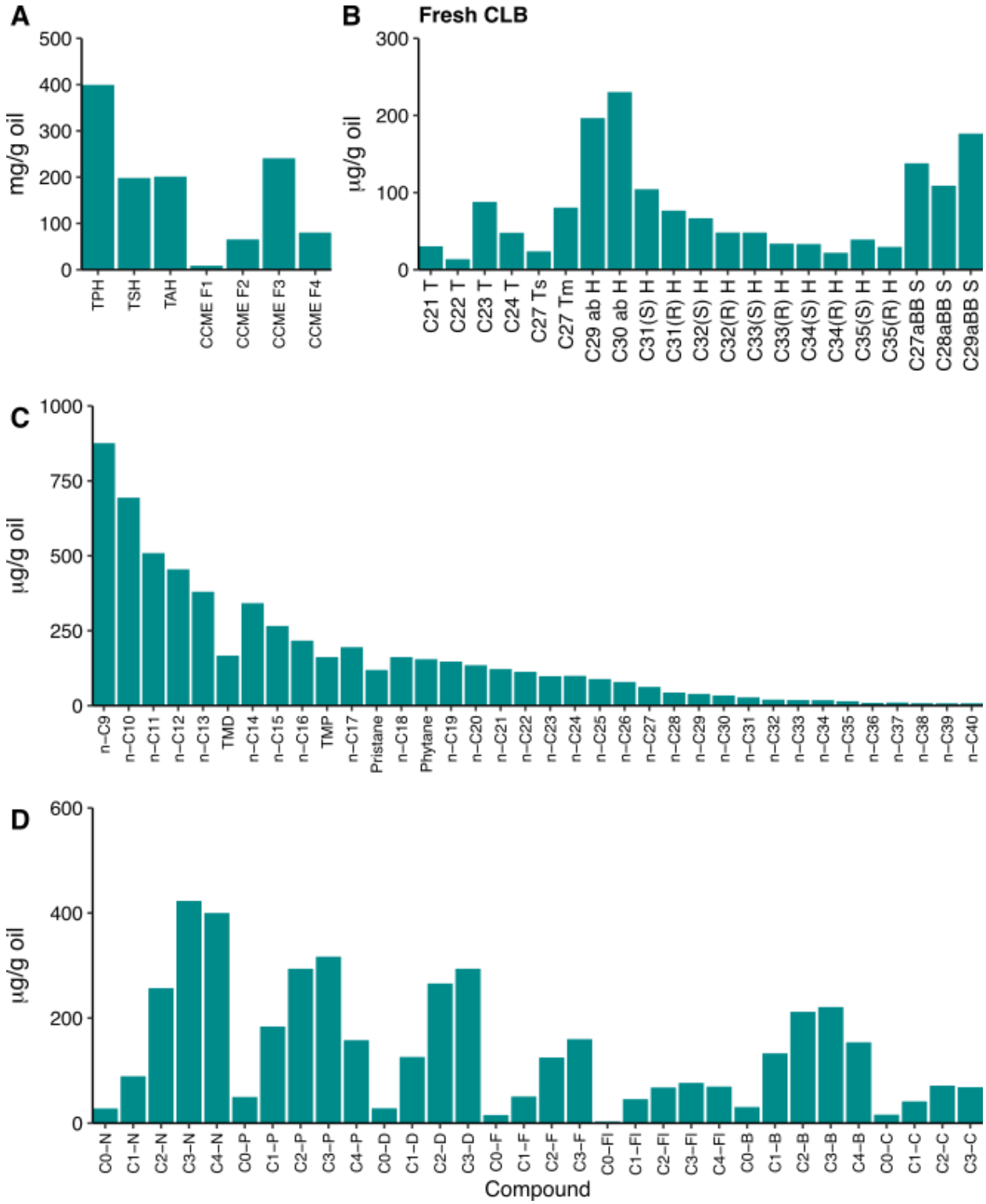

Figure S2. 2. Chemical characterization of fresh, unweathered Cold Lake Winter Blend (CLWB) dilbit used in this study. Petroleum hydrocarbons (A), biomarkers (B), n-alkanes (C) and polycyclic aromatic hydrocarbon (D) profiles are shown. TMD: 2,6,10-trimethyldodecane , TMP: 2,6,10-trimethylpentadecane, TPH: total petroleum hydrocarbons, TSH: total saturate hydrocarbons, TAH: total aromatic hydrocarbons, F1:

<n-C9, F2: n-C10 – n-C16, F3: n-C16 – n-C34, F4: >n-C34, T: terpanes, H: hopanes, S: steranes, N: naphthalene, P: phenanthrene, D: dibenzothiophene, F: fluorene, Fl: fluoranthene, B: benzonaphthothiophene, C: chrysene.

Figure S2. 3. Surface slick sample collected from the high-treatment microcosm utilizing a section of polyester absorbent pad

Figure S2. 4. High volume dilbit sample collected from the high-treatment microcosm for physical property analysis

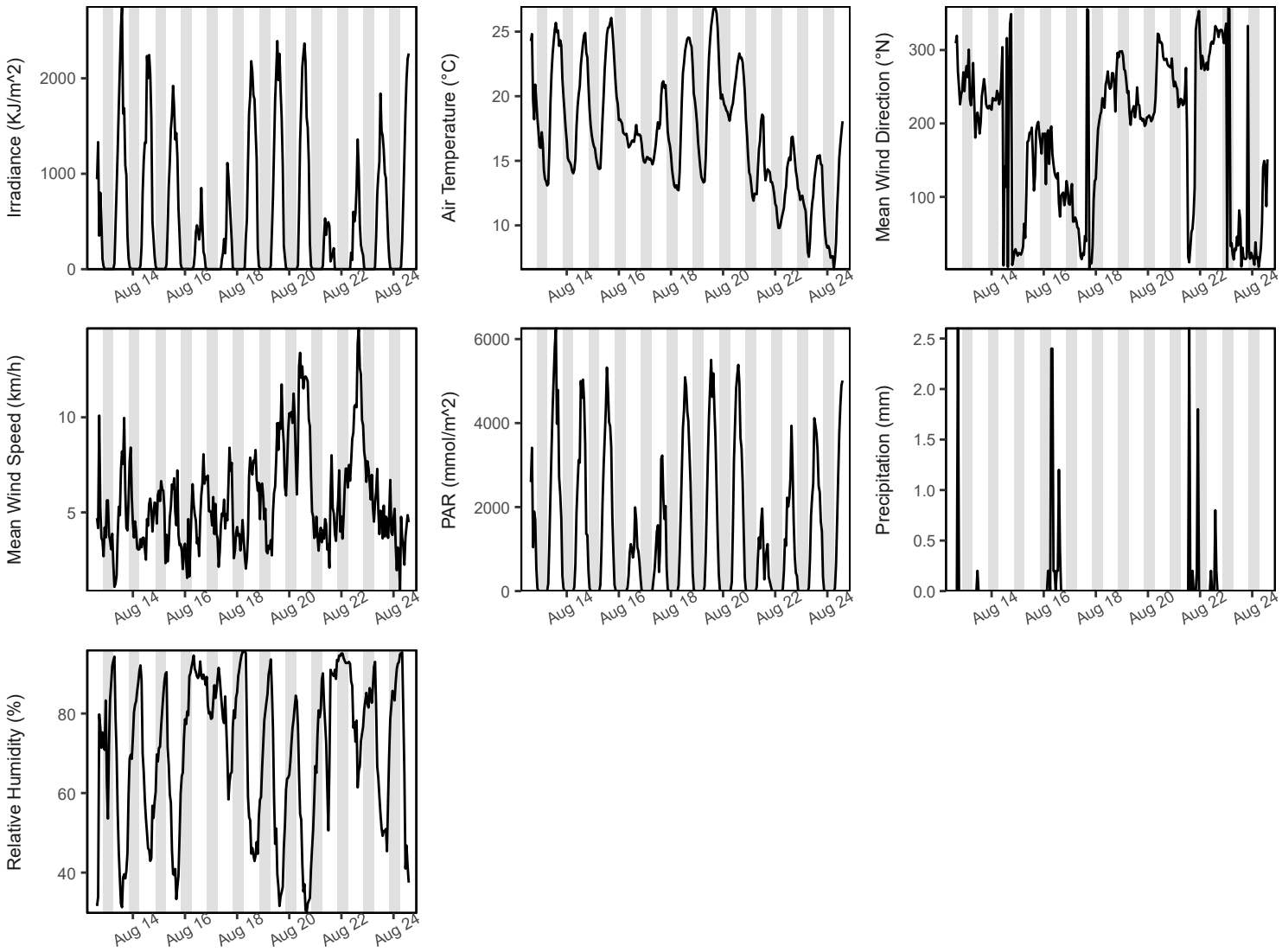

Figure S2. 5. Weather parameters throughout the experimental timeline measured at the meteorological site at IISD-ELA

Supporting Tables

Table S2. 1. Limits of detection for selected PAH compounds in a 1L water sample

Compound	Limit of detection (ng/L)
Naphthalene	0.5
2-Methylnaphthalene	0.5
1-Methylnaphthalene	0.5
2,6-Dimethylnaphthalene	0.6
2,3,5-Trimethylnaphthalene	0.7
Fluorene	0.6
Dibenzothiophene	0.4
Phenanthrene	0.4
1-Methylphenanthrene	0.7
Fluoranthene	0.5
Chrysene	0.8

Table S2. 2. Daily water quality parameters measured within each of the treatment microcosms over the 11-day period of the simulated dilbit spills. All measurements made between 9:00am – 10:30am unless otherwise indicated. Values for water temperature, pressure, dissolved oxygen (DO), conductivity (Cond) and total suspended sediments (TSS) are shown.

	Control (0L)					Low (0.15L)					High (1.5L)				
Day	Water Temp (°C)	Pressure (mmHg)	DO (mg/L)	Cond. (µS)	TSS (mg/L)	Water Temp (°C)	Pressure (mmHg)	DO (mg/L)	Cond. (µS)	TSS (mg/L)	Water Temp (°C)	Pressure (mmHg)	DO (%)	Cond. (µS)	TSS (mg/L)
0[a]	19.1	726.3	8.1	0.034	/	19.1	727	6.39	0.061	/	19.1	726.3	8.17	0.034	/
0[b]	22.4	723.1	8.38	0.038	/	22.7	723.2	7.61	0.036	/	21.7	723	7.95	0.035	/
1	19.9	723.1	8.35	0.033	/	20.6	723.1	7.88	0.034	/	20.3	722.9	7.51	0.034	/
2	19.6	725.1	9.03	0.035	8.5	20.2	725.1	8.71	0.034	1.5	20.1	724.8	8.11	0.034	0.5
3	20.1	726.1	8.75	0.032	/	20.7	726	8.39	0.033	/	20.4	726	7.91	0.033	/
4	18.3	722.2	8.39	0.028	/	19	722.1	8.14	0.03	/	18.9	722.2	7.93	0.031	/
5	17.5	721.1	8.83	0.029	/	18.1	720.9	8.64	0.034	/	17.9	720.9	7.66	0.031	/
6	18.5	722	8.88	0.021	/	19.2	721.8	8.91	0.036	/	18.7	721.9	7.67	0.029	/
7	20	721.9	8.6	0.032	1.5	20.8	721.7	8.02	0.034	0	20.5	721.8	7.74	0.033	0
8	18.1	727.3	8.84	0.03	/	19.2	727.2	8.51	0.032	/	18.9	727.2	7.1	0.032	/
9	15.8	724.1	9.19	0.03	/	16.4	724.2	8.64	0.03	/	16.4	724.1	7.95	0.029	/
10	14.7	729.6	9.39	0.027	/	15.4	729.6	8.95	0.029	/	15.3	729.6	8.33	0.028	/
11	13.5	733.2	9.55	0.026	0	13.9	733.3	9.37	0.028	2	14	733.4	8.94	0.027	0

[a]Day 0 measurement made in the morning
[b]Day 0 measurement made in the afternoon

Table S2. 3. Physical properties of source oil and samples collected throughout the spill. Values are a single measurement, otherwise they represent as the mean of 3 measurements

Parameter	Temp (°C)	Time since release (h)			
		0	**24**	**264**	**840**
Density (g/mL)	**0°C**	0.9293 ± 0.00001		1.017 ± 0.0011	1.0120 ± 0.0005
	15°C	0.9186 ± 0.0006	0.9883	1.0034 ± 0.0009	1.0037 ± 0.0008
Viscosity (mPa·s)	**0°C**	944.1 ± 14.9	5.44×10^6	2.47×10^7	2.76×10^7
	15°C	362.1 ± 9.6	367 000 ± 7257	1.67×10^6 ± 44 700	1.84×10^6 ± 18 800
Water Content (%)		0.41 ± 0.02	18.66 ± 0.08	17.62 ± 0.65	22.25 ± 0.89

Table S2. 4. Summary of non-linear model fit parameters for density and viscosity over time. TSS represents total sum of squares.

Property	Model	Parameter	Estimate	95% CI	R^2	TSS
Density (ρ)	$\rho_0 + (\rho_f - \rho_0)\frac{t}{T+t}$	ρ_0	0.9186	0.9103 to 0.9269	0.999	4.312×10^{-7}
		ρ_f	1.005	0.9983 to 1.011		
		T	5.633	1.668 to 10.79		
Viscosity (Log(ν))	$\nu_f - (\nu_f - \nu_0)e^{-kt}$	ν_0	6.243	5.980 to 6.506	0.999	0.0008567
		ν_f	2.560	2.188 to 2.932		
		k	0.07047	0.05004 to 0.11		

Table S2. 5. Summary of the degradation kinetics of CCME fractions present in dilbit samples taken from both the low and high tank

Tank	CCME Fraction	Decay Equation	Degradation rate (h^{-1})	95% CI	*p*-value[a]	$t_{1/2}$ (h)
Low	F1 (<nC9)	F1 = 12.6*e* - 0.32*t*	0.32	0.15 - 0.50	0.005*	2.13
	F2 (nC10 - nC15)	F2 = 51.1*e* - 0.0036*t*	0.0036	0.00026 - 0.0069	0.039*	194.8
	F3 (nC16 - nC34)	F3 = 217.9*e* - 0.00049*t*	0.00049	-0.00087 - 0.0018	0.40	1415.7
	F4 (>nC34)	F4 = 87.9*e* - 0.00067*t*	0.00067	-0.00091 - 0.0024	0.32	1035.2
High	F1 (<nC9)	F1 = 12.6*e* - 0.35*t*	0.35	0.24 - 0.47	0.0006*	1.95
	F2 (nC10 - nC15)	F2 = 52.1*e* - 0.0074*t*	0.0074	0.0018 - 0.013	0.02*	93.1
	F3 (nC16 - nC34)	F3 = 205.6	0	-0.0014 - 0.0014	1	0
	F4 (>nC34)	F4 = 85.4*e* - 0.000059*t*	0.000059	-0.00087 - 0.0010	0.88	11806.3

[a]alpha = 0.05,

Supporting References

ASTM D3325-90 Standard Practice for Preservation of Waterborne Oil Samples, 2013. . ASTM Int. https://doi.org/10.1520/D3325-90R13

ASTM D4489-95 Standard Practices for Sampling of Waterborne Oils, 2017. . ASTM Int. https://doi.org/10.1520/D4489-95R17

Government of Canada, 2013. Properties, composition and marine spill behaviour, fate and transport of two diluted bitumen products from the Canadian oil sands (No. ISBN 987-1-100-23004-7), Federal Government Technical Report.

King, T.L., Robinson, B., Boufadel, M., Lee, K., 2014. Flume tank studies to elucidate the fate and behavior of diluted bitumen spilled at sea. Mar. Pollut. Bull. 83, 32–37. https://doi.org/10.1016/j.marpolbul.2014.04.042

King, T.L., Robinson, B., McIntyre, C., Toole, P., Ryan, S., Saleh, F., Boufadel, M.C., Lee, K., 2015. Fate of surface spills of Cold Lake blend diluted bitumen treated with dispersant and mineral fines in a wave tank. Environ. Eng. Sci. 32, 250–261.

REFERENCES

Alberta's Energy Reserves, 2018. ST98: Alberta's Energy Reserves and Supply/Demand Outlook - Google Search.

American Petroleum Institute, 1999. Fate of oil spilled in marine waters (No. 4691). Health and Environmental Science Department.

Andersson, J.T., Achten, C., 2015. Time to say goodbye to the 16 EPA PAHs? Toward an up-to-date use of PACs for environmental purposes. Polycycl. Aromat. Compd. 35, 330–354. https://doi.org/10.1080/10406638.2014.991042

ASTM D7042-16, 2016. Standard test method for dynamic viscosity anddensity of liquids by Stabinger viscometer (and the calculation of kine-matic viscosity). ASTM Int. West Conshohocken PA Vol 05.04. https://doi.org/10.1520/D7042-16E03

ASTM E203-16, 2016. Standard test method for water using volumetric Karl Fischer titration. ASTM Int. West Conshohocken PA E203-16. https://doi.org/10.1520/E0203-16

Bobra, M., Tennyson, E.J., 1989. Photooxidation of petroleum. Env. CanEnviron Prot Dir River Road 129–147.

Canadian Council of Ministers of the Environment, 2001. Method for the Canada-Wide Standard for Petroleum Hydrocarbons in Soil—Tier 1 Method. CCME Winnipeg (MB).

Crosby, S., Fay, R., Groark, C., Smith, J.R., Sullivan, T., Pavia, R., Shigenaka, G., 2013. Transporting Alberta oil sands products: defining the issues and assessing the risks (No. NOAA Technical Memorandum NOS OR&R 43). U.S. Dept. of Commerce, Seattle, WA: Emergency Response Division, NOAA.

Dew, W.A., Hontela, A., Rood, S.B., Pyle, G.G., 2015. Biological effects and toxicity of diluted bitumen and its constituents in freshwater systems. J. Appl. Toxicol. 35, 1219–1227. https://doi.org/10.1002/jat.3196

Federici, C., Mintz, J., 2014. Oil Properties and Their Impact on Spill Response Options.

Fingas, M., 2015. Review of The Properties and Behaviour of Diluted Bitumen, in: Proceeding of the 39th Arctic and Marine Oil-Spill Program Technical Seminar. Environment and Climate Change Canada, Vancouver, B.C., Canada, pp. 470–494.

Fingas, M., 2014. Handbook of oil spill science and technology. John Wiley & Sons.

Fingas, M., Fieldhouse, B., 2009. Studies on crude oil and petroleum product emulsions: Water resolution and rheology. Colloids Surf. Physicochem. Eng. Asp. 333, 67–81.

Fingas, M., Fieldhouse, B., 2004. Formation of water-in-oil emulsions and application to oil spill modelling. J. Hazard. Mater. 107, 37–50. http://dx.doi.org/10.1016/j.jhazmat.2003.11.008

Fitzpatrick, F.A., Boufadel, M.C., Johnson, R., Lee, K.W., Graan, T.P., Bejarano, A.C., Zhu, Z., Waterman, D., Capone, D.M., Hayter, E., 2015. Oil-particle interactions and submergence from crude oil spills in marine and freshwater environments: Review of the science and future research needs (No. 2015–1076). US Geological Survey.

Gafonova, O.V., Yarranton, H.W., 2001. The stabilization of water-in-hydrocarbon emulsions by asphaltenes and resins. J. Colloid Interface Sci. 241, 469–478.
Garrett, R.M., Pickering, I.J., Haith, C.E., Prince, R.C., 1998. Photooxidation of crude oils. Environ. Sci. Technol. 32, 3719–3723.
Government of Canada, 2013. Properties, composition and marine spill behaviour, fate and transport of two diluted bitumen products from the Canadian oil sands (No. ISBN 987-1-100-23004-7), Federal Government Technical Report.
Gustitus, S.A., Clement, T.P., 2017. Formation, Fate, and Impacts of Microscopic and Macroscopic Oil-Sediment Residues in Nearshore Marine Environments: A Critical Review. Rev. Geophys. 55, 1130–1157. https://doi.org/10.1002/2017RG000572
Hollebone, B.P., Fieldhouse, B., Sergey, G., Lambert, P., Wang, Z., Yang, C., Landriault, M., 2011. The Behaviour of Heavy Oil in Fresh Water Lakes, in: Proceedings of the 34th Arctic and Marine Oilspill Program (AMOP) Technical Seminar on Environmental Contamination and Response. Environment Canada, Ottawa. pp. 668–789.
Hua, Y., Mirnaghi, F.S., Yang, Z., Hollebone, B.P., Brown, C.E., 2018. Effect of evaporative weathering and oil-sediment interactions on the fate and behavior of diluted bitumen in marine environments. Part 1. Spill-related properties, oil buoyancy, and oil-particulate aggregates characterization. Chemosphere 191, 1038–1047. https://doi.org/0.1016/j.chemosphere.2017.10.156
Incardona, J.P., Day, H.L., Collier, T.K., Scholz, N.L., 2006. Developmental toxicity of 4-ring polycyclic aromatic hydrocarbons in zebrafish is differentially dependent on AH receptor isoforms and hepatic cytochrome P4501A metabolism. Toxicol. Appl. Pharmacol. 217, 308–321.
King, T.L., Robinson, B., Boufadel, M., Lee, K., 2014. Flume tank studies to elucidate the fate and behavior of diluted bitumen spilled at sea. Mar. Pollut. Bull. 83, 32–37. https://doi.org/10.1016/j.marpolbul.2014.04.042
Lee, K. (chair), Boufadel, M., Chen, B., Foght, J., Hodson, P., Swanson, S., Venosa, A., 2015. Expert Panel Report on the Behaviour and Environmental Impacts of Crude Oil Released into Aqueous Environments (No. ISBN: 978-1-928140-02-3). Royal Society of Canada, Ottawa, ON, Canada.
Mackay, D., Matsugu, R.S., 1973. Evaporation rates of liquid hydrocarbon spills on land and water. Can. J. Chem. Eng. 51, 434–439.
Mackay, D., Shiu, W.-Y., Ma, K.-C., Lee, S.C., 2006. Handbook of Physical-Chemical Properties and Environmental Fate for Organic Chemicals; Volume 1-Introduction and Hydrocarbons.
Madison, B.N., Hodson, P.V., Langlois, V.S., 2017. Cold Lake Blend diluted bitumen toxicity to the early development of Japanese medaka. Environ. Pollut. 225, 579–586.
Marty, J., Potter, S., 2014. Risk Assessment for Marine Spills in Canadian Waters, Phase 1: Oil Spills South of the 60th Parallel. WSP Can.
McGenity, T.J., Folwell, B.D., McKew, B.A., Sanni, G.O., 2012. Marine crude-oil biodegradation: a central role for interspecies interactions. Aquat. Biosyst. 8, 10.

National Academies of Sciences, Medicine, 2016. Spills of Diluted Bitumen from Pipelines: A Comparative Study of Environmental Fate, Effects, and Response. National Academies Press.
Philibert, D.A., Philibert, C.P., Lewis, C., Tierney, K.B., 2016. Comparison of diluted bitumen (dilbit) and conventional crude oil toxicity to developing zebrafish. Environ. Sci. Technol. 50, 6091–6098.
Reed, M., Johansen, Ø., Brandvik, P.J., Daling, P., Lewis, A., Fiocco, R., Mackay, D., Prentki, R., 1999. Oil spill modeling towards the close of the 20th century: overview of the state of the art. Spill Sci. Technol. Bull. 5, 3–16.
Sebastiao, P., Soares, C.G., 1995. Modeling the fate of oil spills at sea. Spill Sci. Technol. Bull. 2, 121–131.
SL Ross, 2012. Meso-scale weathering of Cold Lake bitumen/condensate blend. SL Ross Environ. Res. Ltd 200–1140.
Speight, J.G., 2010. Handbook of industrial hydrocarbon processes. Gulf Professional Publishing.
Stogiannidis, E., Laane, R., 2015. Source characterization of polycyclic aromatic hydrocarbons by using their molecular indices: an overview of possibilities, in: Reviews of Environmental Contamination and Toxicology. Springer, pp. 49–133.
US EPA, 2013. Dredging Begins on Kalamazoo River, Enbridge Oil Spill, Marshall, Michigan. U.S. Environmental Protection Agency (US EPA).
Wadsworth, T., 1995. Containment & Recovery of Oil Spills at Sea: Methods and Limitations.
Winter, J., Haddad, R., 2014. Ecological impacts of dilbit spills: Considerations for natural resource damage assessment, in: 37th AMOP Technical Seminar on Environmental Contamination and Response, Alberta, Canada, June. pp. 3–5.
Yan, Z., Elliott, J.A., Masliyah, J.H., 1999. Roles of various bitumen components in the stability of water-in-diluted-bitumen emulsions. J. Colloid Interface Sci. 220, 329–337.
Yang, C., Hollebone, B.P., Brown, C.E., Yang, Z., Landriault, M., 2015. Chromatographic fingerprinting analysis of crude oils and petroleum products. Handb. Oil Spill Sci. Technol. 93–164. https://doi.org/10.1002/978111898992.ch5
Yang, C., Lambert, P., Zhang, G., Yang, Z., Landriault, M., Hollebone, B., Fieldhouse, B., Mirnaghi, F., Brown, C.E., 2017. Characterization of chemical fingerprints of unconventional Bakken crude oil. Environ. Pollut. 230, 609–620. https://doi.org/0.1016/j.envpol.2017.07.011
Yang, C., Wang, Z., Yang, Z., Hollebone, B., Brown, C.E., Landriault, M., Fieldhouse, B., 2011. Chemical fingerprints of Alberta oil sands and related petroleum products. Environ. Forensics 12, 173–188.
Yang, Z., Hua, Y., Mirnaghi, F., Hollebone, B.P., Jackman, P., Brown, C.E., Yang, C., Shah, K., Landriault, M., Chan, B., 2018. Effect of evaporative weathering and oil-sediment interaction on the fate and behavior of diluted bitumen in marine environments. Part 2. The water accommodated and particle-laden hydrocarbon species and toxicity of the aqueous phase. Chemosphere 191, 145–155. https://doi.org/10.1016/j.chemosphere.2017.10.033

Yarranton, H.W., Hussein, H., Masliyah, J.H., 2000. Water-in-hydrocarbon emulsions stabilized by asphaltenes at low concentrations. J. Colloid Interface Sci. 228, 52–63.

CHAPTER 3: SIMULATING DILUTED BITUMEN SPILLS IN BOREAL LAKE LIMNOCORRALS- PART 2: FACTORS AFFECTING THE PHYSICAL CHARACTERISTICS AND SUBMERGENCE OF DILUTED BITUMEN

Stoyanovich, S[a]., Rodríguez-Gil, JR[b]., Hanson, M[c]., Hollebone, B.P[d]., Orihel, D. M[e]., Palace, V[b]., Faragher, R[d]., Mirnaghi, F.S[d]., Shah, K[d]., Yang, Z[d]., Blais, J.M[a*]

[a] Department of Biology, University of Ottawa, Ottawa, Ontario, K1N 6N5, Canada

[b] International Institute for Sustainable Development - Experimental Lakes Area, 111 Lombard Avenue, Suite 325, Winnipeg, Manitoba R3N 0T4, Canada

[c] Department of Environment and Geography, University of Manitoba, Winnipeg, MB, R3T 2N2, Canada.

[d] Emergencies Science and Technology Section, Environment and Climate Change Canada, Ottawa, Ontario, Canada

[e] Department of Biology and School of Environmental Studies, Queen's University, Kingston, ON K7L 3N6

*Corresponding Author: Jules Blais (jules.blais@uottawa.ca)

STATEMENT OF CONTRIBUTIONS

Stoyanovich, S: conceptualization, writing, formal analysis, analytical, field work
Rodriguez-Gil, J: conceptualization, reviewing
Hanson, M: reviewing, funding acquisition
Hollebone, B: reviewing, funding acquisition, analytical
Orihel, D: reviewing, funding acquisition
Palace, V: reviewing, funding acquisition
Faragher, R: reviewing, field work, analytical
Mirnaghi, F: reviewing, analytical
Shah, K: field work, analytical
Yang, Z: analytical, reviewing
Blais, J: supervision, reviewing, funding acquisition, conceptualization, corresponding author

Science of the Total Environment published this chapter:

Stoyanovich, S., Rodríguez-Gil, J.R., Hanson, M., Hollebone, B.P., Orihel, D.M., Palace, V., Faragher, R., Mirnaghi, F.S., Shah, K., Yang, Z., 2021. Simulating diluted bitumen spills in boreal lake limnocorrals-Part 2: Factors affecting the physical characteristics and submergence of diluted bitumen. Sci. Total Environ. 148580.

ABSTRACT

The propensity for diluted bitumen (dilbit) to sink in freshwater remains uncertain. In the Part 1 companion to this paper, we described a series of experimental dilbit spills into freshwater limnocorrals (10 m diameter x 1.5 m depth) ranging in spill volume from 1.5 to 180 L (oil:water- 1:71 000 to 1:500 v/v). In Part 2, we further examine the fate and behaviour of dilbit as it weathered for 70 days under realistic environmental conditions. Volatile hydrocarbons in the dilbit slick decreased rapidly after the dilbit was spilled on the water's surface, and dilbit density and viscosity significantly increased (> 1 g mL^{-1} and > 5 000 000 mPa s, respectively). Dilbit sank to the bottom sediments in all treatments, and the time to sinking was positively correlated with spill volume. The lowest dilbit treatment began to sink on day 12, whereas the highest dilbit treatment sank on day 31. Dilbit submerged when its density surpassed the density of freshwater (> 0.999 g mL^{-1}), with wind, rain, and other factors contributing to dilbit sinking by promoting the break-up of the surface slick. This experiment improves our ability to predict dilbit's aquatic fate and behaviour, and its tendency to sink in a boreal lake. Our findings should be considered in future pipeline risk assessments to ensure the protection of these important aquatic systems.

1 INTRODUCTION

Landlocked deposits of bitumen are found in many places worldwide, including Venezuela, the United States, and Russia, but the largest deposits are found in Alberta. Following extraction, crude bitumen is too dense and viscous to flow and must be engineered to meet pipeline specifications. Diluents, consisting of light hydrocarbon condensates, are mixed with bitumen to reduce its density and viscosity to pipeline specifications (0.940 g mL^{-1} and 350 mPa·S, respectively), generating a blend of crude oil known as diluted bitumen, or dilbit (Fingas, 2015a). Pipelines, despite being one of the safest modes of transporting Canada's dilbit to market (Green and Jackson, 2015; Transport Canada, 2013), are still vulnerable to oil spills. From 2010 to 2018, a total 1 300 billion L of crude oil was transported out of Canada, by pipeline and railway combined (CER, 2019), of which an estimated 14 million L was spilled in Canada (Oliver Wyman, 2019). Such spills are likely to continue, in part because some estimates forecast a million barrels per day (b/d) increase in oil sands production in the next decade (CAPP, 2019; CER, 2016).

Several recent reports identified knowledge gaps in the fate and behaviour of spilled dilbit in freshwater (Lee et al., 2015; NASEM, 2016; 2014, 2013; Transportation Research Board and National Research Council, 2014). Following a spill to water, dilbit's physical and chemical characteristics change due to evaporation, emulsion, and other processes. Evaporation results in significant loss of oil mass as lighter hydrocarbons are lost to the atmosphere. Evaporation increases both the viscosity and density of the oil, and contributes to eventual oil submergence (Stoyanovich et al. 2019; King et al., 2017, 2014; Lee et al., 2015; NASEM, 2016). These weathering processes

affect oil spill remediation strategies that must consider the physical properties of the spilled oil. For example, *in-situ* burning can remove oil from the water surface but it is only efficient when the volatile components are still present and the slick is >2 mm thick (Fingas, 2015a). For any heavy oil, including dilbit, the window of opportunity to ignite the oil is within the first 1 to 2 hours of the spill (Federici and Mintz, 2014). Chemical dispersants can diffuse the oil into the water column (Canevari, 1978), but dispersants don't work when oil viscosity exceeds 10 000 mPa·s (Federici and Mintz, 2014; Nordvik, 1995; Zhao et al., 2014). Mechanical skimmers and booms are ineffective when oil viscosity is > 100 000 mPa·s (Federici and Mintz, 2014; ITOPF, 2012; Wadsworth, 1995).

Uncertainty remains about the environmental fate of dilbit, including its tendency to sink or float in freshwater (Lee et al., 2015). For example, studies documented dilbit submergence after a pipeline ruptured in Marshall, Michigan in 2010. The rupture released 3.2 million litres of dilbit into Talmadge Creek and eventually the Kalamazoo River, where 10-20% of the spilled oil sank upon entering the river (Fitzpatrick et al., 2015; Lee et al., 2015; US EPA, 2013). The spill occurred during high rainfall and flooding that increased the turbulence and suspended sediments in the river flows (Fitzpatrick et al., 2015). Interaction between suspended sediment and floating oil forms macroscopic sediment-oil aggregates (SOAs, > 1 mm) and microscopic oil-particulate aggregates (OPAs, < 1 mm) that may become dense enough to sink (Gustitus and Clement, 2017), which was likely the case in the Kalamazoo River spill (Fitzpatrick et al., 2015). Only 6 – 10 % of the submerged oil was recoverable by dredging three years

following the spill (US EPA, 2013), an estimated ~ 300 000 L of submerged dilbit remained at the bottom of the Kalamazoo River (NASEM, 2016).

Experimental studies under controlled environments have also documented dilbit weathering and sinking. Hua et al. (2018) mixed artificially weathered Cold Lake Blend (CLB) dilbit with saltwater containing 10 000 mg L^{-1} suspended sediments in test tubes and found that the resulting OPAs sank. Waterman and Garcia (2015) mixed artificially weathered dilbit with river sediments to form small oil droplets coated in sediments that experienced both neutral buoyancy and submergence in tap water. Laboratory studies, however, may not capture important environmental factors like solar radiation, microbial interactions, or diurnal and seasonal changes (Lee et al., 2015). Short (2013) noted that laboratory studies consider low wind speeds and high slick thicknesses that may be unrealistic of an actual spill scenario. Field experiments are therefore needed to assess dilbit weathering over longer timespans and under natural environmental conditions (Lee et al., 2015).

Several studies have investigated the fate of dilbit in outdoor field experiments to address some of the limitations of laboratory experiments. King et al. (2014) simulated dilbit spills in a flume tank containing filtered seawater and allowed the oil to weather for 13 days, noting increases in dilbit's density and the presence of small submerged oil droplets. Stoyanovich et al. (2019) added dilbit into outdoor tanks containing natural lake water and sediments. The researchers found that dilbit sank after 8 days when evaporation and emulsification caused dilbit density to surpass freshwater density. Despite these developments, questions remain about whether dilbit will float, disperse, or sink, especially in freshwater systems (Lee et al., 2015).

Here, we investigated the fate of dilbit in a large-scale spill experiment to assess dilbit's propensity to weather and submerge in a natural lake environment. This study was part of the BOREAL project (Boreal Lake Oil Release Experiments by Additions to Limnocorrals), a multi-phase program to examine the fate, behaviour, and impacts of dilbit spills in freshwater environments. This study expands on a pilot study involving dilbit additions into three outdoor 2-meter diameter tanks (Cederwall et al., 2020; Stoyanovich et al., 2019). We installed nine 10-m diameter limnocorrals in a boreal lake near Kenora, Ontario, Canada to simulate a pipeline spill to freshwater. To these limnocorrals we added dilbit in volumes ranging from 1.5 L to 180 L, employing a regression design to simulate dilbit spills ranging in actual oil:volume ratios between 1:71 000 and 1:500 (Rodriguez-Gil et al., 2021). This study reports the physical and chemical changes associated with dilbit spills exposed to natural biotic and abiotic environmental conditions typical of a boreal lake for 70 days. We examined each limnocorral treatment individually and utilized our regression design to determine how spill volume correlated to different outcomes, namely, sinking times and weathering rates. This study provides a novel approach to determine environmentally relevant timelines for major dilbit weathering processes in a natural freshwater system to inform risk assessors, spill responders, and regulators involved in oil spill countermeasures.

2 MATERIALS AND METHODS

2.1. Study Site

We performed this study in Lake 260 at the International Institute for Sustainable Development - Experimental Lakes Area (IISD-ELA) near Kenora, Ontario, Canada

during the summer of 2018. The IISD-ELA is a remote freshwater research site located on the Precambrian Shield of northwestern Ontario (49°40'N, 93°44'W). IISD-ELA consists of 58 boreal lakes of various dimensions. In 1968, the federal government of Canada and the province of Ontario designated this site for experimental freshwater studies (Johnson and Vallentyne, 1971). Lake 260 is a clear, oligotrophic lake 32.8 ha in area with a maximum depth of 15.7 m and an approximate water volume of 1 975 000 m^3.

2.2. Experimental Design

We installed nine limnocorrals in a ~ 2-m deep littoral zone on the northern shore of Lake 260 at the IISD-ELA. Rodríguez-Gil et al. (2021) provided details about the limnocorrals, their construction, and other elements of the larger study design. Briefly, we installed limnocorrals that consisted of a 10 m diameter floating ring to which we attached a high-density polyethylene (HDPE) cylindrical membrane extending down to the sediments. We used sandbags to seal the plastic membrane to the lake bottom (Figure 3.1A), a typical procedure in limnocorral studies (Baulch et al., 2003; Orihel et al., 2006). We accounted for potential water leakage throughout the experiment by tracking tritium (^3H) that we initially spiked to all limnocorrals.

We randomly assigned seven of the nine limnocorrals a nominal dilbit spill volume of either 1.5, 2.9, 5.5, 18, 42, 82, or 180 L in the form of a regression design. Our selected spill volumes were based on published onshore crude oil spill occurrences throughout North America between 2008 and 2017 obtained from the U.S Department of Transportation (USDOT, 2017) and the National Energy Board of Canada (NEB, 2017). We then predicted the resulting oil:water (%v/v) ratios that would be expected if

these spills were to occur in our study lake (Lake 260 ~ $2x10^6$ m^3). Our lowest treatment volume, 1.5 L (oil:water 1:66000 %v/v), results in an oil:water ratio within the same range as the most common spill volume in North America, and our highest treatment, 180 L (oil:water 1:590 %v/v) is similar to the largest on-shore spill to date, the 2010 Kalamazoo River Spill. With our lower and upper spill volume ranges set, we selected the remaining 5 volumes equidistant along a logarithmic scale between 1.5 and 180 L. The full rationale for spill volume selection is described in detail elsewhere (Rodriguez-Gil et al., 2021). The remaining two limnocorrals were controls; one located adjacent to dilbit treatments (near field) and one located roughly 100m from any dilbit treatments (far field) (Figure 3.1BC). We added Cold Lake Winter Blend (CLWB) dilbit to the water's surface of these limnocorrals on June 20th 2018, between 8:30am and 10:00am. We pumped CLWB from cans to the water surface using a Flojet diaphragm pump (FLOJET Corp, California) at a rate of approximately 7.5 L min^{-1} (Figure S3.1). We weighed all empty cans, hoses, and pumps before and after the dilbit additions to precisely determine the mass of dilbit added to each limnocorral. We then estimated spill volumes from the mass of CLWB added and its density measured at 15 ºC (0.9215 g mL^{-1}). Shah et al. (2019) provides additional details of the procedure for pumping dilbit to water. We monitored these limnocorrals for 70 days, tracking changes in dilbit properties until we decommissioned the experiment on September 8th, 2018, and remediated the site (Rodriguez-Gil et al., 2021).

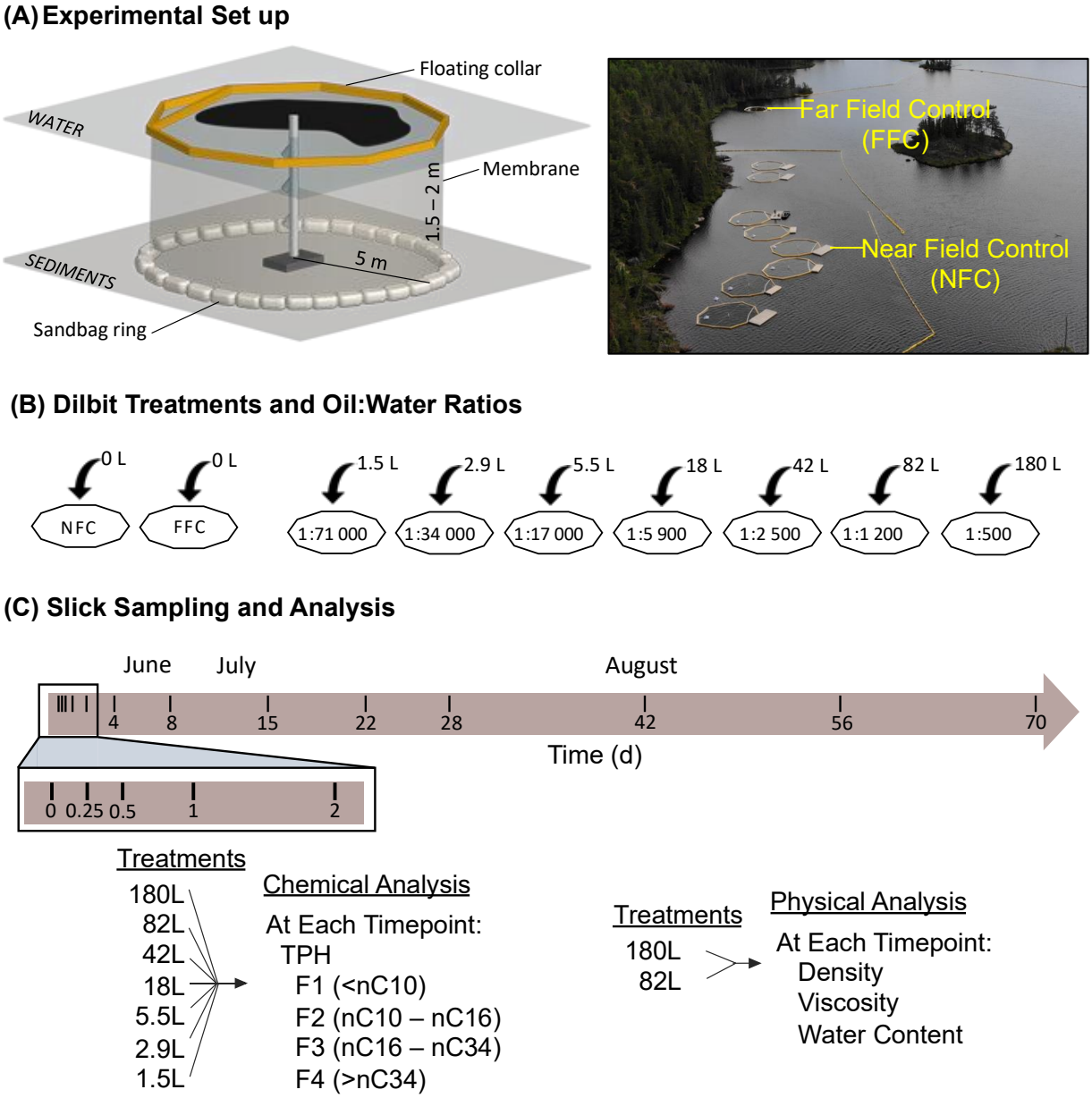

Figure 3. 1. Experimental design of limnocorrals and simulated CLWB dilbit spills. (A) Main aspects of limnocorral and distribution of limnocorrals throughout the NW littoral zone of L260 at the IISD-ELA. (B) The distribution dilbit treatments including two controls, one near field (NFC) and one far field (FFC). (C) Overview of dilbit slick sampling timepoints and associated analyses.

2.3. Environmental and Water Quality Monitoring

We installed a portable meteorological station on a small island adjacent to the study site at lake-level on June 15th 2019, 5 days before the dilbit addition. The meteorological station recorded wind speed and direction, precipitation, air temperature, humidity, and solar radiation every hour for the study's duration. We installed HOBO® data loggers at 0.5 m below water surface in each of the limnocorrals that recorded light intensity and water temperature every 4 minutes for the duration of the study. We sampled water for a full suite of water quality parameters (e.g. turbidity, ions, and nutrients) in each of the nine limnocorrals throughout the experiment. These details are in a companion paper (Rodriguez-Gil et al., 2021).

2.4. Dilbit Slick Behavioural Monitoring

We monitored the dilbit slicks daily, taking note of any changes in colour, thickness, surface area coverage, and sinking patterns. Underwater cameras (GoPro Hero 5 Session®) enabled the qualitative assessment of dilbit dispersal and presence on the sediment bottom. We recorded the surface behaviour of the low, medium, and high treatment (1.5, 18, and 180 L) from sunrise to sunset using time-lapse cameras (Brinno TLC200 Pro HDR®) mounted 3m above the limnocorrals. Additionally, we recorded aerial drone photos and videos regularly at a height of 10 m above the limnocorrals to further assess slick behaviour (DJI Mavic Air Quadcopter®). We processed aerial photos using ImageJ software version 1.50 to estimate temporal changes in the surface area coverage of the dilbit slicks and sheens at each time a photo was taken.

2.5. Dilbit Slick Samples

We collected two sets of dilbit surface slick samples from each of the limnocorral treatments, one for physical measurements and one for chemical analysis, after 0.25, 2, 4, 8, 15, 22, 28, 42, 56, and 70 d post-spill (Figure 3.1D). The dilbit slicks eventually submerged, which affected the dilbit sampling, and therefore the final slick sampling days ranged from 15 d to 70 d depending on when submergence in each treatment occurred (discussed in section 3.1).

We additionally collected higher volume dilbit samples (~50 mL) from the two highest dilbit treatments (82 and 180 L) for physical property analysis. An Anton Paar DMA 5000 and DMA 48 density meter enabled the measurement of oil density at 0, 15, and 30 °C following ASTM D5002 (ASTM D5002-19, 2019). We measured dynamic viscosity at three different temperatures (0, 15, and 30 °C) using Anton Parr Stabinger SVM 3000 Viscometer following standard D7042 (ASTM D7042-16, 2016) and a HAAK VTiQ Viscotester (Thermo Fischer Scientific). We evaluated the Newtonian and Non-Newtonian behaviour of the oil, and measured viscosity at different shear rates in any samples exhibiting non-Newtonian behaviour (i.e., viscosity dependent on shear rate). Karl Fischer titration with a Metrohm 901 automatic titrator following ASTM E203 (ASTM E203-16, 2016) enabled water content determinations of each dilbit sample. We ran all dilbit samples collected for physical properties in triplicate to assess analytical accuracy. We sampled the dilbit slick by passing a small piece of Teflon sheet along the dilbit slick until roughly 2 – 5 mL of dilbit had adhered to the material. An Agilent 7890A gas chromatograph equipped with a flame ionization detector (GC-FID) enabled analysis of total petroleum hydrocarbons, which we then grouped into four chemical fractions; F1 (<

nC_{10}), F2 (*n*C_{10} - *n*C_{16}), F3 (*n*C_{16} – *n*C_{34}), and F4 (> *n*C_{34}). We used an Agilent 7890A gas chromatograph equipped with an Agilent 5975C mass selective detector (GC-MSD) to analyze petroleum biomarker compounds including: terpanes, hopanes, and steranes following the procedure in Yang et al. (2017). See section 2.0 of supporting info for more information on analytical procedures.

2.6. Chemical Weathering

We normalized TPH concentrations to 17α(H) 21β(H) hopane (C_{30} hopane), a highly recalcitrant compound termed "biomarker" to act as a recalcitrant tracer to assess weathering (Prince et al., 1994; Stout and Wang, 2016; Venosa et al., 1997). The percentage of chemical remaining can be calculated by Eq. (1) adapted from Douglas et al. (1996) and Radović et al (2014):

$$\% \text{ analyte depleted} = [1 - (C_t/C_o)(H_o/H_t) \times 100] \quad (1)$$

where C_t and C_o are the concentrations of a compound in a weathered (*t)* and original (o) sample, respectively and H_t and H_o are the concentrations of C_{30} Hopane in those same samples.

2.7. Physical Property Models

We carried out a temporal analysis of physical properties (density and viscosity) on the two highest dilbit treatments (82 and 180 L) due to sample volume requirements. We fit the experimental data to a monod-type model adapted from King et al. (2019, 2017, 2014):

$$\rho = \rho_0 + (\rho_f - \rho_0)\left(\frac{t}{T+t}\right)^n \quad (2)$$

$$\nu = \nu_0 + (\nu_f - \nu_0)\left(\frac{t}{T+t}\right)^n \quad (3)$$

Equations 2 and 3 predict temporal changes in density (ρ) and viscosity (ν) from initial (ρ_0 and ν_0) to final (ρ_f and ν_f). Where "*t*" represents time (d), *"T"* is a time constant representing the time (d) it takes for the density and/or viscosity to increase half-way between initial and final values, and the power *"n"* controls the rate of increase.

3 RESULTS AND DISCUSSION

3.1. Physical Behaviour

The slicks began to spread across the surface area of the limnocorrals immediately following the addition. The average wind speed and air temperature was 1.4 m s^{-1} and 22.4 °C, respectively on the day of dilbit addition (Rodriguez-Gil et al., 2021). The experiment was in a sheltered boreal lake and therefore did not experience any breaking waves over the study duration. We noted that the distribution and thickness of the dilbit slicks were largely dependent on wind speed and direction throughout the experiment. Days of high wind forced the slicks to accumulate along the leeward side of the limnocorral walls, increasing slick thickness, and days of low wind allowed the slicks to spread, decreasing the thickness (Figure 3.2).

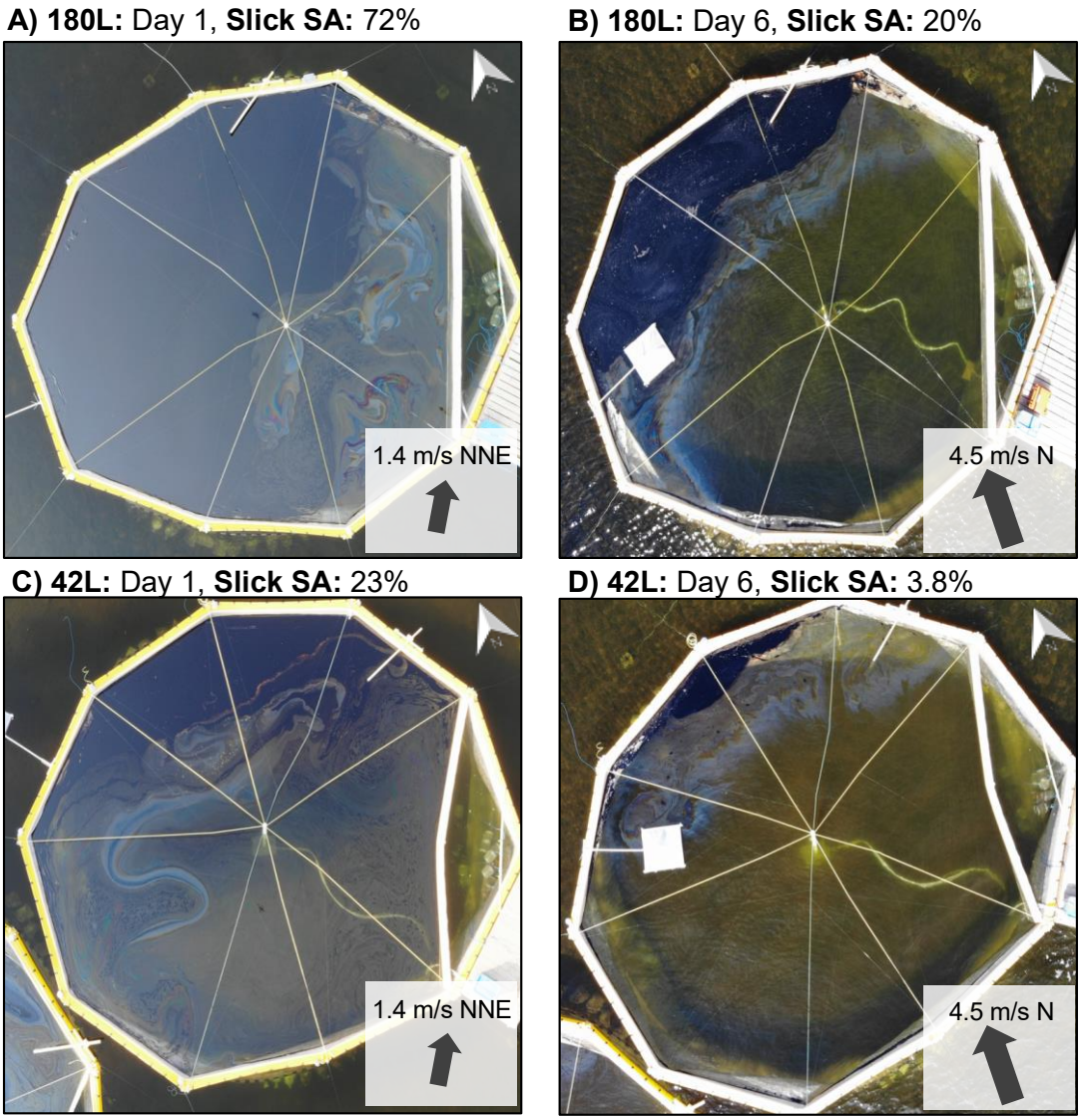

Figure 3. 2. Aerial photographs showing changes in percentage surface area (SA) coverage of the dilbit slick from day 1 to day 6 for the 180L (A,B) and 42L treatment (C,D). North Arrows and average wind speed/direction during the time of the photo are indicated.

The dilbit slicks changed considerably in overall appearance (i.e., colour, thickness, and surface skin) during the 70-d experiment (Figure S3.2, S3.3, S3.4, & S3.5). Colour changes from dark black to light brown began as early as day 6 (June 26) and were caused by the uptake of water droplets (Lee et al., 2015) and exposure to sunlight (Bobra and Tennyson, 1989). We also observed the formation of a skin on the

surface of the dilbit slicks, a similar finding to a previous study by Stoyanovich et al. (2019). Surface skins tend to persist in low energy systems that lack substantial turbulence or agitation energy, such as Lake 260. The skins are caused by the accumulation of polar compounds, including asphaltenes and resins, at the oil – water interface (Fingas, 2015a; Hollebone et al., 2011; Lee et al., 2015).

The slicks broke apart into discrete masses as weathering proceeded. We observed the presence of tar balls (<10 cm in diameter), tar patties (>10 cm in diameter), and tar mats (≥1 m) (Lee et al., 2015; Warnock et al., 2015) that encompass a highly weathered exterior crust and a less-weathered interior (Figure S3.3A). A precipitation event (14.3 mm in 3 h) and high winds (maximum of 6.6 m s^{-1}) on day 14 contributed to the break-up of the surface slicks. The tar balls remained intact for the remainder of the study, becoming neutrally buoyant in the water column, and eventually began to submerge to the bottom sediments (Figure S3.3).

Notably, the surface slicks in all seven treatments sank to the sediments during the study period as small discrete tar balls and patties (Figure S3.6 & S3.7) and in some cases large tar mats (Figure S3.8). The onset and completion of sinking differed among treatments. Sinking onset (i.e., time when dilbit was first observed on sediments) and completion (i.e., no remaining surface oil) proceeded in the following order for each treatment: Day 12 – 19 (1.5 L), 14 – 22 (2.9 L), 15 – 25 (5.5 L), 14 – 28 (18 L), 15 – 43 (42 L), 22 – 61 (82 L), and 31 – 77 d (180 L), respectively (Figure 3.3A, Figure S3.9). We found a significant positive correlation between the amount of dilbit added and the time to sinking onset (*slope*=0.10, R^2 = 0.92, *p*<0.0005, Figure 3.3B), and the time to complete submergence (*slope*=0.33, R^2 = 0.97, *p*<0.0005, Figure 3.3B). Note that

sinking times were based on the first visual appearance of dilbit on the sediment bottom, and do not consider dilbit droplets dispersed or neutrally buoyant in the water column. We performed visual underwater scans of the sediments every morning upon arrival at the site, so any observed submergence could have occurred the previous evening, night or early morning. Therefore, we may have slightly overestimated our sinking times by several hours.

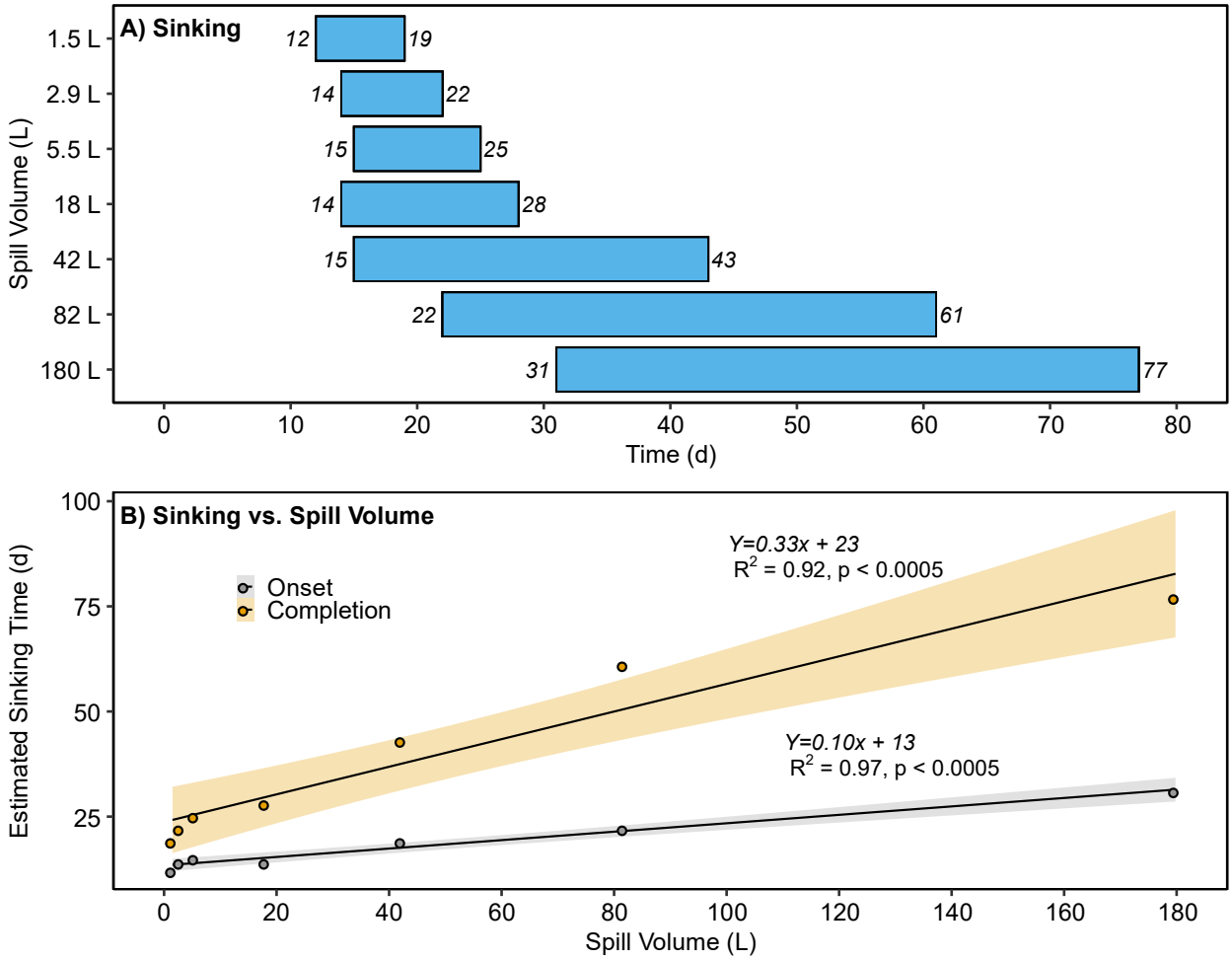

Figure 3. 3. Submergence patterns observed in the seven dilbit treatments throughout the experiment. The timespan between when dilbit was first noticed on the sediments and when no floating dilbit slick remained (A) and the linear relationship between spill volume and sinking times (B) are shown. Monitoring continued past the 70 day sampling timeline.

According to Hansen et al. (2015), the four major criteria that influence crude oil submergence are oil density, water turbidity, water salinity, and suspended sediment load. These researchers suggested dilbit submergence will most likely occur in shallow streams or rivers with high suspended sediment load. When oil mixes with sediments, the newly formed sediment-oil aggregates, SOAs (Gustitus and Clement, 2017), can become denser than the water and sink. This situation may be expected when oil strands on shore and mixes with sediments suspended by wave action (Michel et al., 2014). Johannessen et al. (2019) remarked that most lab studies demonstrated dilbit sinking when dilbit was mixed with suspended sediment concentrations ranging from 1000 to 10 000 mg L^{-1}, loadings similar to maximum concentrations found in coastal river outflows (Hua et al., 2018). These total suspended sediment (TSS) loads are three to four times greater than the greatest TSS value, 2.0 mg L^{-1}, observed in any of the limnocorrals throughout our study (Figure S3.10). Furthermore, turbulent mixing is required to promote the interaction of the oil with the sediments (Yang et al., 2018). The low TSS concentrations along with the low mixing energy of our limnocorral systems suggests that the formation of SOAs did not play a major role in the observed submergence patterns, similar to results found in previous tank-based studies by Stoyanovich et al. (2019) and King et al. (2014).

Precipitation may have also influenced dilbit sinking. We noted that slick weathering rates were not equal among treatments, as shown by their differences in colour and buoyancy. Furthermore, small sections of the bulk floating slicks would sink below the water level while remaining attached to the floating portion (Figure S3.11). A number of early precipitation events (25 mm on day 7 and 8mm on day 9) occurred prior

to any observed submergence (Figure S3.10). On days of heavy precipitation, rain was sufficient to break the slicks apart, thus separating the discrete floating and sinking sections, in a similar manner to a previous study (Stoyanovich et al., 2019).

3.2. Temporal Changes in Physical and Chemical Properties

3.2.1. Volatile Loss

The most volatile components of dilbit were the first to evaporate from the residual floating slicks (Figure 3.5A). We used the depletion of $\leq C_{16}$ hydrocarbons, obtained by summing concentrations of F1 and F2 fractions generated by GC-FID, to assess early evaporation of volatile components. For example, Gros et al. (2014) found that 50% of hydrocarbons $\leq C_{16}$ disappeared from oil sheens after 1 h of an experimental spill of Norwegian Grane crude oil in the open sea.

In all treatments, > 80% of the initial amount of $\leq C_{16}$ hydrocarbons was lost by the final sampling day (Figure 3.4A). The volatile hydrocarbon fraction nearly disappeared entirely from the slicks by the end of the study, consistent with the predictions of Gros et al. (2014)'s transport model. Conversely, the higher molecular weight F3 (C_{16} – C_{34}) and F4 (> C_{34}) fractions varied throughout the study (Figure S3.12) but never exceeded losses greater than 47 % across all treatments. These compounds would not likely evaporate and would be less susceptible to other forms of degradation, explaining their relative stability. Overall, the majority of volatile loss occurred within the first four days of the study, during which the average air temperature and wind speed was 21 ºC and 1.7 ms^{-1}, respectively. This rapid loss of volatile constituents is likely attributable to evaporation, an important weathering process that is responsible for early mass loss in oil residues (Gros et al., 2014; Harrison et al., 1975).

Evaporation affects all crude oil types differently and will depend on air temperature (Fingas, 2004), film thickness (Fingas, 2015b; Yarranton et al., 2015), and wind speed (Gros et al., 2014). Dilbit is unique because it is a heavy oil that still retains a high proportion of lower molecular weight compounds in its diluent, and thus it evaporates more than other conventional heavy oils (Government of Canada, 2014; Hansen et al., 2015). Yarranton et al. (2015) found that CLWB evaporation accelerated at higher temperature and lower film thickness, however unlike light crude oil, it was unaffected by wind speed. The researchers suggested that dilbit evaporation was limited by the mass transfer of volatiles in bitumen, which is limited by it's high viscosity.

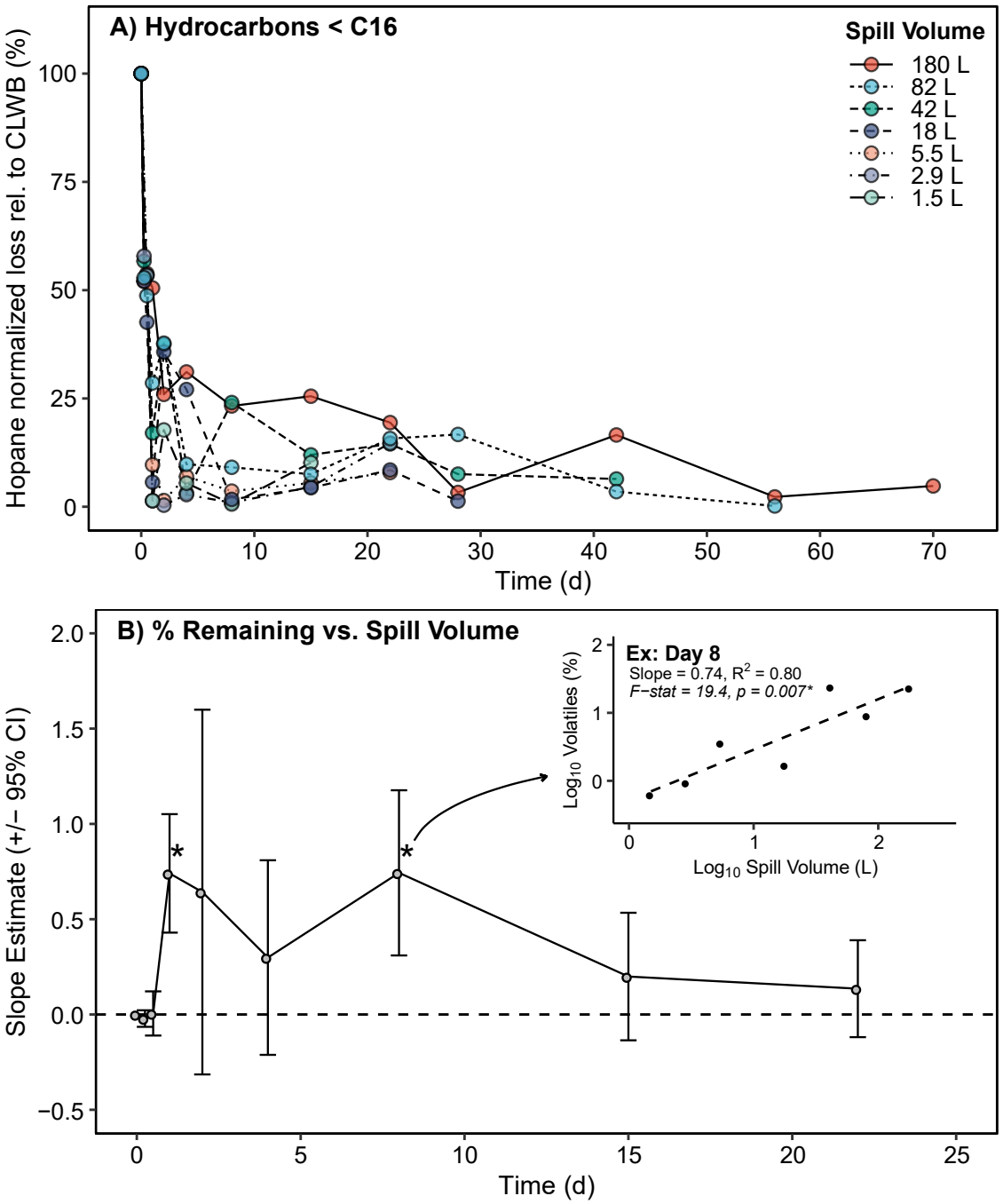

Figure 3. 4. The loss of volatile hydrocarbons from surface dilbit slicks. (A) Temporal changes of ≤ C_{16} hydrocarbons relative to the source dilbit in samples collected surface of dilbit slicks. (B) Regression coefficients obtained by regressing hopane normalized loss relative to CLWB against spill volume over time (example from day 8 shown in inset). Slope estimates and 95% CI's are from individual regressions, asterisks represent slopes that are significantly different from zero (i.e., $p < 0.05$). Regressions are only shown up to sampling day 22 (July 12, 2018) since the majority of slicks had submerged following this day yielding insufficient sample size to perform further regressions for subsequent sampling days.

The thickness of the dilbit layer can affect the diffusion of volatiles at the oil – air interface, resulting in less evaporation from thick slicks compared to thin sheens (Lee et al., 2015). For example, King et al (2017) found that increasing the thickness of dilbit slicks from 4 to 7 mm reduced the weathering of the oil in tank based studies. In our study, we were unable to track slick thickness, however we used spill volume as a proxy for slick thickness because the surface area of the limnocorrals was fixed. The regression design allowed us to analyze the relationship between volatile loss and dilbit-spill volume at each of the sampling timepoints using simple linear regressions (Figure 3.4B). A significant slope estimate (i.e., $p < 0.05$) indicates a relationship between the volatiles remaining in the dilbit slick and the amount of dilbit spilled. We observed significant positive slope estimates at only two time points (1 and 8 d) throughout the study, individual regressions can be found in Figure S3.13. In general, slopes were greater than 0 for the majority of sampling time points, indicating that the volatiles remained in the higher volume slicks for longer periods of time. The thin sheens found in lower dilbit treatments evaporated faster than the sheens from the thicker oil slicks in the higher treatments. These findings corroborated both laboratory and mesoscale field studies where mass transfer of volatile compounds through the dilbit film decreased with increasing film thickness (Brandvik and Faksness, 2009; Yarranton et al., 2015). Other factors affecting evaporation rates are climatic parameters including temperature and wind speed (Fingas 2004; Gros et al. 2014; King et al. 2019). We conducted our study during the warm summer months on a relatively small, sheltered lake (i.e., high air temperature and low wind speed), therefore we may have observed higher evaporation

rates in a large open area (i.e., higher wind speeds), and lower evaporation rates at lower temperatures.

The dilbit slicks remained heterogeneous throughout the entire study, therefore sample variability was high. The dilbit samples in the lowest volume treatments would consist of a sheen on low wind days (i.e., more spread out) and thick oil slick on high wind days (i.e., when dilbit accumulated at one side of the limnocorral), which may explain some of the variability in the results. Without controlling and differentiating between surface and bulk dilbit slick samples, processes such as photooxidation, which would be most prominent on the outermost film of the dilbit slick, are difficult to discern in this study. Biodegradation may have played a role in the removal of the lower molecular weight hydrocarbons because these simple compounds are most susceptible to microbial decomposition (Prince et al., 2003). For example, Schreiber et al. (2019) found that the microbial degradation of dilbit targets mainly the *n*-alkanes, with reductions of $\geq$ 84% over 28 days in microcosms spiked with a natural microbe consortia from the Douglas Channel, British Columbia, Canada. Microbes are unlikely to affect the rapid and early losses of low molecular weight hydrocarbons in this study. Biodegradation tends to occur over long timeframes (Lee et al., 2015) and in systems that are naturally exposed to petroleum hydrocarbons, such as natural oil seeps, which facilitate the proliferation of hydrocarbon degrading bacteria (Atlas and Hazen, 2011). Future work is thus planned to analyze compositional changes in the weathered dilbit samples in order to differentiate between other roles of degradation, including biodegradation and photooxidation.

3.2.2. Density and Viscosity

The rheological changes that occur to oil following a spill are important to consider as they can influence the spill response options that follow. We fit dilbit density data obtained from the surface slicks of our two highest treatments (180 and 82 L) to equation (2) and obtained the following:

180 L; $\rho = 0.9215 + (1.0024 - 0.9215)\left(\frac{t}{6.35+t}\right)^{0.148}$

82 L; $\rho = 0.9215 + (1.0112 - 0.9215)\left(\frac{t}{49.7+t}\right)^{0.128}$

Dilbit density (measured at 15 °C) increased rapidly within the first 8 days and then at a more gradual rate for the remainder of the study (Figure 3.5A). After just 24 hours of environmental exposure, density values in both the 82 and 180 L treatments were 0.9854 and 0.9785 g mL^{-1}, respectively. These reported 24 hour values were slightly greater than values reported from wave tank studies by King et al. (2014), where CLB reached a density of 0.96 g mL^{-1} after 24 h, and similar to our previous tank based study where the density of CLB reached 0.9883 g mL^{-1} after 24 h (Stoyanovich et al., 2019). Maximum densities occurred on day 28 in the 82 L treatment (1.0057 g mL^{-1}) and day 56 in the 180 L treatment (1.0072 g mL^{-1}) and were substantially higher than the density of the fresh dilbit (Table S3.1). Sunken tar balls collected from the sediment bottom of the 180, 82, 42, and 18 L treatments had densities of 0.9999, 1.0016, 1.0042, and 1.0094 g mL^{-1}, respectively. These values are equal to or higher than the density range of freshwater that would be expected throughout the experiment considering a maximum water density of 0.9999 g mL^{-1} is reached at 4 ºC (Weast et al., 1988). Dilbit density can increase from the loss of volatiles. We noted that the density of the weathered dilbit was linearly correlated with the amount of volatile hydrocarbon loss in

both 180 and 82 L treatments (Slope = 0.00071, R^2= 0.79, p <0.005, Figure S3.15A). Dilbit returns to a physical state similar to dense and viscous bitumen as the diluent evaporates away (Government of Canada, 2014; Yarranton et al., 2015). Water uptake through emulsification may have also affected the density increases, where water content increased to approximately 20% in the residual dilbit and then stabilized after 15 d, roughly the same time that density measurements stabilized (Figure 3.5A, Figure S3.15).

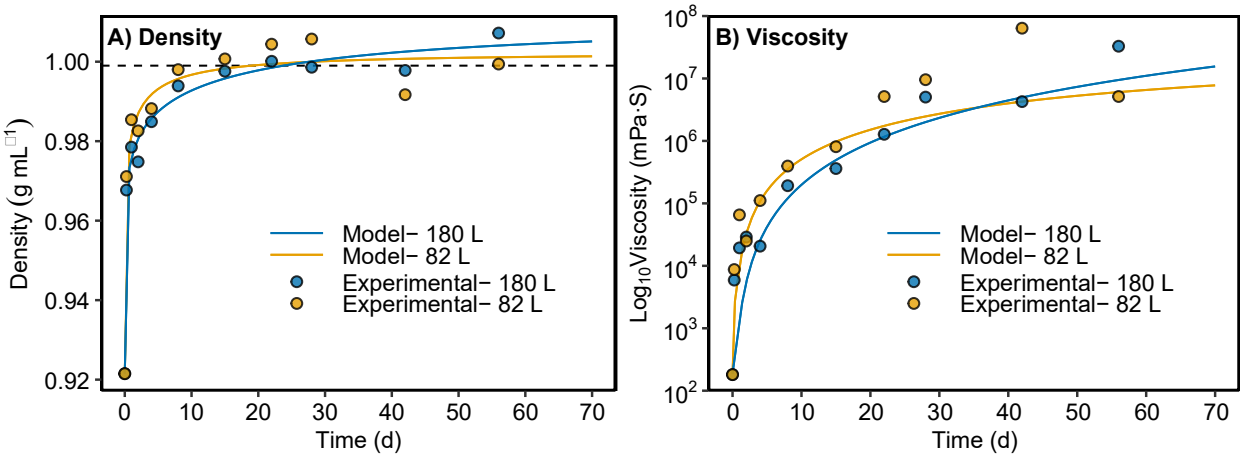

Figure 3. 5. Temporal changes in (A) density (g mL^{-1}; at 15 °C) and (B) viscosity (mPa·S at shear rate between 0.01 – 100 s^{-1}; at 15 °C) of samples collected from the two highest treatments (82 and 180 L) throughout the experimental spills. Monod-type models fitted to each data set are presented. The horizontal dashed line represents the density of freshwater at 15 °C.

We fit the log_{10} transformed viscosity data to equation (3) and yielded:

$$180\ \text{L},\ \upsilon = 188 + (1.0 \times 10^{12} - 188)\left(\frac{t}{9717+t}\right)^{2.25}$$

$$82\ \text{L},\quad \upsilon = 184 + (4.0 \times 10^{7} - 184)\left(\frac{t}{104+t}\right)^{1.79}$$

Viscosity (measured at 15 °C) increased rapidly after the onset of the spills, exceeding 100 000 mPa·s after just 4 and 8 d in the 82 and 180 L treatments, respectively,

resulting in a > 500-fold change from the initial viscosity (Figure 3.5B). Throughout the remainder of the study, viscosity measurements continued to increase, eventually reaching > 5 000 000 (27 000-fold change) and 30 000 000 mPa·s (170 000-fold change) in the 82 and 180 L treatments, respectively at the end of the study. The temporal change in viscosity was similar to density in that the 82 L treatment reached greater values early on, and then was surpassed by the 180 L treatment between day 42 and 56. These high viscosity values would limit the potential for dispersion into the water column in the form of small droplets, thus further reducing the potential to interact with suspended sediments.

Viscosity changes can be attributable to multiple processes. First, evaporation alone can return the viscosity to a value similar to crude bitumen (i.e., 100 000 – 450 000 mPa·S) (Fingas, 2015a), similarly to density, viscosity was linearly correlated with the amount of volatile hydrocarbon loss in both 180 and 82 L treatments (Slope = 0.047, R^2= 0.79, p <0.005, Figure S3.15B). Second, the dispersion of small water droplets into the dilbit slick can further increase viscosity due to internal friction between water droplets and the dilbit structure (Brandvik and Faksness, 2009; Fingas, 2015a; Fingas and Fieldhouse, 2004). The water content of collected dilbit samples increased early in the study and then plateaued at values between 18 – 25% after 8 d, remaining stable for the remainder of the study (Figure S3.14). The interaction of water droplets with dilbit under various environmental conditions can lead to the formation of water-in-oil emulsions of which there exists four main types; 1) stable, 2) meso-stable, 3) entrained, and 4) unstable. These are classified according to the visual appearance, water content, stability and rheological properties of the oil which are often dependent on the oil's

chemical composition and environmental factors such as temperature, mixing energy of the system (Fingas and Fieldhouse, 2014a), and salinity of water (Lee et al., 2015). Based on the properties of each emulsion outlined by Fingas and Fieldhouse (2014b), the slicks measured in this study fit into the entrained category. This classification is similar to our earlier pilot study, where the water content of dilbit samples remained <20%, becoming too dense and viscous for any additional water droplet penetration (Stoyanovich et al., 2019).

Wave energy can often facilitate the formation of emulsions by forcing small water droplets into the oil matrix, but if the oil is too viscous the droplets will not efficiently enter the oil slick (Fingas, 2015a). Rainfall could provide some turbulence to promote water uptake, however the first major rainfall event post-spill (25 mm) did not occur until day 7 (Figure S3.10). In our study, the dilbit viscosity exhibited greater than 5000-fold increase by day 8, the same time at which the water content stabilized, suggesting that the dilbit was too viscous to further incorporate any water droplets (Fingas, 2015a). Therefore, it is likely that the high viscosity of the dilbit paired with the relatively low energy of our study lake limited the formation of any stable form of emulsion, which would require water content to be between 70-80% (Fingas and Fieldhouse, 2014a).

The substantial increases in viscosity observed in this study could limit the feasibility of many response options following the spill. Viscosities exceeded the threshold for chemical dispersant use (i.e., 10 000 mPa·S) after just 6 h of environmental exposure (Federici and Mintz, 2014; Nordvik, 1995; Zhao et al., 2014). Viscosities surpassed the limit for efficient mechanical recovery techniques (i.e., 100

000 mPa·S), including booms and skimmers, after just 4 d (Federici and Mintz, 2014; ITOPF, 2012; Wadsworth, 1995). Our results suggest that following a summer dilbit spill in a boreal lake, spill responders would need to employ recovery techniques within the first 6 hours to 4 days of the spill in order to achieve efficient recovery. Response times are largely dependent on the remoteness of the spill site. The Canadian response organization standards require on-water recovery operations to be completed within 10 operational days after the recovery equipment is first deployed on site (Transport Canada, 1995). While deployment times for accessible coastal areas can range from 6 hours to 3 days (Transport Canada, 1995), the logistical challenges of a spill in a remote location could extend response timelines and result in a significant amount of dilbit that has sunken to the sediments.

4 CONCLUSION

Reports have suggested the potential for dilbit to sink in fresh and marine water under high energy conditions with high suspended sediment loads and after sufficient weathering (Fitzpatrick et al., 2015; Government of Canada, 2014; Hansen et al., 2015; Hua et al., 2018). Here we showed that dilbit is capable of sinking under natural conditions of an oligotrophic freshwater lake with very low suspended sediment loads and mixing energy, suggesting that dilbit will sink due to weathering alone and was not likely attributable to the interaction with suspended particles. The evaporative loss of volatiles coincided with increases in density and viscosity, returning dilbit to a condition similar to that of crude bitumen. Dilbit's viscosity quickly surpassed important threshold values for different spill response methods. Therefore, under these environmental

conditions, the use of traditional response techniques including *in-situ* burning, chemical dispersants, booms, and skimmers would become highly inefficient within the early days of the spill.

This study highlights the rapid physical and chemical changes that follow dilbit spills under realistic conditions typical of a boreal lake. The realistic nature of this work provides novel information on dilbit's fate in freshwater, building from laboratory and tank studies, and focusing on realistic conditions typical of a boreal lake. Simulating a wide variety of spill sizes over long periods of time (i.e., 70 days) has allowed us to determine for the first time the influence that spill volume can have on important physical processes including sinking. The outcome of this study will provide decision makers with critical new information to consider when planning dilbit transport in the future.

ACKNOWLEDGEMENTS

Funding for the present study was provided by a Natural Sciences and Engineering Research Council Strategic Partnership Grant (STPGP 493786-16 awarded to J.M. Blais, M. Hanson, and D.M. Orihel), a grant under the Oceans Protection Program, in-kind contributions from Environment and Climate Change Canada (ECCC), and in-kind support from the IISD-Experimental Lakes Area. A special thank you to J. Séguin, T. Black, J. Cederwall, L. Timlick, S. Patterson, J. Mason, D. Denton, H. Kosichek, K. Watson, and D. Dey for their contributions to the project.

SUPPORTING INFORMATION

Supporting Methods

1. Set Up and Sampling

See Shah et al., (2019) for an in-depth overview of the design and execution of the controlled dilbit spills. This study was carried out at the International Institute for Sustainable Development Experimental Lakes Area (IISD-ELA), a unique research station in northwestern Ontario, Canada, dedicated to holistic, interdisciplinary field research and ecosystem manipulation studies.

1.1 Dilbit Slick Sampling

Subsamples of oil for chemical analysis were collected from the surface slick in each limnocorral using Teflon strips following ASTM Methods D4489 and D3325 (2013; 2017). The Teflon strip was passed through the oil slick until a sample approximately 2 – 5 mL had adhered. Oil samples for physical property analysis were collected using a pre-cleaned stainless-steel spoon which was passed through the dilbit slick until approximately 50 mL of sample was collected. Both types of samples were then placed in a certified 125mL wide mouth amber glass jar with a lid lined with a TFE-fluorocarbon polymer film and sealed. In the case of the control limnocorrals, we simply passed the wipe through the water surface. We placed samples immediately in a cooler and stored them away from any potential light sources to prevent further photochemical reactions.

2. Analytical Methods

2.1 Sample Preparation

Prior to use, we rinsed all glassware with acetone, dichloromethane (DCM) and hexane. Teflon strips were ultrasonicated with DCM three times and dried at ambient temperature. The analysis of the concentrated solvent blank demonstrated the glassware and Teflon strips were clean and target-analyte free. To extract collected oil samples, Teflon strips spiked with appropriate surrogates (o-terphenyl, d_{50}-tetracosane, d_8-naphthalene, d_{10}-acenaphthene, d_{10}-phenanthrene, d_{12}-benz[a]anthracene, and d_{12}-perylene) were ultrasonicated with DCM for 10 minutes, then the extracts were passed through sodium sulfate to get rid of water residues. Teflon strips were further rinsed with DCM until they are color free. The final extracts were diluted to 10 mL with DCM. Total solvent extractable materials (TSEM) were measured by gravimetric method by drying one-mL of above extracts to estimate the appropriate amount of extracts used for column clean-up. Appropriate amount of DCM extracts were solvent exchanged to hexane, and then quantitatively transferred onto a chromatographic column packed with 3 g of silica gel, which was topped with about 1 cm of anhydrous granular sodium sulfate that had been pre-conditioned with 20 mL of hexane, for sample cleanup and fractionation. Hexane and a hexane-DCM mixture (1:1, v:v) were used to sequentially elute the saturated and aromatic compounds, respectively. These two fractions were concentrated under a gentle stream of nitrogen to appropriate volumes, spiked with internal standards (IS) (including 5-α-androstane for total (GC-detectable) petroleum hydrocarbons (TPHs) and alkanes, C_{30} 17β(H),21β(H)-hopane for petroleum biomarker compounds and d_{14}-terphenyl, for polycyclic aromatic compound (PACs) analysis,

respectively), and then adjusted to a volume of 1.0 mL for GC-MS and GC-FID analyses. The saturated fraction was used for analysis of aliphatics (total saturated hydrocarbons, TSHs), *n*-alkanes, and biomarker terpanes and steranes; the aromatic fraction was used for analysis of aromatic hydrocarbons (TAHs), alkylated homologous PACs and other unsubstituted PACs.

2.2 Instrument and Sample Analysis

We determined TPH concentration (largely *n*-C_9 through *n*-C_{40}) on an Agilent 7890A gas chromatograph equipped with a flame ionization detector (FID) using Agilent OpenLAB ChemStation for data collection. We performed chemical separation using a DB-5HT fused silica column (30 m × 0.25 mm i.d., 0.10 μm film thickness) and hydrogen (1.3 mL/min) as a carrier gas. The injector and detector temperatures were 290°C and 300°C, respectively. The temperature program used for TPH determination was: 40°C for 2 min, ramp at 20°C/min to 340°C, and held for 20 min.

We analyzed target petroleum biomarker compounds using an Agilent 7890A GC equipped with an Agilent 5975C mass selective detector (MSD). The GC separation employed a DB-5MS capillary column (30 m × 0.25 mm i.d. × 0.25 μm film thickness). Samples (1.0 μL) injected into the GC in splitless mode (injector temperature at 290°C) with 1.0 mL/min of helium as carrier gas. The MSD operated in select ion monitoring (SIM) mode. The column temperature was held at 60°C for 2.0 min, and then programmed 6°C/min to 300 °C and held for 20 min. Data was acquired and analyzed with Agilent Enhanced MSD ChemStation. Recoveries of *o*-terphenyl and d_{50}-

tetracosane, surrogates for GC-FID analysis of TPH, were determined to be 90 ± 9% and 94 ± 9% for all the oil samples.

3. Monod-type density and viscosity modelling

The following model has been previously described by King et al., (2014; 2017) to describe changes in density and viscosity of surface oil samples (note density- ρ can be interchanged with viscosity- ν):

$$\rho = \rho_0 + (\rho_f - \rho_0)\left(\frac{t}{T+t}\right)^n \qquad (2)$$

Using density as an example, ρ_0 and ρ_f are the initial and final densities, T is a time constant representing the time to reach the plateau, and *n* is the rate at which ρ_0 approaches ρ_f, and t is time. The same approach can be used for viscosity measurements.

Supporting Tables and Figures

Table S3. 1. Physical Properties of fresh, unweathered CLWB

Measurement	Mean ± SD (n =3)
Density at 15°C (g mL^{-1})	0.9215 ± 0.0003
Density at 0 °C (g mL^{-1})	0.932 ± 0
API Gravity	21.5
Viscosity at 15 °C (mPa·S)	181 ± 0.2
Viscosity at 0 °C (mPa·S)	547 ± 0.5
Flash Point (°C)	-6 ± 0
Pour Point (°C)	-43 ± 3
Sulfur Content (%)	3.3 ± 0.01

Table S3. 2. Identified targets and abbreviations

n-Alkanes	Biomarker compounds		Alkylated PAHs	
n-C_9	C21 tricyclic terpane	C_{21}terpane	C_0-Naphthalene	C_0-N
n-C_{10}	C22 tricyclic terpane	C_{22}terpane	C_1-Naphthalenes	C_1-N
n-C_{11}	C23 tricyclic terpane	C_{23}terpane	C_2-Naphthalenes	C_2-N
n-C_{12}	C24 tricyclic terpane	C_{24}terpane	C_3-Naphthalenes	C_3-N
n-C_{13}	18α(H),21β(H)-22,29,30-trinorhopane	C_{27}Ts	C_4-Naphthalenes	C_4-N
2,6,10-trimethyldodecane		C_{27}Tm		
(TMD)	17α(H),21β(H)-22,29,30-trinorhopane		C_0-Phenanthrene/anthracene	C_0-P
n-C_{14}	17α(H),21β(H)-30-norhopane	C_{29}αβ hopane	C_1-Phenanthrenes/anthracenes	C_1-P
n-C_{15}	17α(H),21β(H)-hopane	C_{30}αβ hopane	C_2-Phenanthrenes/anthracenes	C_2-P
n-C_{16}	22*S*-17α(H),21β(H)-30-homohopane	C_{31}(S) hopane	C_3-Phenanthrenes/anthracenes	C_3-P
2,6,10-trimethylpentadecane		C_{31}(R) hopane	C_4-Phenanthrenes/anthracenes	
(TMP)	22*R*-17α(H),21β(H)-30-homohopane			C_4-P
n-C_{17}	22*S*-17α(H),21β(H)-30,31-bishomohopane	C_{32}(S) hopane	C_0-Dibenzothiophene	C_0-D
Pristane	22*R*-17α(H),21β(H)-30,31-bishomohopane	C_{32}(R) hopane	C_1-Dibenzothiophenes	C_1-D
n-C_{18}	22*S*-17α(H),21β(H)-30,31,32-trishomohopane	C_{33}(S) hopane	C_2-Dibenzothiophenes	C_2-D
Phytane	22*R*-17α(H),21β(H)-30,31,32-trishomohopane	C_{33}(R) hopane	C_3-Dibenzothiophenes	C_3-D
n-C_{19}	22*S*-17α(H),21β(H)-30,31,32,33-tetrakishomohopane	C_{34}(S) hopane	C_0-Fluorene	C_0-F
n-C_{20}	22*R*-17α(H),21β(H)-30,31,32,33-tetrakishomohopane	C_{34}(R) hopane	C_1-Fluorenes	C_1-F
n-C21	22S-17α(H),21β(H)-30,31,32,33,34-pentakishomohopane	C_{35}(S) hopane	C_2-Fluorenes	C_2-F
n-C_{22}	22*R*-17α(H),21β(H)-30,31,32,33,34-pentakishomohopane	C_{35}(R) hopane	C_3-Fluorenes	C_3-F
n-C_{23}	C_{27} 20-5α(H),14β(H),17β(H)-cholestane	C_{27}αββ sterane	C_0-Fluroanthene/pyrene	C_0-Fl
n-C_{24}	C_{28} 20-5α(H),14β(H),17β(H)-ergostane	C_{28}αββ sterane	C_1-Fluroanthenes/pyrenes	C_1-Fl
n-C_{25}	C_{29} 20-5α(H),14β(H),17β(H)-stigmastane	C_{29}αββ sterane	C_2-Fluroanthenes/pyrenes	C_2-Fl
n-C_{26}	C21 tricyclic terpane	C_{21}terpane	C_3-Fluroanthenes/pyrenes	C_3-Fl
n-C_{27}			C_4-Fluroanthenes/pyrenes	C_4-Fl
n-C_{28}			C_0-Benzonaphthothiophenes	C_0-B
n-C_{29}			C_1-Benzonaphthothiophenes	C_1-B
n-C_{30}			C_2-Benzonaphthothiophenes	C_2-B
n-C_{31}			C_3-Benzonaphthothiophenes	C_3-B
n-C_{32}			C_4-Benzonaphthothiophenes	C_4-B
n-C_{33}			C_0-Chrysene	C_0-C
n-C_{34}			C_1-Chrysenes	C_1-C
n-C_{35}			C_2-Chrysenes	C_2-C
n-C_{36}			C_3-Chrysenes	C_3-C
n-C_{37}			Biphenyl	Bph
n-C_{38}			Acenaphthylene	Acl
n-C_{39}			Acenaphthene	Ace
n-C_{40}			Anthracene	An
			Pyrene	Py
			Benz(a)anthracene	BaA
			Benzo(b)fluoranthene	BbF
			Benzo(k)fluoranthene	BkF
			Benzo(e)pyrene	BeP
			Benzo(a)pyrene	BaP
			Perylene	Pe
			Indeno(1,2,3-cd)pyrene	IP
			Dibenzo(a,h)anthracene	DA
			Benzo(g,h,i)perylene	BgP

Table S3. 3. Chemical composition of fresh, unweathered 2018 CLWB. Full chemical names provided in Table S3.2.

Aromatics	Conc. (µg/g)	*n*-Alkanes	Conc. (µg/g)	Biomarkers	Conc. (µg/g)	Metals[4]	Conc. (µg/g)
ΣAromatics	**7298**	**Σ*n*-alkanes**	**19260**	**ΣBiomarkers**	**1201**	Barium	0.00
ΣParent & Alkyl PAHs	**7220**	n-C9	2469	C23 Terpane	70.4	Cadmium	0.00
ΣNAP C0 - C4	2154	n-C10	2135	C24 Terpane	35.6	Chromium	0.00
ΣPHE C0 - C4	1392	n-C11	1585	C27 Ts[3]	17.6	Iron	3.66
ΣDBT C0 - C3	1353	n-C12	1525	C27 Tm[4]	61.6	Molybdenum	6.41
ΣFLU C0 - C3	769	n-C13	505	C29αß Hopane	146	Nickel	60.51
ΣFLA C0 - C4	318	TMD[1]	1313	C30αß Hopane	178	Titanium	1.29
ΣBNT C0 - C4	992	n-C14	1258	C31(S) Hopane	32.1	Vanadium	137.2
ΣCHR C0 - C3	241	n-C15	978	C31(R) Hopane	80.0	Zinc	0.00
ΣEPA PAHs	**77.8**	n-C16	781	C32(S) Hopane	54.8		
Biphenyl	13.36	TMP[2]	485	C32(R) Hopane	50.4		
Acenaphthylene	0.26	n-C17	730	C33(S) Hopane	36.9		
Acenaphthene	10.99	Pristane	377	C33(R) Hopane	38.3		
Anthracene	3.59	n-C18	608	C34(S) Hopane	25.4		
Fluoranthene	4.94	Phytane	432	C34(R) Hopane	40.0		
Pyrene	7.40	n-C19	562	C35(S) Hopane	16.2		
Benz(a)anthracene	5.58	n-C20	490	C35(R) Hopane	34.4		
Benzo(b)fluoranthene	5.42	n-C21	453	C27αßß Sterane	30		
Benzo(k)fluoranthene	1.45	n-C22	400	C28αßß Sterane	122		
Benzo(e)pyrene	5.83	n-C23	356	C29αßß Sterane	104		
Benzo(a)pyrene	3.57	n-C24	313				
Perylene	9.28	n-C25	281				
Indeno(1,2,3-cd)pyrene	2.14	n-C26	257				
Dibenzo(ah)anthracene	0.84	n-C27	206				
Benzo(ghi)perylene	3.11	n-C28	156				
ΣBTEX	**10948**	n-C29	133				
Benzene	1469	n-C30	128				
Toluene	4146	n-C31	99.0				
Ethylbenzene	410	n-C32	66.0				
o,m,p-Xylenes	4924	n-C33	47.8				
		n-C34	34.4				
		n-C35	28.3				
		n-C36	21.4				
		n-C37	14.1				
		n-C38	13.2				
		n-C39	12.3				
		n-C40	7.54				

C0 are parent unsubstituted PAHs and C1 – C4 are alkylated PAHs.[1]TMD represents 2,6,10-trimethyldodecane and [2]TMP represents 2,6,10-trimethylpentadecane. [3]*Ts* represents 18α(H) 22,29,30 trisnorphopane and [4]*Tm* represents 17α(H) 22,29,30 trisnorhopane. [4]Metal analysis on the source oil was performed via ASTM method D7111 with a detection limit of 0.1 µg/g

Figure S3. 1. The addition of 180 L of CLWB (1:590 oil:water, v/v) onto the water surface of the limnocorral. (A) Overview of addition method, (B) View of telescopic arm and pumping system being held at approximately 5 – 10 cm from the water's surface. The oil exited the hose parallel to the waters surface to avoid forcing oil below the water surface and allowing it to spread out during the addition.

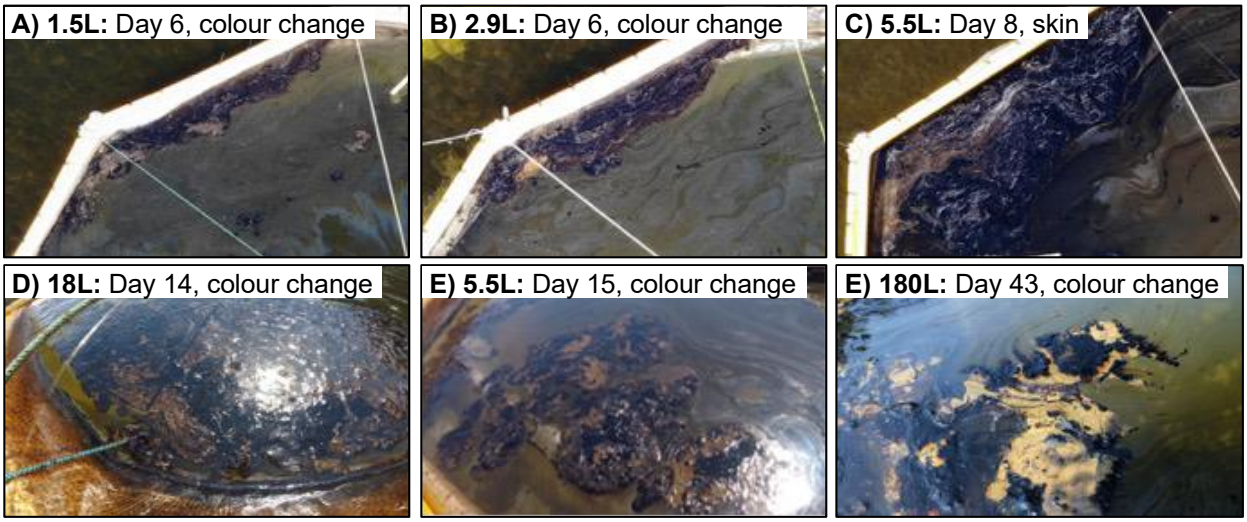

Figure S3. 2. Examples of colour change and skin formation observed throughout the experiment.

Figure S3. 3. Examples of tar balls observed floating on the water surface (A), neutrally buoyant in the water column (B), and submerged on the sediments (C).

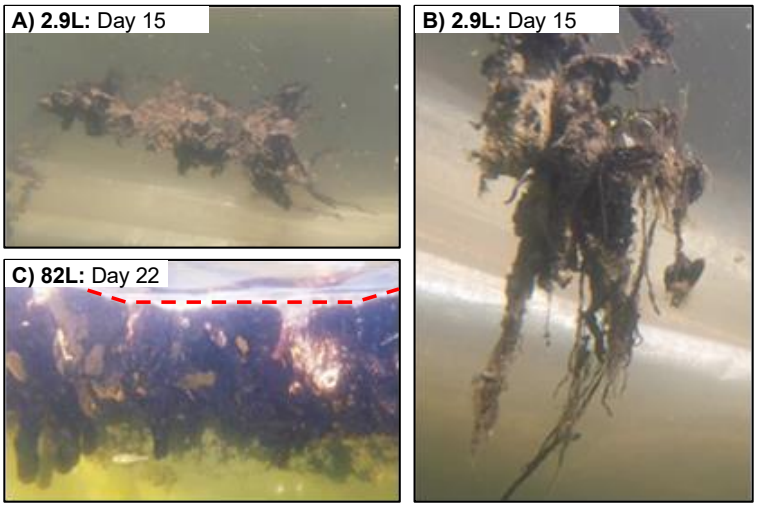

Figure S3. 4. Changes in thickness of slick and formation of strings, water level represented by red dashed line in (C).

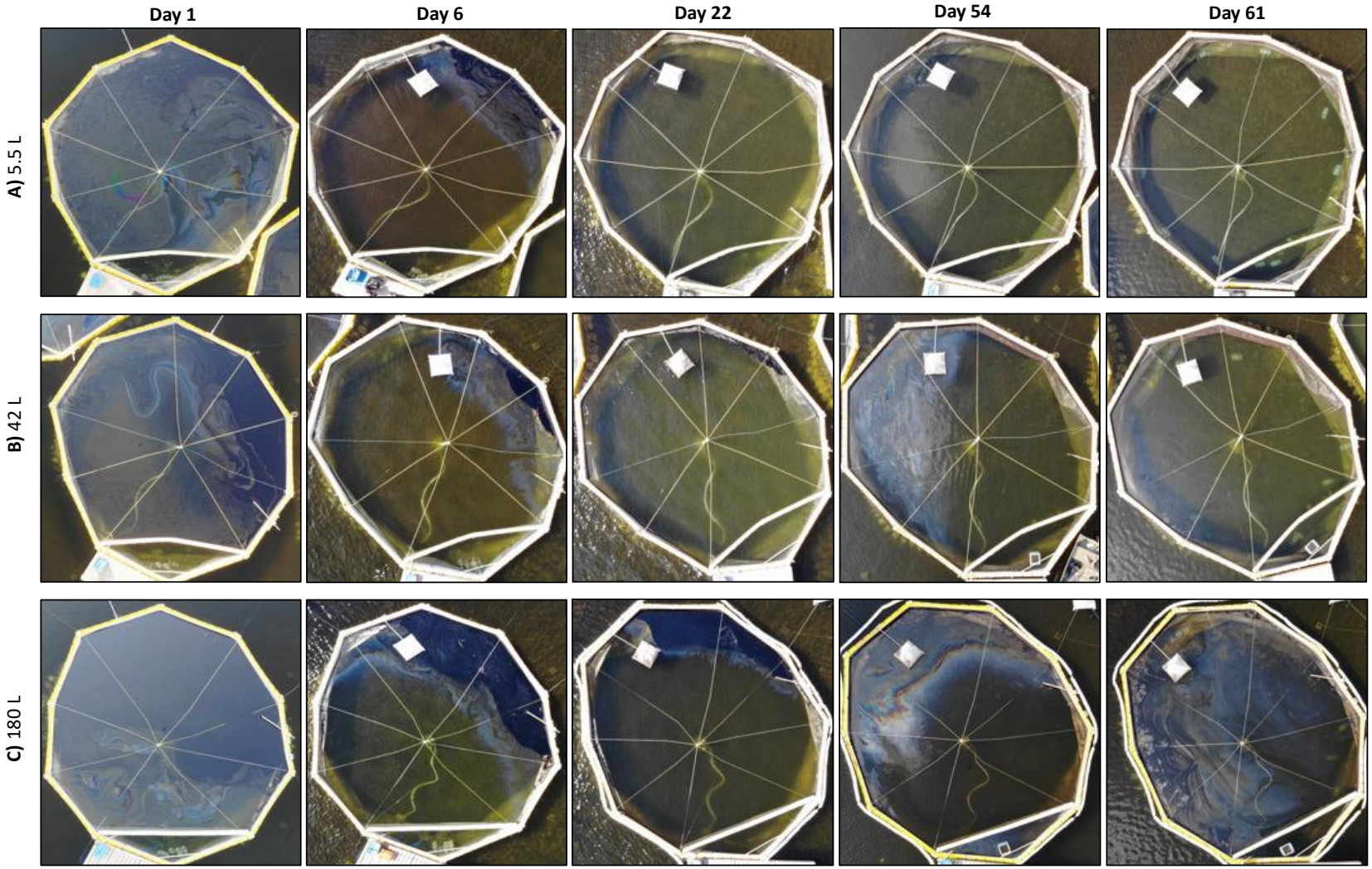

Figure S3. 5. Aerial photograph timelines for a low (A), medium (B), and high (C) treatment showing changes in slick coverage and eventual disappearance.

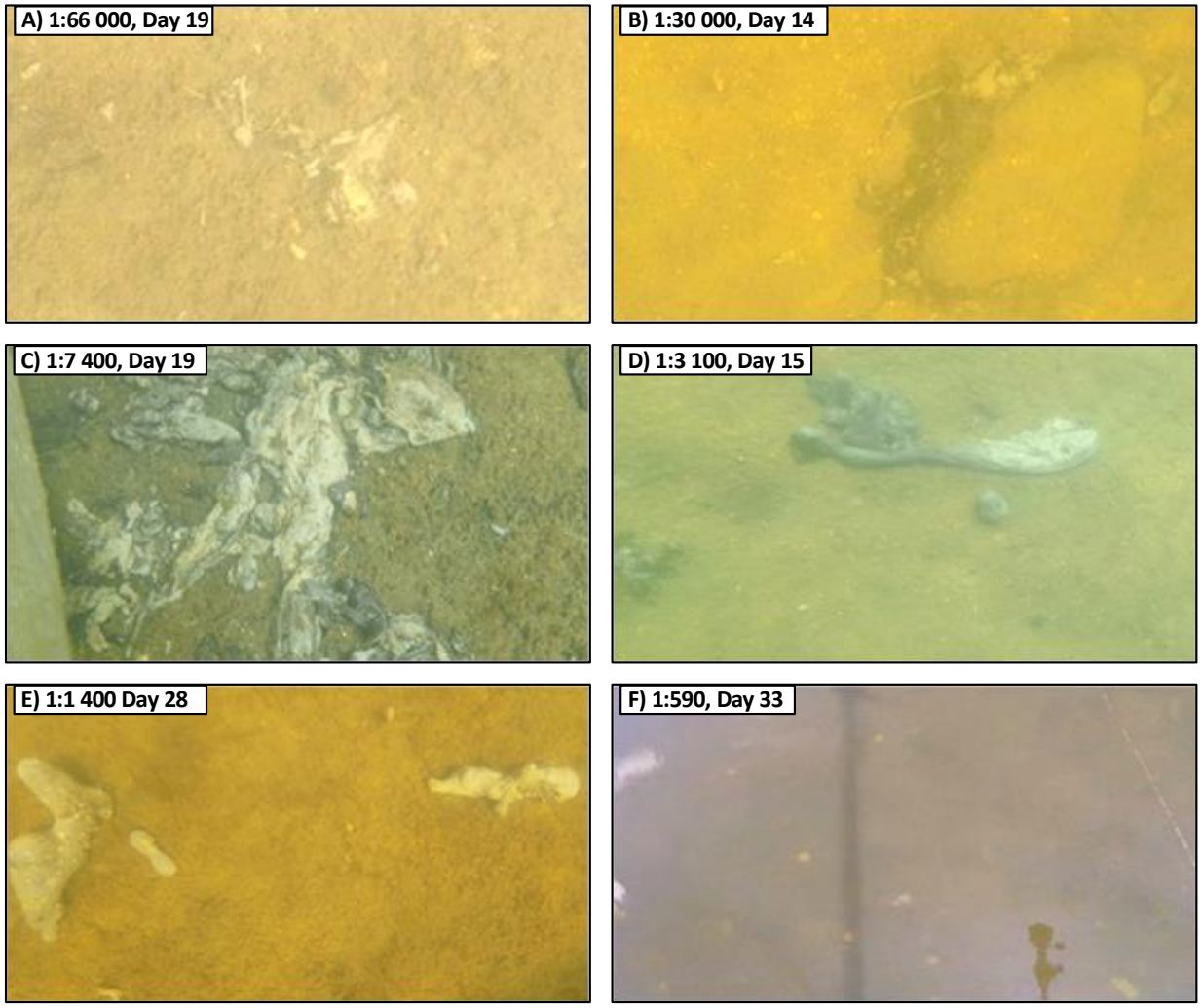

Figure S3. 6. Examples of dilbit submergence in selected treatments early on in the experiment. All photographs were taken underwater directly above the sediment layer except for panel (F) which was taken above the water surface, the small white globules are dilbit lying on the sediments. While tarballs appear white in colour, this is an effect of the water column on the lighting, the tarballs appeared light to dark brown when removed from the water.

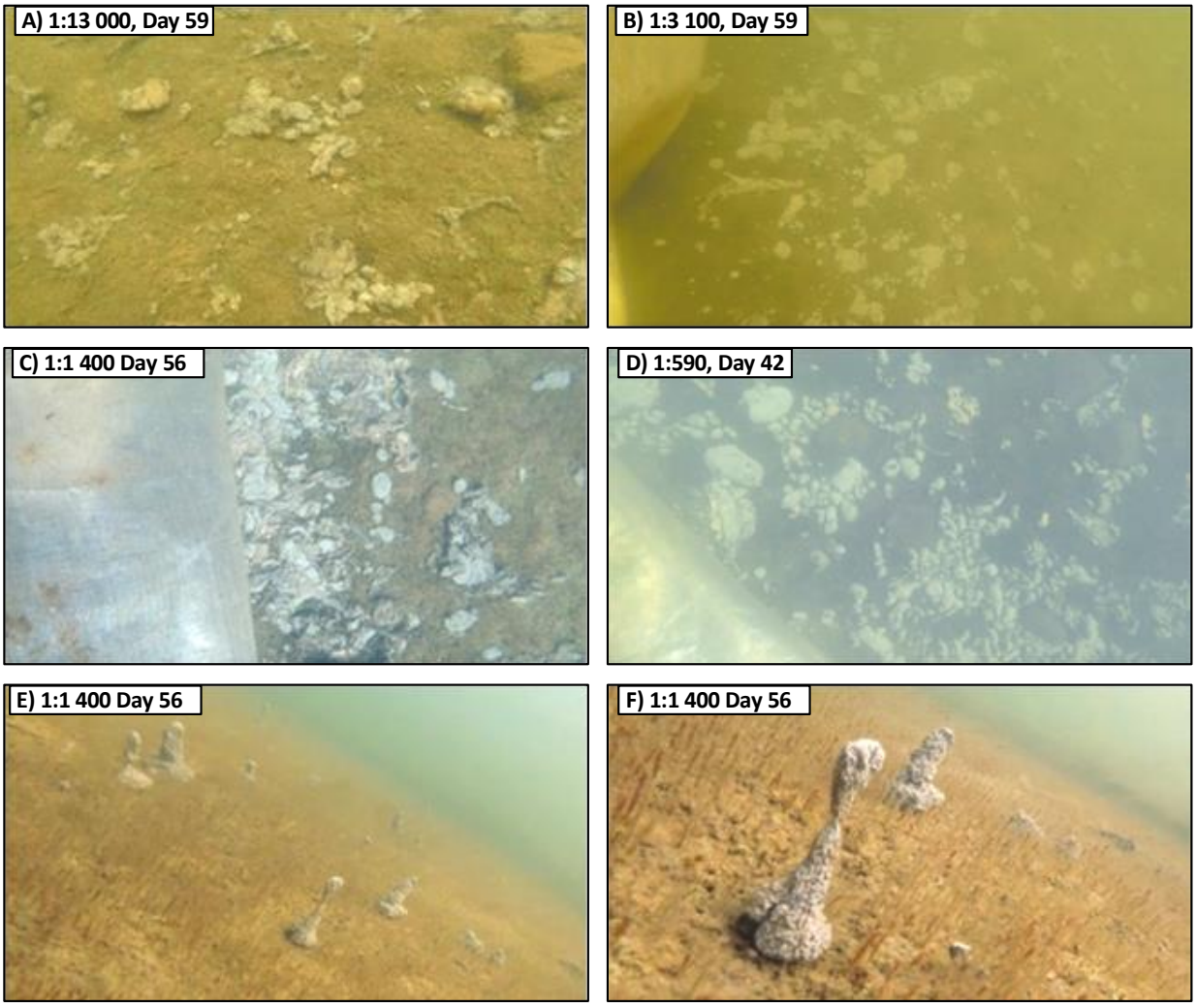

Figure S3. 7. Examples of dilbit submergence in selected treatments later on in the experiment. All photographs were taken underwater directly above the sediment layer. Panels E) and F) depict the unique behaviour of tarballs that was observed only in the two highest treatments. Sections of the tarballs appear to be extending upward while being held down by the bulk oil suggesting that there may be density differences across the tarballs. While tarballs appear white in colour, this is an effect of the water column on the lighting, the tarballs appeared light to dark brown when removed from the water.

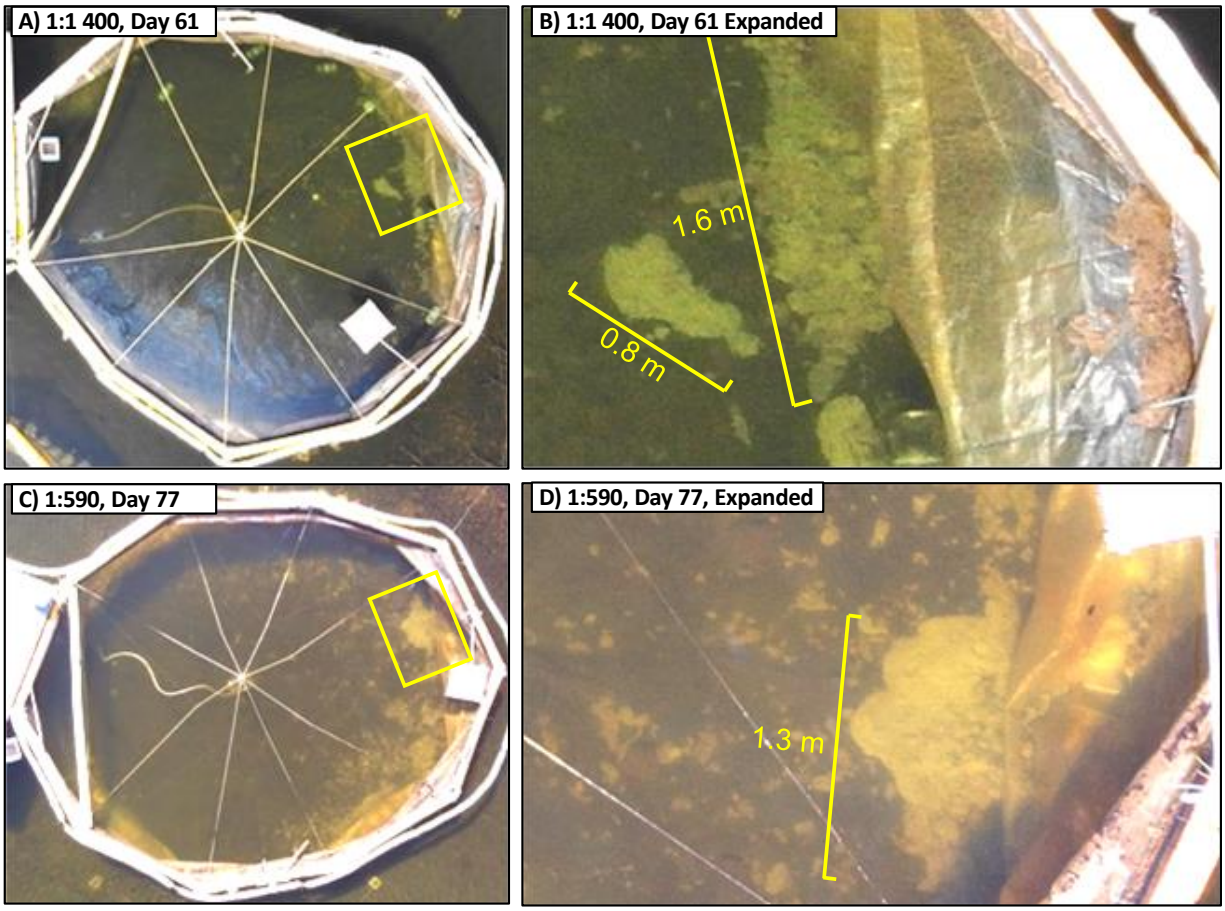

Figure S3. 8. Examples of tar mats on the sediment bottom of the two highest treatments towards the end of the experiments. Panels B and C are zoomed in versions of the aerial photographs A and C. Tar mat measurements were made using ImageJ software version 1.50.

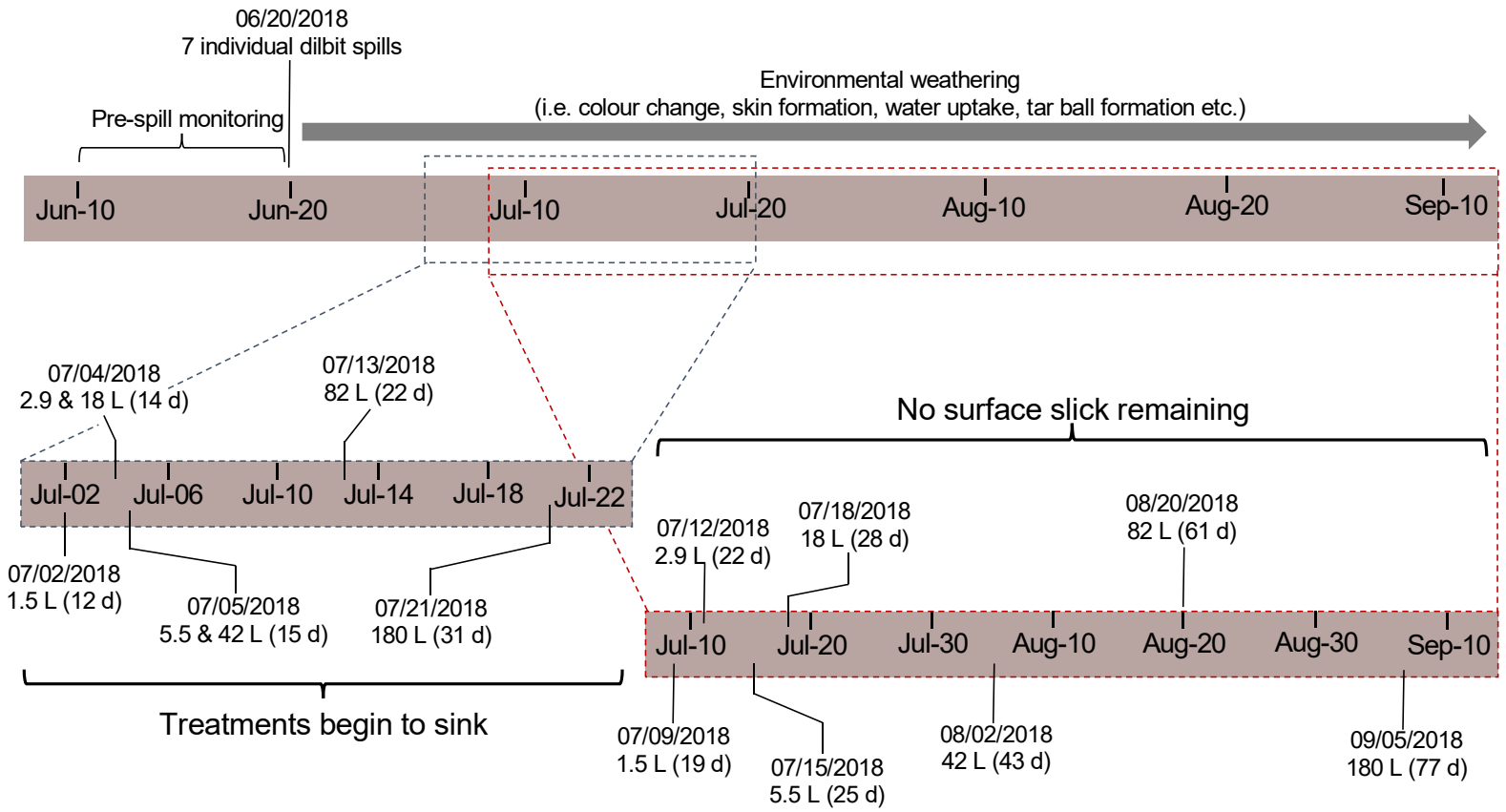

Figure S3. 9. Detailed submergence timelines for each of the seven dilbit amended treatments during the summer of 2018.

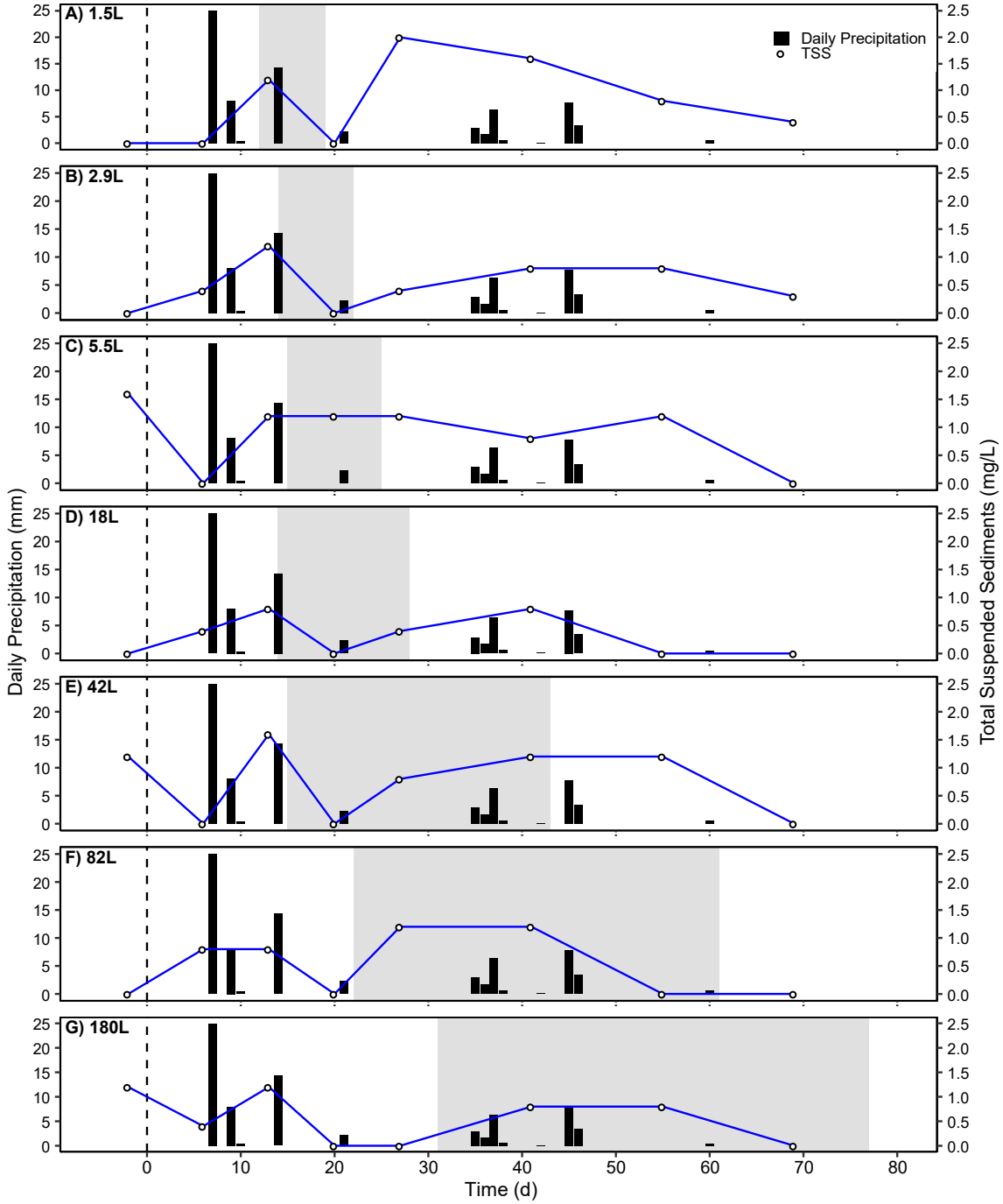

Figure S3. 10. Monitoring of daily precipitation (black bars) and total suspended solids (open circles) over time in each of the dilbit treatments. Gray rectangles mark the onset and completion of submergence.

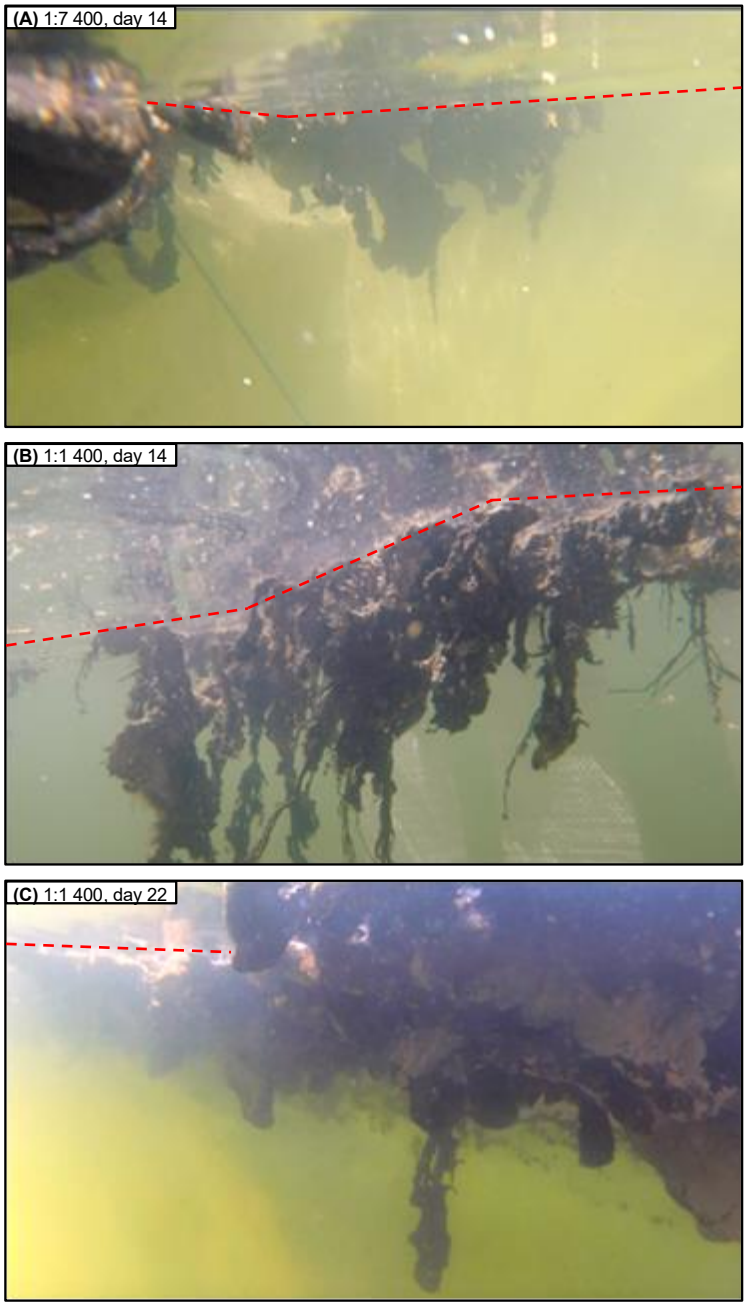

Figure S3. 11. Photographs of floating slicks showing examples of sections of slick that are extending down into the water column while still remaining attached to the bulk surface slick. The red dashed lines represent the location of the water's surface for reference. With sufficient precipitation energy, it is possible that these slicks would break up, thus allowing the sinking sections to fully submerge to the sediments.

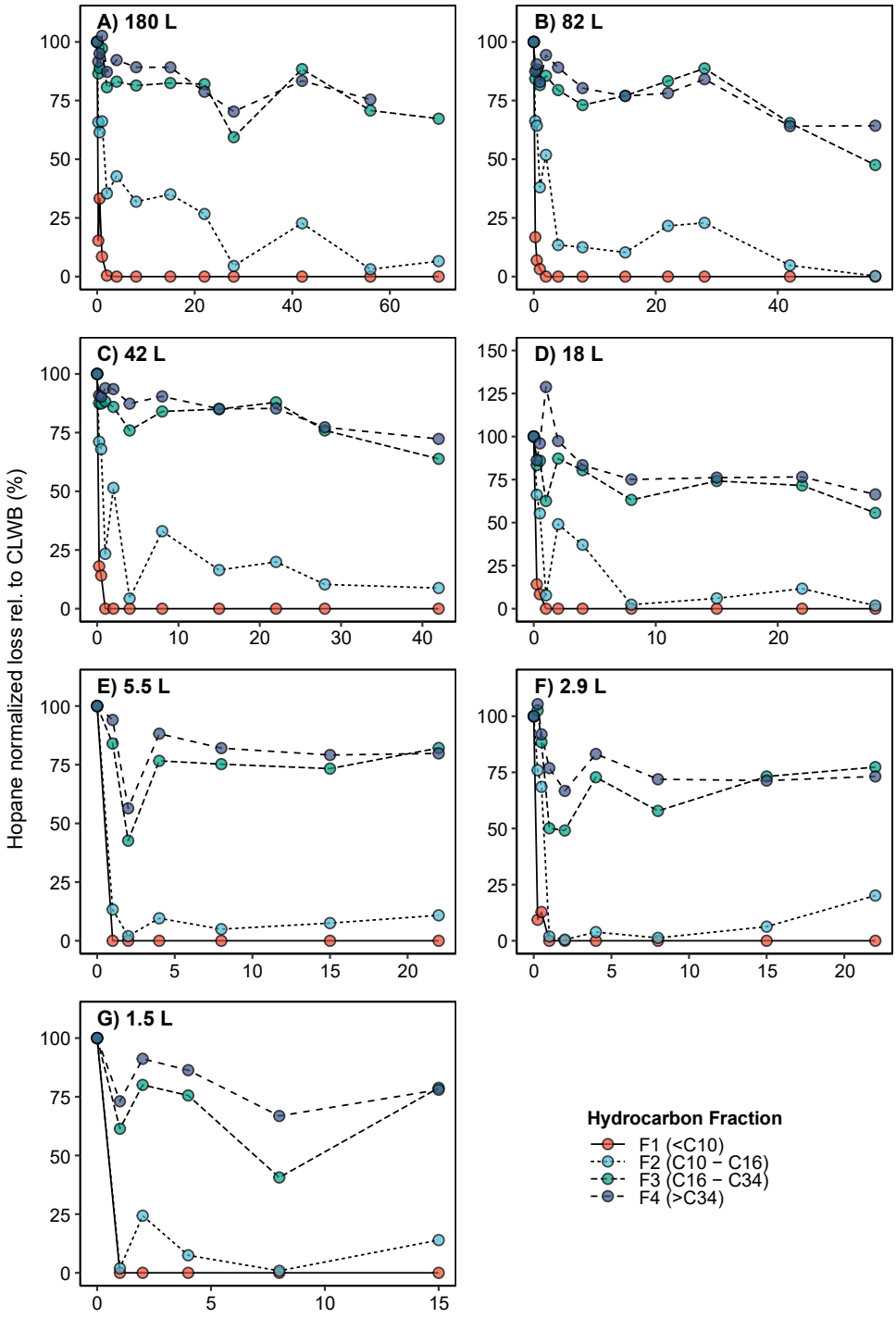

Figure S3. 12. Temporal changes of the four petroleum hydrocarbon fractions separated by GC-FID in dilbit slicks samples. Concentrations were normalized to C_{30} $\alpha\beta$ hopane and presented as percentage loss relative to the source CLWB dilbit. The varying x axis scale reflects when the respective dilbit slick was completely submerged, leaving no residual surface oil to sample. F3 and F4 fractions from panel G on day 8 and 15 were omitted due to analytical issues.

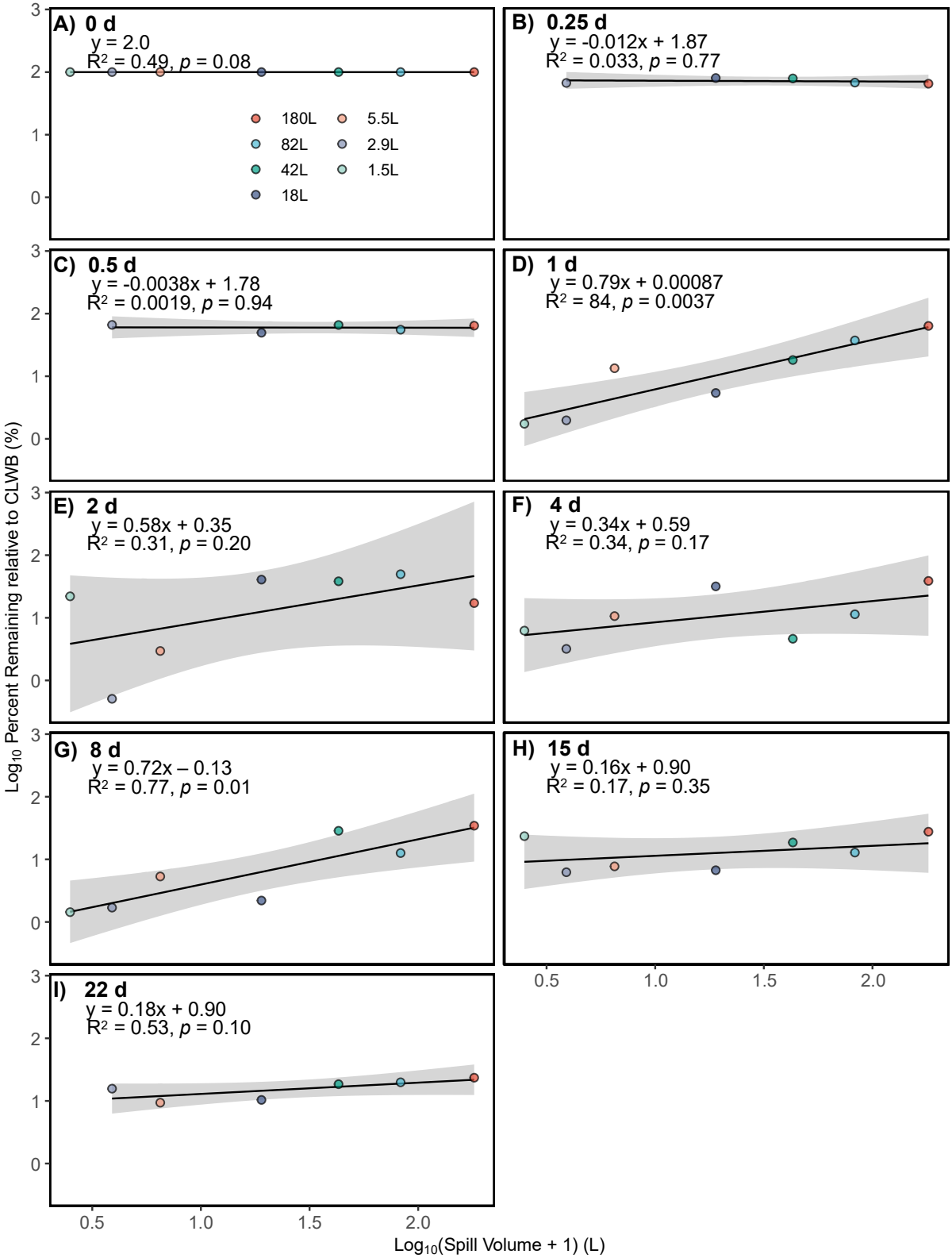

Figure S3. 13. Individual regressions performed on slick samples collected at each time point. Data used to generate figure 3.4B in main research article. Each panel represents a sampling timepoint.

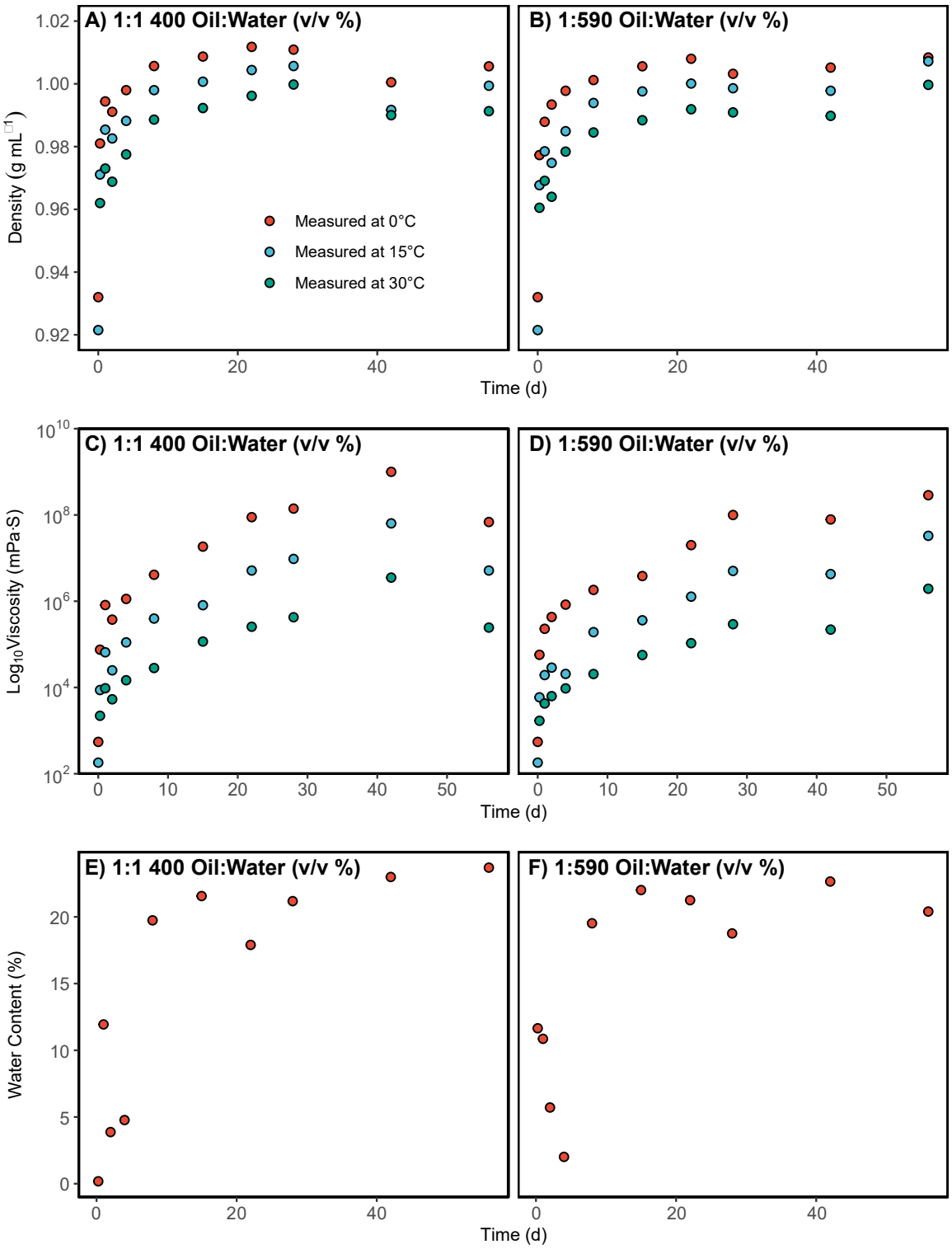

Figure S3. 14. Temporal changes in physical properties (AB- density, CD- viscosity, EF- water content). Density and viscosity were measured at three different temperatures (0, 15, and 30 ºC), whereas water content was measured at room temperature.

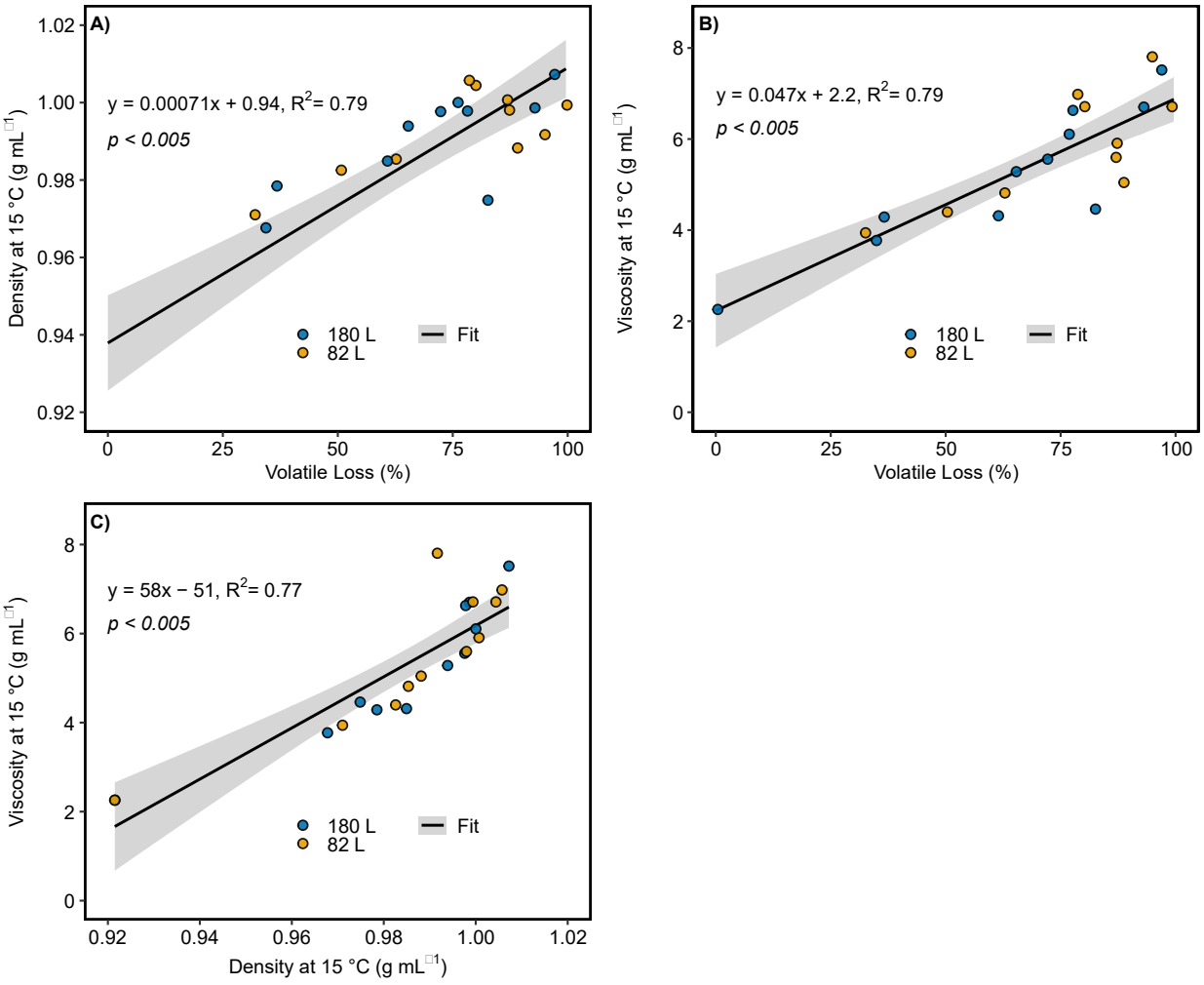

Figure S3. 15. The relationship between (A) density measured at 15 ºC, (B) viscosity measured at 15 ºC, and the percentage of volatile hydrocarbon (<C16) loss relative to the source CLWB. (C) The relationship between viscosity measured at 15 ºC and density measured a Lines represent a fitted linear regression model and associated standard error.

Supporting References

ASTM D3325-90 Standard Practice for Preservation of Waterborne Oil Samples. 2013. ASTM Int. doi:10.1520/D3325-90R13.

ASTM D4489-95 Standard Practices for Sampling of Waterborne Oils. 2017. ASTM Int. doi:10.1520/D4489-95R17.

Fingas M, Fieldhouse B. 2014. Water-in-oil emulsions: formation and prediction. Handb Oil Spill Sci Technol. 225. doi:http://dx.doi.org/10.14355/jpsr.2014.0301.04.

King TL, Robinson B, Boufadel M, Lee K. 2014. Flume tank studies to elucidate the fate and behavior of diluted bitumen spilled at sea. Mar Pollut Bull. 83(1):32–37. doi:10.1016/j.marpolbul.2014.04.042.

King TL, Robinson B, Cui F, Boufadel M, Lee K, Clyburne JA. 2017. An oil spill decision matrix in response to surface spills of various bitumen blends. Environ Sci Process Impacts. 19(7):928–938. doi:https://doi.org/10.1039/C7EM00118E.

Shah K, Watson K, Hollebone B, Yang Z, Lambert P, Faragher R, Aljawahari M, Dey D, Mirnaghi F, Stoyanovich S, et al. 2019. The BOREAL Project: The Design and Execution of a Controlled Oil Spill Study in a Canadian Freshwater Lake. In: Proceedings of the Forty-second AMOP Technical Seminar. Environment and Climate Change Canada, Ottawa, ON, Canada. p. 276–294.

Yarranton H, Motahhari HR, Schoeggl F, Zhou JZ. 2015. Evaporative Weathering of Diluted Bitumen Films. J Can Pet Technol. 54(04):223–244. doi:https://doi.org/10.2118/174557-PA.

REFERENCES

ASTM D5002-19, 2019. Standard Test Method for Density, Relative Density, and API Gravity of Crude Oils by Digital Density Analyzer. ASTM Int. West Conshohocken PA Vol 05.02. https://doi.org/10.1520/D5002-19

ASTM D7042-16, 2016. Standard test method for dynamic viscosity anddensity of liquids by Stabinger viscometer (and the calculation of kine-matic viscosity). ASTM Int. West Conshohocken PA Vol 05.04. https://doi.org/10.1520/D7042-16E03

ASTM E203-16, 2016. Standard test method for water using volumetric Karl Fischer titration. ASTM Int. West Conshohocken PA E203-16. https://doi.org/10.1520/E0203-16

Atlas, R.M., Hazen, T.C., 2011. Oil biodegradation and bioremediation: a tale of the two worst spills in US history. ACS Publications.

Baulch, H.M., Nord, T.W., Ackerman, M.Y., Dale, J.D., Hazewinkel, R.R.O., Schindler, D.W., Vinebrooke, R.D., 2003. Climate warming experiments: Design of a mesocosm heating system. Limnol. Oceanogr. Methods 1, 10–15. https://doi.org/10.4319/lom.2003.1.10

Bobra, M., Tennyson, E.J., 1989. Photooxidation of petroleum. Env. CanEnviron Prot Dir River Road 129–147.

Brandvik, P.J., Faksness, L.-G., 2009. Weathering processes in Arctic oil spills: Meso-scale experiments with different ice conditions. Cold Reg. Sci. Technol. 55, 160–166. http://dx.doi.org/10.1016/j.coldregions.2008.06.006

Canevari, G.P., 1978. Some observations on the mechanism and chemistry aspects of chemical dispersion,. ASTM Int. West Conshohocken PA Chemical dispersants for the control of oil spills, 5–17. https://doi.org/10.1520/STP35706S

CAPP, 2019. 2019 Crude Oil Forecast, Markets and Transportation (No. 2019– 0018). Canadian Association of Petroleum Producers (CAPP), Calgary, AB.

Cederwall, J., Black, T.A., Blais, J.M., Hanson, M.L., Hollebone, B.P., Palace, V.P., Rodríguez-Gil, J.L., Greer, C.W., Maynard, C., Ortmann, A.C., 2020. Life under an oil slick: response of a freshwater food web to simulated spills of diluted bitumen in field mesocosms. Can. J. Fish. Aquat. Sci. 1–10. https://doi.org/10.1139/cjfas-2019-0224

CER, 2019. Crude Oil annual Export Summary - 2018 [WWW Document]. URL www.cer-rec.gc.ca/nrg/sttstc/crdlndptrlmprdct/stt/crdlsmmr/crdlsmmr-eng.html (accessed 3.10.19).

CER, 2016. Canada's Energy Future 2016: Energy Supply and Demand Projections to 2040 (No. ISSN 2292-1710). Canada Energy Regulator (CER).

Douglas, G.S., Bence, A.E., Prince, R.C., McMillen, S.J., Butler, E.L., 1996. Environmental stability of selected petroleum hydrocarbon source and weathering ratios. Environ. Sci. Technol. 30, 2332–2339.

Federici, C., Mintz, J., 2014. Oil properties and their impact on spill response options literature review (No. IRM-2014-U-007490). CNA Anal. Solutions, Arlington, VA, USA.

Fingas, M., 2015a. Review of The Properties and Behaviour of Diluted Bitumen, in: Proceeding of the 39th Arctic and Marine Oil-Spill Program Technical Seminar.

Environment and Climate Change Canada, Vancouver, B.C., Canada, pp. 470–494.
Fingas, M., 2015b. Oil and Petroleum Evaporation, in: Handbook of Oil Spill Science and Technology. Wiley Online Library, pp. 205–223.
Fingas, M., Fieldhouse, B., 2014a. Water-in-oil emulsions: formation and prediction. Handb. Oil Spill Sci. Technol. 225.
Fingas, M., Fieldhouse, B., 2014b. Water-in-oil emulsions: formation and prediction. Handb. Oil Spill Sci. Technol. 225. http://dx.doi.org/10.14355/jpsr.2014.0301.04
Fingas, M., Fieldhouse, B., 2004. Formation of water-in-oil emulsions and application to oil spill modelling. J. Hazard. Mater. 107, 37–50. http://dx.doi.org/10.1016/j.jhazmat.2003.11.008
Fingas, M.F., 2004. Modeling evaporation using models that are not boundary-layer regulated. J. Hazard. Mater. 107, 27–36. https://doi.org/10.1016/j.jhazmat.2003.11.007
Fitzpatrick, F.A., Boufadel, M.C., Johnson, R., Lee, K.W., Graan, T.P., Bejarano, A.C., Zhu, Z., Waterman, D., Capone, D.M., Hayter, E., 2015. Oil-particle interactions and submergence from crude oil spills in marine and freshwater environments: Review of the science and future research needs (No. 2015–1076). US Geological Survey.
Government of Canada, Gas and Energy Research (Canada), 2014. Federal government technical report - properties, composition and marine spill behaviour, fate and transport of two diluted bitumen products from the Canadian oil sands.
Green, K.P., Jackson, T., 2015. Safety in the transportation of Oil and Gas: pipelines or rail? Fraser Institute Vancouver, BC.
Gros, J., Nabi, D., Würz, B., Wick, L.Y., Brussaard, C.P., Huisman, J., van der Meer, J.R., Reddy, C.M., Arey, J.S., 2014. First day of an oil spill on the open sea: Early mass transfers of hydrocarbons to air and water. Environ. Sci. Technol. 48, 9400–9411. https://doi.org/10.1021/es502437e
Gustitus, S.A., Clement, T.P., 2017. Formation, Fate, and Impacts of Microscopic and Macroscopic Oil-Sediment Residues in Nearshore Marine Environments: A Critical Review. Rev. Geophys. 55, 1130–1157. https://doi.org/10.1002/2017RG000572
Hansen, K., Sprague, M., Joeckel, J., Rockley, M., 2015. Response to Oil Sands Products Assessment (No. CG-D-16-15). U.S, Coast Guard Research and Development Center, New London, CT.
Harrison, W., Winnik, M.A., Kwong, P.T., Mackay, D., 1975. Crude oil spills. Disappearance of aromatic and aliphatic components from small sea-surface slicks. Environ. Sci. Technol. 9, 231–234. https://doi.org/10.1021/es60101a006
Hollebone, B.P., Fieldhouse, B., Sergey, G., Lambert, P., Wang, Z., Yang, C., Landriault, M., 2011. The Behaviour of Heavy Oil in Fresh Water Lakes, in: Proceedings of the 34th Arctic and Marine Oilspill Program (AMOP) Technical Seminar on Environmental Contamination and Response. Environment Canada, Ottawa. pp. 668–789.
Hua, Y., Mirnaghi, F.S., Yang, Z., Hollebone, B.P., Brown, C.E., 2018. Effect of evaporative weathering and oil-sediment interactions on the fate and behavior of diluted bitumen in marine environments. Part 1. Spill-related properties, oil

buoyancy, and oil-particulate aggregates characterization. Chemosphere 191, 1038–1047. https://doi.org/10.1016/j.chemosphere.2017.10.156
ITOPF, 2012. Use of Skimmers in Oil Pollution Response. International Tanker Owners Pollution Federation (ITOPF).
ITOPF, 2011. Use of dispersants to treat oil spills, Technical Information Paper 4. International Tanker Owners Pollution Federation (ITOPF), London.
Johannessen, S.C., Greer, C.W., Hannah, C.G., King, T.L., Lee, K., Pawlowicz, R., Wright, C.A., 2019. Fate of diluted bitumen spilled in the coastal waters of British Columbia, Canada. Mar. Pollut. Bull. 110691. https://doi.org/10.1016/j.marpolbul.2019.110691
Johnson, W.E., Vallentyne, J.R., 1971. Rationale, background, and development of experimental lake studies in northwestern Ontario. J. Fish. Board Can. 28, 123–128. https://doi.org/10.1139/f71-026
King, T., Toole, P., Robinson, B., Ryan, S., Lee, K., Boufadel, M.C., Li, H., Clyburne, J.A., 2019. Influence of Climatic Parameters on Changes in the Density and Viscosity of Diluted Bitumen after a Spill. J. Rnvion. Sci. Pollut. Res. 5, 373–382. https://doi.org/doi.org/10.30799/jespr.176.19050305
King, T.L., 2019. Physical properties dynamics of oil sands products and their influence on spill response (PhD Thesis). Sain Mary's University, Halifax, Nova Scotia, Canada.
King, T.L., Robinson, B., Boufadel, M., Lee, K., 2014. Flume tank studies to elucidate the fate and behavior of diluted bitumen spilled at sea. Mar. Pollut. Bull. 83, 32–37. https://doi.org/10.1016/j.marpolbul.2014.04.042
King, T.L., Robinson, B., Cui, F., Boufadel, M., Lee, K., Clyburne, J.A., 2017. An oil spill decision matrix in response to surface spills of various bitumen blends. Environ. Sci. Process. Impacts 19, 928–938. https://doi.org/10.1039/C7EM00118E
Lee, K. (chair), Boufadel, M., Chen, B., Foght, J., Hodson, P., Swanson, S., Venosa, A., 2015. Expert Panel Report on the Behaviour and Environmental Impacts of Crude Oil Released into Aqueous Environments (No. ISBN: 978-1-928140-02-3). Royal Society of Canada, Ottawa, ON, Canada.
Michel, J., Ploen, M., Elliot, J., 2014. API Study on Detection and Recovery of Sunken Oil., in: International Forum on Group V Oils. Presented at the International Spill Control Organization (ISCO), Detroit, MI.
NASEM, 2016. Spills of Diluted Bitumen from Pipelines: A Comparative Study of Environmental Fate, Effects, and Response (No. ISBN: 978-0-309-38010-2). National Academies of Sciences, Engineering and Medicine (NASEM), Washington, DC.
Nordvik, A.B., 1995. The technology windows-of-opportunity for marine oil spill response as related to oil weathering and operations. Spill Sci. Technol. Bull. 2, 17–46. https://doi.org/10.1016/1353-2561(95)00013-T
Oliver Wyman, 2019. Canadian Crude Oil Transportation: Comparing the Safety of Pipelines and Railways, Prepared for The Railway Association of Canada. Marsh & McLennan Companies.
Orihel, D.M., Paterson, M.J., Gilmour, C.C., Bodaly, R.A., Blanchfield, P.J., Hintelmann, H., Harris, R.C., Rudd, J.W., 2006. Effect of loading rate on the fate of mercury in

littoral mesocosms. Environ. Sci. Technol. 40, 5992–6000. https://doi.org/10.1021/es060823+
Prince, R.C., Elmendorf, D.L., Lute, J.R., Hsu, C.S., Haith, C.E., Senius, J.D., Dechert, G.J., Douglas, G.S., Butler, E.L., 1994. 17. alpha.(H)-21. beta.(H)-hopane as a conserved internal marker for estimating the biodegradation of crude oil. Environ. Sci. Technol. 28, 142–145. https://doi.org/10.1021/es00050a019
Prince, R.C., Garrett, R.M., Bare, R.E., Grossman, M.J., Townsend, T., Suflita, J.M., Lee, K., Owens, E.H., Sergy, G.A., Braddock, J.F., 2003. The roles of photooxidation and biodegradation in long-term weathering of crude and heavy fuel oils. Spill Sci. Technol. Bull. 8, 145–156. https://doi.org/10.1016/S1353-2561(03)00017-3
Radović, J.R., Aeppli, C., Nelson, R.K., Jimenez, N., Reddy, C.M., Bayona, J.M., Albaigés, J., 2014. Assessment of photochemical processes in marine oil spill fingerprinting. Mar. Pollut. Bull. 79, 268–277. https://doi.org/10.1016/j.marpolbul.2013.11.029
Rodriguez-Gil, J.L., Stoyanovich, S., Hanson, M.L., Hollebone, B., Orihel, D.M., Palace, V., Faragher, R., Mirnaghi, F.S., Shah, K., Yang, Z., 2021. Simulating diluted bitumen spills in boreal lake limnocorrals-Part 1: Experimental design and responses of hydrocarbons, metals, and water quality parameters. Sci. Total Environ. 148537.
Short, J.W., 2013. Susceptibility of Diluted Bitumen Products from the Alberta Tar Sands to Sinking in Water (No. D72-80–2). JWS Consulting LLC.
Stout, S.A., Wang, Z., 2016. Chemical fingerprinting methods and factors affecting petroleum fingerprints in the environment. Stand. Handb. Oil Spill Environ. Forensics 61–129.
Stoyanovich, S., Yang, Z., Hanson, M., Hollebone, B., Orihel, D., Palace, V., Rodriguez-Gil, J., Faragher, R., Mirnaghi, F., Shah, K., Blais, J., 2019. Simulating a spill of diluted bitumen: Environmental weathering and submergence in a model freshwater system. ET&C. https://doi.org/10.1002/etc.4600
Transport Canada, 2014. A Review of Canada's Ship-Source Spill Preparedness and Response: Setting the Course for the Future, Phase II, Requirements for the Arctic and for Hazardous and Noxious Substances Nationally (No. ISBN 978-1-100-24991-9). Tanker Safety Panel Secretariat Ottawa, Canada.
Transport Canada, 2013. Tanker Safety Expert Panel - A review of Canada's Ship-source Oil Spill Preparedness And Response Regime: Setting the course for the future (No. ISBN 978-1-100-54627-8). Tanker Safety Panel Secretariat Ottawa, Canada.
Transport Canada, 1995. Response Organization Standards. Marine Safety Directorate, Ottawa, Canada.
Transportation Research Board and National Research Council, 2014. TRB Special Report 311: Effects of Diluted Bitumen on Crude Oil Transmission Pipelines (No. https://doi.org/10.17226/18381). The National Academies Press, Washington, DC.
US EPA, 2013. Dredging Begins on Kalamazoo River, Enbridge Oil Spill, Marshall, Michigan. U.S. Environmental Protection Agency (US EPA).

Venosa, A.D., Suidan, M.T., King, D., Wrenn, B.A., 1997. Use of hopane as a conservative biomarker for monitoring the bioremediation effectiveness of crude oil contaminating a sandy beach. J. Ind. Microbiol. Biotechnol. 18, 131–139. https://doi.org/10.1038/sj.jim.2900304

Wadsworth, T., 1995. Containment & Recovery of Oil Spills at Sea: Methods and Limitations.

Warnock, A.M., Hagen, S.C., Passeri, D.L., 2015. Marine tar residues: a review. Water. Air. Soil Pollut. 226, 68. https://doi.org/10.1007/s11270-015-2298-5

Waterman, D.M., Garcia, M.H., 2015. Laboratory Tests of Oil-Particle Interactions in a Freshwater Riverine Environment with Cold Lake Blend Weathered Bitumen. Ven Te Chow Hydrosystems Lab. Univ. Ill.

Weast, R.C., Astle, M.J., Beyer, W.H., 1988. CRC handbook of chemistry and physics. CRC press Boca Raton, FL.

Yang, C., Lambert, P., Zhang, G., Yang, Z., Landriault, M., Hollebone, B., Fieldhouse, B., Mirnaghi, F., Brown, C.E., 2017. Characterization of chemical fingerprints of unconventional Bakken crude oil. Environ. Pollut. 230, 609–620. https://doi.org/0.1016/j.envpol.2017.07.011

Yang, Z., Hua, Y., Mirnaghi, F., Hollebone, B.P., Jackman, P., Brown, C.E., Yang, C., Shah, K., Landriault, M., Chan, B., 2018. Effect of evaporative weathering and oil-sediment interaction on the fate and behavior of diluted bitumen in marine environments. Part 2. The water accommodated and particle-laden hydrocarbon species and toxicity of the aqueous phase. Chemosphere 191, 145–155. https://doi.org/10.1016/j.chemosphere.2017.10.033

Yarranton, H., Motahhari, H.R., Schoeggl, F., Zhou, J.Z., 2015. Evaporative Weathering of Diluted Bitumen Films. J. Can. Pet. Technol. 54, 223–244. https://doi.org/10.2118/174557-PA

Zhao, L., Torlapati, J., Boufadel, M.C., King, T., Robinson, B., Lee, K., 2014. VDROP: A comprehensive model for droplet formation of oils and gases in liquids-Incorporation of the interfacial tension and droplet viscosity. Chem. Eng. J. 253, 93–106. https://doi.org/10.1016/j.cej.2014.04.082

CHAPTER 4: CHEMICAL WEATHERING PATTERNS OF DILUTED BITUMEN SPILLED INTO FRESHWATER LIMNOCORRALS

Stoyanovich, S[a]., Saunders, L[a]., Yang, Z[b]., Hanson, M[d]., Hollebone, B.P[b]., Orihel, D. M[c]., Palace, V[e]., Rodriguez-Gil, JR[a]., Mirnaghi, F.S[b]., Shah, K[b]., Blais, J.M[a*]

[a] Department of Biology, University of Ottawa, Ottawa, Ontario, K1N 6N5, Canada

[b] Emergencies Science and Technology Section, Environment and Climate Change Canada, Ottawa, Ontario, Canada

[c] Department of Biology and School of Environmental Studies, Queen's University, Kingston, ON K7L 3N6

[d] Department of Environment and Geography, University of Manitoba, Winnipeg, MB, R3T 2N2, Canada.

[e] International Institute for Sustainable Development, Experimental Lakes Area, 111 Lombard Avenue, Suite 325, Winnipeg, Manitoba R3N 0T4, Canada

*Corresponding Author: Jules Blais (jules.blais@uottawa.ca)

STATEMENT OF CONTRIBUTIONS

Stoyanovich, S: conceptualization, writing, formal analysis, analytical, field work
Saunders, L: analysis, writing, reviewing
Yang, Z: analytical, reviewing
Hanson, M: reviewing, funding acquisition
Hollebone, B: reviewing, funding acquisition, analytical
Orihel, D: reviewing, funding acquisition
Palace, V: reviewing, funding acquisition
Rodriguez-Gil, J: reviewing
Faragher, R: reviewing, field work, analytical
Mirnaghi, F: reviewing, analytical
Shah, K: field work, analytical
Blais, J: supervision, reviewing, funding acquisition, conceptualization, corresponding author

This chapter was prepared for submission to the journal: *Environmental Science and Technology*

ABSTRACT

We determined the weathering patterns of Cold Lake Winter Blend diluted bitumen (dilbit) by performing a series of controlled spills onto the water's surface of 10m diameter limnocorrals installed in a freshwater lake in Northern Ontario, Canada. Utilizing a regression-based design, we added seven different dilbit spill volumes, ranging from 1.5 to 180 L, resulting in oil-to-water ratios between 1:71 000 (v/v, %) and 1:500 (v/v, %). GC-MS-based methods for oil fingerprinting were used to track changes in dilbit's chemical composition as it weathered in the environment for 70 days. Depletion rate constants of *n*-alkanes and PAHs ranged from 0.00091 to 0.41 d^{-1} and 0.00075 to 0.38 d^{-1}, respectively. We observed no significant relationship between the magnitude of individual hydrocarbon depletion rate constants and the amount of dilbit spilled, suggesting that the size of the dilbit spill had no effect on the depletion rate of hydrocarbons. The major diagnostic ratios developed from *n*-alkanes, isoprenoids, and PAHs (e.g., LMW/HMW, *n*-C_{17}/pris, *n*-C_{18}/phy, $C_{1+2}N/C_{3+4}N$, C_2N/C_2F, C_3N/C_3F, C_1P/C_1C, C_1F+C_2F/C_3F, C_3C/C_0C, C_3P/C_3C, C_4Fl/C_0Fl) indicated that evaporation, dissolution, photooxidation, and to a lesser degree biodegradation were acting on the surface slicks. This study provides quantitative estimates of dilbit weathering under relevant environmental conditions crucial for understanding the fate of dilbit in Canadian Boreal lakes.

1 INTRODUCTION

Diluted bitumen's (dilbits) are a form of heavy crude oils produced by mixing highly dense and viscous bitumen with lighter hydrocarbons to facilitate pipeline transport (Government of Canada, 2013). The diluents involved in this process include naphtha's, condensates, and synthetic crude oils (Fingas, 2015a) and the ratio at which they are added varies seasonally to maintain pipeline specifications for viscosity (Lee et al., 2015).

Dilbit spills are more complex than conventional crude oils because of dilbit's seasonal changes in chemical composition and differential fate of the diluent and bitumen components, as the oil weathers (Lee et al., 2015; NASEM, 2016). Weathering is the biotic and abiotic modification of its physical and chemical characteristics following its release into the environment (Lee et al., 2015; NASEM, 2016). Processes such as evaporation, biodegradation, and photooxidation can all alter the physical and chemical properties of dilbit, affecting its long term fate in the environment (Atlas and Hazen, 2011; Fingas, 2015b; Prince et al., 2003a). These processes are poorly defined in inland lakes, where limited research is available on dilbit weathering (Lee et al., 2015). Weathering processes depend heavily on the chemical composition of the spilled oil (Radović et al., 2014) as well as a variety of environmental factors such as sunlight, temperature, and wind speed. Lower molecular weight compounds ($\leq C_{16}$) are typically prone to evaporation (Gros et al., 2014; Lee et al., 2015; Prince et al., 2003a). Larger aromatics are prone to photooxidation and can be transformed into oxygenated polar species when exposed to sunlight (Aeppli et al., 2012; Z. Yang et al., 2017) while alkanes are not (Garrett et al., 1998). The opposite is true for biodegradation, where the

increased stability provided by aromatic rings makes PAHs less susceptible to microbial degradation than alkanes (Prince et al., 2003a). For example, Bacosa et al., (2015) found that biodegradation was the main contributor to the transformation of *n*-alkanes, while photooxidation was the key process for the degradation of PAHs and alkylated PAHs.

The most widely used approach to characterize spilled oil employs the use of gas chromatography either coupled with flame ionization detection (GC-FID) or a mass spectrometer (GC-MS) (Wang and Fingas, 2003). The chemical distribution and diagnostic ratios of certain hydrocarbon groups including *n*-alkanes, polycyclic aromatic hydrocarbons (PAHs), and biomarkers, generate a unique chemical 'fingerprint' that can be used to determine the source of the oil (Stout and Wang, 2016) and to characterize weathering processes occurring over time (Wang and Fingas, 2003). This approach was extensively used following the *Deepwater Horizon* disaster and other marine spills alike (Aeppli et al., 2014; Bacosa et al., 2015; Bagby et al., 2017; Bociu et al., 2019). Identifying the chemical composition and source of the spilled oil allows responders to better predict the potential for transport and weathering, and ultimately the resulting environmental impact of the spill (Owens et al., 2016).

The majority of research on the fate and behaviour of oil in aqueous systems focuses on marine spills as they garner more public attention due to the vast and far-reaching environmental and economic damages (ex: 2010 *Deepwater Horizon* Disaster, 2002 Prestige Tanker spill, 1989 Exxon Valdez spill). Conversely, inland freshwater oil spills receive much less attention (Bhattacharyya et al., 2003) even though historically they have occurred more frequently than their marine counterparts (Owens et al., 1993;

Vandermeulen and Ross, 1995). We currently lack information on the effects of environmental weathering of diluted bitumen under prevailing conditions of the Boreal shield region of Canada. In particular, no studies to date have derived depletion rates for hydrocarbons present in a dilbit slick under natural biotic and abiotic conditions of a boreal lake. Following an accidental spill, the collection of environmental samples is often delayed for several days as spill containment and recovery are of top priority. By this time, the majority of the early weathering processes, such as evaporation, have already occurred and cannot be tracked.

This study is part of the BOREAL project (Boreal Lake Oil Release Experiments by Additions to Limnocorrals), a multi-phase project aimed at providing much-needed information on the fate, behaviour, and impacts of dilbit spills in freshwater environments. Here we monitored the compositional changes of the dilbit slicks for 70 days following experimental spills to 10 m diameter in-lake limnocorrals, beginning our sampling immediately following the spills. With this study, we aim to address the lack of early compositional dilbit slick data following a spill and specifically shed light on weathering processes that alter dilbit spilled in a boreal freshwater system.

2 MATERIALS AND METHODS

2.1. Experimental Set Up

We installed nine 10 m diameter limnocorrals in a ~ 2 m deep littoral zone on the northern shore of Lake 260 at the International Institute for Sustainable Development – Experimental Lakes Area (IISD-ELA), located near Kenora, Ontario, Canada. The limnocorrals consisted of a 10 m diameter floating ring to which we attached a high-

density polyethylene (HDPE) cylindrical membrane curtain extending down to the sediment surface. We used sandbags to seal the plastic membrane to the lake bottom (SI Figure S4.1). Each limnocorral created a section of the water column (approx. 100 000 L) that we could manipulate experimentally without otherwise affecting the entire lake. A detailed account of the construction and installation of our limnocorrals has been described elsewhere (Rodriguez-Gil et al., 2021).

We employed a regression design to simulate dilbit spills of different sizes. We performed seven individual dilbit spills by releasing dilbit into separate limnocorrals in the following distinct volumes (L): 1.5, 2.9, 5.5, 18, 42, 82, or 180. Our selected spill volumes were based on published onshore crude oil spill occurrences throughout North America between 2008 and 2017 obtained from the U.S Department of Transportation (USDOT, 2017) and the National Energy Board of Canada (NEB, 2017). We then predicted the resulting oil:water (%v/v) ratios that would be expected if these spills were to occur in our study lake (Lake 260 ~ $2x10^6$ m^3). Our lowest treatment volume, 1.5 L (oil:water 1:66000 %v/v), results in an oil:water ratio within the same range as the most common spill volume in North America, and our highest treatment, 180 L (oil:water 1:590 %v/v) is similar to the largest on-shore spill to date, the 2010 Kalamazoo River Spill. With our lower and upper spill volume ranges set, we selected the remaining 5 volumes equidistant along a logarithmic scale between 1.5 and 180 L. The full rationale for spill volume selection is described in detail elsewhere (Rodriguez-Gil et al., 2021). The remaining two limnocorrals were controls; one located adjacent to dilbit treatments (near field control) and one located roughly 100 m from any dilbit treatment (far field control).

We added Cold Lake Winter Blend (CLWB) dilbit to the water's surface of these limnocorrals on June 20th, 2018, between 8:30am and 10:00am. Shah et al. (2019) provided additional details of the procedure for pumping dilbit to water. Briefly, we pumped CLWB from cans to the water surface using a Flojet diaphragm pump (FLOJET Corp, California) at a rate of approximately 7.5 L min^{-1} (SI Figure S4.2). We weighed all empty cans, hoses, and pumps before and after the dilbit additions to precisely determine the mass of dilbit added to each limnocorral. We then estimated spill volumes from the mass of CLWB added and its density measured at 15 ºC (0.9215 g mL^{-1}). We monitored these limnocorrals for 70 days, tracking changes in dilbit properties until we decommissioned the experiment on September 8th, 2018, and remediated the site.

2.2. Sample Collection

We collected and stored surface oil samples for chemical analysis from each dilbit treatment using Teflon strips following ASTM Methods D4489 and D3325 ("ASTM D3325-90 Standard Practice for Preservation of Waterborne Oil Samples," 2013; "ASTM D4489-95 Standard Practices for Sampling of Waterborne Oils," 2017). We passed the Teflon strips through the oil slick until a volume of approximately 2 – 5 mL had adhered and then stored them in 125 mL wide mouth amber glass jars. The jars were sealed and refrigerated prior to further processing. Following the onset of the spills, we collected samples from the dilbit slicks at 0.25, 2, 4, 8, 15, 22, 28, 42, 56, and 70 d post-spill. The dilbit slicks eventually submerged to the limnocorral sediments (Stoyanovich et al., 2021) which limited the amount of surface oil available for sample collection. Therefore day 15 was the final day that we collected a sample from each treatment. We halted dilbit sampling after day 15 for any treatments where complete

dilbit submergence had already occurred. The detailed sampling protocol can be found in SI Figure S4.3.

2.3. Analytical

Prior to extraction, we cut a strip of the oiled Teflon sheet, weighed, and spiked it with surrogates as recovery standards (o-terphenyl, d_{50}-tetracosane, d_8-naphthalene, d_{10}-acenaphthene, d_{10}-phenanthrene, d_{12}-benz[a]anthracene, and d_{12}-perylene) and then ultrasonicated in dichloromethane (DCM) for 10 minutes. We then passed the extracts through sodium sulfate to remove any residual water and rinsed them with DCM until they were colour free, and then diluted to 10 mL with DCM. Gravimetric analysis enabled the determination of total solvent extractable materials (TSEM). We blew down 1 mL of the above extract to complete dryness to measure TSEM weight. Appropriate amounts of extracts were than solvent exchanged into *n*-hexane prior to transferring to a preconditioned chromatographic column packed with 3 g of silica gel for cleanup. We performed fractionation following the same procedure as Yang et al. (2017).

An Agilent 7890A gas chromatograph (GC) equipped with an Agilent 5975C mass selective detector (MSD) enabled the analysis of target *n*-alkanes, PAHs (including 7 alkylated PAH homologous groups and other unsubstituted PAHs) and petroleum biomarker compounds (SI Table S4.1). We analyzed all concentrations using Agilent Enhanced MSD ChemStation. Mean (± standard deviation) recovery rates for d_8-naphthalene, d_{10}-acenaphthene, d_{10}-phenanthrene, d_{12}-benz(a)anthracene, d_{12}-perylene, and *n*-tetracosane were 67 ± 13%, 77 ± 10%, 87 ± 8%, 96 ± 9%, 96 ± 9%, and 94 ± 9%, respectively across all samples.

To account for uncertainty arising from analytical procedures and manual integration, we performed a reference oil injection (13.1% weathered Prudhoe Bay crude oil) after every 20 environmental samples from July 2018 – March 2019, resulting in a total of 13 individual GC-MSD injections. RSDs ranged from 9 to 40% and was typically higher for compounds present at low concentrations in the source oil (SI Table S4.2). Finally, we performed a method blank analysis to monitor the laboratory background at every 10 samples.

2.4. Interpretation and Calculations

In order to determine depletion rates of individual analytes, we applied a quantitative method to monitor depletion in the form of a conserved internal standard (Douglas et al., 1996). We normalized all analyte concentrations to 17α(H) 21β(H) hopane (C_{30} hopane), a useful biomarker in this context due to its recalcitrance to biotic and abiotic weathering processes (Garrett et al., 1998; Prince et al., 1994; Stout and Wang, 2016; Venosa et al., 1997). As weathering proceeds, the hopane concentration in the residual oil increases as other compounds are removed from the slick (Douglas et al., 1996, 1994). Therefore the concentration of hopane in the weathered oil (H_t) relative to the concentration in the source oil (H_o) is a function of the amount of oil depleted.

$$\% \text{ oil depletion} = [1 - (H_o/H_t)] \times 100 \qquad (1)$$

We then calculated individual analyte depletion in an equation adapted from Radović et al. (2014) and Douglas et al. (1996) (eq. 2):

$$\% \text{ analyte depleted} = [1 - (C_t/C_o)(H_o/H_t))] \times 100 \quad (2)$$

Where C_t and C_o are the concentrations of a compound in a weathered (*t*) and original (o) sample.

2.5. Statistical Analyses

R Studio version 1.1.383 (RStudio., Boston, MA, USA) enabled the calculation of rate constants from the temporal changes in concentration over time in dilbit slick samples. By assuming first-order kinetics, we determined individual rate constants (*k;* d^{-1}) using the integrated rate method by which the natural log of the normalized concentration is regressed against time (Bacosa et al., 2015; Bociu et al., 2019; De Bruyn et al., 2012):

$$\ln(C/H)_t = \ln(C/H)_0 - kt \quad (3)$$

where $(C/H)_0$ and $(C/H)_t$ are biomarker normalized ratios of the selected analyte at time 0 and time *t* (d). We use the term “depletion” rather than degradation to represent these rate constants since we are unable to accurately differentiate between biotic and abiotic processes acting on the slicks. In order to assess and compare depletion across each spill volume, we first normalized concentrations of the individual compound (C; $\mu g\ g^{-1}$) to concentrations of C_{30} Hopane (H; $\mu g\ g^{-1}$). We only calculated depletion rate constants over the first 15 days of the study due to differences in submergence trends affecting our ability to collect surface oil samples (SI Figure S4.3). This prevents any skewing of rate constants by the extended sampling timelines in some of the higher dilbit

treatments compared to the lower volume treatments. We also carried out principle component analyses (PCA) in R Studio using the package "*factoextra*" (Kassambara and Mundt, 2017). Nonlinear regression models were fit using JMP version 14 (SAS., Cary, NC, USA). Nonlinear regression enabled the evaluation of the differences in *k* with respect to molecular weight. To evaluate for possible treatment effects, we evaluated the differences in *k* with respect to spill volume by linear regression. Slopes derived from these regression relationships (i.e., $k_{treatment}$) were then compared against the degree of alkylation (alkylated PAHs) to determine if treatment effects were compound specific.

2.6. Weathering Ratio Analysis

We utilized 14 commonly used diagnostic ratios to identify potential weathering processes acting upon the dilbit slicks throughout the study, a summary of each is described in detail in SI Table S4.3. These ratios reflect the higher susceptibility of smaller, more volatile compounds to evaporation, dissolution, and biodegradation (Miller and Mudge, 1997; Mudge, 2016; Prince and Walters, 2016; Vergeynst et al., 2019; Wang et al., 1998) and the larger, more alkylated compounds to photooxidation (Charrié-Duhaut et al., 2000; Lima et al., 2005; Prince et al., 2003b).

We determined the relative standard deviation (%RSD) following a total of 13 individual injections of our reference oil for each of the 15 diagnostic and weathering ratios (SI Table S4.4). For these 13 replicates, we obtained RSDs of 4 to 11% for the 15 ratios (average of 7%).

3 RESULTS AND DISCUSSION

3.1. Depletion of *n*-alkanes

Total *n*-alkanes in the surface dilbit slick samples experienced a rapid decrease in the first 2 days of the experiment, followed by a more gradual decrease for the remainder of the study, resulting in total losses between 43 and 91%, across each treatment (Figure 4.1AB). First-order depletion rate constants of total *n*-alkanes calculated over the first 15 days of study ranged from 0.040 – 0.093 d^{-1} (SI Table S4.6). *N*-alkane fingerprints of dilbit samples exhibited a significant loss of the lower molecular weight compounds (*n*-C_9 – *n*-C_{16}) within the first 6 hours of the spills, followed by further loss of the larger compounds (*n*-C_{17} – *n*-C_{40}) later on (SI Figure S4.5A). Nearly 100% of the volatile *n*-alkanes (*n*-C_9 – *n*-C_{16}) were removed in each treatment by the final sampling timepoint (SI Figure S4.6). Patterns of *n*-alkane depletion become apparent when observed in the form of a PCA. Figure S4.7 tracks the progression of *n*-alkane fingerprints in collected dilbit samples over time, we observe two major phases. The first occurs during the initial hours of the spills (< 1 day), where short chain volatile *n*-alkanes dominate. Following the rapid loss of these compounds, likely due to evaporation, there was a significant shift towards longer chained *n*-alkanes dominating, as these compounds are more resistant to loss over time. These trends are most pronounced in the higher treatment volumes which remained on the water's surface for longer periods of time (Stoyanovich et al., 2021) and therefore experienced prolonged weathering.

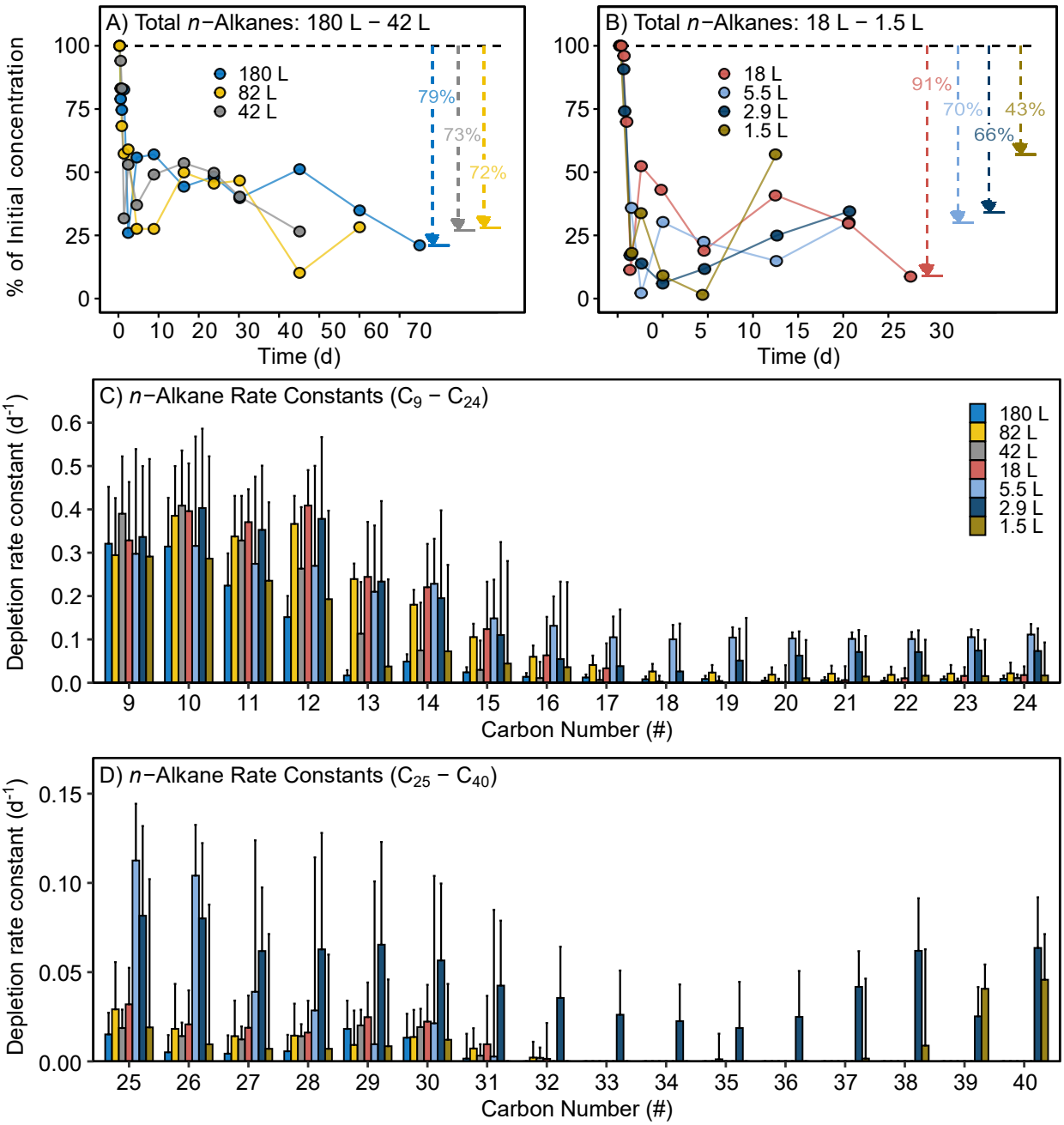

Figure 4. 1. Depletion of total n-alkanes in each dilbit amended treatment over time (AB) and first order depletion rate constants of individual n-alkanes (CD). Absolute rates are presented, error bars represent standard error of the slope coefficient. Missing data bars represent treatments where the specific analyte did not exhibit any degradation over time (i.e., $k>0$). Timelines of collected surface slick samples differ due to differences in dilbit submergence times.

Individual *n*-alkane regressions of the natural logarithm transformed concentration over time can be found in SI Table S4.7 and Figure S4.8 and the resulting

rate constants in Figure 4.1CD. Overall, the highest rate constant of 0.41 d^{-1} for *n*-C_{10} and *n*-C_{12} was observed in the 18 and 42 L treatments, respectively (Figure 4.1CD, SI Table S4.6). Positive rate constants were found for *n*-C_{17}, *n*-C_{18}, pristane, phytane, and the majority of compounds >*n*-C_{31} (Figure 4.1CD). Previous studies involving conventional crude oil have shown that the depletion of *n*-alkanes are highest for the shorter, smaller compounds, and decrease with increasing chain length (Atlas and Bartha, 1992; Bociu et al., 2019; Knightes and Peters, 2003; Wardlaw et al., 2011). We also report an inverse correlation between depletion rate and *n*-alkane chain length here. We consistently found in each treatment that depletion rate constants decreased exponentially with molecular weight, from 0.029 – 0.39 d^{-1} for *n*-C_9 to 0 – 0.065 d^{-1} for *n*-C_{40}, across all treatments (Figure 4.2A, SI Table S4.7). These findings support the recalcitrance of higher molecular weight *n*-alkanes. Depletion patterns of branched alkanes differed from their *n*-alkane counterparts of similar molecular weight in all cases except for TMD (2,6,10-trimethyldodecane), where rate constants were still generally high, ranging from 0.12 to 0.29 d^{-1} across all treatments (SI Figure S4.9). The volume of dilbit spilled did not have a significant effect on the magnitude of rate constants for any of the *n*-alkanes over the initial 15 days of weathering. Collectively, these results suggest that spill volume does not impact the rate at which individual *n*-alkanes are depleted.

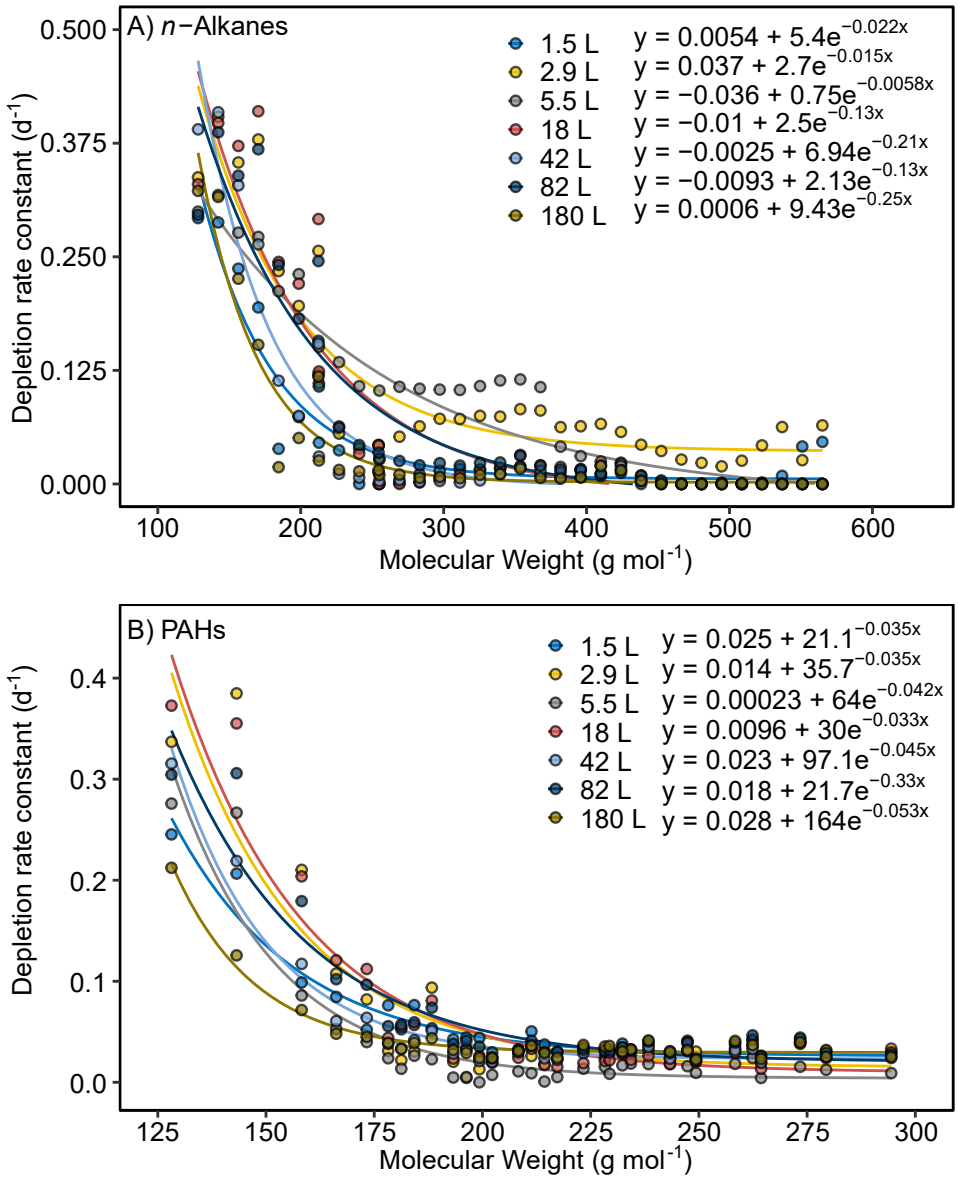

Figure 4. 2. Individual n-alkane (A) and PAHs (B) absolute rate constants (|k|) as a function of molecular weight in each of the dilbit amended treatments. Compounds that did not show evidence of loss over time (i.e., *k*>0) were omitted from this analysis.

3.2. Depletion of PAHs

Total PAHs in the surface dilbit slick samples experienced a rapid decrease in the first 2 days of the experiment, followed by more gradual decrease for the remainder of the study, resulting in between 42 and 70% across each treatment (Figure 4.3AB).

First-order depletion rate constants of total PAHs calculated over the first 15 days of study ranged from 0.017 – 0.047 d^{-1} (SI Table S4.6). Similar to *n*-alkanes, the changes in PAH fingerprints in dilbit samples were marked by a general depletion of the low molecular weight 2-ring constituents early, followed by depletions of the remaining 3 – 4 ring compounds (SI Figure S4.5B). The parent and methyl substituted naphthalenes (C_0-NAP and C_1-NAP) showed >95% depletion by the final sampling day in all treatments (SI Figure S4.10). Similar to *n*-alkanes, we observed shifts in the PCAs from more volatile 2-ring PAHs that dominated during the initial hours of the spills, to highly alkylated 4-ring PAHs dominating towards the end of the study (SI Figure S4.11).

Individual PAH rate constants decreased exponentially with increasing molecular weight from 0.21 – 0.37 d^{-1} for C_0-NAP to 0.009 – 0.033 d^{-1} for C_4-benzonaphthothiophene, across all treatments, reflecting a decrease in depletion rate with an increase in the number of benzene rings and alkylation (Figure 4.2B, Figure 4.3CD). Aside from C_1- and C_2-DBT in the 5.5 L treatment, all other individual PAHs exhibited loss over time (SI Table S4.8). Overall, the highest depletion rate constant of 0.38 d^{-1} was observed for C_1- NAP in the 2.9 L treatment, while the lowest depletion rate of 0.0022 d^{-1} was observed for C_2-BNT (C_2-benzonaphthothiophene) in the 5.5 L treatment (Figure 4.3, SI Table S4.8).

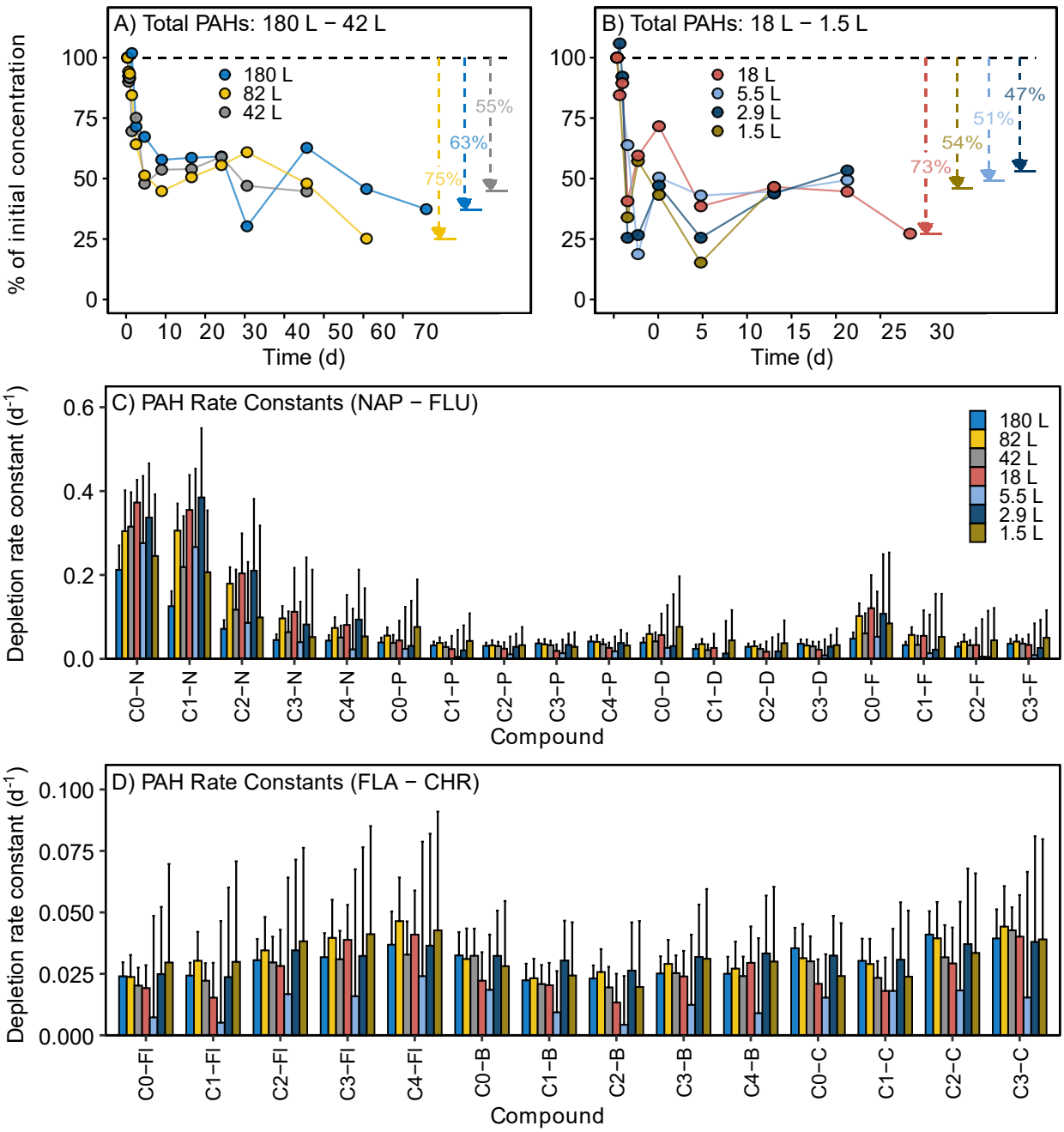

Figure 4. 3. Depletion of total PAHs in each dilbit amended treatment over time (A,B) and first order depletion rate constants of individual PAHs (C,D). Absolute rates are presented, error bars represent standard error of the slope coefficient. Missing data bars represent treatments where the specific analyte did not exhibit any degradation over time (i.e., $k>0$). Timelines of collected surface slick samples differ due to differences in dilbit submergence times.

Individual PAH regressions of the natural logarithm transformed concentration against time can be found in SI Table S4.8 and Figure S4.12. In general, the two-ringed NAP's had the highest depletion rate constants of all the PAHs, varying between 0.023 – 0.38 d^{-1} across all treatments. The three-ringed PAHs (phenanthrenes; PHE, dibenzothiophenes; DBT, and fluorenes; FLU) all had similar rate constants ranging from 0.00075 – 0.12 d^{-1} across each treatment. Finally, the four-ring PAHs (fluoranthenes; FLA, benzonaphthothiophenes; BNT, and chrysenes; CHR) had similar rate constants varying from 0.0042 to 0.046 d^{-1} across all treatments.

The level of alkylation had a significant impact on the depletion rate constants for both NAP and FLA (SI Figure S4.13 & Table S4.9). Rate constants within the NAP group significantly decreased with an increasing level of alkylation. This is likely driven by evaporation, where a decrease in vapor pressure is associated with greater molecular weight (Garrett et al., 1998). In the case of FLA and CHR, the opposite held true. In all treatments except for 2.9 L, rate constants increased with increased alkylation, suggesting that the more alkylated FLA's and CHR's were depleted faster than their lesser-alkylated counterparts, indicative of photooxidation (Aeppli et al., 2012; Charrié-Duhaut et al., 2000; Prince et al., 2003b).

Similar to *n*-alkanes, the depletion of PAHs in the respective dilbit slicks did not depend on the volume of dilbit spilled. This is contrary to our original hypothesis that the depletion rate constants would be inversely proportional to spill volume, especially for the more volatile components. Theoretically, thicker oil slicks (i.e., higher volume spilled) would lose components at a slower rate than thinner slicks because the thickness of the slick can limit mass transfer of compounds through the oil (Arey et al.,

2007; Gros et al., 2014).The observed error associated with our calculated rate constants is a plausible explanation for this discrepancy between observed and expected results. Larger standard error was significantly associated with the lower spill volumes for the majority of *n*-alkanes and all PAHs (SI Figure S4.14), overshadowing any effects of treatment.

We attribute the high standard error associated with rate constants, particularly in the lower volume treatments, with sample inconsistency. During the initial days of the study, the surface slicks in the higher volume spills formed a thick uniform film on the water's surface, whereas the slicks in the lower treatments spread very thin and were heterogeneous in appearance (SI Figure S4.15). Therefore, each collected sample from the lower treatment volumes was less uniform. This had a clear impact on the concentration over time profiles (Figure 4.1AB, Figure 4.2AB) and relatively low coefficient of determinations (R^2) accompanying total *n*-alkane and PAH rate constants (SI Table S4.6).

3.3. Comparison among hydrocarbon groups

In this study, the range of measured rate constants span three orders of magnitude across the hydrocarbon groups. Both the *n*-alkanes and PAHs had similar maximum observed rate constants that decreased with increasing chain length or molecular weight. The highest recorded rate constant of an *n*-alkane was 0.29 d^{-1} (*n*-C_9) in the 1.5 L treatment, whereas the highest PAH rate constant was 0.25 d^{-1} (C0-naphthalene), also in the 1.5 L treatment.

Previous small-scale lab and tank studies have begun to elucidate the depletion of hydrocarbons present in dilbit over time. King et al. (2014) performed CLB weathering

experiments in a flume tank using filtered seawater from the Bedford Basin, NS, Canada for 13 days. Cobanli et al. (2015) performed CLB degradation experiments in flasks using enriched microbial consortia obtained from seawater from the Douglas Channel and Hecate Strait, BC, Canada for 42 days. Deshpande et al. (2018) performed CLB degradation experiments in flasks using enriched microbial consortiums obtained from the Kalamazoo River oil spill site at 5 ºC and 25 ºC for 60 days. Comparisons between rate constants obtained from the present study and those listed above are found in Table S4.10. Our results for the depletion of total *n*-alkanes were similar to those from Cobanli et al. (2015), but different than the other studies. King et al. (2014) used a similar timeline to our study, however their rates for total *n*-alkane and PAH depletion were much lower than what was observed in our study. This difference could be due to the differences in oil spill volume to surface area ratios (V:SA). The resulting V:SA ratios in our study were between 4 and 400X (SI Table S4.11) lower than those employed in the study by King et al., (2014). Increased surface area can accelerate depletion by both biotic and abiotic degradation processes (Prince et al., 2003b; Yarranton et al., 2015) and is likely why our rates were much higher. The rate constants obtained by Deshpande et al. (2018) were roughly an order of magnitude greater than those calculated in our study. Here, the researchers used freshwater media that was inoculated with microbes that were previously enriched on dilbit, which would have accelerated degradation beyond rates that would be experienced in the natural environment.

3.4. Weathering Ratios

Weathering processes including evaporation, biodegradation, and photooxidation, can change the relative abundance of *n*-alkanes and PAHs in a dilbit slick over time. While these processes are often interlinked, detailed analysis of compositional changes allow us to discriminate among these processes. We determined the progressive weathering behaviour of the dilbit slicks by tracking diagnostic ratios of *n*-alkanes and alkylated PAHs that are indicative of different weathering processes (SI Table S4.3). A major change observed in the aliphatic content of collected dilbit slick samples was the decrease of *n*-alkanes in the $\leq n\text{-}C_{16}$ range relative to the larger compounds, presented as $\Sigma n\text{-}C_9 – n\text{-}C_{16} / \Sigma n\text{-}C_{22} – n\text{-}C_{32}$, adapted from Mudge (2016), in Figure 4.4A. This ratio decreased rapidly at the early stage in all treatments indicating that evaporation was a prominent weathering process acting on the dilbit surface slicks. Evaporation is of particular importance to dilbit as the loss of the lighter hydrocarbons can increase density and viscosity, and in some cases lead to submergence (King et al., 2017, 2014; Lee et al., 2015; NASEM, 2016; Stoyanovich et al., 2019) which we highlighted in a separate study (Stoyanovich et al., 2021).

We employed recently defined diagnostic ratios by Vergeynst et al., (2019) to distinguish between dissolution and other processes including: C_1N+C_2N/C_3N+C_4N, $C_1P+C2P/C3P$, C_2N/C_2F, and C_3N/C_3F. Figure 4.4BCEF shows each of these ratios decreasing rapidly with time in each of the dilbit amended treatments except for 180 L. These ratios reflect the lower susceptibility of larger, highly alkylated PAHs towards dissolution and biodegradation and greater susceptibility to photooxidation. Therefore, a decrease in these ratios can likely be attributed to either dissolution or biodegradation.

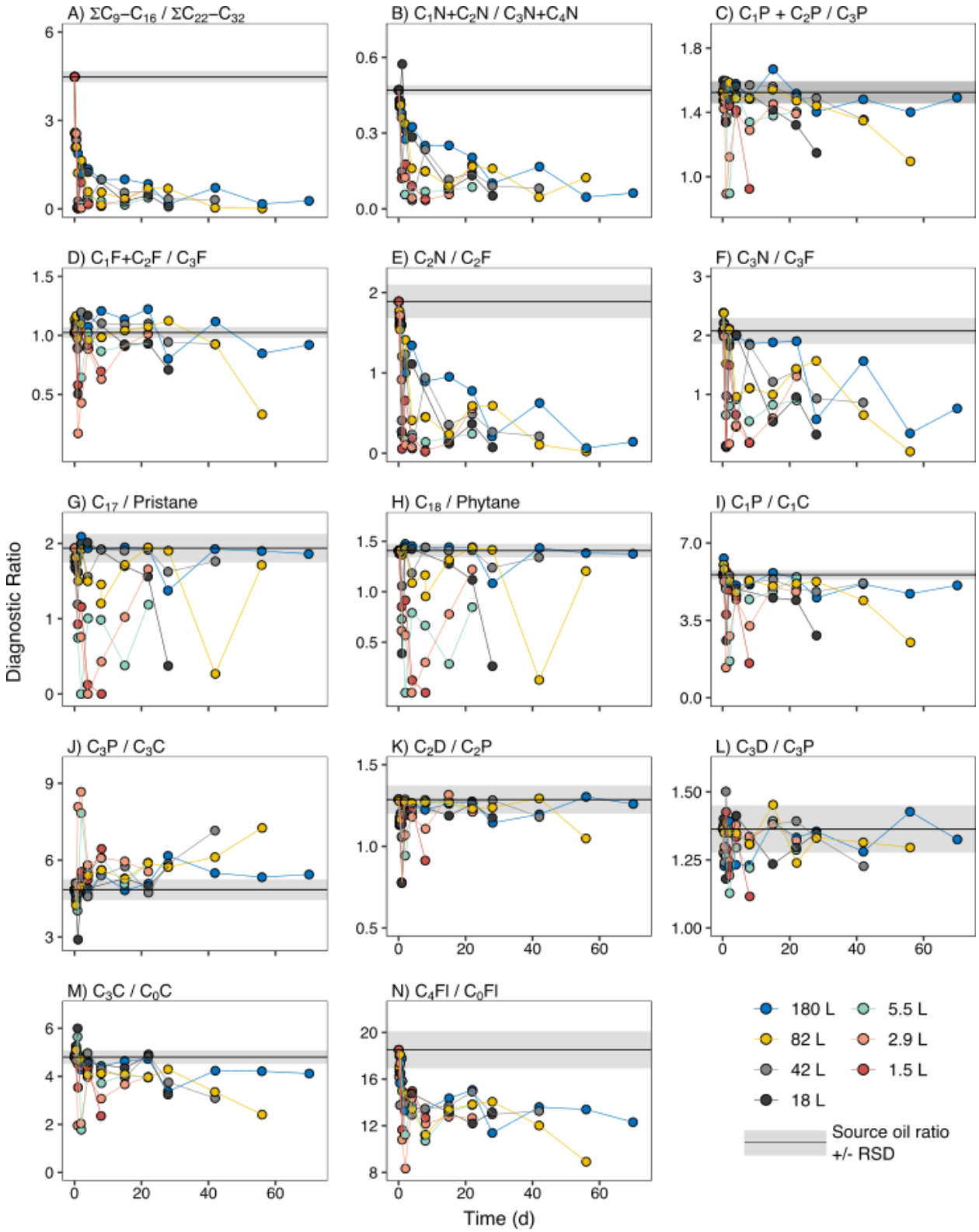

Figure 4. 4. Diagnostic weathering ratios of alkanes and PAHs. Solid black horizontal line represents the ratio in the source CLWB dilbit. The gray shaded area marks the ±RSD analytical uncertainty for each diagnostic ratio determined by calculating %RSD on the reference oil (n = 13).

For the three highest dilbit treatments (42, 82 and 180 L) treatments, the *n*-C_{17}/pris and *n*-C_{18}/phy ratios showed relatively constant values similar to that of the source dilbit at each time point except on days 8 and 28, where values dropped slightly below the range of %RSD (Figure 4.4GH). However, for the remaining treatments (18 – 1.5 L), the ratio values were quite variable. At some timepoints, these ratios decreased substantially, suggesting that biodegradation may have played a more important role in the removal of these shorter chain alkanes. Prince and Douglas (2005) note that as compounds approach detection limits, they will no longer provide reliable ratios. In the lower volume treatments, concentrations of *n*-C_{17}, *n*-C_{18}, pristane, and phytane all approach zero at multiple time points, suggesting these ratios may not be reliable indicators of biodegradation.

We observed a decrease of smaller C_1-PHE compared to larger C_1-CHR (Figure 4.4I) in each of the treatments as 2-ring PHE would be biodegraded at a faster rate than 4-ring CHR (Aeppli et al., 2012; Leblond et al., 2001). Another useful indicator of biodegradation is a decrease in the C_3-PHE/C_3-CHR ratio (Garrett et al., 1998), however in our study this ratio increased with time (Figure 4.4J), suggesting greater loss of the highly alkylated CHR compared to PHE. This discrepancy is likely attributed to photooxidation targeting the higher alkylated 4-ring PAHs such as C_3-CHR, discussed further below. Both C_2-DBT/C_2-PHE and C_3-DBT/C_3-PHE ratios remained relatively constant throughout the study duration in all the treatments (Figure 4.4KL), with only some cases of values below the %RSD range around the source dilbit. If microbes were degrading the oil slicks, we would expect to see the non-sulfur containing compounds (i.e., C_2-PHE and C_3-PHE) removed at a faster rate than the sulfur containing C_2-DBT

and C_3-DBT, and a resulting increase in the ratios (Olson et al., 2017), which was not the case in our study. These results therefore contrast the findings concluded from the *n*-C_{17}/pris and *n*-C_{18}/phy ratios in the lower volume treatments. Considering the previously discussed shortcomings of the *n*-alkane and isoprenoid relationship, the PAH ratios provide more concrete evidence that biodegradation was not an important weathering process observed in this study. Furthermore, given the pristine conditions of this boreal lake, the likelihood of hydrocarbon degrading bacteria being present at significant quantities is low (Atlas, 1981; Ron and Rosenberg, 2014) it is unlikely that any biodegradation of petrogenic hydrocarbons would occur. Instead, observed hydrocarbons depletions were likely driven by abiotic processes.

In contrast to biodegradation, evidence suggests alkylated PAHs are photooxidized at a faster rate than equivalent parent compounds (Garrett et al., 1998). For four ring PAHs including chrysene and fluoranthene, the parent compounds had lower degradation rates than the more alkylated congeners in most treatments, further supported by the decreasing trend of C_3-CHR/C_0-CHR and C_4-FLA/C_0-FLA (Figure 4.4MN). These findings are consistent with more rapid photooxidative loss in larger PAHs than smaller ones, and more rapid photooxidation of more alkylated PAHs than their less alkylated counterparts (Aeppli et al., 2012; Bacosa et al., 2015; Charrié-Duhaut et al., 2000; Garrett et al., 1998; Prince et al., 2003a).

The relative standard deviation (%RSD) for each weathering ratio measured over time can be used to assess which processes had the greatest impact on the slicks. The higher the %RSD, the more the ratio has changed with time (Wang et al., 2013). Ratios with %RSD <5% suggest are likely not affected by weathering, whereas %RSD >5%

suggests weathering is responsible for the observed variation (Li et al., 2009; Stout et al., 2001). Figure 4.5 demonstrates that aside from the ratios C_1P+C_2P/C_3 in 42 L, C_3D/C_3P in 82 and 2.9 L, and C_2D/C_2P in 180 L, all other ratios display changes over time across each treatment. Ratios with the highest RSD often involved LMW compounds including naphthalenes and short chain alkanes, which would be subject to early evaporation and dissolution processes. Whereas ratios involving higher molecular weight compounds would be more affected by biodegradation and photooxidation.

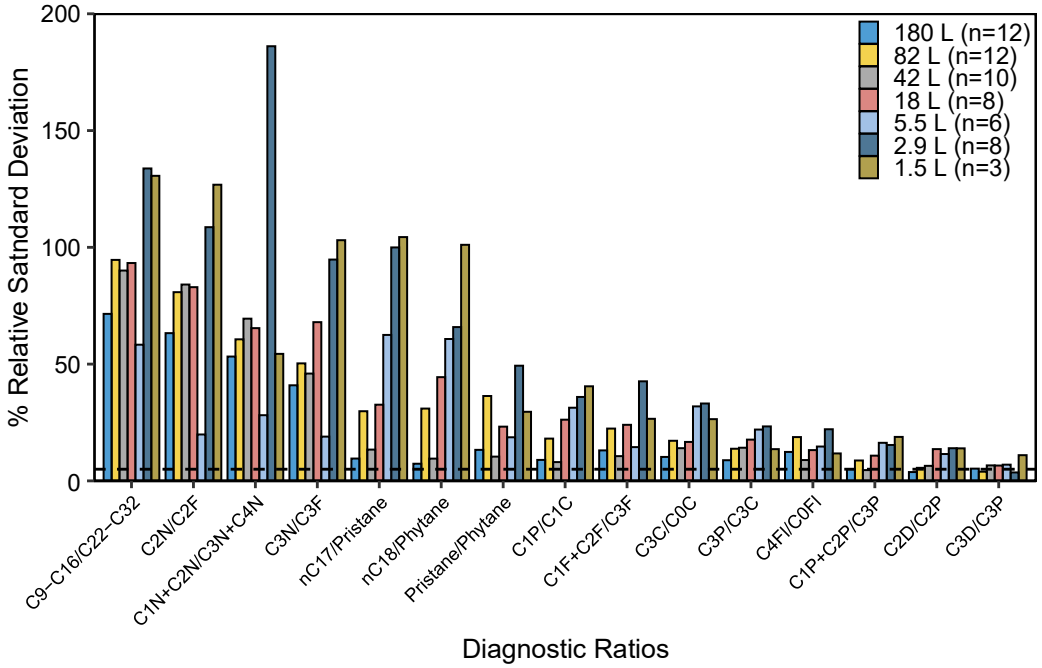

Figure 4. 5. Percent relative standard deviation (RSD) of selected analyte diagnostic ratios for dilbit samples collected from the water's surface between 6 h – 70 d after the experimental dilbit additions. Sample sizes for each treatment are in the legend. Fresh, unweathered CLB samples were not considered in this analysis. The RSD threshold value of 5% is labelled in the black dashed line.

Hydrocarbon weathering cannot be explained by a single process (SI Figure S4.16). Weathering alters the relative abundance of PAH compounds differently depending on ring number and alkylation. Biodegradation potential decreases with increasing ring number and, within a homologue series, increasing alkylation (Prince

and Douglas, 2005), whereas the opposite is true for photooxidation (Garrett et al., 1998). For PAHs, weathering patterns are difficult to discern because a combination of evaporation, dissolution, photooxidation, and biodegradation may be active (Vergeynst et al., 2019).

4 CONCLUSION

This study demonstrates the effects of prolonged environmental weathering on the composition of dilbit slicks under natural summer conditions of a Boreal-shield lake. It provides a unique first glimpse into the real-time fate of dilbit's constituents following a spill while providing novel findings for the immediate time points following a spill that are not typically monitored. We've shown that evaporation, dissolution, and photooxidation are prominent weathering processes under these conditions and biodegradation is not. This suggests that although bioremediation is a proven technique for spill management in marine systems, it may not be a viable option in pristine freshwater lakes such as those located in the Boreal shield of Canada. Finally, this study bridges the gap between weathering studies performed under non-realistic laboratory and tank conditions and the natural environment, which is ultimately the area most affected by a dilbit spill.

ACKNOWLEDGEMENTS

Funding for the present study was provided by a Natural Sciences and Engineering Research Council Strategic Partnership Grant (STPGP 493786-16 awarded to J.M. Blais, M. Hanson, and D.M. Orihel), a grant under the Oceans Protection Program, in-kind contributions from Environment and Climate Change Canada (ECCC), and in-kind support from the IISD-Experimental Lakes Area. A special thank you to J. Séguin, T. Black, J. Cederwall, L. Timlick, S. Patterson, J. Mason, D. Denton, H. Kosichek, K. Watson, and D. Dey for their contributions to the project.

SUPPORTING INFORMATION

1.0 SUPPLEMENTING MEATERIALS AND METHODS

1.1 Experimental Set Up

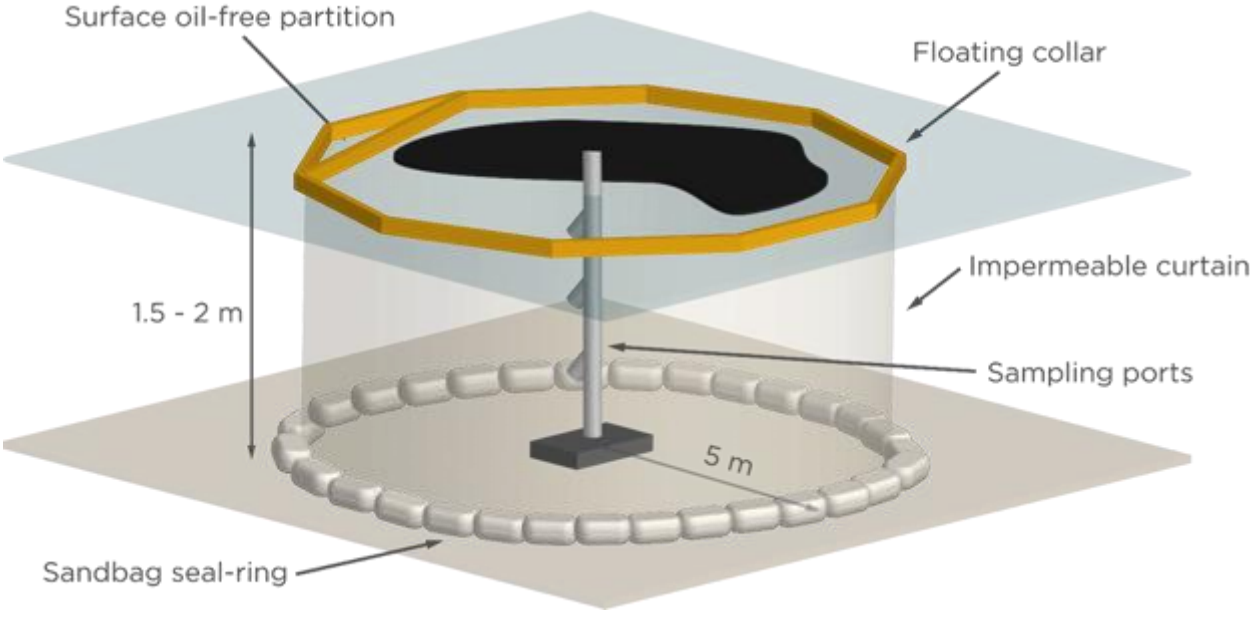

Figure S4. 1. Limnocorral design employed in the 2018 in-situ dilbit experiment.

See Shah et al., (2019) for an in-depth overview of the design and execution of the controlled dilbit spills. This study was carried out at the International Institute for Sustainable Development Experimental Lakes Area (IISD-ELA), a unique research station in northwestern Ontario, Canada, dedicated to holistic, interdisciplinary field research and ecosystem manipulation studies.

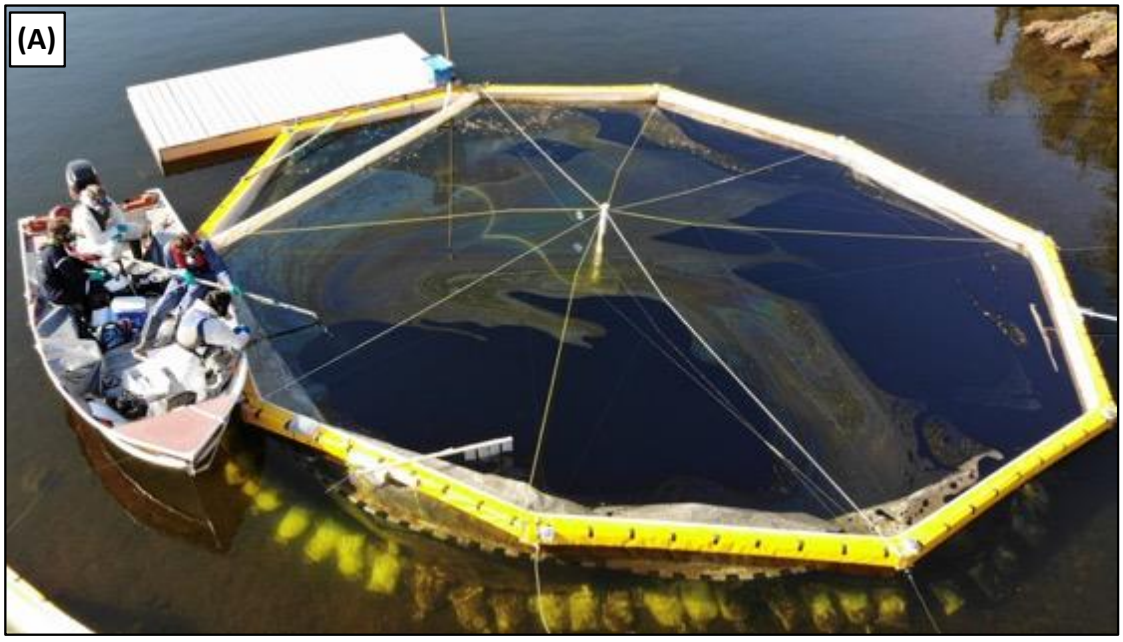

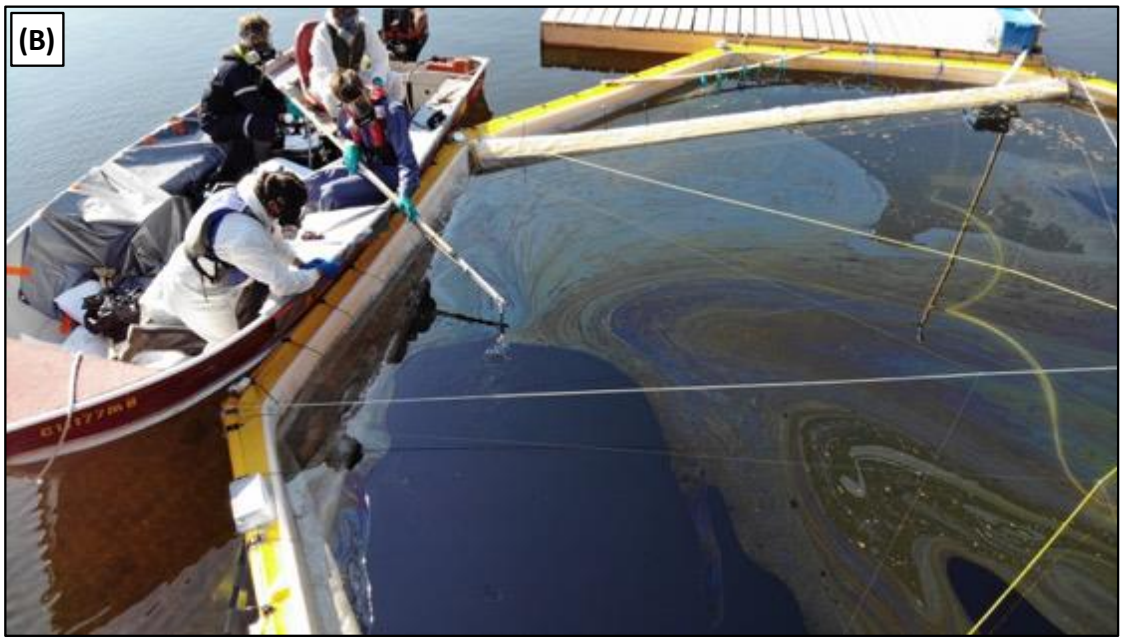

Figure S4. 2. The addition of 180 L of CLWB (1:590 oil:water, v/v) onto the water surface of the limnocorral. (A) Overview of addition method, (B) View of telescopic arm and pumping system being held at approximately 5 – 10 cm from the water's surface. The oil exited the hose parallel to the water's surface to avoid forcing oil below the water surface and allowing it to spread out during the addition.

1.2 Dilbit Slick Sampling

Figure S4.3 outlines the dilbit slick sampling regime employed in this study. The primary goal was to intensively sample the slicks early on in order to capture the early evaporative losses of volatile compounds and then to continue to monitor the slicks for the remainder of the study to assess any long-term changes in chemical distributions. Eventually due to density increases, each slick began to submerge at different onset times of 12 – 31 d and were completely submerged between 19 – 77 d, reported by Stoyanovich et al. (2021). This affected our ability to continue to collect dilbit samples from the water's surface according to the pre-defined sampling regime (SI Figure S4.3).

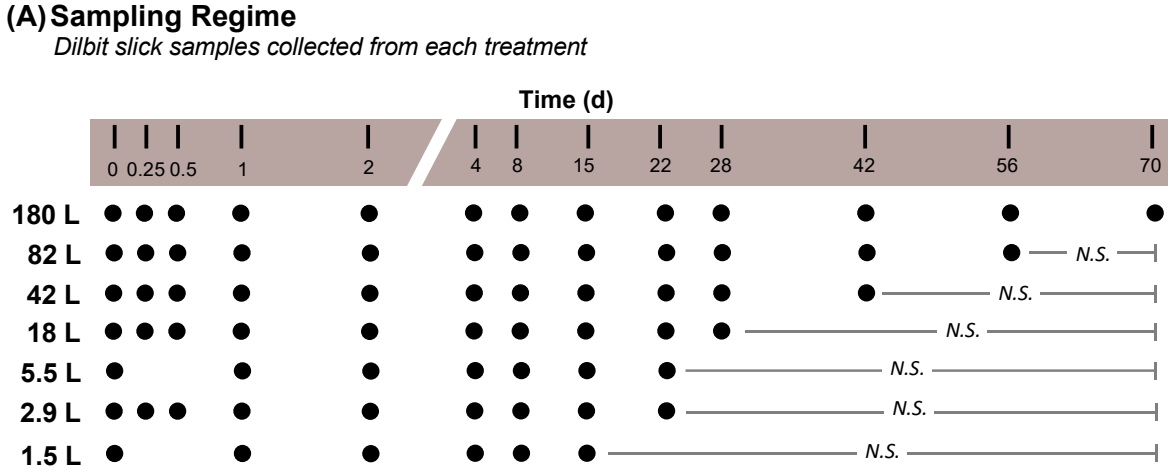

Figure S4. 3. Dilbit slick sampling regime employed throughout this study. Each black circle represents when a sample from each treatment was collected along the pre-determined sampling timeline. Following submergence of the surface slick, there was not sufficient floating dilbit remaining to be collected, and is marked as N.S., no sample. Samples were not collected in the 5.5 and 1.5 L treatments at 6 and 12 hours.

1.3 Analytical

Table S4. 1. Identified targets and abbreviations

n-Alkanes	Biomarker compounds		Alkylated PAHs	
n-C_9	C21 tricyclic terpane	C_{21}terpane	C_0-Naphthalene	C_0-N
n-C_{10}	C22 tricyclic terpane	C_{22}terpane	C_1-Naphthalenes	C_1-N
n-C_{11}	C23 tricyclic terpane	C_{23}terpane	C_2-Naphthalenes	C_2-N
n-C_{12}	C24 tricyclic terpane	C_{24}terpane	C_3-Naphthalenes	C_3-N
n-C_{13}	18α(H),21β(H)-22,29,30-trinorhopane	C_{27}Ts	C_4-Naphthalenes	C_4-N
2,6,10-trimethyldodecane (TMD)	17α(H),21β(H)-22,29,30-trinorhopane	C_{27}Tm	C_0-Phenanthrene/anthracene	C_0-P
n-C_{14}	17α(H),21β(H)-30-norhopane	C_{29}αβ hopane	C_1-Phenanthrenes/anthracenes	C_1-P
n-C_{15}	17α(H),21β(H)-hopane	C_{30}αβ hopane	C_2-Phenanthrenes/anthracenes	C_2-P
n-C_{16}	22*S*-17α(H),21β(H)-30-homohopane	C_{31}(S) hopane	C_3-Phenanthrenes/anthracenes	C_3-P
2,6,10-trimethylpentadecane (TMP)	22*R*-17α(H),21β(H)-30-homohopane	C_{31}(R) hopane	C_4-Phenanthrenes/anthracenes	C_4-P
n-C_{17}	22*S*-17α(H),21β(H)-30,31-bishomohopane	C_{32}(S) hopane	C_0-Dibenzothiophene	C_0-D
Pristane	22*R*-17α(H),21β(H)-30,31-bishomohopane	C_{32}(R) hopane	C_1-Dibenzothiophenes	C_1-D
n-C_{18}	22*S*-17α(H),21β(H)-30,31,32-trishomohopane	C_{33}(S) hopane	C_2-Dibenzothiophenes	C_2-D
Phytane	22*R*-17α(H),21β(H)-30,31,32-trishomohopane	C_{33}(R) hopane	C_3-Dibenzothiophenes	C_3-D
n-C_{19}	22*S*-17α(H),21β(H)-30,31,32,33-tetrakishomohopane	C_{34}(S) hopane	C_0-Fluorene	C_0-F
n-C_{20}	22*R*-17α(H),21β(H)-30,31,32,33-tetrakishomohopane	C_{34}(R) hopane	C_1-Fluorenes	C_1-F
n-C21	22S-17α(H),21β(H)-30,31,32,33,34-pentakishomohopane	C_{35}(S) hopane	C_2-Fluorenes	C_2-F
n-C_{22}	22*R*-17α(H),21β(H)-30,31,32,33,34-pentakishomohopane	C_{35}(R) hopane	C_3-Fluorenes	C_3-F
n-C_{23}	C_{27} 20-5α(H),14β(H),17β(H)-cholestane	C_{27}αββ sterane	C_0-Fluroanthene/pyrene	C_0-Fl
n-C_{24}	C_{28} 20-5α(H),14β(H),17β(H)-ergostane	C_{28}αββ sterane	C_1-Fluroanthenes/pyrenes	C_1-Fl
n-C_{25}	C_{29} 20-5α(H),14β(H),17β(H)-stigmastane	C_{29}αββ sterane	C_2-Fluroanthenes/pyrenes	C_2-Fl
n-C_{26}			C_3-Fluroanthenes/pyrenes	C_3-Fl
n-C_{27}			C_4-Fluroanthenes/pyrenes	C_4-Fl
n-C_{28}			C_0-Benzonaphthothiophenes	C_0-B
n-C_{29}			C_1-Benzonaphthothiophenes	C_1-B
n-C_{30}			C_2-Benzonaphthothiophenes	C_2-B
n-C_{31}			C_3-Benzonaphthothiophenes	C_3-B
n-C_{32}			C_4-Benzonaphthothiophenes	C_4-B
n-C_{33}			C_0-Chrysene	C_0-C
n-C_{34}			C_1-Chrysenes	C_1-C
n-C_{35}			C_2-Chrysenes	C_2-C
n-C_{36}			C_3-Chrysenes	C_3-C
n-C_{37}			Biphenyl	Bph
n-C_{38}			Acenaphthylene	Acl
n-C_{39}			Acenaphthene	Ace
n-C_{40}			Anthracene	An
			Fluoranthene	Fl
			Pyrene	Py
			Benz(a)anthracene	BaA
			Benzo(b)fluoranthene	BbF
			Benzo(k)fluoranthene	BkF
			Benzo(e)pyrene	BeP
			Benzo(a)pyrene	BaP
			Perylene	Pe
			Indeno(1,2,3-cd)pyrene	IP
			Dibenzo(a,h)anthracene	DA
			Benzo(g,h,i)perylene	BgP

Table S4. 2. Relative standard deviation (%RSD) for each individual analyte measured in reference oil (13.1% Prudhoe Bay Crude Oil) throughout the analytical period of the experimental samples (n = 13).

n-Alkane	%RSD	Alkyl PAH	%RSD	EPA PAH	%RSD	Biomarker	%RSD
n-C9	11	C0-N	14	Bph	32	C21 T	13
n-C10	11	C1-N	14	Acl	33	C22 T	22
n-C11	11	C2-N	14	Ace	32	C23 T	14
n-C12	13	C3-N	13	An	35	C24 T	13
n-C13	23	C4-N	11	Fl	37	C27 Ts	12
TMD	71	C0-P	12	Py	37	C27 Tm	10
n-C14	13	C1-P	12	BaA	35	C29 aß H	11
n-C15	14	C2-P	11	BbF	36	C30 aß H	11
n-C16	13	C3-P	14	BkF	NA	C31 (S) H	26
TMP	9	C4-P	13	BeP	34	C31 (R) H	14
n-C17	11	C0-D	12	BaP	43	GAM	NA
Pristane	19	C1-D	13	Pe	35	C32 (S) H	12
n-C18	13	C2-D	12	IP	37	C32 (R) H	14
Phytane	10	C3-D	12	DA	36	C33 (S) H	11
n-C19	13	C0-F	12	BgP	35	C33 (R) H	17
n-C20	13	C1-F	14			C34 (S) H	12
n-C21	13	C2-F	16			C34 (R) H	27
n-C22	13	C3-F	15			C35 (S) H	17
n-C23	13	C0-Fl	14			C35 (R) H	16
n-C24	15	C1-Fl	12			C27 aßß S	30
n-C25	11	C2-Fl	27			C28 aßß S	14
n-C26	12	C3-Fl	12			C29 aßß S	15
n-C27	10	C4-Fl	11				
n-C28	12	C0-B	27				
n-C29	11	C1-B	17				
n-C30	13	C2-B	18				
n-C31	12	C3-B	18				
n-C32	13	C4-B	15				
n-C33	15	C0-C	13				
n-C34	17	C1-C	12				
n-C35	21	C2-C	12				
n-C36	22	C3-C	14				
n-C37	28						
n-C38	32						
n-C39	37						
n-C40	40						

2.4 Weathering Ratio Analysis

Table S4. 3. Commonly used weathering ratios to elucidate the role of different weathering processes acting on surface slicks

#	Ratio	Description
	Evaporation	
1	*n*-C_9 – *n*-C_{16} / *n*-C_{22} – *n*-C_{32}	(1) Values at time "0" should be high and decrease rapidly early on indicating the preferential loss of the more volatile compounds relative to the non-volatile constituents (Miller and Mudge, 1997; Mudge, 2016).
	Photooxidation/ Dissolution + Biodegradation	
2	$C_{1+2}N$ / $C_{3+4}N$	(2 – 6) PAHs with more alkylation and aromatic rings are less susceptible to dissolution, biodegradation, and evaporation and more susceptible to photooxidation. Therefore a decreasing ratio indicates dissolution + biodegradation + evaporation whereas an increasing ratio indicates photooxidation (Vergeynst et al., 2019b).
3	$C_{1+2}P$ / $C_{3+4}P$	
4	$C_{1+2}D$ / C_3D	
5	$C_{1+2}F$ / C_3F	
6	C_2N / C_2F C_3N / C_3F	
	Biodegradation	
7	*n*-C_{17} / pristane	(7-9) Branched isoprenoids (pristane, phytane) are more recalcitrant than their straight chain counterparts (*n*-C_{17}, *n*-C_{18}), a decrease in these ratios is evidence of biodegradation (Christensen and Larsen, 1993; Mudge, 2016). The preferential removal of shorter over longer branched alkanes is also diagnostic for biodegradation (Vergeynst et al., 2019a; Wang et al., 1998).
8	*n*-C_{18} / phytane	
9	C_1P / C_1C	(10) A decrease of smaller PAH such as phenanthrene compared to chrysene is indicative of biodegradation (Aeppli et al., 2012; Leblond et al., 2001)
10	C_3P / C_3C	(11) C_3 phenanthrene (2 rings) would be biodegraded at a faster rate than C_3 chrysene (4 rings). A decrease in their ratio is a useful indicator of biodegradation (Garrett et al., 1998).
11	C_2D/C_2P	
12	C_3D/C_3P	(12 – 13) A decrease in ratios of sulfur containing to non-sulfur containing PAHs of similar molecular weight is indicative of biodegradation, whereas no observable change is indicative of physical weathering (Olson et al., 2017).
	Photooxidation	
13	C_3C / C_0C	(14 – 15) Larger PAHs lost before smaller ones, and more alkylated PAHs lost before less alkylated congeners (i.e., decrease in ratio) are patterns indicative of photooxidative loss (Charrié-Duhaut et al., 2000; Lima et al., 2005; Prince et al., 2003)
14	C_4Fl / C_0Fl	

Table S4. 4. Relative standard deviation (%RSD) for each individual weathering ratio measured in the reference oil (13.1% Prudhoe Bay Crude Oil) throughout the analytical period of the experimental samples (n = 13).

Ratio	%RSD
1	4.3
2	4.1
3	4.5
4	4.5
5	11.1
6	10.7
7	9.8
8	4.7
9	10.4
10	3.8
11	8.4
12	6.7
13	6.4
14	5.9
15	8.6
Average	**6.9**
Sd	**2.7**

2.0 SUPPLEMENTING RESULTS AND DISCUSSION

2.1 Crude Oil characteristics

We quantified the concentrations of various groups of *n*-alkanes, PAHs and petroleum biomarkers (see Table S1) in the fresh CLWB source dilbit Figure S3.5). The same set of compounds were also quantified for a reference oil (13.1% weathered Prudhoe Bay Crude).

Fresh, unweathered CLWB has density and viscosity values of 0.9215 g mL^{-1} and 547 mPa·S at 0 °C and 0.9320 g mL^{-1} and 181 mPa·S at 15 °C, with an API gravity value of 21.5 (SI Table S5). The *n*-alkane profile of the fresh dilbit shows a decreasing trend in quantity from low (LMW) to high (HMW) molecular weight compounds (*n*-C_9 – *n*-C_{40}), where the LMW compounds are most abundant (SI Figure S4.5A). This can be

attributed to the dilution of crude bitumen (70 – 80 %) with LMW gas condensates (20 – 30 %) to produce diluted bitumen (Yang et al. 2016). Out of the 46 PAHs evaluated, the chemical fingerprint of CLWB demonstrates an enrichment in the alkylated homologs in comparison to the unsubstituted parent compounds (SI Figure S4.5B) consistent with its petrogenic origin and low geologic heat present during formation (Yang et al. 2011; Stout and Wang 2016). In general, the distribution of alkylated forms in each PAH group follows a "bell shape", which is characteristic of most crude oils (Stogiannidis and Laane 2015; Stout and Wang 2016). The US priority PAHs were at such low concentrations in the source CLWB (0.26 – 13.4 μg g oil^{-1}) that their concentrations are negligible and were not described in this study.

Table S4. 5. Physical properties of the studied CLWB dilbit

Measurement	Mean ± SD (n =3)
Density at 15°C (g mL^{-1})	0.9215 ± 0.0003
Density at 0 °C (g mL^{-1})	0.932 ± 0
API Gravity	21.5
Viscosity at 15 °C (mPa·S)	181 ± 0.2
Viscosity at 0 °C (mPa·S)	547 ± 0.5
Flash Point (°C)	-6 ± 0
Pour Point (°C)	-43 ± 3
Sulfur Content (%)	3.3 ± 0.01

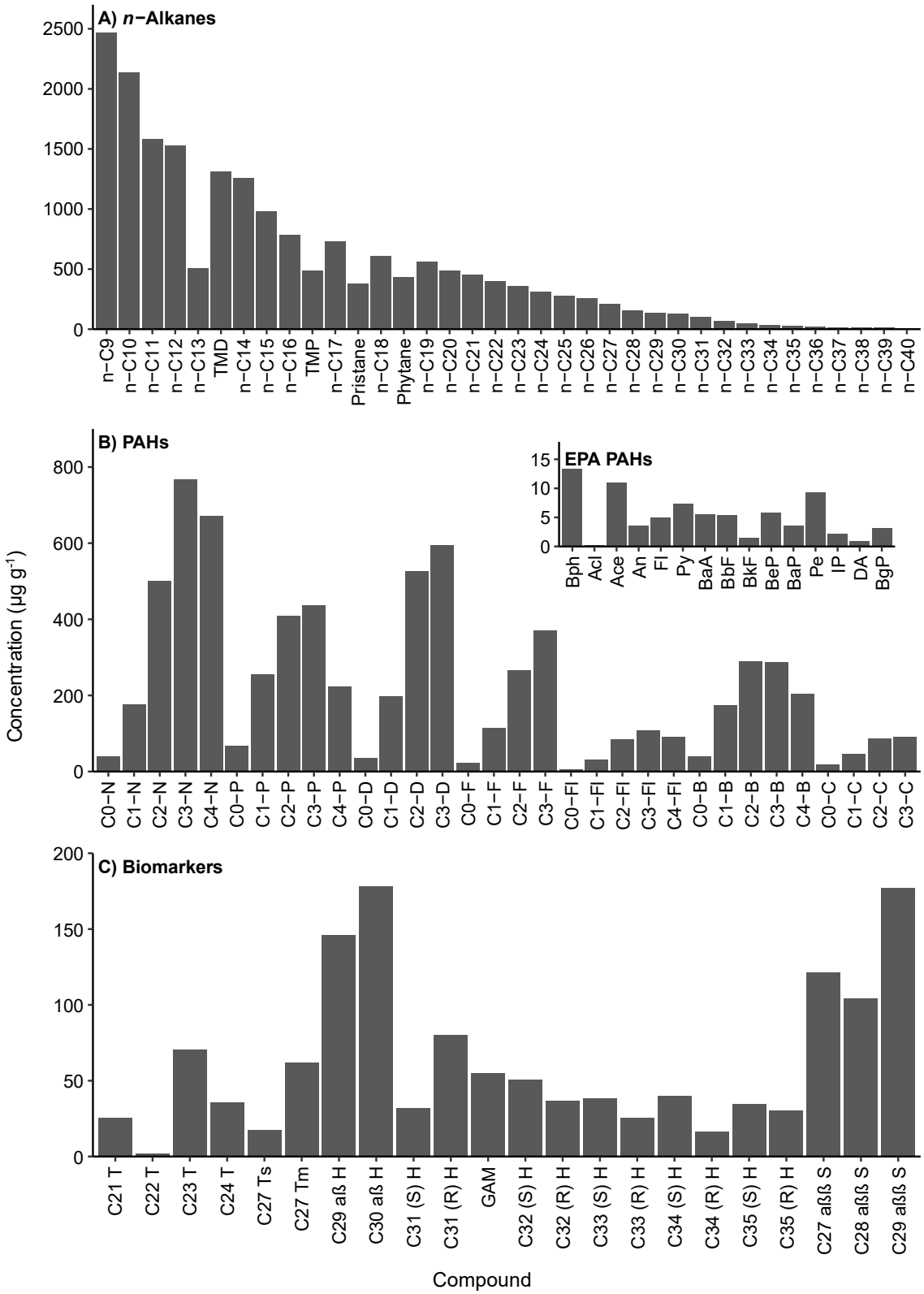

Figure S4. 4. Chemical composition of CLWB used in this study. A) n-alkanes, B) aromatics, and C) petroleum biomarkers.

Table S4. 6. Total n-alkane and PAH depletion rate constants measured in each of the dilbit amended treatments. Negative values represent depletion rates. SE represents the standard error associated with the rate constant.

Treatment	Total *n*-alkanes			Total PAHs		
	k **(d^{-1})**	**SE**	**R^2**	***k*** **(d^{-1})**	**SE**	**R^2**
180 L	-0.041	0.020	0.41	-0.037	0.010	0.69
82 L	-0.071	0.031	0.46	-0.049	0.016	0.61
42 L	-0.044	0.032	0.24	-0.038	0.015	0.51
18 L	-0.064	0.052	0.20	-0.042	0.023	0.35
5.5 L	-0.047	0.130	0.03	-0.019	0.048	0.04
2.9 L	-0.093	0.082	0.18	-0.045	0.045	0.14
1.5 L	-0.094	0.140	0.10	-0.041	0.051	0.14

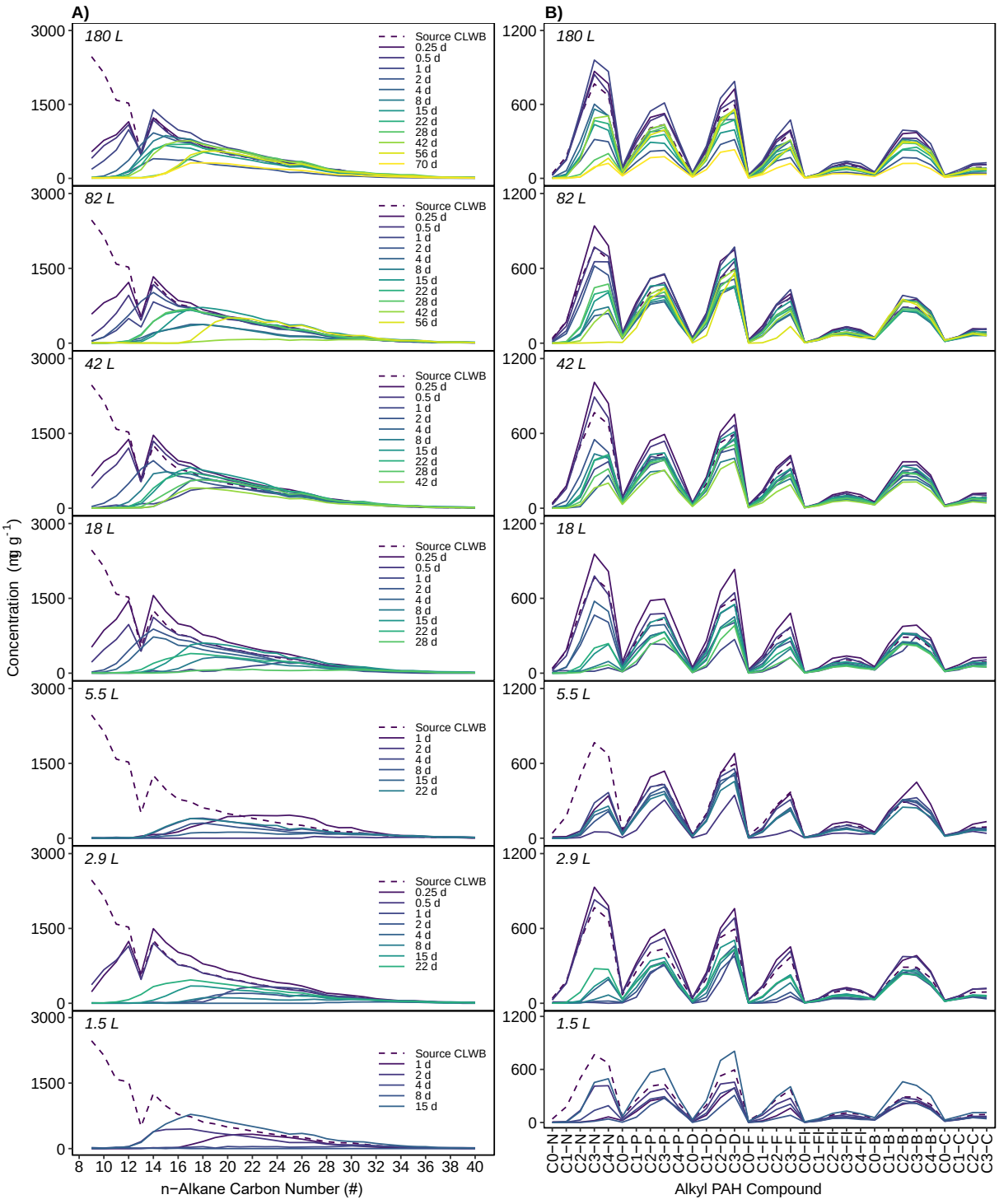

Figure S4. 5. Concentrations of n-alkanes (A) and alkylated PAHs (B) in surface dilbit-slick samples collected during the 70-day study in each of the seven dilbit-amended treatments. Legends presented in panel A are shared with panel B. Temporal trends in sample collection differ in each treatment (ex: 0 – 70 d for 180L, 0 – 15 d for 1.5 L) due to submergence of floating slicks.

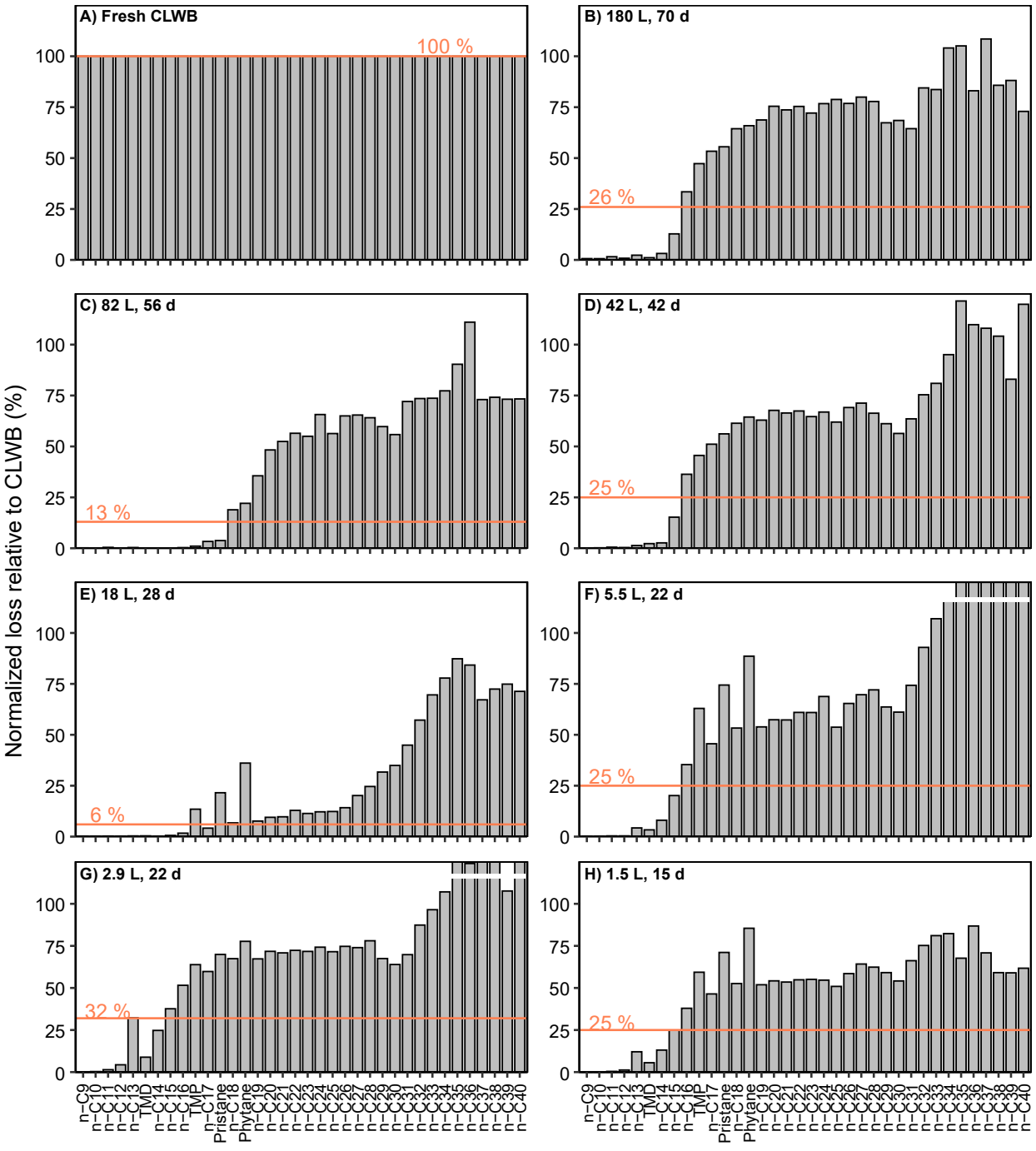

Figure S4. 6. N-Alkane loss in dilbit slick samples during weathering. Concentrations were normalized to C_{30} $\alpha\beta$ Hopane. Horizontal red lines represent the total *n*-alkane loss relative to the CLWB dilbit. Each panel corresponds to the final sampling day of that particular treatment. Final sampling days vary due to submergence of the dilbit slicks which limited surface sample collection. Broken bars represent percentages greater than 150%.

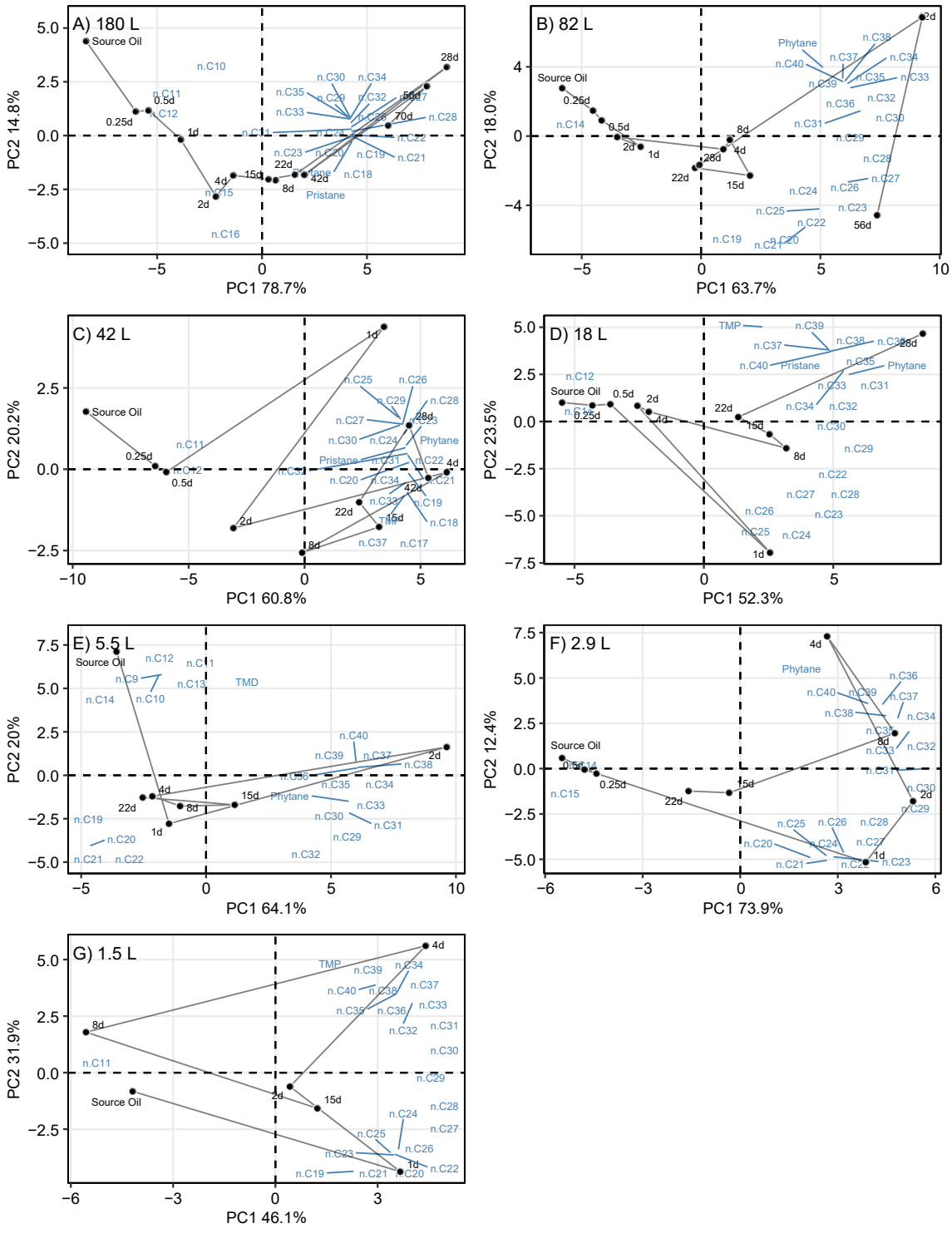

Figure S4. 7. Principal component analysis of n-alkane profiles normalized Hopane in dilbit slick samples collected throughout the entire study from each treatment.

Table S4. 7. First order rate constants (± standard error) for individual n-alkanes in each of the dilbit amended treatments. Cases when concentrations of the individual compounds in the dilbit slicks were below detection limits were omitted from the computation of rate coefficients. Negative rate constants identify cases of depletion whereas positive rate constants identify cases of no observable depletion.

Compound	*k* (d^{-1}) ± SE						
	1.5 L	2.9 L	5.5 L	18 L	42 L	82 L	180 L
n-C_9	-0.293 ± 0.226	-0.337 ± 0.164	-0.3 ± 0.243	-0.33 ± 0.135	-0.39 ± 0.133	-0.296 ± 0.132	-0.323 ± 0.132
n-C_{10}	-0.288 ± 0.237	-0.404 ± 0.184	-0.318 ± 0.253	-0.397 ± 0.111	-0.409 ± 0.128	-0.387 ± 0.115	-0.316 ± 0.113
n-C_{11}	-0.237 ± 0.182	-0.354 ± 0.149	-0.277 ± 0.202	-0.372 ± 0.076	-0.329 ± 0.103	-0.339 ± 0.094	-0.226 ± 0.075
n-C_{12}	-0.194 ± 0.206	-0.379 ± 0.19	-0.272 ± 0.232	-0.41 ± 0.082	-0.264 ± 0.142	-0.368 ± 0.065	-0.153 ± 0.049
n-C_{13}	-0.039 ± 0.202	-0.234 ± 0.187	-0.212 ± 0.154	-0.244 ± 0.129	-0.114 ± 0.119	-0.241 ± 0.036	-0.019 ± 0.012
TMD	-0.158 ± 0.213	-0.256 ± 0.185	-0.121 ± 0.145	-0.292 ± 0.096	-0.154 ± 0.126	-0.245 ± 0.054	-0.118 ± 0.046
n-C_{14}	-0.074 ± 0.201	-0.196 ± 0.204	-0.231 ± 0.104	-0.22 ± 0.102	-0.075 ± 0.111	-0.182 ± 0.034	-0.051 ± 0.017
n-C_{15}	-0.045 ± 0.238	-0.111 ± 0.216	-0.151 ± 0.09	-0.124 ± 0.112	-0.03 ± 0.068	-0.107 ± 0.031	-0.026 ± 0.012
n-C_{16}	-0.037 ± 0.198	-0.055 ± 0.18	-0.134 ± 0.068	-0.063 ± 0.091	-0.011 ± 0.037	-0.062 ± 0.026	-0.015 ± 0.009
TMP	-0.042 ± 0.146	-0.043 ± 0.103	0.03 ± 0.136	-0.042 ± 0.073	-0.013 ± 0.019	-0.034 ± 0.017	-0.015 ± 0.01
n-C_{17}	0.019 ± 0.129	-0.039 ± 0.132	-0.108 ± 0.048	-0.033 ± 0.06	-0.007 ± 0.021	-0.043 ± 0.022	-0.014 ± 0.007
Pristane	-0.026 ± 0.094	0.034 ± 0.126	0.02 ± 0.095	-0.026 ± 0.054	-0.017 ± 0.012	-0.031 ± 0.013	-0.018 ± 0.009
n-C_{18}	0.008 ± 0.102	-0.027 ± 0.111	-0.103 ± 0.033	0.002 ± 0.071	-0.003 ± 0.013	-0.028 ± 0.018	-0.01 ± 0.007
Phytane	-0.018 ± 0.073	0.021 ± 0.073	0.023 ± 0.074	-0.008 ± 0.038	-0.008 ± 0.006	-0.016 ± 0.009	-0.012 ± 0.008
n-C_{19}	-0.002 ± 0.148	-0.052 ± 0.074	-0.107 ± 0.024	0.004 ± 0.063	-0.004 ± 0.011	-0.025 ± 0.018	-0.01 ± 0.008
n-C_{20}	-0.011 ± 0.089	-0.063 ± 0.057	-0.105 ± 0.014	-0.002 ± 0.041	-0.002 ± 0.008	-0.021 ± 0.017	-0.007 ± 0.007
n-C_{21}	-0.015 ± 0.094	-0.072 ± 0.052	-0.104 ± 0.015	-0.006 ± 0.034	-0.003 ± 0.007	-0.023 ± 0.018	-0.008 ± 0.007
n-C_{22}	-0.016 ± 0.083	-0.072 ± 0.051	-0.103 ± 0.016	-0.01 ± 0.026	-0.002 ± 0.007	-0.02 ± 0.019	-0.006 ± 0.007
n-C_{23}	-0.016 ± 0.084	-0.075 ± 0.048	-0.108 ± 0.018	-0.016 ± 0.022	-0.004 ± 0.007	-0.023 ± 0.02	-0.01 ± 0.006
n-C_{24}	-0.017 ± 0.077	-0.074 ± 0.053	-0.114 ± 0.024	-0.018 ± 0.021	-0.011 ± 0.009	-0.024 ± 0.025	-0.011 ± 0.008
n-C_{25}	-0.019 ± 0.083	-0.082 ± 0.051	-0.115 ± 0.032	-0.032 ± 0.02	-0.019 ± 0.011	-0.031 ± 0.027	-0.017 ± 0.013
n-C_{26}	-0.01 ± 0.079	-0.081 ± 0.043	-0.107 ± 0.028	-0.021 ± 0.019	-0.015 ± 0.008	-0.02 ± 0.025	-0.007 ± 0.01
n-C_{27}	-0.007 ± 0.065	-0.063 ± 0.036	-0.041 ± 0.086	-0.019 ± 0.018	-0.013 ± 0.008	-0.016 ± 0.02	-0.006 ± 0.011
n-C_{28}	-0.007 ± 0.053	-0.064 ± 0.065	-0.031 ± 0.086	-0.016 ± 0.018	-0.014 ± 0.007	-0.016 ± 0.018	-0.007 ± 0.01
n-C_{29}	-0.009 ± 0.038	-0.066 ± 0.058	-0.012 ± 0.092	-0.025 ± 0.02	-0.02 ± 0.009	-0.011 ± 0.02	-0.02 ± 0.016
n-C_{30}	-0.012 ± 0.033	-0.057 ± 0.043	-0.023 ± 0.083	-0.022 ± 0.022	-0.02 ± 0.011	-0.015 ± 0.015	-0.015 ± 0.014
n-C_{31}	0.001 ± 0.034	-0.043 ± 0.037	-0.005 ± 0.083	-0.01 ± 0.029	-0.004 ± 0.007	-0.009 ± 0.012	-0.003 ± 0.014
n-C_{32}	0.007 ± 0.033	-0.036 ± 0.029	0.018 ± 0.091	-0.001 ± 0.022	-0.002 ± 0.006	-0.004 ± 0.009	0.002 ± 0.015
n-C_{33}	0.013 ± 0.04	-0.027 ± 0.025	0.018 ± 0.063	0.006 ± 0.028	0.007 ± 0.009	0.003 ± 0.01	0.011 ± 0.016
n-C_{34}	0.016 ± 0.051	-0.023 ± 0.021	0.023 ± 0.05	0.005 ± 0.029	0.007 ± 0.007	0.011 ± 0.008	0.015 ± 0.016
n-C_{35}	0.003 ± 0.059	-0.019 ± 0.026	0.004 ± 0.05	0.025 ± 0.042	-0.002 ± 0.014	0.024 ± 0.018	0.025 ± 0.021
n-C_{36}	0.022 ± 0.046	-0.026 ± 0.026	0.012 ± 0.032	0.001 ± 0.019	0.011 ± 0.012	0.002 ± 0.017	-0.001 ± 0.018
n-C_{37}	-0.002 ± 0.045	-0.042 ± 0.02	0.029 ± 0.023	0.005 ± 0.024	0.029 ± 0.02	0.015 ± 0.014	0.033 ± 0.028
n-C_{38}	-0.009 ± 0.055	-0.063 ± 0.029	0.037 ± 0.026	0.014 ± 0.023	0.029 ± 0.018	0.01 ± 0.012	0.044 ± 0.035
n-C_{39}	-0.041 ± 0.012	-0.026 ± 0.016	0.044 ± 0.026	0.005 ± 0.027	0.024 ± 0.019	0.018 ± 0.017	0.036 ± 0.036
n-C_{40}	-0.046 ± 0.024	-0.065 ± 0.028	0.031 ± 0.018	0.01 ± 0.022	0.03 ± 0.011	0.039 ± 0.018	0.042 ± 0.038

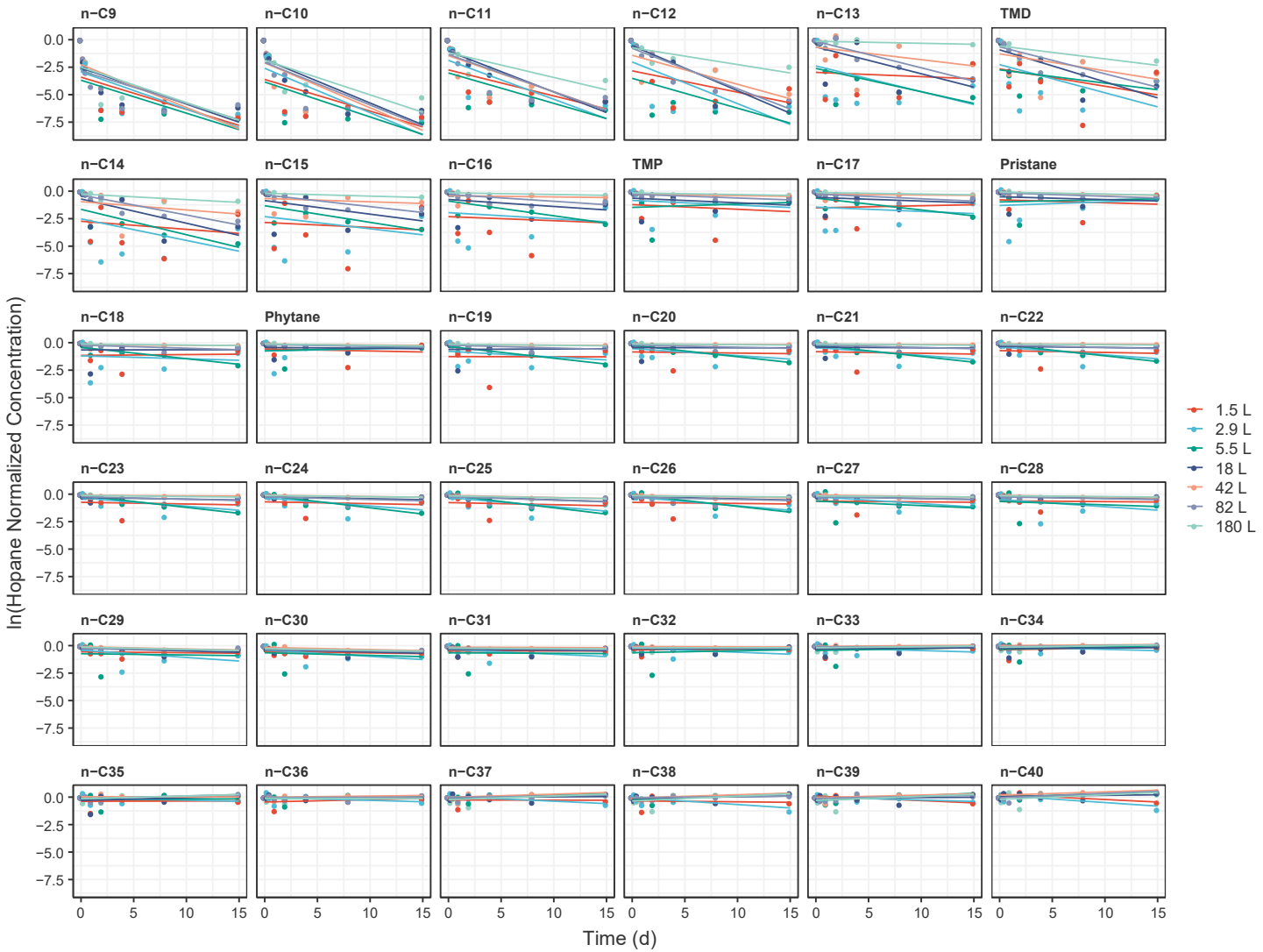

Figure S4. 8. Linear regressions of natural logarithm transformed n-alkane normalized concentrations over time during the first 15 days of the study.

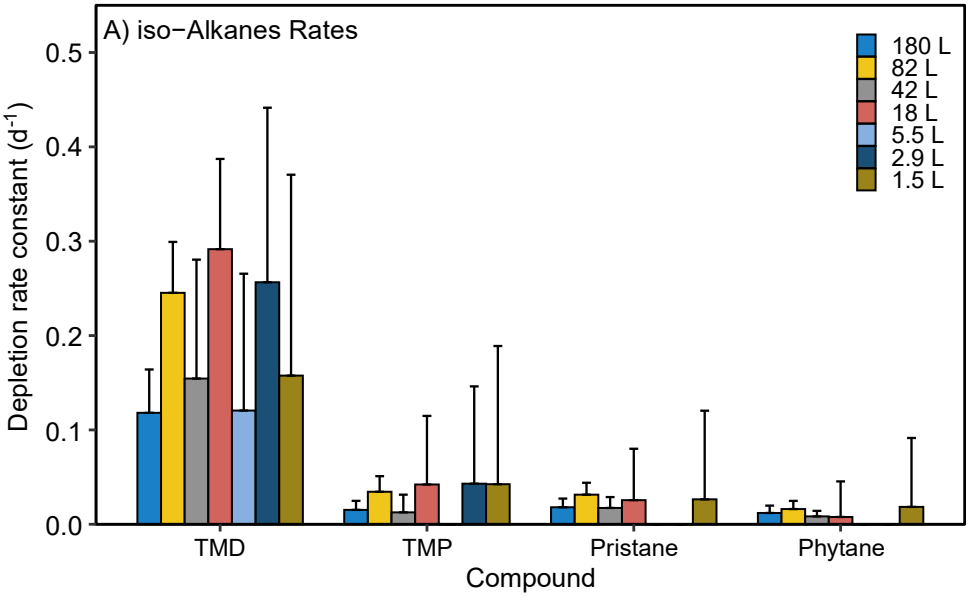

Figure S4. 9. Rate constants of isoprenoid alkanes. No significant relationship between spill volume and rate constants was observed for any of the isoprenoid alkanes. Missing data bars represent treatments where the specific analyte did not exhibit any degradation.

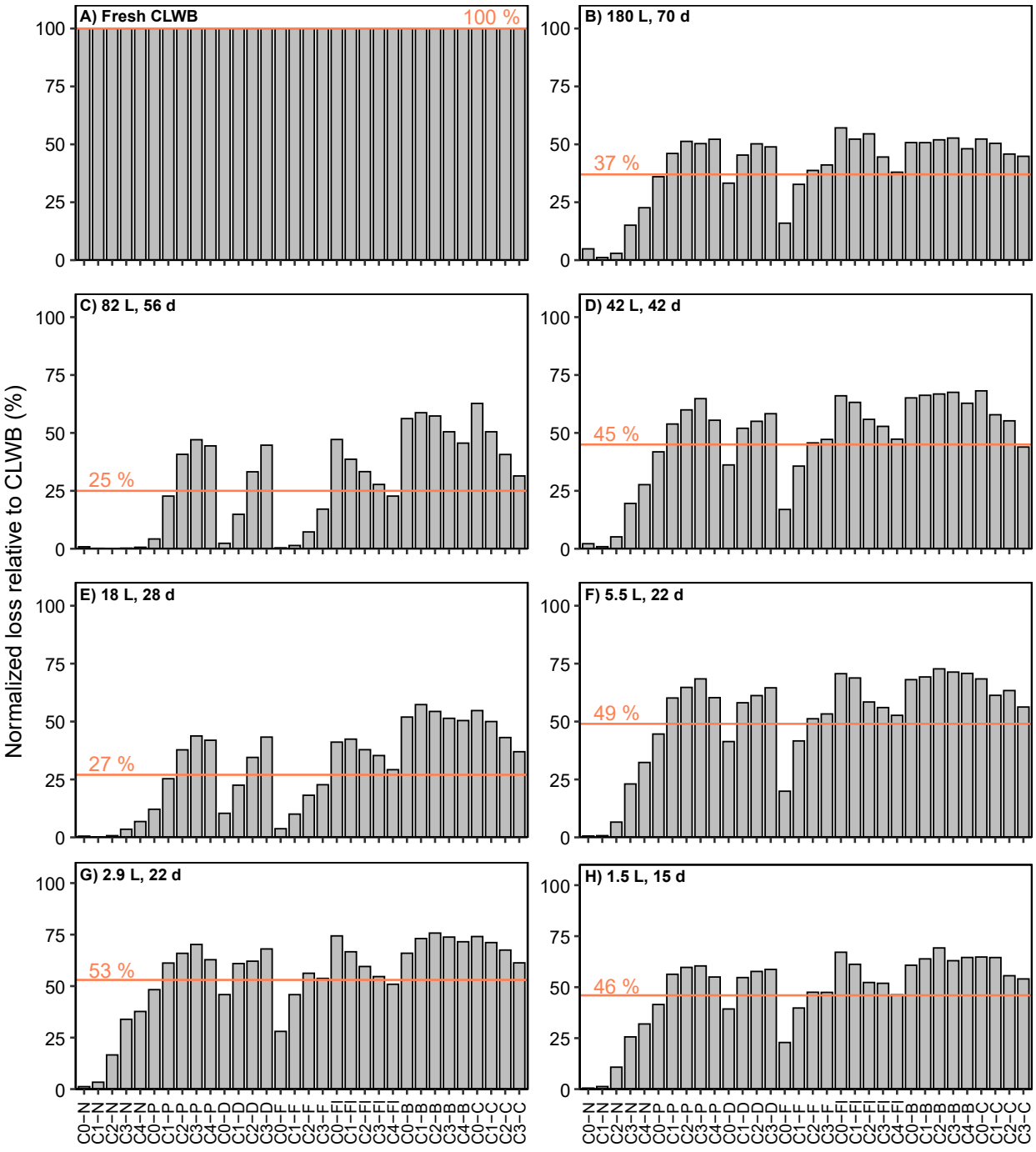

Figure S4. 10. PAH loss in dilbit slick samples during weathering. Concentrations were normalized to C_{30} $\alpha\beta$ Hopane. Horizontal red lines represent the total PAH loss relative to the CLWB dilbit. Each panel corresponds to the final sampling day of that particular treatment. Final sampling days vary due to submergence of the dilbit slicks which limited surface sample collection.

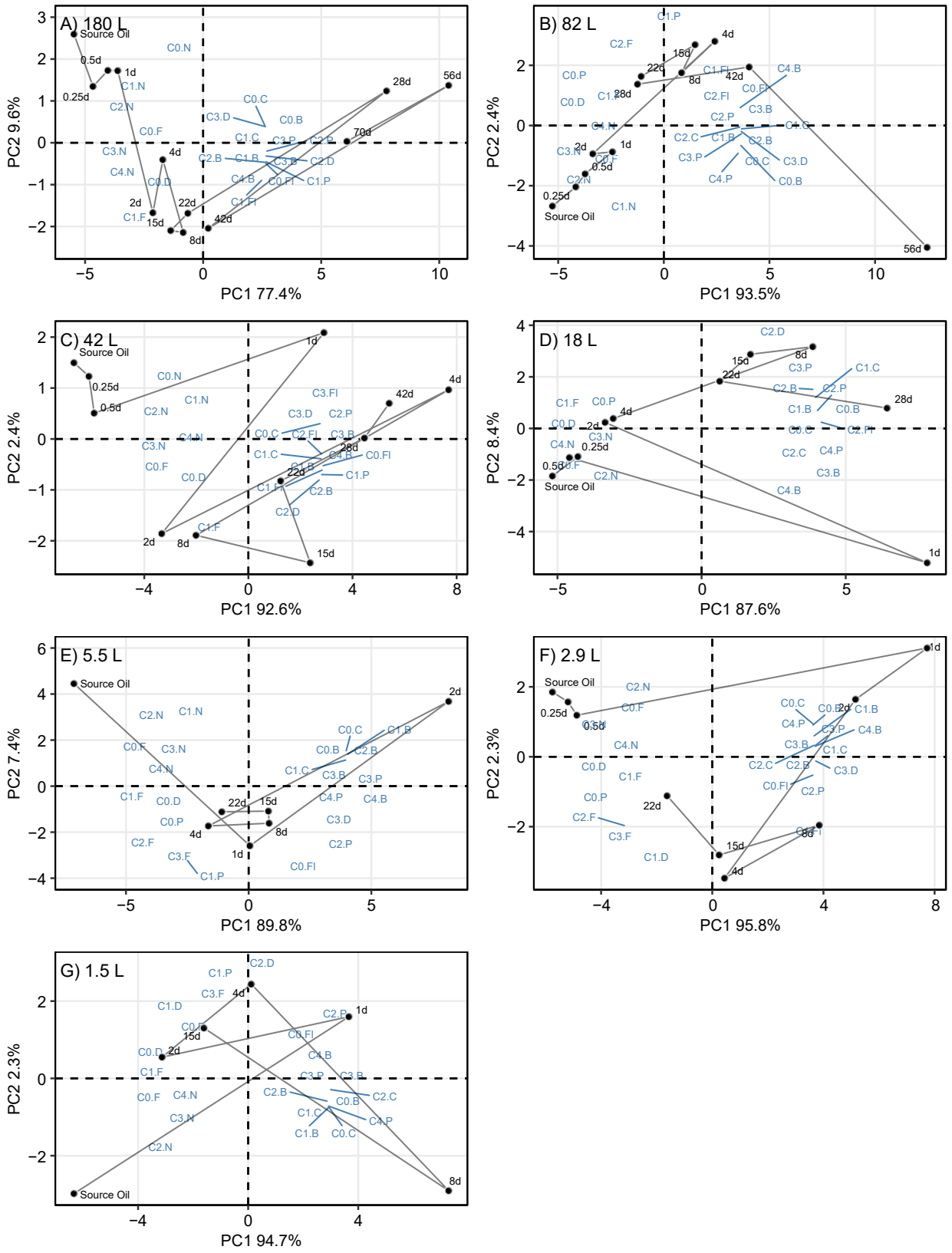

Figure S4. 11. Principal component analysis of PAH profiles normalized Hopane in dilbit slick samples collected throughout the entire study from each treatment.

Table S4. 8. First order rate constants (± standard error) for individual parent and alkylated PAHs in each of the dilbit amended treatments. Cases when concentrations of the individual compounds in the dilbit slicks were below detection limits were omitted from the computation of rate coefficients. Negative rate constants identify cases of depletion whereas positive rate constants identify cases of no observable depletion.

Compound	*k* (d^{-1}) ± SE						
	1.5 L	2.9 L	5.5 L	18 L	42 L	82 L	180 L
C0-N	-0.245 ± 0.147	-0.337 ± 0.129	-0.276 ± 0.16	-0.373 ± 0.054	-0.315 ± 0.082	-0.304 ± 0.097	-0.212 ± 0.058
C1-N	-0.207 ± 0.147	-0.385 ± 0.165	-0.267 ± 0.187	-0.355 ± 0.083	-0.219 ± 0.121	-0.306 ± 0.064	-0.126 ± 0.036
C2-N	-0.099 ± 0.219	-0.21 ± 0.171	-0.086 ± 0.145	-0.204 ± 0.095	-0.117 ± 0.096	-0.179 ± 0.039	-0.072 ± 0.021
C3-N	-0.052 ± 0.16	-0.082 ± 0.16	-0.04 ± 0.096	-0.112 ± 0.105	-0.064 ± 0.049	-0.097 ± 0.029	-0.045 ± 0.014
C4-N	-0.054 ± 0.115	-0.094 ± 0.119	-0.023 ± 0.097	-0.081 ± 0.072	-0.051 ± 0.028	-0.074 ± 0.026	-0.044 ± 0.013
C0-P	-0.076 ± 0.113	-0.031 ± 0.107	-0.024 ± 0.1	-0.044 ± 0.047	-0.038 ± 0.019	-0.056 ± 0.019	-0.039 ± 0.011
C1-P	-0.043 ± 0.066	-0.02 ± 0.059	-0.005 ± 0.064	-0.023 ± 0.031	-0.028 ± 0.011	-0.038 ± 0.013	-0.032 ± 0.009
C2-P	-0.033 ± 0.043	-0.029 ± 0.031	-0.011 ± 0.042	-0.024 ± 0.015	-0.03 ± 0.011	-0.032 ± 0.012	-0.031 ± 0.008
C3-P	-0.029 ± 0.035	-0.033 ± 0.027	-0.013 ± 0.032	-0.019 ± 0.015	-0.032 ± 0.011	-0.035 ± 0.013	-0.037 ± 0.009
C4-P	-0.032 ± 0.029	-0.038 ± 0.031	-0.018 ± 0.035	-0.026 ± 0.012	-0.035 ± 0.011	-0.04 ± 0.016	-0.041 ± 0.012
C0-D	-0.076 ± 0.12	-0.03 ± 0.124	-0.026 ± 0.102	-0.057 ± 0.051	-0.042 ± 0.022	-0.059 ± 0.021	-0.039 ± 0.011
C1-D	-0.044 ± 0.072	-0.013 ± 0.078	0.005 ± 0.073	-0.026 ± 0.034	-0.021 ± 0.014	-0.035 ± 0.012	-0.024 ± 0.01
C2-D	-0.037 ± 0.054	-0.018 ± 0.041	-0.001 ± 0.051	-0.017 ± 0.024	-0.024 ± 0.011	-0.03 ± 0.012	-0.029 ± 0.008
C3-D	-0.033 ± 0.04	-0.029 ± 0.028	-0.008 ± 0.038	-0.022 ± 0.019	-0.03 ± 0.011	-0.032 ± 0.014	-0.036 ± 0.01
C0-F	-0.084 ± 0.169	-0.108 ± 0.142	-0.053 ± 0.108	-0.121 ± 0.079	-0.061 ± 0.048	-0.102 ± 0.03	-0.048 ± 0.015
C1-F	-0.052 ± 0.102	-0.022 ± 0.133	-0.013 ± 0.092	-0.055 ± 0.061	-0.033 ± 0.022	-0.057 ± 0.018	-0.033 ± 0.008
C2-F	-0.044 ± 0.077	-0.004 ± 0.11	-0.005 ± 0.089	-0.033 ± 0.041	-0.032 ± 0.012	-0.041 ± 0.017	-0.029 ± 0.009
C3-F	-0.05 ± 0.065	-0.026 ± 0.067	-0.009 ± 0.076	-0.033 ± 0.025	-0.036 ± 0.011	-0.041 ± 0.015	-0.036 ± 0.011
C0-Fl	-0.03 ± 0.04	-0.025 ± 0.027	-0.007 ± 0.041	-0.019 ± 0.009	-0.02 ± 0.007	-0.024 ± 0.009	-0.024 ± 0.006
C1-Fl	-0.03 ± 0.041	-0.024 ± 0.036	-0.005 ± 0.041	-0.015 ± 0.014	-0.022 ± 0.007	-0.03 ± 0.012	-0.024 ± 0.005
C2-Fl	-0.038 ± 0.038	-0.035 ± 0.037	-0.017 ± 0.047	-0.028 ± 0.015	-0.03 ± 0.01	-0.035 ± 0.014	-0.031 ± 0.009
C3-Fl	-0.041 ± 0.044	-0.032 ± 0.044	-0.016 ± 0.052	-0.039 ± 0.014	-0.031 ± 0.012	-0.04 ± 0.015	-0.032 ± 0.01
C4-Fl	-0.043 ± 0.048	-0.036 ± 0.046	-0.024 ± 0.055	-0.041 ± 0.018	-0.033 ± 0.014	-0.046 ± 0.018	-0.037 ± 0.014
C0-B	-0.028 ± 0.026	-0.032 ± 0.018	-0.019 ± 0.022	-0.022 ± 0.012	-0.032 ± 0.011	-0.031 ± 0.012	-0.033 ± 0.009
C1-B	-0.024 ± 0.022	-0.03 ± 0.016	-0.009 ± 0.017	-0.02 ± 0.009	-0.021 ± 0.008	-0.023 ± 0.008	-0.022 ± 0.007
C2-B	-0.02 ± 0.027	-0.026 ± 0.02	-0.004 ± 0.02	-0.013 ± 0.012	-0.019 ± 0.008	-0.026 ± 0.009	-0.023 ± 0.005
C3-B	-0.031 ± 0.028	-0.032 ± 0.021	-0.012 ± 0.029	-0.024 ± 0.01	-0.025 ± 0.007	-0.029 ± 0.01	-0.025 ± 0.007
C4-B	-0.03 ± 0.03	-0.033 ± 0.024	-0.009 ± 0.03	-0.029 ± 0.015	-0.024 ± 0.008	-0.027 ± 0.011	-0.025 ± 0.007
C0-C	-0.024 ± 0.021	-0.032 ± 0.016	-0.015 ± 0.018	-0.021 ± 0.01	-0.03 ± 0.01	-0.031 ± 0.014	-0.035 ± 0.008
C1-C	-0.024 ± 0.027	-0.031 ± 0.023	-0.018 ± 0.025	-0.018 ± 0.014	-0.023 ± 0.007	-0.029 ± 0.01	-0.03 ± 0.009
C2-C	-0.034 ± 0.032	-0.037 ± 0.031	-0.018 ± 0.036	-0.029 ± 0.015	-0.032 ± 0.013	-0.039 ± 0.015	-0.041 ± 0.009
C3-C	-0.039 ± 0.041	-0.038 ± 0.043	-0.015 ± 0.051	-0.04 ± 0.017	-0.043 ± 0.009	-0.044 ± 0.016	-0.039 ± 0.012

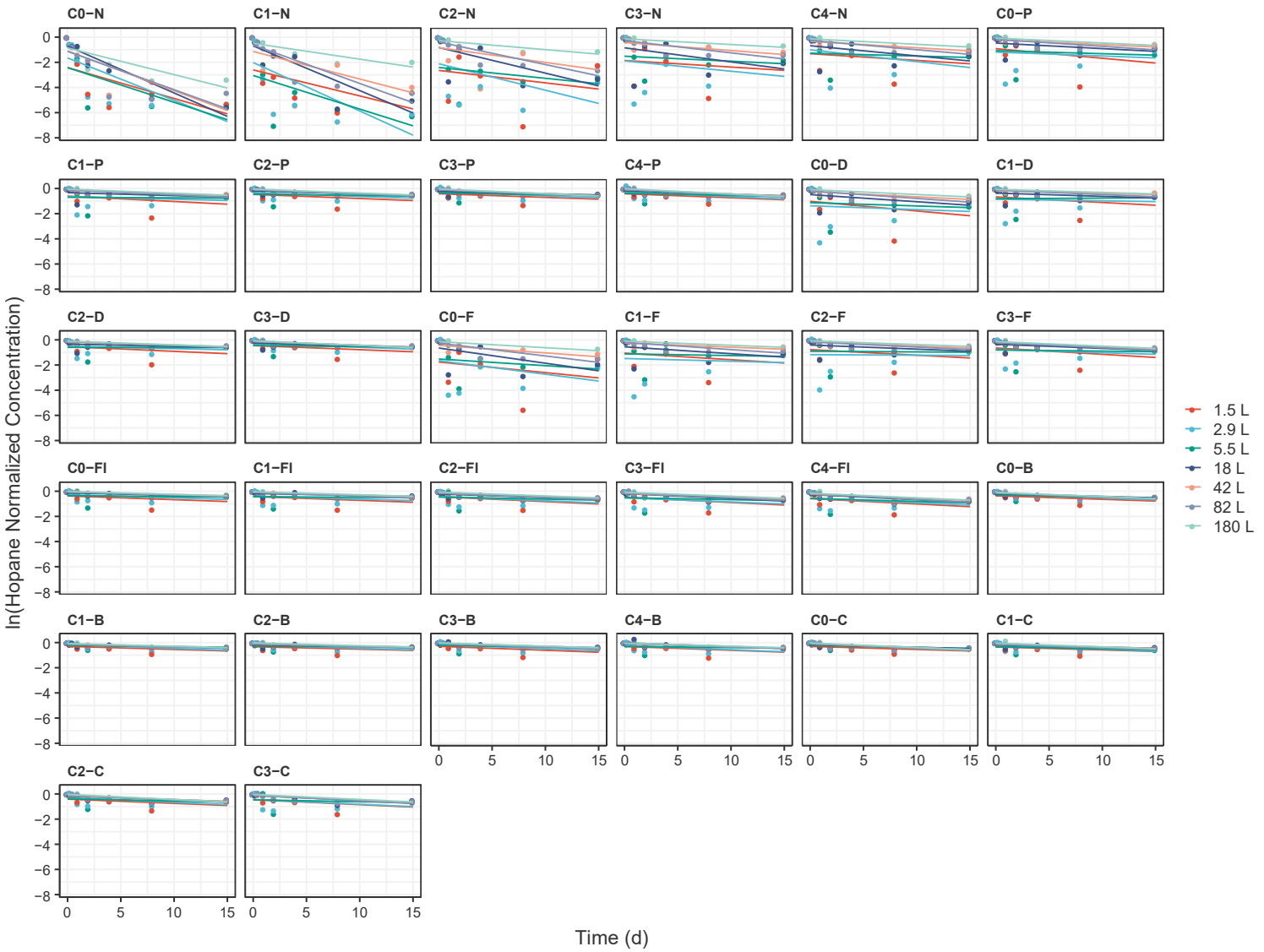

Figure S4. 12. Linear regressions of natural logarithm transformed PAH normalized concentrations over time during the first 15 days of the study.

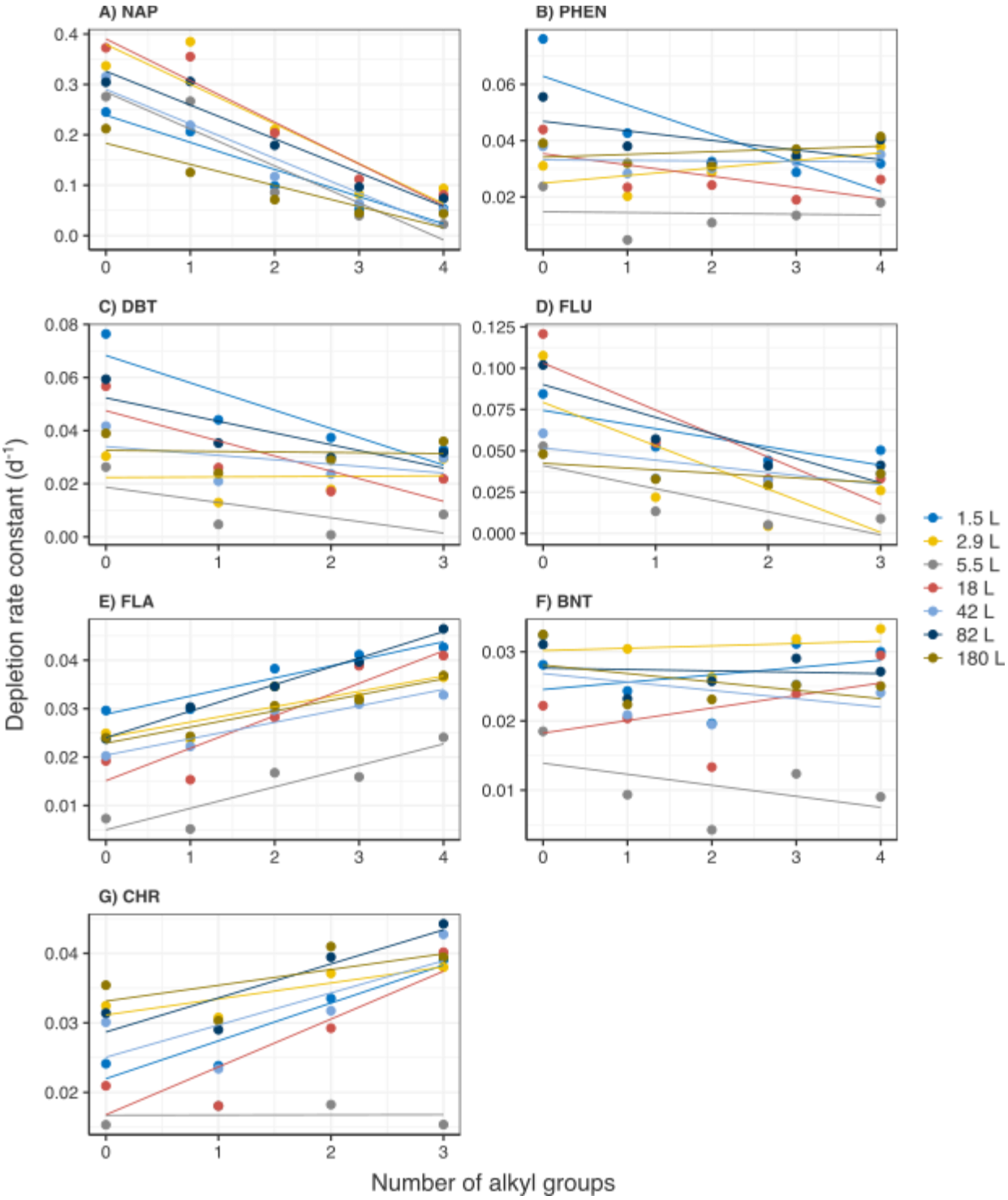

Figure S4. 13. Relationship between individual PAH degradation rate constants and the degree of alkylation in each of the seven dilbit amended treatments.

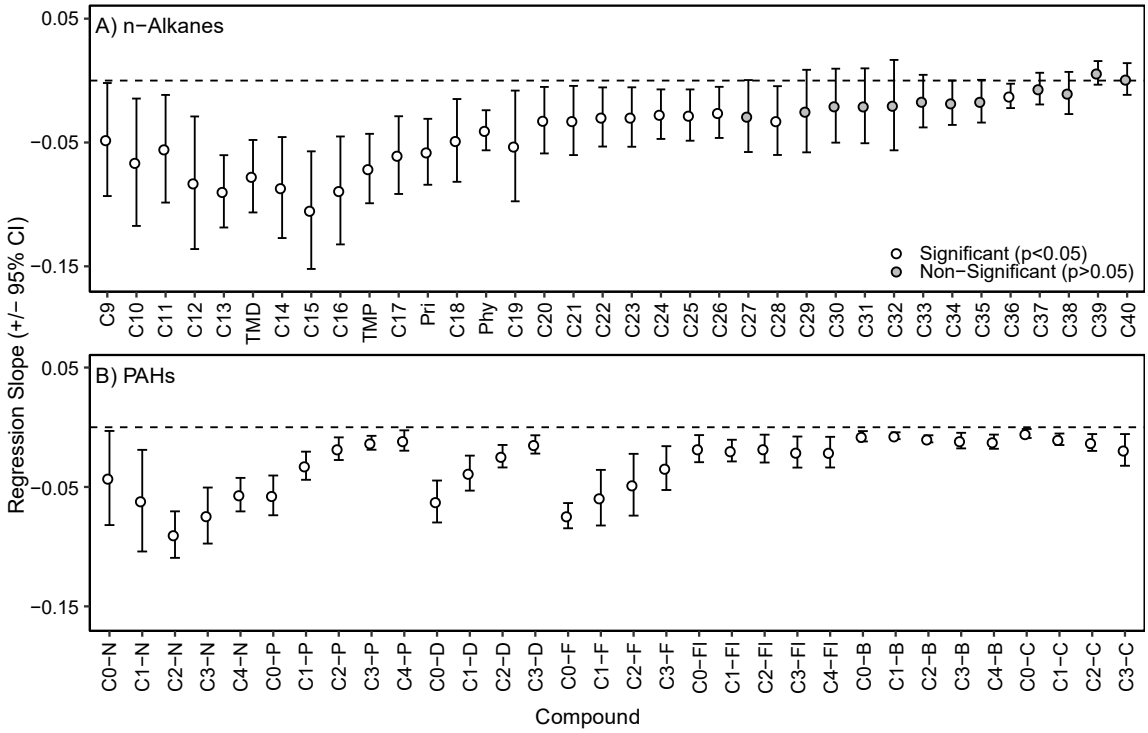

Figure S4. 14. Compound specific regression outputs for n-alkanes (A) and PAHs (B) following linear regression of the standard error associated with each calculated rate constant and spill volume. A negative slope (i.e., below horizontal dashed line) represents an inverse relationship between standard error and spill volume. Relationships that are statistically significant are white.

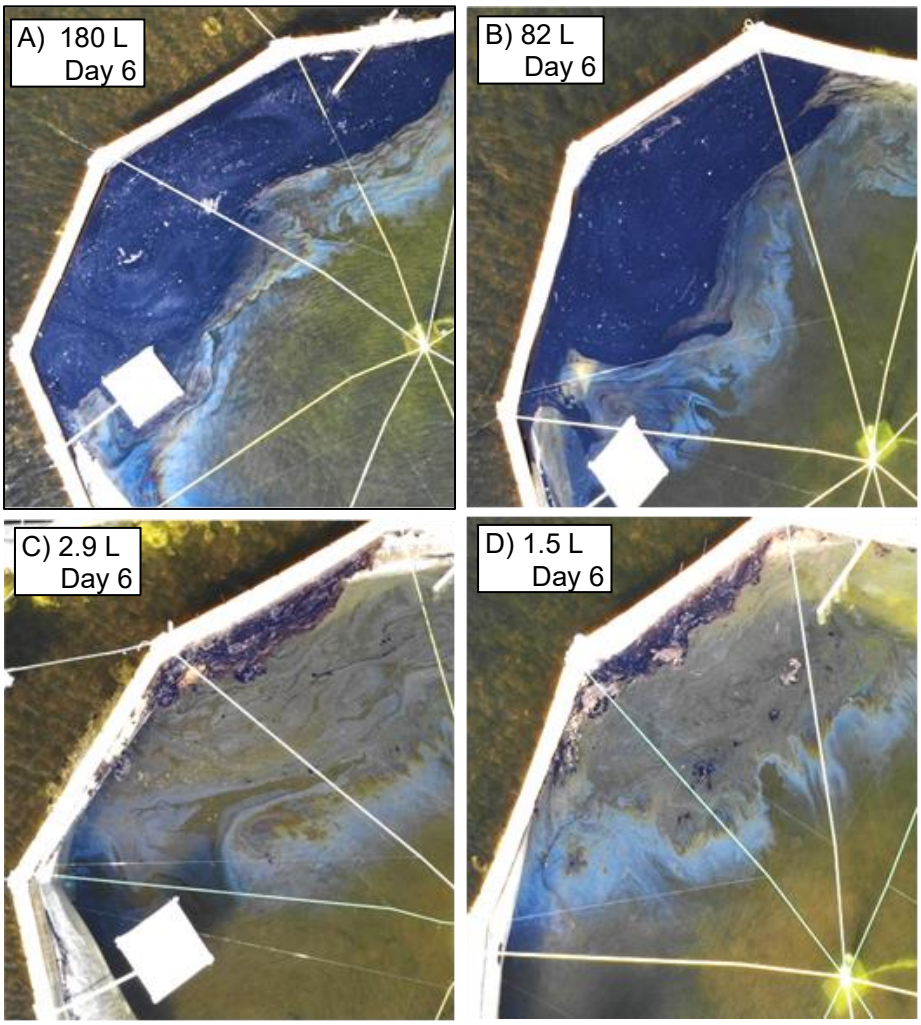

Figure S4. 15. Differences in slick appearance on the same day (day 6) in two higher volume treatments (AB) and two lower treatments (CD).

Table S4. 9. Regression outputs from linear regressions performed in Figure S3.15.

Treatment	PAH Group	Slope	R^2	*p*-value
1.5 L	NAP	-0.054	0.90	**0.01**
	PHEN	-0.010	0.69	0.08
	DBT	-0.014	0.81	0.10
	FLU	-0.011	0.62	0.21
	FLA	0.004	0.91	**0.01**
	BNT	0.001	0.13	0.56
	CHR	0.005	0.89	0.06
2.9 L	NAP	-0.079	0.82	**0.03**
	PHEN	0.003	0.42	0.24
	DBT	0.0002	0.00	0.97
	FLU	-0.026	0.54	0.26
	FLA	0.003	0.76	0.06
	BNT	0.0003	0.04	0.75
	CHR	0.002	0.71	0.16
5.5 L	NAP	-0.073	0.88	**0.02**
	PHEN	-0.0003	0.00	0.92
	DBT	-0.006	0.43	0.34
	FLU	-0.014	0.67	0.18
	FLA	0.004	0.83	**0.03**
	BNT	-0.002	0.23	0.41
	CHR	0.00003	0.00	0.98
18 L	NAP	-0.083	0.94	**0.01**
	PHEN	-0.004	0.43	0.23
	DBT	-0.011	0.67	0.18
	FLU	-0.028	0.78	0.11
	FLA	0.007	0.86	**0.02**
	BNT	0.002	0.24	0.40
	CHR	0.007	0.80	0.10
42 L	NAP	-0.068	0.93	**0.01**
	PHEN	0.000	0.01	0.91
	DBT	-0.003	0.22	0.54
	FLU	-0.007	0.51	0.29
	FLA	0.003	0.92	**0.01**
	BNT	-0.001	0.15	0.53
	CHR	0.005	0.55	0.26
82 L	NAP	-0.067	0.92	**0.01**
	PHEN	-0.003	0.34	0.30
	DBT	-0.009	0.69	0.17
	FLU	-0.020	0.79	0.11
	FLA	0.005	0.99	**0.0002**
	BNT	0.000	0.01	0.87
	CHR	0.005	0.80	0.11
180 L	NAP	-0.042	0.86	**0.02**
	PHEN	0.001	0.12	0.58
	DBT	-0.0004	0.01	0.92
	FLU	-0.004	0.39	0.38
	FLA	0.003	0.94	**0.01**
	BNT	-0.001	0.23	0.42
	CHR	0.002	0.38	0.39

Table S4. 10. Comparison of rate constants between the present study and others using Cold Lake blend (CLB) dilbit. Rates marked as "0" represent no depletion (i.e., a positive rate constant).

		k (d^{-1})			
	Compound	**Present Study[a]**	**Deshpande et al., (2018)[b]**	**Cobanli et al., (2015)[c]**	**King et al., (2014)[d]**
Timeline (d)		15	60	42	13
Totals	**Total *n*-alkanes**	0.041 - 0.094	0.52 - 1.13	0.06*	0.0011
	Total PAHs	0.019 - 0.41	0.05 - 0.14	0.0045 - 0.0053*	0.0005
Alkanes	***n*-C_9**	0.293 - 0.39	/	/	/
	***n*-C_{10}**	0.288 - 0.409	0.42	/	/
	***n*-C_{11}**	0.226 - 0.372	0.4	/	/
	***n*-C_{12}**	0.153 - 0.41	0.37	/	/
	***n*-C_{13}**	0.019 - 0.244	0.35	/	/
	TMD	0.118 - 0.292	/	/	/
	***n*-C_{14}**	0.051 - 0.231	0.23	/	/
	***n*-C_{15}**	0.026 - 0.151	0.28	/	/
	***n*-C_{16}**	0.011 - 0.134	0.27	/	/
	TMP	0 - 0.043	/	/	/
	***n*-C_{17}**	0 - 0.108	0.25	/	/
	Pristane	0 - 0.031	/	/	/
	***n*-C_{18}**	0 - 0.103	0.28	/	/
	Phytane	0 - 0.018	/	/	/
	***n*-C_{19}**	0 - 0.107	0.26	/	/
	***n*-C_{20}**	0.002 - 0.105	0.28	/	/
	***n*-C_{21}**	0.003 - 0.104	0.3	/	/
	***n*-C_{22}**	0.002 - 0.103	0.3	/	/
	***n*-C_{23}**	0.004 - 0.108	0.3	/	/
	***n*-C_{24}**	0.011 - 0.114	0.29	/	/
	***n*-C_{25}**	0.017 - 0.115	0.3	/	/
	***n*-C_{26}**	0.007 - 0.107	0.31	/	/
	***n*-C_{27}**	0.006 - 0.063	0.28	/	/
	***n*-C_{28}**	0.007 - 0.064	0.3	/	/
	***n*-C_{29}**	0.009 - 0.066	0.36	/	/
	***n*-C_{30}**	0.012 - 0.057	0.28	/	/
	***n*-C_{31}**	0 - 0.043	0.26	/	/
	***n*-C_{32}**	0 - 0.036	0.33	/	/
	***n*-C_{33}**	0 - 0.027	0.2	/	/
	***n*-C_{34}**	0 - 0.023	0.25	/	/
	***n*-C_{35}**	0 - 0.019	0.19	/	/
	***n*-C_{36}**	0 - 0.026	/	/	/
	***n*-C_{37}**	0 - 0.042	/	/	/
	***n*-C_{38}**	0 - 0.063	/	/	/
	***n*-C_{39}**	0 - 0.041	/	/	/
	***n*-C_{40}**	0 - 0.065	/	/	/
PAHs	**C0-N**	0.212 - 0.373	0.88 - 2.16	/	/
	C1-N	0.126 - 0.385	0.49 - 2.14	/	/
	C2-N	0.072 - 0.21	0.44 - 0.61	/	/
	C3-N	0.04 - 0.112	0.12 - 0.41	/	/
	C4-N	0.023 - 0.094	0.03 - 0.13	/	/
	C0-P	0.024 - 0.076	0.32 - 0.74	/	/
	C1-P	0.005 - 0.043	0.1 - 0.42	/	/
	C2-P	0.011 - 0.033	0.03 - 0.13	/	/
	C3-P	0.013 - 0.037	NA - 0.11	/	/
	C4-P	0.018 - 0.041	NA - 0.13	/	/
	C0-D	0.026 - 0.076	0.28 - 0.49	/	/

	C1-D	0 - 0.044	0.08 - 0.31	/	/
	C2-D	0.001 - 0.037	0.03 - 0.13	/	/
	C3-D	0.008 - 0.036	NA - 0.09	/	/
	C0-F	0.048 - 0.121	0.41 - 0.89	/	/
	C1-F	0.013 - 0.057	0.06 - 0.22	/	/
	C2-F	0.004 - 0.044	0.05 - 0.19	/	/
	C3-F	0.009 - 0.05	NA - 0.11	/	/
	C0-Fl	0.007 - 0.03	/	/	/
	C1-Fl	0.005 - 0.03	/	/	/
	C2-Fl	0.017 - 0.038	/	/	/
	C3-Fl	0.016 - 0.041	/	/	/
	C4-Fl	0.024 - 0.046	/	/	/
	C0-B	0.019 - 0.033	NA.- 0.1	/	/
	C1-B	0.009 - 0.03	NA - 0.08	/	/
	C2-B	0.004 - 0.026	NA - 0.09	/	/
	C3-B	0.012 - 0.032	NA - 0	/	/
	C4-B	0.009 - 0.033	/	/	/
	C0-C	0.015 - 0.035	NA - 0.11	/	/
	C1-C	0.018 - 0.031	NA - 0.08	/	/
	C2-C	0.018 - 0.041	NA - 0.04	/	/
	C3-C	0.015 - 0.044	NA - 0.04	/	/

[a]The values recorded from the present study are presented as the minimum and maximum rates across all seven treatment levels

[b]Deshpande et al. (2018) performed CLB degradation experiments using enriched microbial consortiums obtained from the Kalamazoo River oil spill site at 5 ºC and 25 ºC. Values presented as ranges represent degradation rates at 5 ºC - 25 ºC, respectively measured over a period of 60 days. Degradation rate data for individual *n*-alkanes was only measured at 5 ºC.

[c]Cobanli et al. (2015) performed CLB degradation experiments microbial consortiums obtained from seawater from the Douglas Channel and Hecate Strait, BC, Canada. Rate constants were only generated for total *n*-alkanes and total PAHs over a period of 42 days. Values presented as ranges represent degradation rates from the Hecate Strait – Douglas Channel, respectively.

[d]King et al. (2014) performed CLB weathering experiments in a flume tank using filtered seawater from the Bedford Basin, NS, Canada for 13 days. Rate constants were only generated for total *n*-alkanes and total PAHs.

Table S4. 11. Comparison of study characteristics between the present study and the tank study of King et al., (2014). Fold changes recorded in green represent values greater than those of King et al. (2014) and fold changes recorded in red represent values lower than those of King et al., (2014).

Study Parameters	Present Study	King et al., (2014)
Enclosure area (m^2)	~77.3 (590x ↑)	0.13
Volume of dilbit added (L)	1.5 to 180 (1.4x to 167x ↑)	1.08[a]
Volume of dilbit added (m^3)	0.0015 to 0.18 (1.4x to 167x ↑)	0.00108
Estimated slick thickness on day 0 (cm)	0.0019 to 0.23 (437x to 4x ↓)	0.83
V:SA (L m^{-2})	0.019 to 2.33 (437x to 4x ↓)	8.3

[a]The volume (L) of dilbit added in the King et al., (2014) study was calculated based on the density of the

Supporting References

Aeppli, C., Carmichael, C.A., Nelson, R.K., Lemkau, K.L., Graham, W.M., Redmond, M.C., Valentine, D.L., Reddy, C.M., 2012. Oil weathering after the Deepwater Horizon disaster led to the formation of oxygenated residues. Environmental Science & Technology 46, 8799–8807.

Aeppli, C., Nelson, R.K., Radovic, J.R., Carmichael, C.A., Valentine, D.L., Reddy, C.M., 2014. Recalcitrance and degradation of petroleum biomarkers upon abiotic and biotic natural weathering of Deepwater Horizon oil. Environmental science & technology 48, 6726–6734.

Charrié-Duhaut, A., Lemoine, S., Adam, P., Connan, J., Albrecht, P., 2000. Abiotic oxidation of petroleum bitumens under natural conditions. Organic Geochemistry 31, 977–1003.

Christensen, L.B., Larsen, T.H., 1993. Method for determining the age of diesel oil spills in the soil. Groundwater Monitoring & Remediation 13, 142–149. https://doi.org/10.1111/j.1745-6592.1993.tb00458.x

Garrett, R.M., Pickering, I.J., Haith, C.E., Prince, R.C., 1998. Photooxidation of crude oils. Environmental Science & Technology 32, 3719–3723.

Huesemann, M.H., Hausmann, T.S., Fortman, T.J., 2003. Biodegradation of hopane prevents use as conservative biomarker during bioremediation of PAHs in petroleum contaminated soils. Bioremediation journal 7, 111–117.

Leblond, J.D., Schultz, T.W., Sayler, G.S., 2001. Observations on the preferential biodegradation of selected components of polyaromatic hydrocarbon mixtures. Chemosphere 42, 333–343. https://doi.org/10.1016/S0045-6535(00)00161-2

Lima, A.L.C., Farrington, J.W., Reddy, C.M., 2005. Combustion-derived polycyclic aromatic hydrocarbons in the environment—a review. Environmental Forensics 6, 109–131.

Luellen, D.R., Shea, D., 2003. Semipermeable membrane devices accumulate conserved ratios of sterane and hopane petroleum biomarkers. Chemosphere 53, 705–713.

Miller, N.J., Mudge, S.M., 1997. The effect of biodiesel on the rate of removal and weathering characteristics of crude oil within artificial sand columns. Spill Science & Technology Bulletin 4, 17–33.

Mudge, S.M., 2016. Statistical analysis of oil spill chemical composition data, in: Standard Handbook Oil Spill Environmental Forensics. Elsevier, pp. 849–867.

Olson, G.M., Gao, H., Meyer, B.M., Miles, M.S., Overton, E.B., 2017. Effect of Corexit 9500A on Mississippi Canyon crude oil weathering patterns using artificial and natural seawater. Heliyon 3, e00269.

Prince, R.C., Elmendorf, D.L., Lute, J.R., Hsu, C.S., Haith, C.E., Senius, J.D., Dechert, G.J., Douglas, G.S., Butler, E.L., 1994. 17. alpha.(H)-21. beta.(H)-hopane as a conserved internal marker for estimating the biodegradation of crude oil. Environmental science & technology 28, 142–145. https://doi.org/10.1021/es00050a019

Prince, R.C., Garrett, R.M., Bare, R.E., Grossman, M.J., Townsend, T., Suflita, J.M., Lee, K., Owens, E.H., Sergy, G.A., Braddock, J.F., 2003. The roles of photooxidation and biodegradation in long-term weathering of crude and heavy

fuel oils. Spill Science & Technology Bulletin 8, 145–156. https://doi.org/10.1016/S1353-2561(03)00017-3
Shah, K., Watson, K., Hollebone, B., Yang, Z., Lambert, P., Faragher, R., Aljawahari, M., Dey, D., Mirnaghi, F., Stoyanovich, S., Blais, J.M., 2019. The BOREAL Project: The Design and Execution of a Controlled Oil Spill Study in a Canadian Freshwater Lake, in: Proceedings of the Forty-Second AMOP Technical Seminar. Environment and Climate Change Canada, Ottawa, ON, Canada, pp. 276–294.
Stoyanovich, S., Yang, Z., Hanson, M., Hollebone, B., Orihel, D., Palace, V., Rodriguez-Gil, J., Faragher, R., Mirnaghi, F., Shah, K., Blais, J., 2019. Simulating a spill of diluted bitumen: Environmental weathering and submergence in a model freshwater system. ET&C. https://doi.org/10.1002/etc.4600
Venosa, A.D., Suidan, M.T., King, D., Wrenn, B.A., 1997. Use of hopane as a conservative biomarker for monitoring the bioremediation effectiveness of crude oil contaminating a sandy beach. Journal of Industrial Microbiology and Biotechnology 18, 131–139. https://doi.org/10.1038/sj.jim.2900304
Vergeynst, L., Christensen, J.H., Kjeldsen, K.U., Meire, L., Boone, W., Malmquist, L.M., Rysgaard, S., 2019a. In situ biodegradation, photooxidation and dissolution of petroleum compounds in Arctic seawater and sea ice. Water research 148, 459–468. https://doi.org/10.1016/j.watres.2018.10.066
Vergeynst, L., Greer, C.W., Mosbech, A., Gustavson, K., Meire, L., Poulsen, K.G., Christensen, J.H., 2019b. Biodegradation, photo-oxidation, and dissolution of petroleum compounds in an Arctic fjord during summer. Environmental Science & Technology 53, 12197–12206. https://doi.org/10.1021/acs.est.9b03336
Wang, Z., Fingas, M., Blenkinsopp, S., Sergy, G., Landriault, M., Sigouin, L., Foght, J., Semple, K., Westlake, D.W.S., 1998. Comparison of oil composition changes due to biodegradation and physical weathering in different oils. Journal of Chromatography A 809, 89–107. https://doi.org/10.1016/S0021-9673(98)00166-6

REFERENCES

Aeppli, C., Carmichael, C.A., Nelson, R.K., Lemkau, K.L., Graham, W.M., Redmond, M.C., Valentine, D.L., Reddy, C.M., 2012. Oil weathering after the Deepwater Horizon disaster led to the formation of oxygenated residues. Environ. Sci. Technol. 46, 8799–8807.

Aeppli, C., Nelson, R.K., Radovic, J.R., Carmichael, C.A., Valentine, D.L., Reddy, C.M., 2014. Recalcitrance and degradation of petroleum biomarkers upon abiotic and biotic natural weathering of Deepwater Horizon oil. Environ. Sci. Technol. 48, 6726–6734.

Arey, J.S., Nelson, R.K., Plata, D.L., Reddy, C.M., 2007. Disentangling oil weathering using GCxGC. 2. Mass transfer calculations. Environ. Sci. Technol. 41, 5747–5755.

ASTM D3325-90 Standard Practice for Preservation of Waterborne Oil Samples, 2013. . ASTM Int. https://doi.org/10.1520/D3325-90R13

ASTM D4489-95 Standard Practices for Sampling of Waterborne Oils, 2017. . ASTM Int. https://doi.org/10.1520/D4489-95R17

Atlas, R.M., 1981. Microbial degradation of petroleum hydrocarbons: an environmental perspective. Microbiol. Rev. 45, 180.

Atlas, R.M., Bartha, R., 1992. Hydrocarbon biodegradation and oil spill bioremediation, in: Advances in Microbial Ecology. Springer, pp. 287–338.

Atlas, R.M., Hazen, T.C., 2011. Oil biodegradation and bioremediation: a tale of the two worst spills in US history. ACS Publications.

Bacosa, H.P., Erdner, D.L., Liu, Z., 2015. Differentiating the roles of photooxidation and biodegradation in the weathering of Light Louisiana Sweet crude oil in surface water from the Deepwater Horizon site. Mar. Pollut. Bull. 95, 265–272.

Bagby, S.C., Reddy, C.M., Aeppli, C., Fisher, G.B., Valentine, D.L., 2017. Persistence and biodegradation of oil at the ocean floor following Deepwater Horizon. Proc. Natl. Acad. Sci. 114, E9–E18.

Bhattacharyya, S., Klerks, P.L., Nyman, J.A., 2003. Toxicity to freshwater organisms from oils and oil spill chemical treatments in laboratory microcosms. Environ. Pollut. 122, 205–215. https://doi.org/10.1016/S0269-7491(02)00294-4

Bociu, I., Shin, B., Wells, W.B., Kostka, J.E., Konstantinidis, K.T., Huettel, M., 2019. Decomposition of sediment-oil-agglomerates in a Gulf of Mexico sandy beach. Sci. Rep. 9, 1–13. https://doi.org/10.1038/s41598-019-46301-w

Charrié-Duhaut, A., Lemoine, S., Adam, P., Connan, J., Albrecht, P., 2000. Abiotic oxidation of petroleum bitumens under natural conditions. Org. Geochem. 31, 977–1003.

Cobanli, S.E., Greer, C.W., King, T.L., Robinson, B.J., Ryan, S.A., Fortin, N., Wohlgeschaffen, G.D., Mason, J.A., Thamer, P.M., McIntyre, E.C., 2015. In Field Studies to Monitor Indigenous Microbial Respiration to Determine the Potential Biodegradation of Naturally and Chemically Dispersed Crude Oil, Condensate and Diluted Bitumen, in: British Columbia. Vancouver, B.C., Canada.

De Bruyn, W.J., Clark, C.D., Ottelle, K., Aiona, P., 2012. Photochemical degradation of phenanthrene as a function of natural water variables modeling freshwater to marine environments. Mar. Pollut. Bull. 64, 532–538.

Deshpande, R.S., Sundaravadivelu, D., Techtmann, S., Conmy, R.N., Santo Domingo, J.W., Campo, P., 2018. Microbial degradation of Cold Lake Blend and Western Canadian select dilbits by freshwater enrichments. J. Hazard. Mater. 352, 111–120. https://doi.org/10.1016/j.jhazmat.2018.03.030

Douglas, G.S., Bence, A.E., Prince, R.C., McMillen, S.J., Butler, E.L., 1996. Environmental stability of selected petroleum hydrocarbon source and weathering ratios. Environ. Sci. Technol. 30, 2332–2339.

Douglas, G.S., Prince, R.C., Butler, E.L., Steinhauer, W.G., 1994. The use of internal chemical indicators in petroleum and refined products to evaluate the extent of biodegradation, Hydrocarbon bioremediation. Lewis Publishers: Ann Arbor, MI.

Fingas, M., 2015a. Review of The Properties and Behaviour of Diluted Bitumen, in: Proceeding of the 39th Arctic and Marine Oil-Spill Program Technical Seminar. Environment and Climate Change Canada, Vancouver, B.C., Canada, pp. 470–494.

Fingas, M., 2015b. Oil and Petroleum Evaporation, in: Handbook of Oil Spill Science and Technology. Wiley Online Library, pp. 205–223.

Garrett, R.M., Pickering, I.J., Haith, C.E., Prince, R.C., 1998. Photooxidation of crude oils. Environ. Sci. Technol. 32, 3719–3723.

Government of Canada, 2013. Properties, composition and marine spill behaviour, fate and transport of two diluted bitumen products from the Canadian oil sands (No. ISBN 987-1-100-23004-7), Federal Government Technical Report.

Gros, J., Nabi, D., Würz, B., Wick, L.Y., Brussaard, C.P., Huisman, J., van der Meer, J.R., Reddy, C.M., Arey, J.S., 2014. First day of an oil spill on the open sea: Early mass transfers of hydrocarbons to air and water. Environ. Sci. Technol. 48, 9400–9411. https://doi.org/10.1021/es502437e

Kassambara, A., Mundt, F., 2017. Package 'factoextra.' Extr. Vis. Results Multivar. Data Anal. 76.

King, T.L., Robinson, B., Boufadel, M., Lee, K., 2014. Flume tank studies to elucidate the fate and behavior of diluted bitumen spilled at sea. Mar. Pollut. Bull. 83, 32–37. https://doi.org/10.1016/j.marpolbul.2014.04.042

King, T.L., Robinson, B., Cui, F., Boufadel, M., Lee, K., Clyburne, J.A., 2017. An oil spill decision matrix in response to surface spills of various bitumen blends. Environ. Sci. Process. Impacts 19, 928–938. https://doi.org/10.1039/C7EM00118E

Knightes, C.D., Peters, C.A., 2003. Aqueous phase biodegradation kinetics of 10 PAH compounds. Environ. Eng. Sci. 20, 207–218. https://doi.org/doi.org/10.1089/109287503321671410

Leblond, J.D., Schultz, T.W., Sayler, G.S., 2001. Observations on the preferential biodegradation of selected components of polyaromatic hydrocarbon mixtures. Chemosphere 42, 333–343. https://doi.org/10.1016/S0045-6535(00)00161-2

Lee, K. (chair), Boufadel, M., Chen, B., Foght, J., Hodson, P., Swanson, S., Venosa, A., 2015. Expert Panel Report on the Behaviour and Environmental Impacts of Crude Oil Released into Aqueous Environments (No. ISBN: 978-1-928140-02-3). Royal Society of Canada, Ottawa, ON, Canada.

Li, Y., Xiong, Y., Yang, W., Xie, Y., Li, S., Sun, Y., 2009. Compound-specific stable carbon isotopic composition of petroleum hydrocarbons as a tool for tracing the source of oil spills. Mar. Pollut. Bull. 58, 114–117.

Lima, A.L.C., Farrington, J.W., Reddy, C.M., 2005. Combustion-derived polycyclic aromatic hydrocarbons in the environment—a review. Environ. Forensics 6, 109–131.
Miller, N.J., Mudge, S.M., 1997. The effect of biodiesel on the rate of removal and weathering characteristics of crude oil within artificial sand columns. Spill Sci. Technol. Bull. 4, 17–33.
Mudge, S.M., 2016. Statistical analysis of oil spill chemical composition data, in: Standard Handbook Oil Spill Environmental Forensics. Elsevier, pp. 849–867.
NASEM, 2016. Spills of Diluted Bitumen from Pipelines: A Comparative Study of Environmental Fate, Effects, and Response (No. ISBN: 978-0-309-38010-2). National Academies of Sciences, Engineering and Medicine (NASEM), Washington, DC.
NEB, 2017. Incident Data. National Energy Board. Government of Canada, Calgary, AB.
Olson, G.M., Gao, H., Meyer, B.M., Miles, M.S., Overton, E.B., 2017. Effect of Corexit 9500A on Mississippi Canyon crude oil weathering patterns using artificial and natural seawater. Heliyon 3, e00269.
Owens, E.H., Taylor, E., Marty, R., Little, D.I., 1993. An inland oil spill response manual to minimize adverse environmental impacts, in: International Oil Spill Conference. American Petroleum Institute, pp. 105–109.
Owens, E.H., Taylor, E., Parker, H.A., 2016. Spill site characterization in environmental forensic investigations, in: Standard Handbook Oil Spill Environmental Forensics. Elsevier, pp. 1–24.
Prince, R.C., Douglas, G.S., 2005. Quantification of hydrocarbon biodegradation using internal markers, in: Monitoring and Assessing Soil Bioremediation. Springer, pp. 179–188.
Prince, R.C., Elmendorf, D.L., Lute, J.R., Hsu, C.S., Haith, C.E., Senius, J.D., Dechert, G.J., Douglas, G.S., Butler, E.L., 1994. 17. alpha.(H)-21. beta.(H)-hopane as a conserved internal marker for estimating the biodegradation of crude oil. Environ. Sci. Technol. 28, 142–145. https://doi.org/10.1021/es00050a019
Prince, R.C., Garrett, R.M., Bare, R.E., Grossman, M.J., Townsend, T., Suflita, J.M., Lee, K., Owens, E.H., Sergy, G.A., Braddock, J.F., 2003a. The roles of photooxidation and biodegradation in long-term weathering of crude and heavy fuel oils. Spill Sci. Technol. Bull. 8, 145–156.
Prince, R.C., Garrett, R.M., Bare, R.E., Grossman, M.J., Townsend, T., Suflita, J.M., Lee, K., Owens, E.H., Sergy, G.A., Braddock, J.F., 2003b. The roles of photooxidation and biodegradation in long-term weathering of crude and heavy fuel oils. Spill Sci. Technol. Bull. 8, 145–156. https://doi.org/10.1016/S1353-2561(03)00017-3
Prince, R.C., Walters, C.C., 2016. Biodegradation of oil hydrocarbons and its implications for source identification, in: Standard Handbook Oil Spill Environmental Forensics. Elsevier, pp. 869–916.
Radović, J.R., Aeppli, C., Nelson, R.K., Jimenez, N., Reddy, C.M., Bayona, J.M., Albaigés, J., 2014. Assessment of photochemical processes in marine oil spill fingerprinting. Mar. Pollut. Bull. 79, 268–277. https://doi.org/10.1016/j.marpolbul.2013.11.029

Rodriguez-Gil, J.L., Stoyanovich, S., Hanson, M.L., Hollebone, B., Orihel, D.M., Palace, V., Faragher, R., Mirnaghi, F.S., Shah, K., Yang, Z., 2021. Simulating diluted bitumen spills in boreal lake limnocorrals-Part 1: Experimental design and responses of hydrocarbons, metals, and water quality parameters. Sci. Total Environ. 148537.

Ron, E.Z., Rosenberg, E., 2014. Enhanced bioremediation of oil spills in the sea. Curr. Opin. Biotechnol. 27, 191–194.

Stout, S.A., Uhler, A.D., McCarthy, K.J., 2001. A strategy and methodology for defensibly correlating spilled oil to source candidates. Environ. Forensics 2, 87–98.

Stout, S.A., Wang, Z., 2016. Chemical fingerprinting methods and factors affecting petroleum fingerprints in the environment. Stand. Handb. Oil Spill Environ. Forensics 61–129.

Stoyanovich, S., Rodríguez-Gil, J.R., Hanson, M., Hollebone, B.P., Orihel, D.M., Palace, V., Faragher, R., Mirnaghi, F.S., Shah, K., Yang, Z., 2021. Simulating diluted bitumen spills in boreal lake limnocorrals-Part 2: Factors affecting the physical characteristics and submergence of diluted bitumen. Sci. Total Environ. 148580.

Stoyanovich, S., Yang, Z., Hanson, M., Hollebone, B., Orihel, D., Palace, V., Rodriguez-Gil, J., Faragher, R., Mirnaghi, F., Shah, K., Blais, J., 2019. Simulating a spill of diluted bitumen: Environmental weathering and submergence in a model freshwater system. ET&C. https://doi.org/10.1002/etc.4600

USDOT, 2017. Hazardous Liquid Accident Data, 2010 - 2017, In: Pipeline and Hazardous Materials Safety Administration, ed. Pipeline Data and Statistics. Washington, DC: U.S. Department of Transportation,.

Vandermeulen, J.H., Ross, C.W., 1995. Oil spill response in freshwater: assessment of the impact of cleanup as a management tool. J. Environ. Manage. 44, 297–308. https://doi.org/10.1016/S0301-4797(95)90338-0

Venosa, A.D., Suidan, M.T., King, D., Wrenn, B.A., 1997. Use of hopane as a conservative biomarker for monitoring the bioremediation effectiveness of crude oil contaminating a sandy beach. J. Ind. Microbiol. Biotechnol. 18, 131–139. https://doi.org/10.1038/sj.jim.2900304

Vergeynst, L., Greer, C.W., Mosbech, A., Gustavson, K., Meire, L., Poulsen, K.G., Christensen, J.H., 2019. Biodegradation, photo-oxidation, and dissolution of petroleum compounds in an Arctic fjord during summer. Environ. Sci. Technol. 53, 12197–12206. https://doi.org/10.1021/acs.est.9b03336

Wang, C., Chen, B., Zhang, B., He, S., Zhao, M., 2013. Fingerprint and weathering characteristics of crude oils after Dalian oil spill, China. Mar. Pollut. Bull. 71, 64–68.

Wang, Z., Fingas, M., Blenkinsopp, S., Sergy, G., Landriault, M., Sigouin, L., Foght, J., Semple, K., Westlake, D.W.S., 1998. Comparison of oil composition changes due to biodegradation and physical weathering in different oils. J. Chromatogr. A 809, 89–107. https://doi.org/10.1016/S0021-9673(98)00166-6

Wang, Z., Fingas, M.F., 2003. Development of oil hydrocarbon fingerprinting and identification techniques. Mar. Pollut. Bull. 47, 423–452.

Wardlaw, G.D., Nelson, R.K., Reddy, C.M., Valentine, D.L., 2011. Biodegradation preference for isomers of alkylated naphthalenes and benzothiophenes in marine sediment contaminated with crude oil. Org. Geochem. 42, 630–639.
Yang, C., Lambert, P., Zhang, G., Yang, Z., Landriault, M., Hollebone, B., Fieldhouse, B., Mirnaghi, F., Brown, C.E., 2017. Characterization of chemical fingerprints of unconventional Bakken crude oil. Environ. Pollut. 230, 609–620. https://doi.org/0.1016/j.envpol.2017.07.011
Yang, Z., Zhang, G., Hollebone, B.P., Brown, C.E., Yang, C., Lambert, P., Wang, Z., Landriault, M., Shah, K., 2017. Fate of oxygenated intermediates in solar irradiated diluted bitumen mixed with saltwater. Environ. Pollut. 231, 622–634.
Yarranton, H., Motahhari, H.R., Schoeggl, F., Zhou, J.Z., 2015. Evaporative Weathering of Diluted Bitumen Films. J. Can. Pet. Technol. 54, 223–244. https://doi.org/10.2118/174557-PA

CHAPTER 5: FATE OF POLYCYCLIC AROMATIC HYDROCARBONS (PAHS) FROM DILUTED BITUMEN SPILLED INTO FRESHWATER LIMNOCORRALS

Stoyanovich, S[a]., Yang, Z[b]., Hanson, M[d]., Hollebone, B.P[b]., Orihel, D. M[c]., Palace, V[e]., Rodriguez-Gil, JR[a]., Mirnaghi, F[b]., Shah, K[b]., Blais, J.M[a*]

[a] Department of Biology, University of Ottawa, Ottawa, Ontario, K1N 6N5, Canada

[b] Emergencies Science and Technology Section, Environment and Climate Change Canada, Ottawa, Ontario, Canada

[c] Department of Biology and School of Environmental Studies, Queen's University, Kingston, ON K7L 3N6

[d] Department of Environment and Geography, University of Manitoba, Winnipeg, MB, R3T 2N2, Canada.

[e] International Institute for Sustainable Development, Experimental Lakes Area, 111 Lombard Avenue, Suite 325, Winnipeg, Manitoba R3N 0T4, Canada

*Corresponding Author: Jules Blais (jules.blais@uottawa.ca)

STATEMENT OF CONTRIBUTIONS

Stoyanovich, S: conceptualization, writing, formal analysis, analytical, field work
Yang, Z: analytical, reviewing
Hanson, M: reviewing, funding acquisition
Hollebone, B: reviewing, funding acquisition, analytical
Orihel, D: reviewing, funding acquisition
Palace, V: reviewing, funding acquisition
Rodriguez-Gil, J: reviewing
Mirnaghi, F: reviewing, analytical
Shah, K: field work, analytical
Blais, J: supervision, reviewing, funding acquisition, conceptualization, corresponding author

This chapter was prepared for submission to the journal: *Science of the Total Environment*

ABSTRACT

Diluted bitumen (dilbit) is produced by mixing highly viscous bitumen with low viscosity diluent to facilitate transportation. Dilbit's unique physical and chemical properties may cause it to behave differently than commonly transported crude oils in the event of a spill. We report on 70-d-long experimental spills of Cold Lake Winter Blend (CLWB) dilbit in limnocorrals installed directly in a freshwater Boreal lake. A regression design with 2 controls and 7 treatments was used to assess the fate and behaviour of dilbit-derived polycyclic aromatic hydrocarbons (PAHs) as they partition form the dilbit slick into the water column and sediments. Treatments ranged from 1.5 to 180 L of CLWB, resulting in oil:water ratios ranging between 1:71 000 to 1:500 (v:v). We began to detect elevated concentrations of alkylated and parent PAHs in the limnocorral water columns and sediments within the initial days of the spills. By the end of the experiment, the concentrations of PAHs had largely declined in the water column but remained elevated in the sediments. Our results demonstrate that following dilbit spills under calm, quiescent boreal lake conditions, a very small proportion of PAHs enters the aquatic system but produce concentrations that may cause ecotoxicological harm.

1 INTRODUCTION

The Alberta oil sands make up one of the largest petroleum deposits on Earth, with estimated reserves of 170 billion barrels of bitumen: a form of unconventional heavy crude oil (CAPP, 2019; Lee et al., 2015). Bitumen is a highly viscous form of crude oil that must be diluted with natural gas condensates to facilitate pipeline transport, forming diluted bitumen or dilbit (Crosby et al., 2013; Fingas, 2015). Despite environmental concerns and proposed pipeline expansions, little is known about the environmental fate and effects of dilbit spills, especially in freshwater areas such as inland lakes (Crosby et al., 2013; Fitzpatrick et al., 2015; Lee et al., 2015; NASEM, 2016; Yang et al., 2020).

Oil spills to freshwater can pose major threats to the receiving environment by compromising water supplies and affecting areas of dense human population (Owens et al., 1993). Inland lakes also have limited dispersion and dilution capabilities compared to ocean systems, although oil spills in freshwater are typically much smaller than in ocean settings (Lee et al., 2015). In an open sea system, breaking waves and tidal action can facilitate the transport and dissipation of concentrated oil spills. In low-energy freshwater environments such as sheltered lakes, oil is retained for longer periods of time (Baca and Getter, 1985). A major example of a crude oil spill to freshwater occurred in 2005, when a train derailment caused a 149,500 L spill of Bunker C heavy fuel into Wabamun Lake, Alberta, Canada (Debruyn et al., 2007). In 2010, a pipeline rupture led to the release of 3.2 million L of Cold Lake Blend (CLB) dilbit into Talmadge Creek, and eventually the Kalamazoo River in Marshall, Michigan (US EPA, 2013). In 2013, a pipeline carrying Wabasca heavy crude oil ruptured in Mayflower, Arkansas, releasing approximately 795,000 L of oil into a residential neighborhood that eventually

drained into Lake Conway (Kennon and Bouldin, 2015). In 2016, the rupture of a Husky Energy pipeline in Lloydminster, Saskatchewan released approximately 225, 000 L of diluted heavy crude oil, 40% of which entered the North Saskatchewan River (Husky Energy Inc, 2016; Yang et al., 2020). These spill scenarios have provided an opportunity for researchers to study impacts of a dilbit spill in freshwater. However, since physical recovery of the spilled oil is top priority, environmental sampling is often delayed. Such studies are also hampered by the unexpected nature of a spill; it is difficult to plan a proper study around an accidental spill that occurs without warning.

Following the early stages of an oil spill in an aqueous system, low boiling point compounds that are both volatile and readily water-soluble will partition to the air and water column (Lee et al., 2015), leaving behind a recalcitrant oil residue (Tarr et al., 2016). Certain oil-derived compounds, including polycyclic aromatic hydrocarbons (PAHs) have garnered much attention in the scientific literature due to their toxicity, carcinogenicity and relative resistance to biodegradation (specific to the larger 3-5 ringed PAHs) (Achten and Andersson, 2015; Lee et al., 2015; Van Hamme et al., 2003). Therefore, their water column concentrations following a spill can provide estimates of the potential for toxicity (Neff and Stubblefield, 1995; Reddy and Quinn, 2001). Studies have shown that the dissolution of hydrocarbon occurs within the initial hours following a spill (Brussaard et al., 2016; Gros et al., 2014; Ortmann et al., 2020; Stoyanovich et al., 2019). While dissolution only accounts for a very small portion of the total oil loss (Fingas, 2015; Lee et al., 2015), it can still result in the exposure of aquatic biota to potentially toxic compounds. Contamination can also extend down to the sediments, where hydrophobic compounds may bind to suspended and/or sinking sediment and

persist over long periods of time (Lee et al., 2003). Characterizing the fate of spilled crude oil's chemical constituents in an aquatic system under realistic spill conditions is therefore crucial to understanding potential ecotoxicological effects of a dilbit spill (Bejarano et al., 2014).

Here, we report results from a series of seven controlled dilbit spills (with two controls), ranging in dilbit volume from 1.5 to 180 L, into limnocorrals installed in a small boreal lake located in Northwestern Ontario, Canada. This work focuses on describing the quantity and distribution of aromatic compounds in the water columns and sediments following the spills. Our experimental design is unique in that we began collecting paired dilbit slick, air, water column and sediment samples immediately following the spills (earliest sample 6 h post spill) and over a period of 70 days. This enables us to describe both the short- and long-term behaviour of these compounds as they partition from the dilbit slick to the air, water, and sediments of the limnocorrals. We intended this study to improve models of hydrocarbon partitioning in the environment immediately following a dilbit spill into a Canadian boreal lake.

2 MATERIALS AND METHODS

2.1. Experimental Spills and Sampling

The experiment consisted of nine in-lake limnocorrals deployed along the northwestern littoral zone of Lake 260 at the International Institute for Sustainable Development Experimental Lakes Area (IISD-ELA) in Kenora, Ontario, Canada. The limnocorrals were 10 m in diameter and consisted of a floating ring to which we attached a high-density polyethylene (HDPE) cylindrical membrane that extended to the

sediments at a depth ranging from 1.5 – 2 m (SI Figure S5.1). We used two layers of sandbags around the perimeter to seal the plastic membrane onto the lake bottom (SI Figure S5.2). The experimental set up has been previously described in detail (Rodriguez-Gil et al., 2021). On June 20th, 2018, we pumped Cold Lake Winter Blend dilbit (CLWB) onto the water surface of the treatment limnocorrals. The logistical considerations surrounding the additions have been described by Shah et al. (2019). The addition of water containing a known amount of tritium (^{3}H) to each limnocorral at the beginning of the experiment allowed us to accurately determine the water volume inside the limnocorrals and characterize any potential water exchange through leaks or ruptures with the lake. This method has been described in detail by Rodríguez-Gil et al. (2021). Limnocorral water volumes ranged from 90.7 to 106.5 m^3. Throughout the study no visible gaps, ruptures, or holes were observed in any of the limnocorrals.

The seven treatments received the following dilbit volumes in the form of a regression design, (L): 1.5, 2.9, 5.5, 18, 42, 82, and 180 as well as two controls without any dilbit addition, one near field control (NFC) and one far field control (FFC) (SI Figure S5.3). These spill volumes resulted in oil:water ratios within the limnocorrals ranging from 1:71 000 to 1:500 v/v. We selected these oil:water ratios based on published onshore crude oil spill occurrences throughout North America between 2008 and 2017 (NEB, 2017; USDOT, 2017). The lower limit of 1.5 L replicates the most common onshore spill size, while the upper limit of 180 L produces an oil:water ratio similar to that of the largest inland spill to date, the 2010 Kalamazoo River spill. A detailed rationale for our spill volume selection was published elsewhere (Rodriguez-Gil et al., 2021). These experimental spills lasted a total of 70 days, throughout which we

collected oil slick, air water and sediment samples to assess how these environmental compartments change over time following the introduction of dilbit.

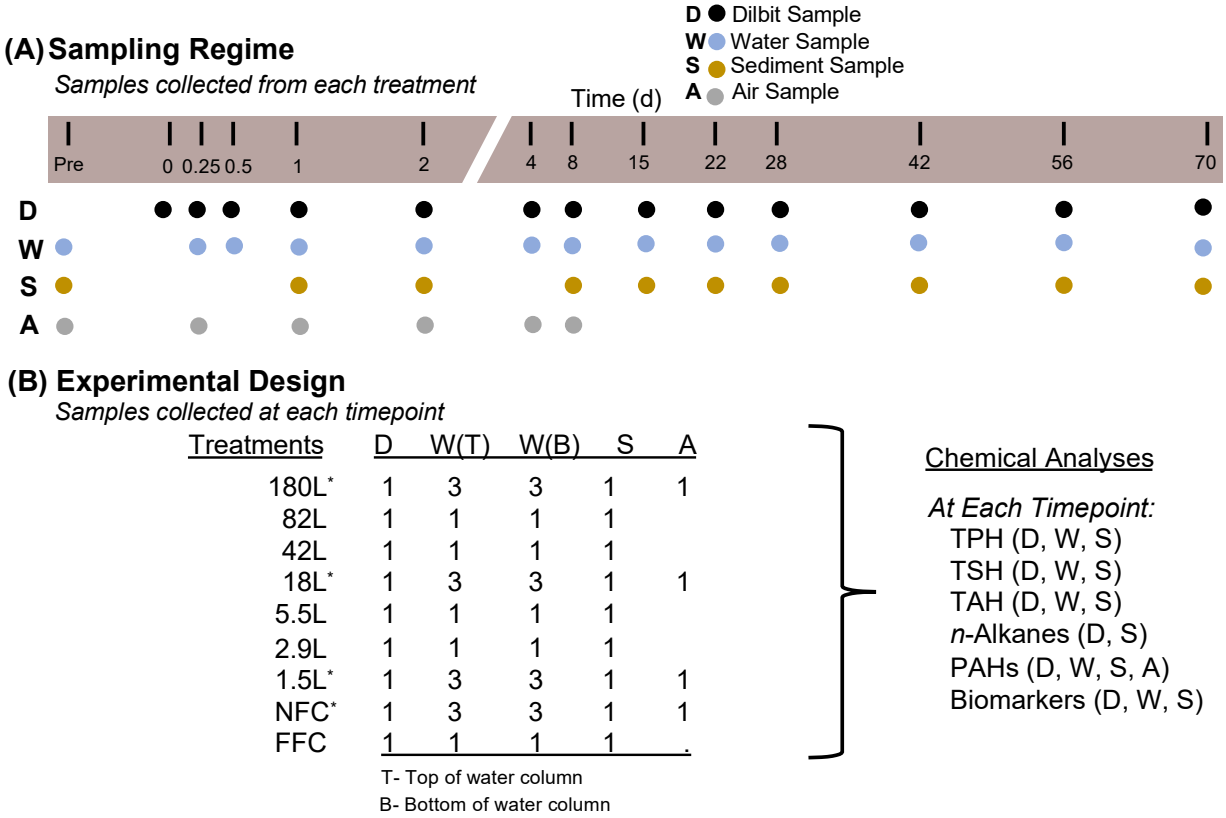

Figure 5. 1. Overview of environmental media sampling timepoints and associated analyses. Panel (A) shows the sampling regime for the dilbit slick (D), water column (W), sediments (S), and air. Panel (B) shows the number of samples collected at each timepoint for each environmental medium (9 oil slick samples, 34 water samples, 9 sediment samples, and 4 air samples- at each timepoint). TPH: total petroleum hydrocarbons, TSH: total saturated hydrocarbons, TAH: total aromatic hydrocarbons.

2.2. Water Column Sampling

We collected water samples for hydrocarbon analysis from the center of each limnocorral at two depths below the water surface (0.1 m and 1.5 m) at -1, 0.25, 1, 2, 4, 8, 15, 22, 28, 42, 56 and 70 days following the dilbit additions (Figure 5.1). The water was pumped from the center-point of each limnocorral through 0.6 cm inner diameter high density polyethylene (HDPE) tubing connected to a Spectra Field-Pro Peristaltic

Pump (flow rate of 1 L min^{-1}) located on the adjacent dock (SI Figure S5.1). The first 1 L of each sample was discarded, after which approximately 1 L of water was collected into pre-weighed, certified-clean amber glass bottles with Teflon film cap liners filled to the top to minimize headspace and any evaporation of volatile compounds. The collected water samples are representative of bulk (unfiltered) samples that include both dispersed and dissolved oil components. There are currently no accepted methods for separating dispersed oil droplets from the dissolved phase in water samples and attempts to do so reduce the realistic nature of field samples (Lee et al., 2015). Preliminary analysis of the total petroleum hydrocarbon (TPH) concentration of these samples indicated no significant differences between the top and bottom water column measurements in any of the treatments, indicating vertical mixing in the water column (Rodriguez-Gil et al., 2021). Because of this, the results from top and bottom measurements were averaged to simplify analyses.

Due to rigorous sampling schedules and intensive analytical demands, only four of the seven treatments: NFC, 1.5 L, 18 L, and 180 L, were chosen to be sampled in triplicate at each depth and timepoint, while single samples were collected from all other treatments.

2.3. Sediment Sampling

Due to the large surface area of the limnocorrals (approx. 75 m^2) and the inability to enter the limnocorrals by boat once the experiment had commenced, all sediment sampling had to be done from the adjacent docks. Invasive techniques such as Ponar dredging, coring, or Ekman grab sampling could not be used as they would significantly

disturb the sediment bottom and re-suspend sediment particles that can in turn alter the fate of the dilbit. Therefore, prior to the beginning of the experiment, a series of 250 mL pre-cleaned glass jars were filled with sediments collected from each limnocorral plot and then placed on the sediment bottom directly below the oil-free partition area (SI Figure S5.1). At each timepoint after the spills, a single jar from each treatment was pulled up through the partition at -3, 1, 2, 8, 15, 22, 28, 42- and 70-days following dilbit addition (Figure 5.1). All samples were stored in a cooler in the field and transferred to a refrigerator in the lab. Due to the placement of these jars below the oil-free partition, no sediment samples showed signs of physical oiling during the study. At the end of the experiment and prior to decommissioning, we entered both the 18 and 82 L treatments and collected 3 sediment cores from both treatments near the centre-point of the limnocorral. We chose areas where the sediments were visibly oiled with dilbit in the form of “tarballs”, in order to get a true estimate of sediment contamination following dilbit submergence. We collected the sediment cores with the tarballs centered in the coring tube (SI Figure S5.4), then removed the tarball and collected the top 1cm of the sediment core for PAH analysis.

2.4. Air Sampling

We conducted air monitoring in the 180L, 18 L, and NFC during the first 8 days of the study. We collected air samples 0.3 m above the water’s surface and roughly 1 m from the northern edge of the limnocorrals (SI Figure S5.1). Air samples were collected at -3, 0.25-, 1-, 2-, 4-, and 8-days post dilbit release from each of the three limnocorrals. At each sampling timepoint, we ran air samplers for a 60-minute period at a flowrate of 5 L min^{-1}. The air samplers consisted of a GilAir® Plus Air Sampling Pump (Levitt Safety,

Ottawa, ON), operated at a flow rate of 5 L min^{-1}, connected to a sampling cartridge via polyvinyl chloride (PVC) connecting tube (Fisher Scientific, Ottawa, ON, Canada). The cartridge contained polyurethane foam (PUF) (URG Corporation, Chapel Hill, NC) and a Quartz filter (25 mm) (Whatman, Maidstone, UK). The pumps were calibrated before sampling using a Gilian Gilibrator-2 Calibrator (Levitt Safety, Ottawa, ON). All Quartz filters were baked at 400°C for 5 h prior to use. Following sample collection, the PUFs and filters were stored in pre-baked aluminum foil and stored in a freezer.

2.5. Sample Analyses

All water samples were processed and extracted for hydrocarbons on the same day of collection. Samples were spiked with surrogates (o-terphenyl, d_{50}-tetracosane, d_8-naphthalene, d_{10}-acenaphthene, d_{10}-phenanthrene, d_{12}-benz[a]anthracene, and d_{12}-perylene) and extracted with 50 mL of dichloromethane (DCM) for 16 hours on a continuous roller apparatus. Triplicate lab blanks were run with ultra-pure Milli-Q water and all PAH concentrations were blank corrected. The sample and instrumental analysis followed the same procedure as Yang et al. (2018). Percent recoveries for water samples are reported in SI Table S5.2.

The top 5cm of the sediments in the jars was removed, homogenized and dried with sodium sulphate, spiked with deuterated PAH surrogate and then Soxhlet extracted with dichloromethane (DCM) for 16 hours. The extracts were then treated in the same manner as the water samples mentioned above. Percent recoveries for sediment samples are reported in SI Table S5.2.

For air samples, prior to extraction, PUFs and filters were spiked with isotopic labeled deuterated PAH standard mix containing d_8-naphthalene, d_{10}-acenaphthene,

d_{10}-phenanthrene, d_{12}-benz[a]anthracene, and d_{12}-perylene obtained from Cambridge Isotope Laboratories (Tewksbury, MA 01876). PUFs and filters were then extracted using Accelerated Solvent Extraction (ASE 200, Dionex Corporation, Sunnyvale, CA, USA). Following extraction, samples were fractionated by silica gel column chromatography and separated into F1 fraction (*n*-alkanes) with hexane and F2 fraction (PAHs) with a 1:1 mixture of dichloromethane (DCM) and hexane. Samples were then spiked with an internal standard, *p*-terphenyl-d14 (Cambridge Isotope Laboratories, Tewksbury, MA 01876) at 1000 pg μl^{-1}, vortexed, and refrigerated until instrumental analysis. PAH (parent and alkylated) concentrations were quantified by gas chromatography coupled with mass spectrometry (GC-MS). All samples were blank corrected to remove background PAH contamination and recovery corrected. Percent recoveries for air samples are reported in SI Table S5.2.

2.6. Data Modelling and Analyses

We used R Studio version 1.1.383 (RStudio., Boston, MA, USA) to perform all statistical analyses and graphical representations. Paired, two-way Student's t-tests enabled the comparison of mean total PAH concentrations, presented as the sum of 46 PAH analytes (ΣPAH_{46})**,** between top and bottom water column replicates (n = 3) within each intensive treatment (180 L, 18 L, 1.5 L, and NFC). This test elucidates whether or not PAH concentrations differ between the top and bottom of the water column and can inform on the impact of vertical mixing on the water column results. We used linear regression to assess dilbit to water ratio as a predictor for PAH contamination in the water column and sediments by regressing the concentration against the nominal oil:water ratio at each sampling timepoint. Here, a significant positive slope estimate

would indicate PAH contamination is proportional to the oil:water ratio at the particular time point. We used principal component analysis (PCA) to explore similarities and differences in the chemical profiles of environmental water, sediment, and the spilled CLWB dilbit samples, similar to the work of Allan et al. (2012).

3 RESULTS AND DICUSSION

3.1. Hydrocarbon Contamination of the Water Column

Analysis by Rodriguez-Gil et al. (2021) has shown no significant difference between hydrocarbon concentrations in water samples collected from the top and bottom of the water column, suggesting mixing in the water column. As such, the results from all top and bottom water samples collected at each time point were averaged. The temporal progression of water column PAHs in each treatment can be characterized by an initial increase phase, a brief plateau at the maxima, and a subsequent decrease phase (Figure 5.2). Maximum PAH concentrations were observed for naphthalenes **(**$\Sigma NAP_{C0\text{-}C4}$) in all treatments except for 2.9 and 1.5 L, where phenanthrenes ($\Sigma PHEN_{C0\text{-}C4}$) and dibenzothiophenes ($\Sigma DBT_{C0\text{-}C3}$) were the most abundant PAH groups, respectively. The treatments reached their maximum PAH concentrations on day 22 for the 180 and 82 L, day 15 for the 42 and 18 L, day 2 in the 5.5 L, and day 8 in the 2.9 and 1.5 L. Compositional patterns of alkylated PAH groups in water samples indicate the dominant PAH groupings were the naphthalenes ($\Sigma NAP_{C0\text{-}C4}$), phenanthrenes ($\Sigma PHEN_{C0\text{-}C4}$), fluorenes ($\Sigma FLU_{C0\text{-}C3}$), and dibenzothiophenes ($\Sigma DBT_{C0\text{-}C3}$), together accounting for 16– 54%, 14 – 26%, 14 – 31%, and 14 – 32% of maximum total PAH, denoted as ΣPAH_{46}, concentrations across all treatments (SI Figure S5.5B). ΣPAH_{46},

ΣAlkyl-PAHs, and ΣEPA-PAHs concentrations in the water column have previously been reported by Rodríguez-Gil et al. (2021).

Notably, we found an uncharacteristic spike of $\Sigma NAP_{C0\text{-}C4}$ between days 1 and 2 in each treatment (Figure 5.2). These results may have arisen from cross-contamination of water samples with the dilbit slicks during sampling, analytical error, field sampling variability, or contamination from boats during sampling. Since we are unable to determine the source of this inconsistency, and since it is possible that these results do reflect the true nature of the experiment, we chose to include them in all analyses.

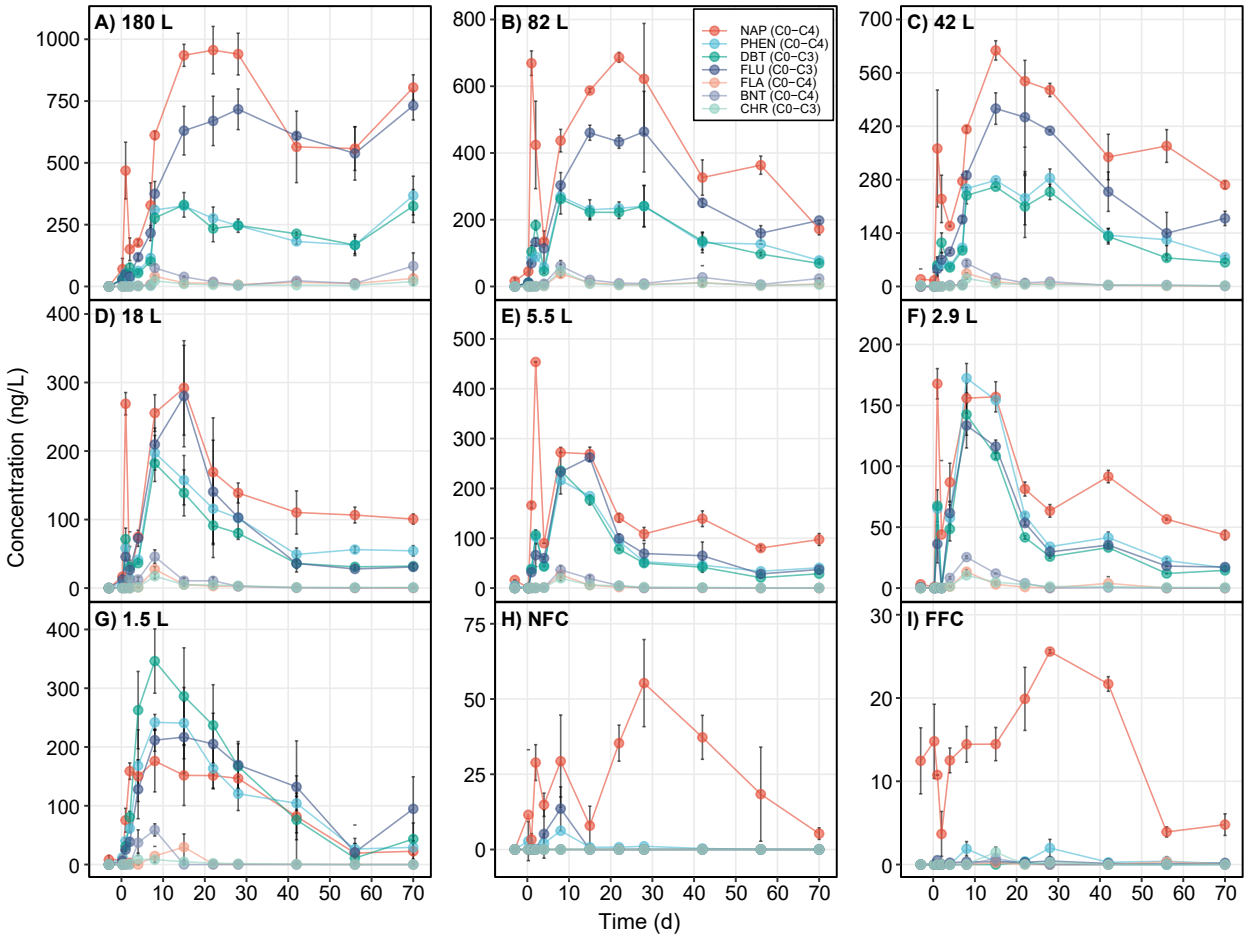

Figure 5. 2. PAH group concentrations in the water column over time. The sum of the parent and each alkylated homolog in each group is presented. Error bars represent standard deviation measured over N= 6 (180 L, 18 L, 1.5 L, and NFC) and n = 2 (82 L, 42 L, 5.5 L, 2.9 L, and FFC). Note changing y-axis scale.

The water samples were typically dominated by C1, C2, and C3 alkylated homologs compared to parent compounds (SI Figure S5.6), likely reflecting the relatively low concentrations of parent PAHs in the source dilbit (SI Figure S5.7). While accumulation in the water column was dominated by 2 – 3 ring PAHs, the concentrations were not significantly proportional to log K_{OW} values when regressed (SI Figure S5.8). The single most abundant PAH groups in the 180, 42, 18, 5.5, and 2.9 L limnocorrals were the C4-NAPs, reaching concentrations of 509 ± 25, 317 ± 10, 150 ± 17, 189 ± 33, and 74 ± 6 ng L^{-1}, respectively. The C3-NAP homologues were the most abundant group in the 82 L treatment (323 ± 7 ng L^{-1}), and C2-DBT group, the most abundant in the 1.5 L treatment (160 ± 17 ng L^{-1}) (SI Figure S5.6). We detected the 4-ring fluoranthenes ($\Sigma FLA_{C0\text{-}C4}$), benzonaphthothiophenes ($\Sigma BNT_{C0\text{-}C4}$), and chrysenes ($\Sigma CHR_{C0\text{-}C3}$) at measurable concentrations on day 8 in all treatments and on day 70 in the 180 L, but they remained otherwise below detection limits, similar to our previous tank study (Stoyanovich et al., 2019). It is important to note that the ^{3}H profiles of the 18 and 82 L treatments suggested significant water exchange with the lake throughout the experiment, at rates of 0.035 and 0.016 d^{-1}, respectively, which were an order of magnitude greater than the leakage rates of the remaining treatments (Rodriguez-Gil et al., 2021). Because of this, we are likely underestimating the PAH concentrations in the 18 and 82 L treatments. These concentrations represent what would occur following a dilbit spill in an enclosed or semi-enclosed boreal lake, where water exchange is low. In large open systems such as coastal environments or large lake systems such as the Great Lakes, water exchange in and out would result in rapid decreases in water column PAHs by dilution (Ortmann et al., 2020).

There are many explanations for the observed depletions in water-borne PAHs (Figure 5.2). Firstly, the thick, highly weathered crust that formed on the exterior of the dilbit slicks early on in experiment (Stoyanovich et al., 2021) may have limited further dissolution as time progressed. This crust is thought to be formed following the loss of low molecular weight compounds (Fingas, 2015), leaving behind heavy resins and asphaltenes that migrate to the oil-water interface during emulsification (Fingas and Fieldhouse, 2009), and decrease dissolution rates (Fingas, 2015). Secondly, the retreating dilbit-slick cover would result in an increase in open water within the limnocorrals. This increase in open water area over the course of the experiment would facilitate PAH evaporation across the water – air interface. Initially the dilbit spread to cover the majority of the water's surface, however with wind action, gaps formed in the slicks and created sections of open water, adding to the oil slick weathering effects. Open water became even more apparent as the slicks began to sink on day 12 in the lowest-concentration treatment and day 31 in the highest-concentration treatment (Stoyanovich et al., 2021). The volatilization rate of a compound from water to air is proportional to the surface area of open water. Surface slicks would act as a barrier to evaporation (King et al., 2019), thus as this barrier is removed, PAH evaporation from the water column would accelerate. This circumstance corroborates our observations in the 180 L treatment, where the surface dilbit slick remained for a longer period of time compared to the other treatments, resulting in a slower PAH depletion rate in the water column (Figure 5.2A). Finally, the PAHs in the water column would eventually partition to the sediments, reflective of their preference for the organic phase (discussed in section 3.3). We do not present any of these factors as a full explanation for the

observed depletions, as it may be a combination of these that are responsible for the depletions.

Drawing comparisons between our results and those of other studies is challenging as factors such as experimental setting, dilbit type, and duration can all have significant effects on PAH dissolution trends. Few studies have reported PAH concentrations in water following a dilbit spill. Stoyanovich et al. (2019) tracked PAHs in the water column following summer spills of CLB into freshwater tanks (~1400 L and 3.1 m^2) at an oil: water ratio of 1:8000 over 11 days. Ortmann et al. (2020) report PAHs in the water column following spills of three different types of dilbit (Access Western Blend, Western Canadian Select, and Synbit) during the summer into flume tank enclosures (~250 L and 0.31 m^2) filled with natural seawater for 14 days. All of the maximum water column concentrations of the seven major PAH groups (NAP, PHEN, DBT, FLU, FLA, BNT, and CHR) of both studies as well as comparisons with our results can be found in SI Table S5.3. When comparing the results at similar oil:water ratios, we find that our maximum concentrations for each PAH group are typically greater than those of Stoyanovich et al. (2019) in all cases except for naphthalenes. Similarly, our maximum naphthalene concentrations were much lower than those of Ortmann et al. (2020). In general, our results were in keeping with the Access Western Blend (AWB) dilbit results, but considerably lower than Synbit and Western Canadian Select (WCS) results (SI Table S5.3). A major difference between the present study and the tank-based studies of both Stoyanovich et al. (2019) and Ortmann et al. (2020) is scale. Our lower profile, in-lake study design along with the large surface area of the limnocorrals (~75 m^2) allows for wind to play a major role in the distribution of the slicks on the water's surface

(Stoyanovich et al., 2021). This creates large areas of open water that promoted the volatilization of low molecular weight (LMW) compounds and is a likely explanation as to why our $\Sigma NAP_{C0\text{-}C4}$ concentrations were lower. Perhaps the most important factor to consider is chemical composition of the different dilbits. Ortmann et al. (2020) noted that the diluent differs across their three test dilbits, the composition of which can impact what PAHs are found in the water column. The effect of dilbit-type on the dissolution patterns of PAHs can be seen by observing the variation in concentrations across each dilbit-type used by Ortmann et al. (2020). A quantitative comparison between studies is difficult since the test dilbits were different.

3.2. Chemical Source Modelling of the Water Column

A principal component analysis enabled us to highlight similarities and differences in the chemical profile of water column samples collected from each treatment and control. In our study, a PCA (Figure 5.3) revealed that pre-spill water samples were similar across each treatment, reflective of background PAH concentrations dominated by naphthalenes. Following the dilbit additions, the controls remained clustered with the pre-spill samples, while the dilbit-amended treatments began to shift away from pre-spill conditions. Interestingly, day 8 samples demonstrated a shift in the direction of the source oil. The day 8 water samples exhibited an enrichment of less soluble hydrocarbons including the 3- or greater number of ring PAHs (SI Figure S5.6) and water-insoluble cyclic alkanes, such as hopanes, terpanes, and steranes (SI Figure S5.9), which is indicative of the presence of oil droplets in the sample. The water column likely experienced a flux of oil droplets forced into the water column following a rain event that occurred on day 7 (25 mm in 6 hours). Day 8 water

samples also showed a biomarker profile that resembled CLWB (SI Figure S5.10), further suggesting the presence of droplets. Aside from day 8 samples, the other timepoints did not shift towards the source oil, likely because the water samples were dominated by water soluble compounds, whereas the source oil contained a significant proportion of high-molecular-weight (HMW) PAHs that would not transfer into the water.

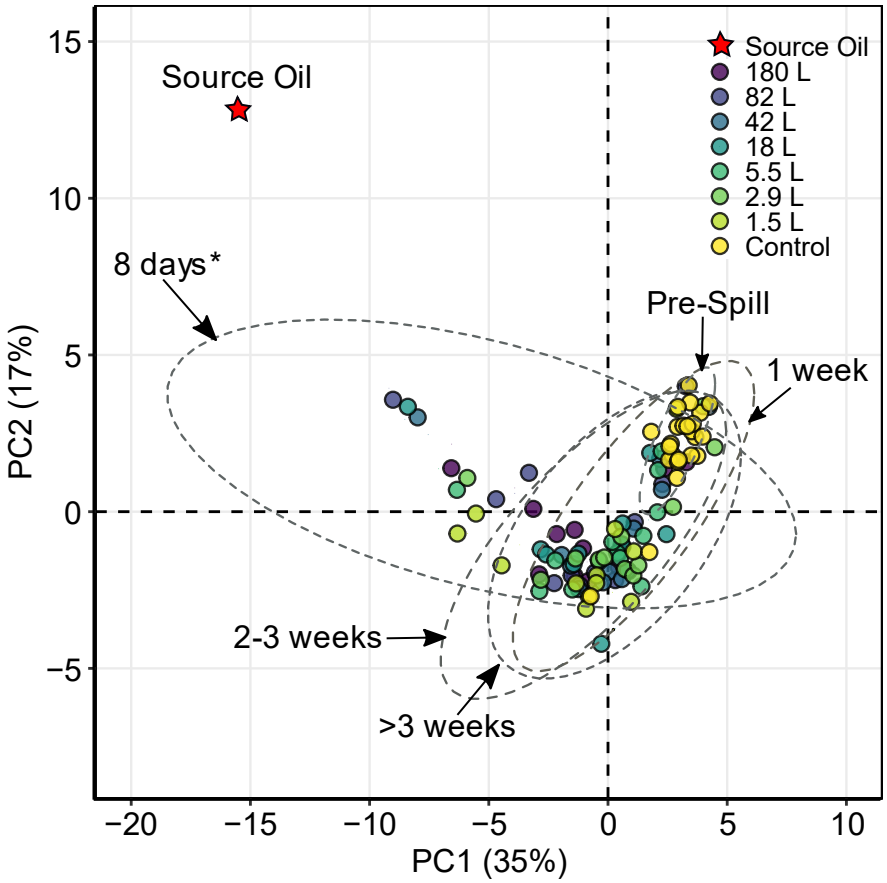

Figure 5. 3. Principal components analysis of PAH profiles normalized to ΣPAH_{46} in water samples collected throughout the entire study from each treatment and control. Principal components 1 and 2 account for 52% of the variability in the data set. Ellipses represent the 95% confidence interval within the 2-D space.

3.3. Hydrocarbon Contamination of the Sediments

Sediment samples collected from pre-positioned jars placed within the limnocorrals allowed us to track temporal changes in concentration of oil components following the spill. The individual PAH profiles in contaminated sediments changed with

time (Figure 5.4), gradually increasing throughout the experiment, showing no clear signs of stabilization. The accumulation of alkylated PAHs in the sediments was proportional to logK_{OW} (SI Figure S5.11), such that PAHs with higher logK_{OW}, such as those with more rings and alkyl groups, were found at higher concentrations, reflective of their affinity for the organic phase (Achten and Andersson, 2015).

Phenanthrenes were the most abundant PAH group ($\Sigma PHEN_{C0\text{-}C4}$) in the 180, 42, 18, 5.5, and 1.5 L treatments accounting for 16 – 51 % of the ΣPAH_{46}, whereas the benzonaphthothiophenes ($\Sigma BNT_{C0\text{-}C4}$) were the most abundant in the 82 and 2.9 L treatments accounting 24 – 36 % of the ΣPAH_{46} (SI Figure S5.12B). Notably, sediment samples collected from the dilbit treatments were enriched in sulfur heterocycles (dibenzothiophene and benzonaphthothiophenes) while the controls were not. These compounds are major components of the organic sulfur content of crude oils (Mössner and Wise, 1999) and bitumen (Lam et al., 2012), and are often used as a marker for oil contamination.

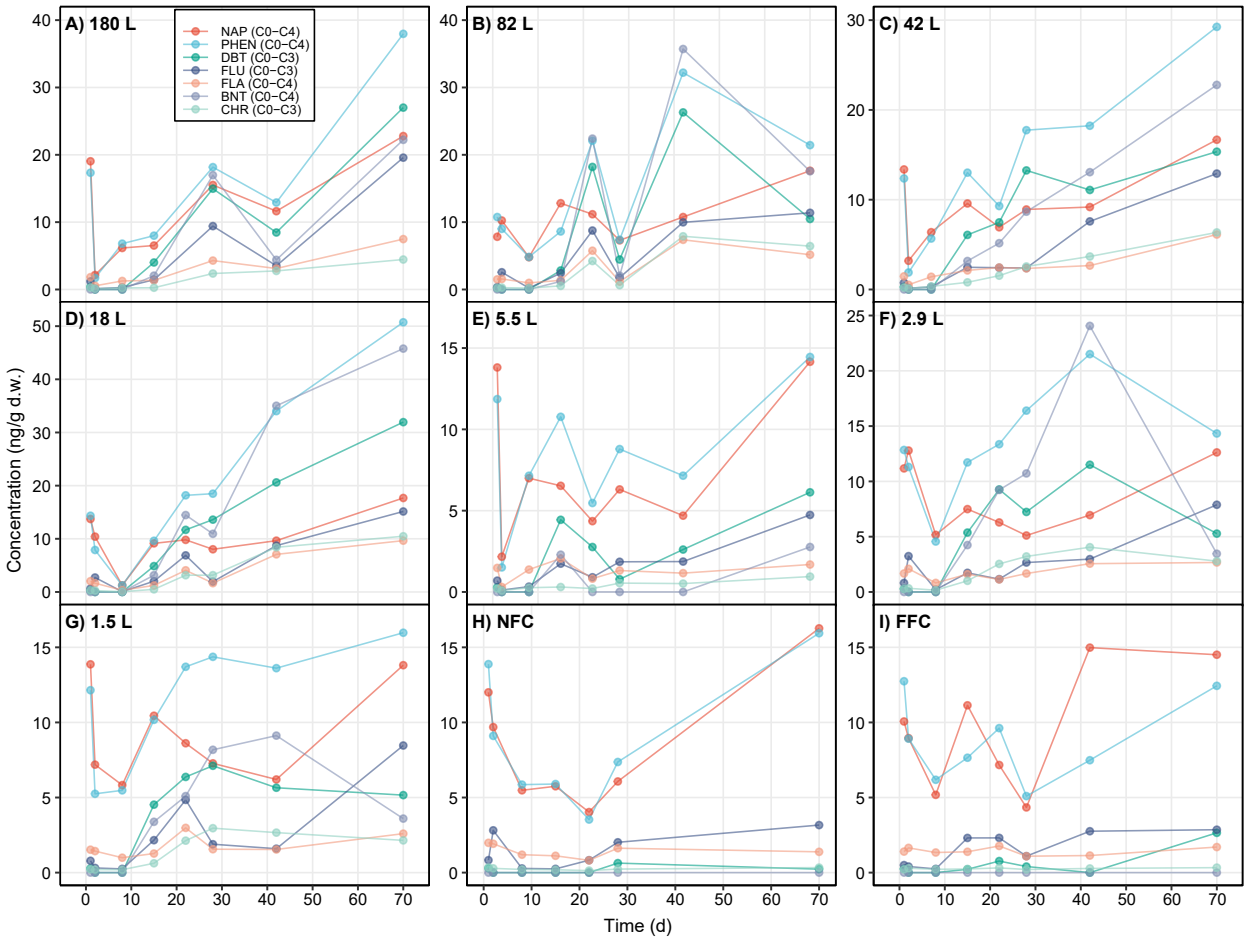

Figure 5. 4. PAH group concentrations over time in the sediments. The sum of the parent and each alkylated homolog in each group is presented. Note changing y-axis scale.

The unalkylated parent compound naphthalene and phenanthrene signals present both in pre-spill and control samples are likely attributable to recent and past forest fires (Murphy and Morrison, 2014), which are common during the summer months in this region. The majority of the alkylated 3-4-ring PAHs remained at or below detection limits in the two controls but showed elevated concentrations in the dilbit-amended treatments. Among the measurable PAHs, concentrations of C_3-DBTs reached the highest concentrations in the 180, 82, and 18 L treatments (14.2, 15.4, and 19.4 ng g^{-1} d.w., respectively), C_3-BNTs reached the highest concentration in the 42 and 2.9 L treatments (10.5 and 7.9 ng g^{-1} d.w., respectively), C_2-BNTs reached the highest

concentration in the 1.5 L treatment (4.3 ng g^{-1} d.w.), and C_3-NAPs reached the highest concentration in the 5.5 L treatment (4.5 ng g^{-1} d.w.) (SI Figure S5.13). In nearly all treatments, the maximum PAH concentrations were reached at the end of the experiment.

Given the placement of the pre-positioned sediment jars below the oil-free partition area (SI Figure S5.1), we did not account for sediments in direct contact with submerged oil. Therefore, following the completion of the study, we collected a total of 6 sediment samples that were in direct contact with sunken dilbit globules in the 18 L (n=3) and 82 L (n=3) treatments (SI Figure S5.4). Core samples collected in triplicate from the 18 L and 82 L treatment had mean ΣPAH_{46} concentrations of 1873 ± 2457 ng g^{-1} and 5643 ± 7817 ng g^{-1}, respectively (Figure 5.5A).

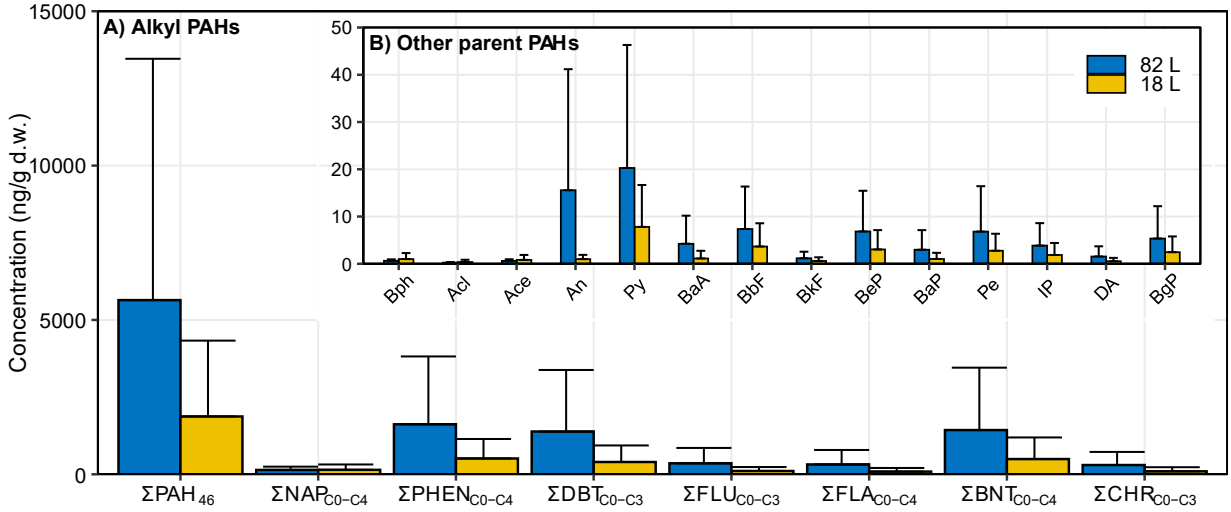

Figure 5. 5. PAH group concentrations in sediment samples in direct contact with sunken dilbit. The sum of the parent and each alkylated homolog in each group is in (A). 14 EPA priority PAHs are in panel (B). Error bars are standard deviations measured over N= 3.

The most abundant PAH groups in both treatments were $\Sigma PHEN_{C0-C4}$, ΣBNT_{C0-C4} and ΣDBT_{C0-C3}, whose concentrations ranged from 398 ± 536 to 512 ± 631 ng g^{-1} in the

18 L and 1385 ± 1994 to 1621 ± 2197 ng g^{-1} in the 82 L treatment (Figure 5.5A). The ΣFLA_{C0-C4}, ΣFLU_{C0-C3}, ΣCHR_{C0-C2}, and ΣNAP_{C0-C4} remained at comparatively lower concentrations ranging from 87.3 ± 117 to 144 ± 174 ng g^{-1} in the 18 L and 142 ± 105 to 356 ± 497 ng g^{-1} in the 82 L treatment (Figure 5.5A). We observed high variation across triplicate samples, as evidenced by the large error bars in Figure 5.5. Uneven submergence of dilbit explains this observation.

Our results uniquely capture two different aspects of sediment contamination following a dilbit spill; (1) sediments that accumulate PAHs by means of natural partitioning or deposition from the water, represented by our jar samples, and (2) sediments in direct contact with submerged oil, represented by our oiled sediment samples. These results highlight the variability in sediment PAH concentrations that can arise if the dilbit submergence. For example, ΣPAH_{46} ranged from 379 – 4708 ng g^{-1} in the 18 L treatment, roughly 2 – 25X higher than the maximum values observed across all jar samples. In the 82 L treatment**,** ΣPAH_{46} concentrations ranged from 587 – 14646 ng g^{-1}, roughly 3 – 77X higher than maximum values observed across all jar samples (SI Table S5.4). Evidences from the July 2007 dilbit spill in Burnaby, British Columbia, Canada show maximum total PAH concentrations in oiled sediments reaching 30300 ng/g (Stantec, 2012). Further, oiled sediment samples collected following the 2010 Kalamazoo River spill in Marshall, Michigan, U.S. show sediment total PAH concentrations ranging from 7000 to 170000 ng g^{-1} (Fitzpatrick et al., 2012). These results suggest that our study only captures a small range of potential sediment PAH concentrations. Further, since dilbit sinks in a heterogeneous manner (Stoyanovich et

al., 2021), certain sections of the sediments will be more oiled than others, stressing the need for a broad sampling approach to capture the full range of contamination.

3.4. Chemical Source Modelling of the Sediments

Similar to water samples, we used a multivariate approach to assess the distribution of PAHs in collected sediment samples and to qualitatively compare them to the spilled CLWB by PCA. All sediment samples collected during the first week of the study clustered together along with the controls (Figure 5.6). As previously discussed, the majority of PAH and biomarker concentrations in the sediments remained below detection limit for the first 15 days of the study, and then began to increase, likely coinciding with dilbit submergence (Stoyanovich et al., 2021). Between weeks 1 and 2, the PAH profiles of the samples began to change, as shown by the distancing of these points from the earlier timepoints on the PCA plot. For the remainder of the study, the PAH profiles of collected sediments shifted towards the data point representing the CLWB dilbit.

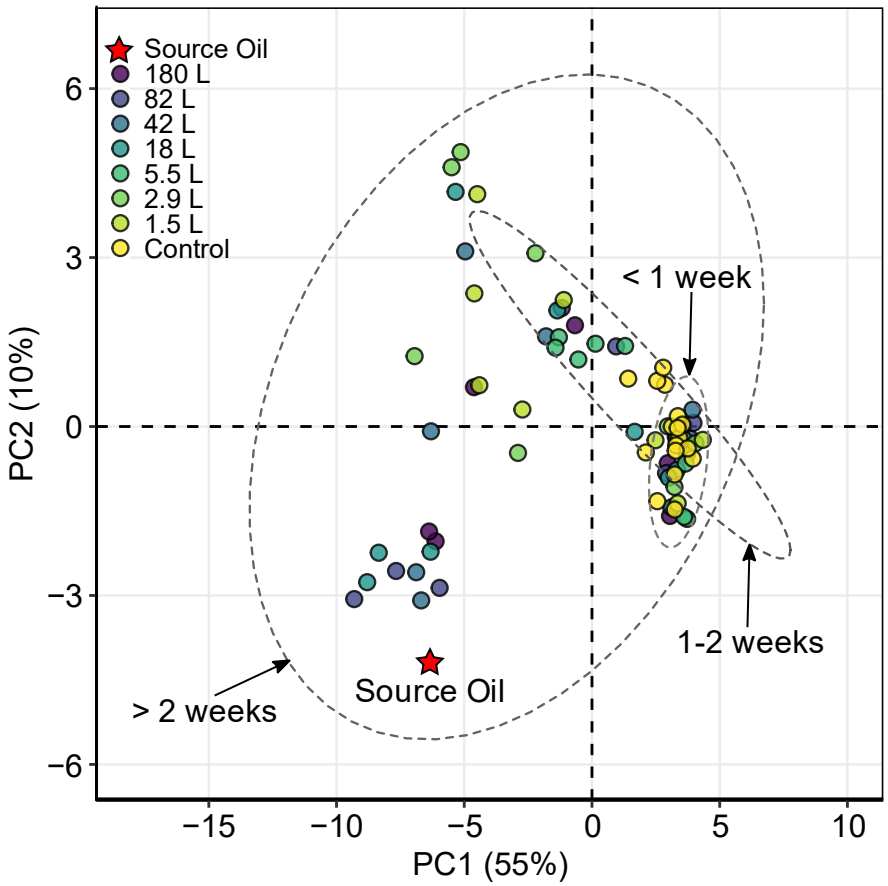

Figure 5. 6. Principal components analysis of the PAH profiles normalized to ΣPAH_{46} in sediment samples collected throughout the entire study from each treatment and control. Principal components 1 and 2 account for 65% of the variability in the data set. Ellipses represent the 95% confidence interval within the 2-D space.

3.5. Hydrocarbons in the Air

Our methods enabled a total of 40 parent and alkylated PAH compounds (denoted as ΣPAH_{40}) to be quantified in air (SI Table S5.1). Pre-spill air samples were highly variable across the three studied treatments (180 L, 18 L, and NFC), with ΣPAH_{40} concentrations ranging from 1133 to 2100 ng m^{-3}. These samples were made up of mostly parent and alkylated naphthalenes and phenanthrenes. Following the onset of the spills, the ΣPAH_{40} concentrations in the 180 L treatment increased from 2099 ng m^{-3} (pre-spill) to a maximum concentration of 6835 ng m^{-3} by day 2 (3.3X greater than background) and then subsequently decreased for the remainder of the sampling period

(SI Figure S5.14). In the 18 L treatment, ΣPAH_{40} concentrations increased from 1132 ng m^{-3} (pre-spill) to a maximum value of 3210 ng m^{-3} after just 6 hours (2.8X greater than background) and then immediately decreased, with a period of slight increase between day 2 and 8. Following the spills, the ΣPAH_{40} concentrations were comprised of between 64 – 90% and 56 – 89% naphthalene's in the 180 and 18 L treatments respectively (SI Figure S5.14). These result are similar to those of Tidwell et al. (2016), who found that naphthalenes made up 90% of the total airborne PAH measurements 11 days following the *Deepwater Horizon* spill in 2010. The NFC also exhibited a slight increase from background levels of 1907 to 3030 ng m^{-3} by day 1 (1.6X greater than background). The ΣPAH_{40} concentrations in the control however were dominated by a wider variety of compounds, with the EPA PAHs, ΣFLA_{C0-C4}, $\Sigma PHEN_{C0-C4}$, and ΣDBT_{C0-C3} making up the majority of ΣPAH_{40} (SI Figure S5.14).

Throughout our experiment, the only compounds that showed a clear increase in the air column over time were the naphthalenes which is reflective of their volatility (Figure 5.7). The ΣNAP_{C0-C4} concentrations in the 180 L treatment increased from 730 ng m^{-3} (pre-spill) to 4916 ng m^{-3} after just 2 days, while the 18 L treatment increased from 814 ng m^{-3} (pre-spill) 2002 ng m^{-3} after just 1 day (Figure 5.7). The near field control also showed evidence of ΣNAP_{C0-C4} concentration increases from 569 ng m^{-3} (pre-spill) to 1278 ng m^{-3} after 4 days, suggesting that the dilbit treatments in close proximity to the control may have influenced air column concentrations.

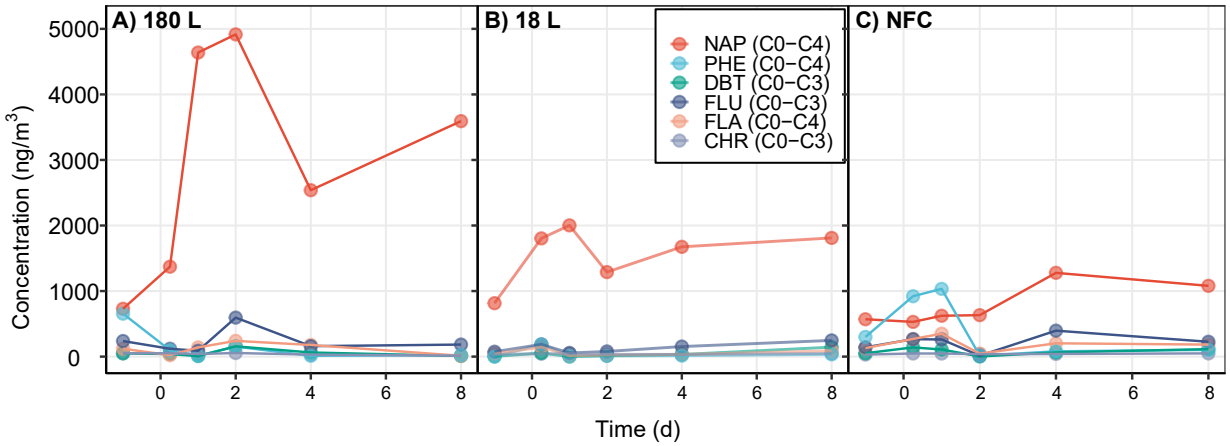

Figure 5. 7. PAH group concentrations over time in the air column above the 180 L (A), 18 L (B), and NFC (C) treatments. The sum of the parent and each alkylated homolog in each group is presented.

The temporal progression of individual parent and alkylated naphthalenes demonstrated slightly different trends across each treatment and control. In the 180 L treatment, C_2-NAP were most abundant group (1710 ng m^{-3} on day 1), followed by C_3>C_1>C_4>C_0. In the 18 L treatment, C_2-NAP were also most abundant (674 ng m^{-3} on day 1), followed by C2>C3>C4>C1>C0. Finally, in the NFC, C3-NAP was the most abundant group (354 ng m^{-3} on day 4), followed by C4>C2>C0>C1 (SI Figure S5.15).

In SI Figure S5.15, it is apparent that following the onset of the spills, the 180 and 18 L treatments began to exhibit a bell-shaped distribution of alkylated naphthalenes, which is indicative of a petrogenic PAH source (Murphy and Morrison, 2014). This bell-shaped pattern was not observed in the control. Since air sampling was carried out in an open system, it is difficult to discern any treatment specific trends. Depending on wind patterns, it is entirely possible that surrounding treatments influenced the PAH profiles of the sampled treatments, which could explain why the control exhibited spikes in naphthalenes at certain timepoints. Furthermore, since air sampling was only carried out from northern edge of the limnocorrals, we are not capturing the entirety of the air

column above each limnocorral, which have a surface area of 75 m^2, and are likely underestimating the PAH levels in the air, especially during the early stages of evaporation. Regardless of the potential caveats mentioned above, these data do highlight the early partitioning of the naphthalenes from the dilbit slick to the air column and may provide useful data to incorporate in mass transfer models in the future.

3.6. Hydrocarbons in the Water Column and Sediments Predicted by Size of Spill

Our regression design offers us the unique ability to analyze the relationship between oil components in environmental samples and the individual oil:water ratios using simple linear regressions. A positive slope would indicate that as the ratio of dilbit to water increases, the concentrations of PAHs in the water column will increase. We observed a significant positive relationship emerge at the majority of timepoints > 8 days for $\Sigma PAH_{46,}$ $\Sigma NAP_{C0\text{-}C4}$, $\Sigma FLU_{C0\text{-}C3}$, $\Sigma FLA_{C0\text{-}C4}$, $\Sigma BNT_{C0\text{-}C4}$, and $\Sigma CHR_{C0\text{-}C3}$ (Figure 5.8, SI Figure S5.16). The PAH groups $\Sigma PHEN_{C0\text{-}C4}$ and $\Sigma DBT_{C0\text{-}C3}$ did not yield significant positive relationships until the end of the experiment (Figure 5.8CD). SI Figure S5.16 further highlights the dynamics of concentration change across spill volumes, specifically the linearity of the relationship between PAH concentrations and oil:water ratios. This figure also shows how the 18 L, which had the highest leakage rate of all the treatments (0.035 d^{-1}), is recurrently found below the regression line for each compound group and sampling timepoint. This suggests that the water exchange occurring between the limnocorral and the lake was likely diluting the observed PAH concentrations.

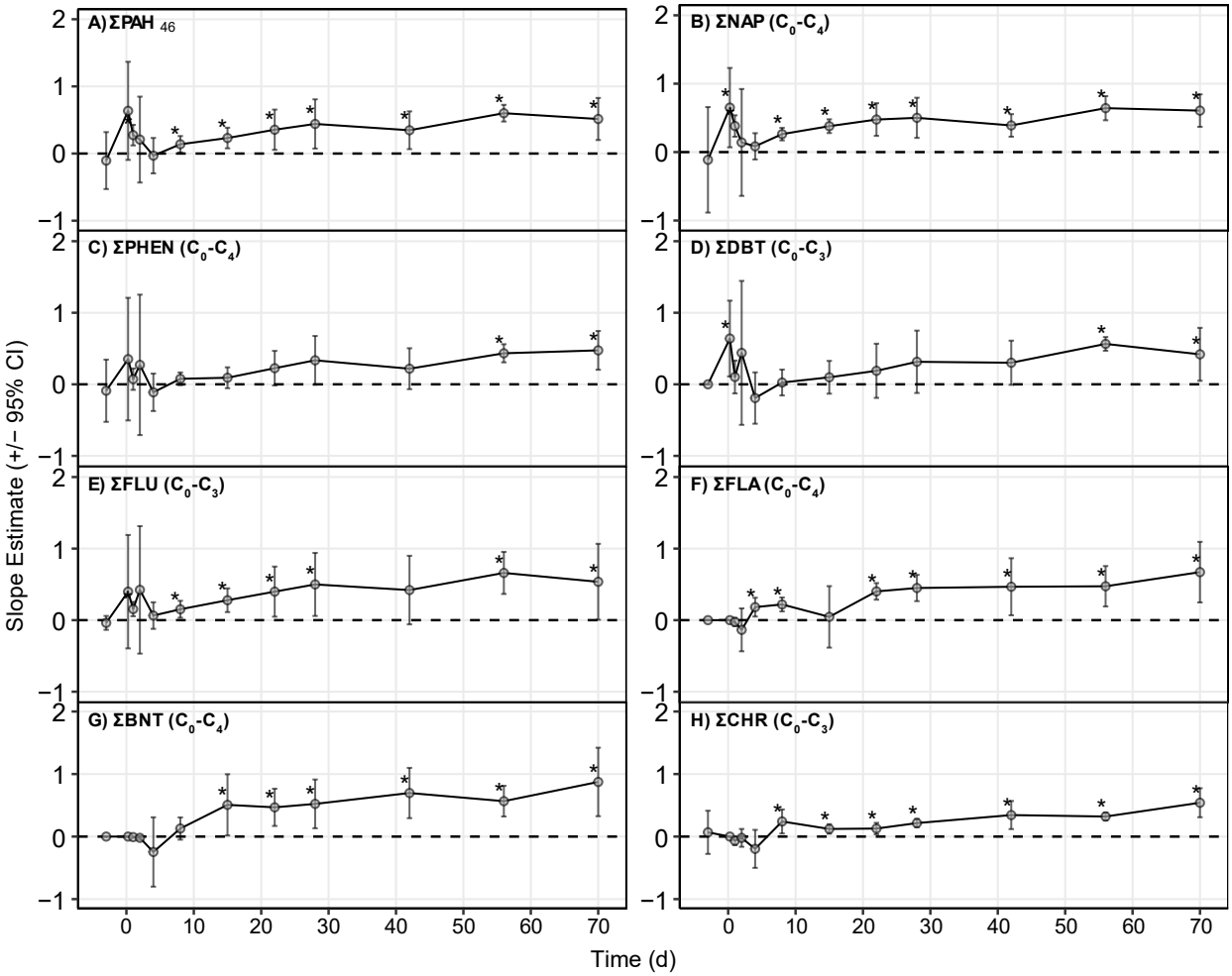

Figure 5. 8. Regression slopes obtained by linear regression of log_{10} transformed oil:water ratio against log_{10} transformed concentration in the water column of each PAH group. Regression parameters are presented in Table S5.5.

Unlike water column PAH concentrations, accumulation trends of PAHs in the sediments over the 70 days were found to be similar between the treatments at most timepoints. While the majority of the regression slopes were positive, significant relationships were only observed between ΣNAP_{C0-C4} and oil:water ratio on days 56 and 70, aside from this, all other relationships were not statistically significant at an alpha level of 0.05 (Figure 5.9, SI Figure S5.17). We conclude that the amount of dilbit spilled has less of an effect on the concentration of naturally dispersed PAHs in the sediments compared to the water column. Other factors aside from spill volume may be limiting

accumulation in the sediment. As previously noted, accumulation in the sediments was proportional to the $LogK_{OW}$ value of the PAHs. Since these compounds do not readily dissolve in water, they would have to reach the sediments by other means, including through the dispersion of oil droplets. Therefore, the accumulation of these HMW compounds in the sediments is likely limited by the compounds migrating through the water column via droplets, which is unrelated to spill volume. By incorporating the oil:water ratio of each individual spill as the independent variable in the regressions, the generated linear models (SI Table S5.5 and S6) can be used to predict PAH contamination at different volumetric scales of dilbit spills that occur in boreal lakes under similar environmental conditions as the present study.

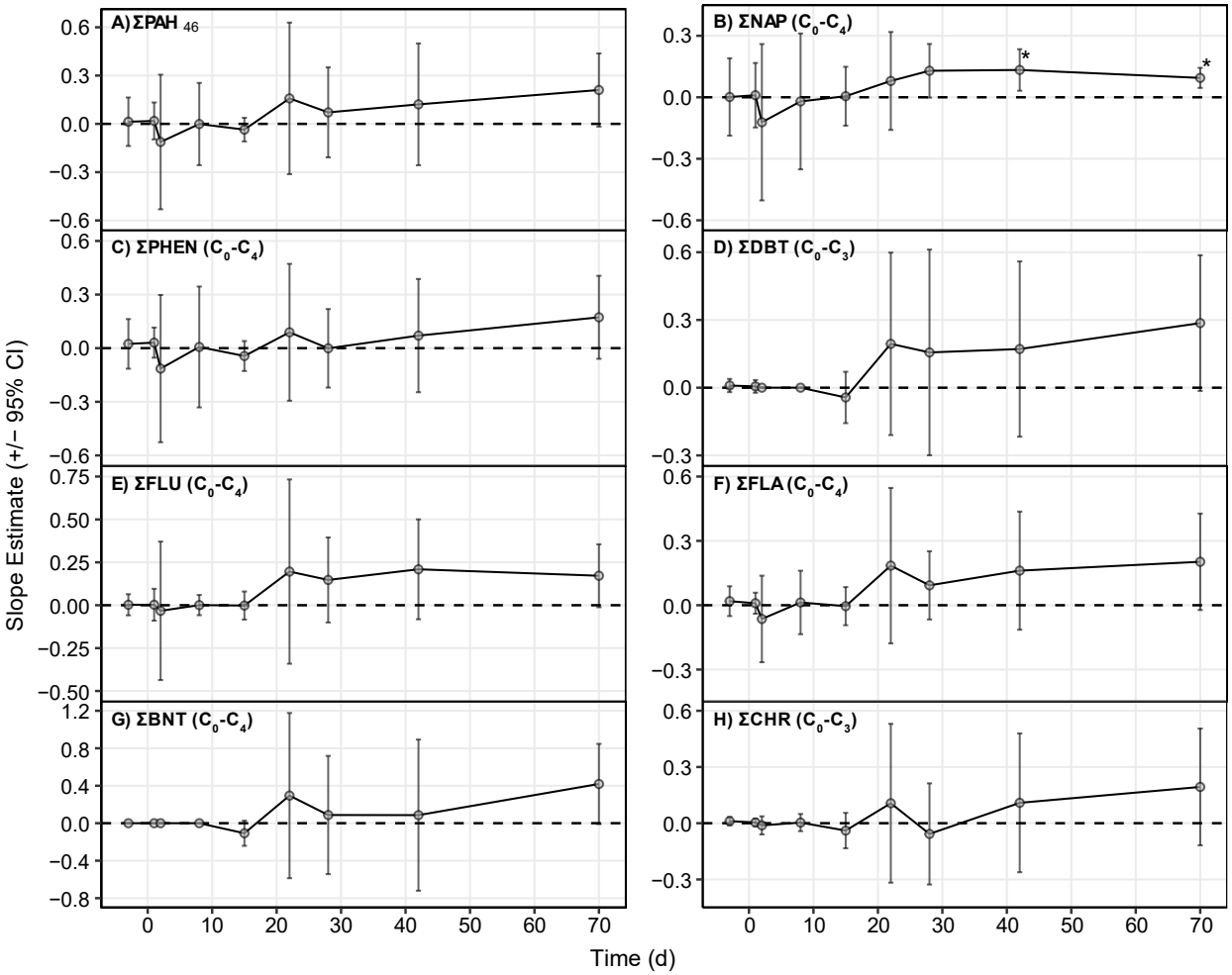

Figure 5. 9. Regression slopes obtained by linear regression of log_{10} transformed oil:water ratio against log_{10} transformed concentration in the sediments of each PAH group. Regression parameters are presented in Table S5.6.

3.7. PAH Mass Balance

We utilized a field mass balance to determine how the water column and sediment results compare to what would be expected based on total dissolvable compound masses in the spilled oil using a similar approach to Brussaard et al. (2016). Since the air samples do not reflect the concentrations of PAHs in the entire air column above the 75 m^2 limnocorrals, we omitted these data from the mass balance. The change in water volume of each limnocorral has previously been reported by Rodriguez-Gil et al. (2021) and we estimated sediment volume using the dimensions of the

limnocorral base (approx. 75 m^2) and the nominal sediment sampling depth (0.05 m). We used the timepoint of highest measured concentrations for the 7 alkylated PAH groups and ΣPAH_{46} in the water column and sediments to determine which percentage of the spilled chemical components are accounted for in the environmental samples (Table 5.1). The water column showed between 0.02 – 1 % of ΣPAH_{46}, 0.02 – 0.6 % of $\Sigma NAP_{C0\text{-}C4}$, 0.01 – 1.3 % of $\Sigma PHE_{C0\text{-}C4,}$ 0.01 – 2 % of $\Sigma DBT_{C0\text{-}C3}$, 0.05 – 2.1 % of $\Sigma FLU_{C0\text{-}C3}$, 0.01 – 0.7 of $\Sigma FLA_{C0\text{-}C4}$, 0.004 – 0.5 % of $\Sigma BNT_{C0\text{-}C4}$, and 0.01 – 0.3 % of $\Sigma CHR_{C0\text{-}C3}$, were released from the slick into the water, across each treatment. These estimates are reasonable, considering that dissolution typically only results in a fraction of a percent of the oil actually dissolving into the water column (Fingas, 2015; Gros et al., 2014). The sediments show between 0.1 – 5.4 % of ΣPAH_{46}, 0.1 – 4.5 % of $\Sigma NAP_{C0\text{-}C4}$, 0.2 – 8.0 % of $\Sigma PHE_{C0\text{-}C4,}$ 0.1 – 3.7 % of $\Sigma DBT_{C0\text{-}C3}$, 0.1 – 7.7 % of $\Sigma FLU_{C0\text{-}C3}$, 0.1 – 6.5 of $\Sigma FLA_{C0\text{-}C4}$, 0.1 – 6.4 % of $\Sigma BNT_{C0\text{-}C4}$, and 0.1 – 8.6 % of $\Sigma CHR_{C0\text{-}C3}$ were detected, across each treatment. Ultimately, these results demonstrate that sediments are a more prominent sink for these PAH groups compared to the water column.

Table 5. 1. Environmental mass balance of PAH groups in the water column and sediments. Percentages are reflective of the maximum concentration observed in the water column and sediments for each compound group.

Environmental Media	Compound Class	Percent Detected (%)						
		180 L	82 L	42 L	18 L	5.5 L	2.9 L	1.5 L
Water[a]	ΣPAH_{46}	0.02	0.03	0.1	0.1	0.3	0.3	1.1
	$\Sigma NAP_{C0\text{-}C4}$	0.02	0.04	0.1	0.1	0.4	0.3	0.6
	$\Sigma PHE_{C0\text{-}C4}$	0.01	0.02	0.1	0.1	0.3	0.5	1.3
	$\Sigma DBT_{C0\text{-}C3}$	0.01	0.02	0.1	0.1	0.3	0.4	2.0
	$\Sigma FLU_{C0\text{-}C3}$	0.05	0.1	0.2	0.2	0.6	0.6	2.1
	$\Sigma FLA_{C0\text{-}C4}$	0.01	0.02	0.03	0.1	0.2	0.2	0.7
	$\Sigma BNT_{C0\text{-}C4}$	0.004	0.01	0.02	0.03	0.1	0.1	0.5
	$\Sigma CHR_{C0\text{-}C3}$	0.01	0.02	0.02	0.05	0.1	0.2	0.3
Sediment[b]	ΣPAH_{46}	0.1	0.2	0.4	1.4	1.2	3.7	5.4
	$\Sigma NAP_{C0\text{-}C4}$	0.1	0.1	0.2	0.5	1.2	2.1	4.5
	$\Sigma PHE_{C0\text{-}C4}$	0.2	0.3	0.5	2.0	1.9	5.5	8.0
	$\Sigma DBT_{C0\text{-}C3}$	0.1	0.2	0.3	1.3	0.8	3.0	3.7
	$\Sigma FLU_{C0\text{-}C3}$	0.1	0.2	0.4	1.1	1.1	3.6	7.7
	$\Sigma FLA_{C0\text{-}C4}$	0.1	0.3	0.5	1.7	1.2	3.0	6.5
	$\Sigma BNT_{C0\text{-}C4}$	0.1	0.4	0.6	2.6	0.5	8.6	6.4
	$\Sigma CHR_{C0\text{-}C3}$	0.1	0.4	0.6	2.4	0.7	5.9	8.6

[a]Total water volume calculated based on modelled predictions from dynamic tritium model by Rodriguez-Gil et al. (2021)

[b]Sediment mass measurements based on assumed dry density of 2.5 g cm^{-3} (Anderson et al., 1987; Beaty, 1994; Bird et al., 1993; Crusius and Anderson, 1991; Durham and Joshi, 1984), surface area of 75 m^2, and sample depth of 0.05m.

3.8. Implications for Ecological Exposure Following Dilbit Spills

The Canadian Council of Ministers of the Environment (CCME) provide water and sediment quality guidelines for the protection of aquatic life for a variety of parent PAHs (SI Table S5.7). However, these values are not typically applicable to dilbit, since dilbit is dominated by alkylated PAHs (Yang et al., 2018). Alkylated PAHs can possess similar toxicities to that of their parent compounds (Andersson and Achten, 2015; Vendrame et al., 1999) and in other cases can be more toxic than their parent counterparts (Marvanová et al., 2008; Turcotte et al., 2011). Therefore, while both water column and sediment samples do not surpass any CCME guidelines for parent

compounds (SI Table S5.7), we cannot completely rule out the potential for toxicity of the alkylated compounds.

The toxicity of dilbit has been assessed by exposing aquatic organisms to water that has been forcibly mixed with dilbit, referred to as a water accommodated fraction (WAF). WAFs are thus a complex mixture of parent and alkylated PAHs and monoaromatics. Philibert et al. (2016) found dilbit water accommodated fractions (WAF) with total PAH concentrations above 28000 ng L^{-1}, made up of approximately 7500 ng L^{-1} $\Sigma NAP_{C0\text{-}C4}$, 1700 ng L^{-1} $\Sigma PHEN_{C0\text{-}C4}$, 1140 ng L^{-1} $\Sigma FLU_{C0\text{-}C3}$, and 2300 ng L^{-1} $\Sigma DBT_{C0\text{-}C3}$ (calculated from 60% of initial WAF, individual concentrations estimated from graphs) significantly reduced survival of zebrafish embryos. Madison et al. (2017) determined 17 day median effective concentrations (EC_{50}) values for embryotoxicity of Japanese medaka to occur at ΣPAH concentrations > 3000 ng L^{-1}. Alderman et al. (2017) exposed juvenile sockeye salmon to CLB WAFs and observed the induction of biomarkers for PAH exposure at ΣPAH of 3500 ng L^{-1} but only observed impacts on swimming performance at ΣPAH concentrations > 66700 ng L^{-1}. Barron et al. (2018) exposed a variety of standard aquatic test species to CLB WAFs and obtained lowest 48 h lethal concentrations (LC_{50}) ranging from 7600 ng ΣPAH L^{-1} for mysid (*Americamysis bahia*) to > 27000 ng ΣPAH L^{-1} for cladocera (*Ceriodaphnia dubia*). Further, the researchers found no observable effect concentrations (NOEC) of 3670 and 5990 ng ΣPAH L^{-1} for Mysid and Cladocera, respectively, following 7 d exposures. The highest ΣPAH_{46} concentration observed in the water column in our study was 2398 ng L^{-1} on day 70 in the 180 L treatment, which is below all reported concentrations for dilbit toxicity in the literature. One aspect not considered in our study is the production of oxygenated

compounds after weathering processes including biodegradation and photooxidation (Charrié-Duhaut et al., 2000; Lee et al., 2015). Weathered oil samples have demonstrated increases in oxygen containing compounds such as carboxylic acids, ketones, and esters (Aeppli et al., 2012), which can be toxic (Jones et al., 2011). Given the prolonged periods of weathering the dilbit slicks endured, it is entirely possible that oxygenated by-products were produced. Since we did not measure this, we cannot comment on whether or not the conditions would be toxic without a full characterization of the water columns and formal toxicity tests.

Barron et al**.** (2020) reported lowest observable effect levels (LOECs) and EC50s for benthic amphipods *Hyalella azteca* and *Leptocheirus plumulosus* exposed to CLB oiled sediment during 10 d survival tests. The LOEC and EC50 values were 17300 and 40800 ng ΣPAH g^{-1} d.w., respectively for *H. azteca*, and 1300 and 1400 ng ΣPAH g^{-1} d.w., respectively for *L. plumulosus* (estimated from wet weight based on reported mean moisture content of 39.4%). While ΣPAH_{46} concentrations in our sediment jar samples are well below these thresholds for toxicity, the oiled sediment samples: OS-18-1, OS-18-2, and OS-82-2 (Figure 5.5), all exceed this range. This stresses the importance of recovering spilled dilbit before submergence occurs. Our results suggest that sediments that are not physically oiled do not pose a threat to aquatic biota based on the current state of sediment toxicity literature. However, sediments that are in direct contact with submerged dilbit can be highly contaminated with PAHs, above thresholds of harm to benthic organisms.

4 CONCLUSION

In conclusion, our study demonstrates that under low-energy spill scenarios typical of a sheltered boreal lake, water column PAH concentrations likely remain below levels that would be toxic to aquatic biota. These findings are also mirrored in the majority of sediment samples. However, sediments in previous contact with submerged dilbit produced elevated PAH concentrations. Therefore, sunken dilbit has the potential to create a substantial long-term risk to freshwater benthic organisms, especially as evidence supporting the hypothesis that dilbit can sink in freshwater continues to emerge. PAH concentrations are much more elevated and enriched in alkylated homologs for which toxicity thresholds are not fully developed. Future work should thus be tailored towards characterizing toxicity thresholds for alkylated PAHs that have been shown to dominate chemical profiles of water and sediment samples following a dilbit spill.

ACKNOWLEDGEMENTS

Funding for the present study was provided by a Natural Sciences and Engineering Research Council Strategic Partnership Grant (STPGP 493786-16 awarded to J.M. Blais, M. Hanson, and D.M. Orihel), a grant under the Oceans Protection Program, in-kind contributions from Environment and Climate Change Canada (ECCC), and in-kind support from the IISD-Experimental Lakes Area. A special thank you to J. Séguin, T. Black, J. Cederwall, L. Timlick, S. Patterson, J. Mason, D. Denton, H. Kosichek, K. Watson, and D. Dey for their contributions to the project.

SUPPORTING INFORMATION

1.0 Supplementing Materials and Methods

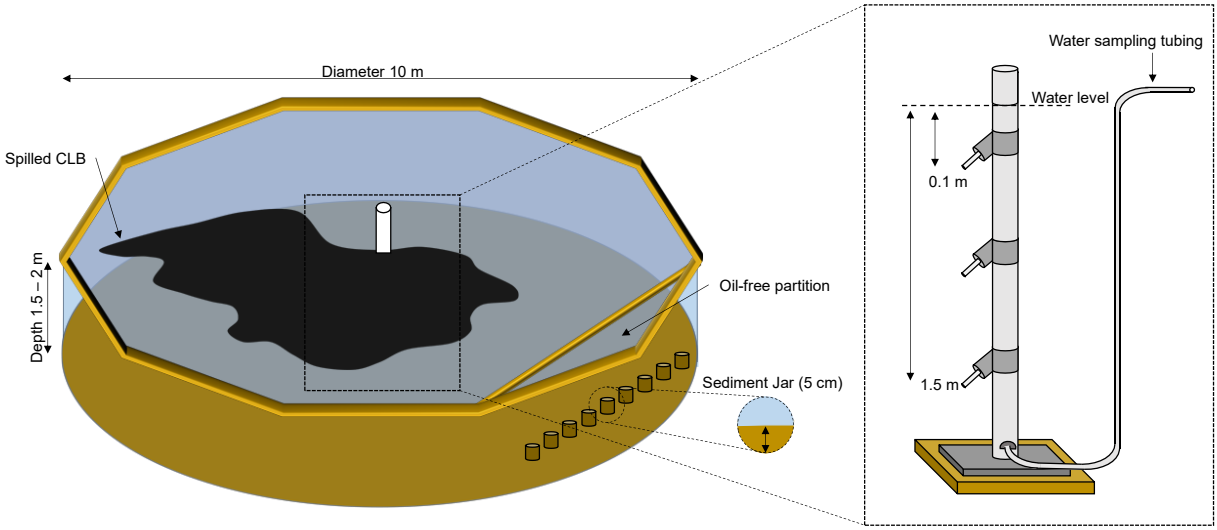

Figure S5. 1. Schematic of limnocorral set up showing water and sediment sampling methods.

Figure S5. 2. The addition of 180 L of CLWB (1:500 oil:water, v/v) onto the water surface of the limnocorral. (A) Overview of addition method and visible sandbags used to seal the membrane to the sediments, (B) View of telescopic arm and pumping system being held at approximately 5 – 10 cm from the water's surface. The oil exited the hose parallel to the water's surface to avoid forcing oil below the water surface and allowing it to spread out during the addition.

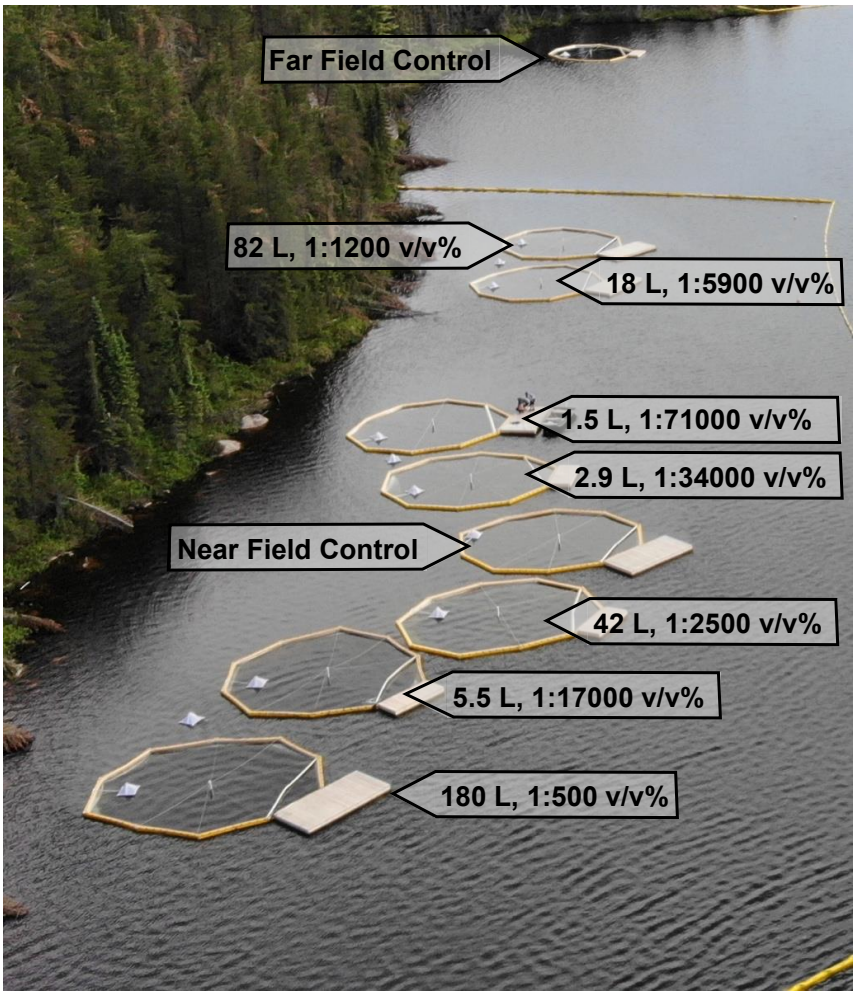

Figure S5. 3. Distribution of spill volumes and resulting oil:water ratios

Figure S5. 4. Example of a tarball sitting on top of the sediment in a coring tube. The tarball was removed and then the top 1cm of the core was processed for PAH analysis.

Table S5. 1. Identified targets and abbreviations. Abbreviations s,w,a represent sediment, water, and air samples.

n-Alkanes	Biomarker compounds		Alkylated PAHs	
^{s}n-C_9	^{s,w}C21 tricyclic terpane	C_{21}terpane	$^{s,w,a}C_0$-Naphthalene	C_0-N
^{s}n-C_{10}	^{s,w}C22 tricyclic terpane	C_{22}terpane	$^{s,w,a}C_1$-Naphthalenes	C_1-N
^{s}n-C_{11}	^{s,w}C23 tricyclic terpane	C_{23}terpane	$^{s,w,a}C_2$-Naphthalenes	C_2-N
^{s}n-C_{12}	^{s,w}C24 tricyclic terpane	C_{24}terpane	$^{s,w,a}C_3$-Naphthalenes	C_3-N
^{s}n-C_{13}	^{s,w}18α(H),21β(H)-22,29,30-trinorhopane	C_{27}Ts	$^{s,w,a}C_4$-Naphthalenes	C_4-N
^{s}2,6,10-trimethyldodecane (TMD)	^{s,w}17α(H),21β(H)-22,29,30-trinorhopane	C_{27}Tm	$^{s,w,a}C_0$-Phenanthrene/anthracene	C_0-P
^{s}n-C_{14}	^{s,w}17α(H),21β(H)-30-norhopane	C_{29}αβ hopane	$^{s,w,a}C_1$-Phenanthrenes/anthracenes	C_1-P
^{s}n-C_{15}	^{s,w}17α(H),21β(H)-hopane	C_{30}αβ hopane	$^{s,w,a}C_2$-Phenanthrenes/anthracenes	C_2-P
^{s}n-C_{16}	^{s,w}22*S*-17α(H),21β(H)-30-homohopane	C_{31}(S) hopane	$^{s,w,a}C_3$-Phenanthrenes/anthracenes	C_3-P
^{s}2,6,10-trimethylpentadecane (TMP)	^{s,w}22*R*-17α(H),21β(H)-30-homohopane	C_{31}(R) hopane	$^{s,w,a}C_4$-Phenanthrenes/anthracenes	C_4-P
^{s}n-C_{17}	^{s,w}22*S*-17α(H),21β(H)-30,31-bishomohopane	C_{32}(S) hopane	$^{s,w,a}C_0$-Dibenzothiophene	C_0-D
^{s}Pristane	^{s,w}22*R*-17α(H),21β(H)-30,31-bishomohopane	C_{32}(R) hopane	$^{s,w,a}C_1$-Dibenzothiophenes	C_1-D
^{s}n-C_{18}	^{s,w}22*S*-17α(H),21β(H)-30,31,32-trishomohopane	C_{33}(S) hopane	$^{s,w,a}C_2$-Dibenzothiophenes	C_2-D
^{s}Phytane	^{s,w}22*R*-17α(H),21β(H)-30,31,32-trishomohopane	C_{33}(R) hopane	$^{s,w,a}C_3$-Dibenzothiophenes	C_3-D
^{s}n-C_{19}	^{s,w}22*S*-17α(H),21β(H)-30,31,32,33-tetrakishomohopane	C_{34}(S) hopane	$^{s,w,a}C_0$-Fluorene	C_0-F
^{s}n-C_{20}	^{s,w}22*R*-17α(H),21β(H)-30,31,32,33-tetrakishomohopane	C_{34}(R) hopane	$^{s,w,a}C_1$-Fluorenes	C_1-F
^{s}n-C21	^{s,w}22S-17α(H),21β(H)-30,31,32,33,34-pentakishomohopane	C_{35}(S) hopane	$^{s,w,a}C_2$-Fluorenes	C_2-F
^{s}n-C_{22}	^{s,w}22*R*-17α(H),21β(H)-30,31,32,33,34-pentakishomohopane	C_{35}(R) hopane	$^{s,w,a}C_3$-Fluorenes	C_3-F
^{s}n-C_{23}	$^{s,w}C_{27}$ 20-5α(H),14β(H),17β(H)-cholestane	C_{27}αββ steranes	$^{s,w,a}C_0$-Fluroanthene/pyrene	C_0-Fl
^{s}n-C_{24}	$^{s,w}C_{28}$ 20-5α(H),14β(H),17β(H)-ergostane	C_{28}αββ steranes	$^{s,w,a}C_1$-Fluroanthenes/pyrenes	C_1-Fl
^{s}n-C_{25}	$^{s,w}C_{29}$ 20-5α(H),14β(H),17β(H)-stigmastane	C_{29}αββ steranes	$^{s,w,a}C_2$-Fluroanthenes/pyrenes	C_2-Fl
^{s}n-C_{26}			$^{s,w,a}C_3$-Fluroanthenes/pyrenes	C_3-Fl
^{s}n-C_{27}			$^{s,w,a}C_4$-Fluroanthenes/pyrenes	C_4-Fl
^{s}n-C_{28}			$^{s,w}C_0$-Benzonaphthothiophenes	C_0-B
^{s}n-C_{29}			$^{s,w}C_1$-Benzonaphthothiophenes	C_1-B
^{s}n-C_{30}			$^{s,w}C_2$-Benzonaphthothiophenes	C_2-B
^{s}n-C_{31}			$^{s,w}C_3$-Benzonaphthothiophenes	C_3-B
^{s}n-C_{32}			$^{s,w}C_4$-Benzonaphthothiophenes	C_4-B
^{s}n-C_{33}			$^{s,w,a}C_0$-Chrysene	C_0-C
^{s}n-C_{34}			$^{s,w,a}C_1$-Chrysenes	C_1-C
^{s}n-C_{35}			$^{s,w,a}C_2$-Chrysenes	C_2-C
^{s}n-C_{36}			$^{s,w,a}C_3$-Chrysenes	C_3-C
^{s}n-C_{37}			^{s,w}Biphenyl	Bph
^{s}n-C_{38}			^{s,w,a}Acenaphthylene	Acl
^{s}n-C_{39}			^{s,w,a}Acenaphthene	Ace
^{s}n-C_{40}			^{s,w,a}Anthracene	An
			^{s,w}Fluoranthene	Fl
			^{s,w,a}Pyrene	Py
			^{s,w,a}Benz(a)anthracene	BaA
			^{s,w,a}Benzo(b)fluoranthene	BbF
			^{s,w,a}Benzo(k)fluoranthene	BkF
			^{s,w}Benzo(e)pyrene	BeP
			^{s,w,a}Benzo(a)pyrene	BaP
			^{s,w}Perylene	Pe
			^{s,w,a}Indeno(1,2,3-cd)pyrene	IP
			^{s,w,a}Dibenzo(a,h)anthracene	DA
			^{s,w,a}Benzo(g,h,i)perylene	BgP

Table S5. 2. Mean percent recoveries (± standard deviation) for deuterated compounds in water, sediment, and air samples

	% Recovery (±sd)		
Compound	**Water Samples**	**Sediment Samples**	**Air Samples**
d_8-naphthalene	71.4 ± 16.7	74.2 ± 13.8	97.4 ± 16.6
d_{10}-Acenaphthene	80.1 ± 16.5	89.2 ± 12.9	83.0 ± 8.0
d_{10}-Phenanthrene	91.8 ± 18.0	97.2 ± 11.8	69.7 ± 3.0
d_{12}-Benz(a)anthracene	92.4 ± 18.7	100.0 ± 14.0	53.1 ± 4.0
d_{12}-Perylene	81.6 ± 16.4	103.7 ± 9.5	52.3 ± 5.7

2.0 Supplementing Results

2.1 Hydrocarbons in the Water Column

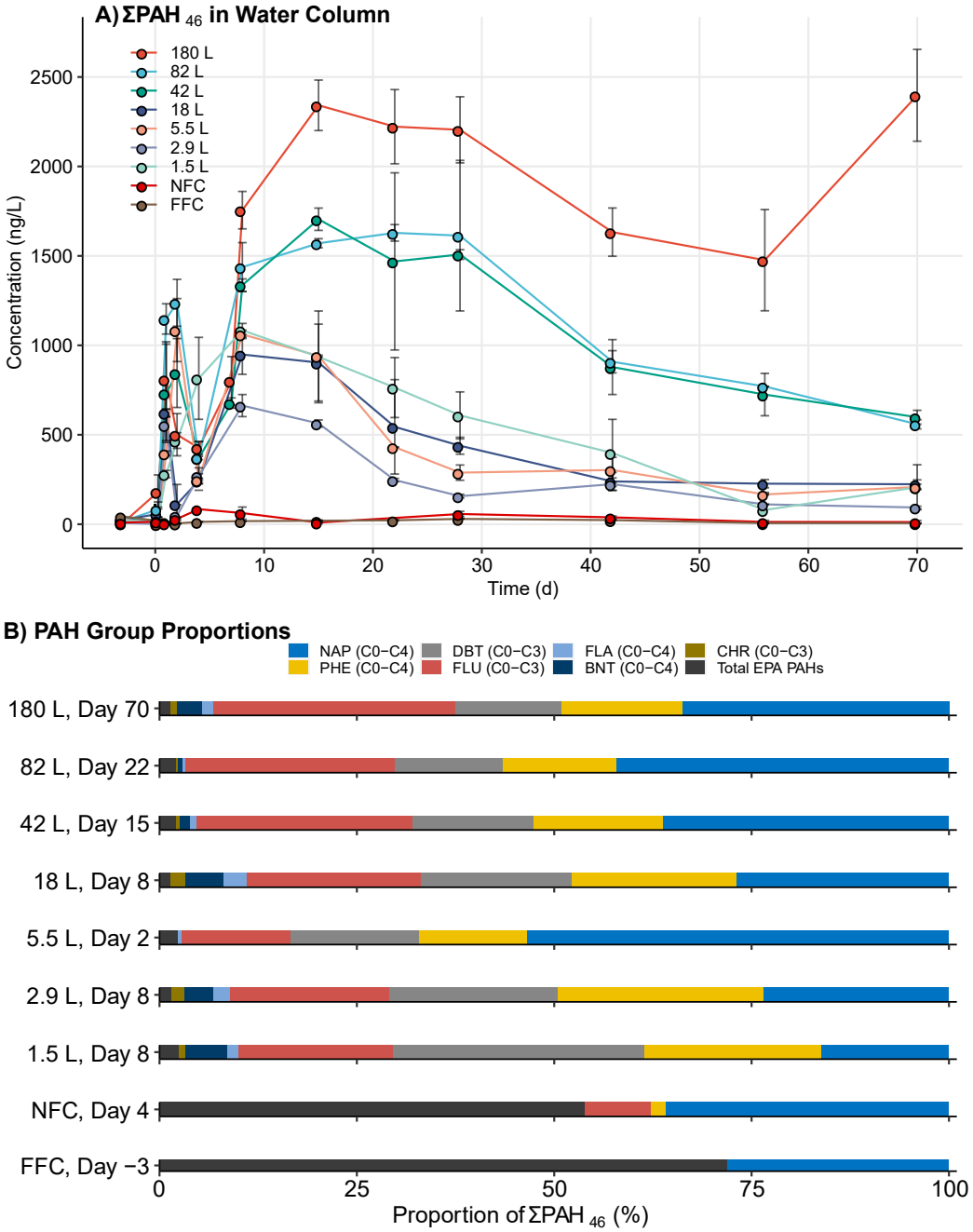

Figure S5. 5. Temporal progression of mean ΣPAH$_{46}$ concentrations in the water column, error bars represent standard deviation (A) and the resulting proportions of each PAH group during the period of maximum ΣPAH$_{46}$ concentration in each treatment (B).

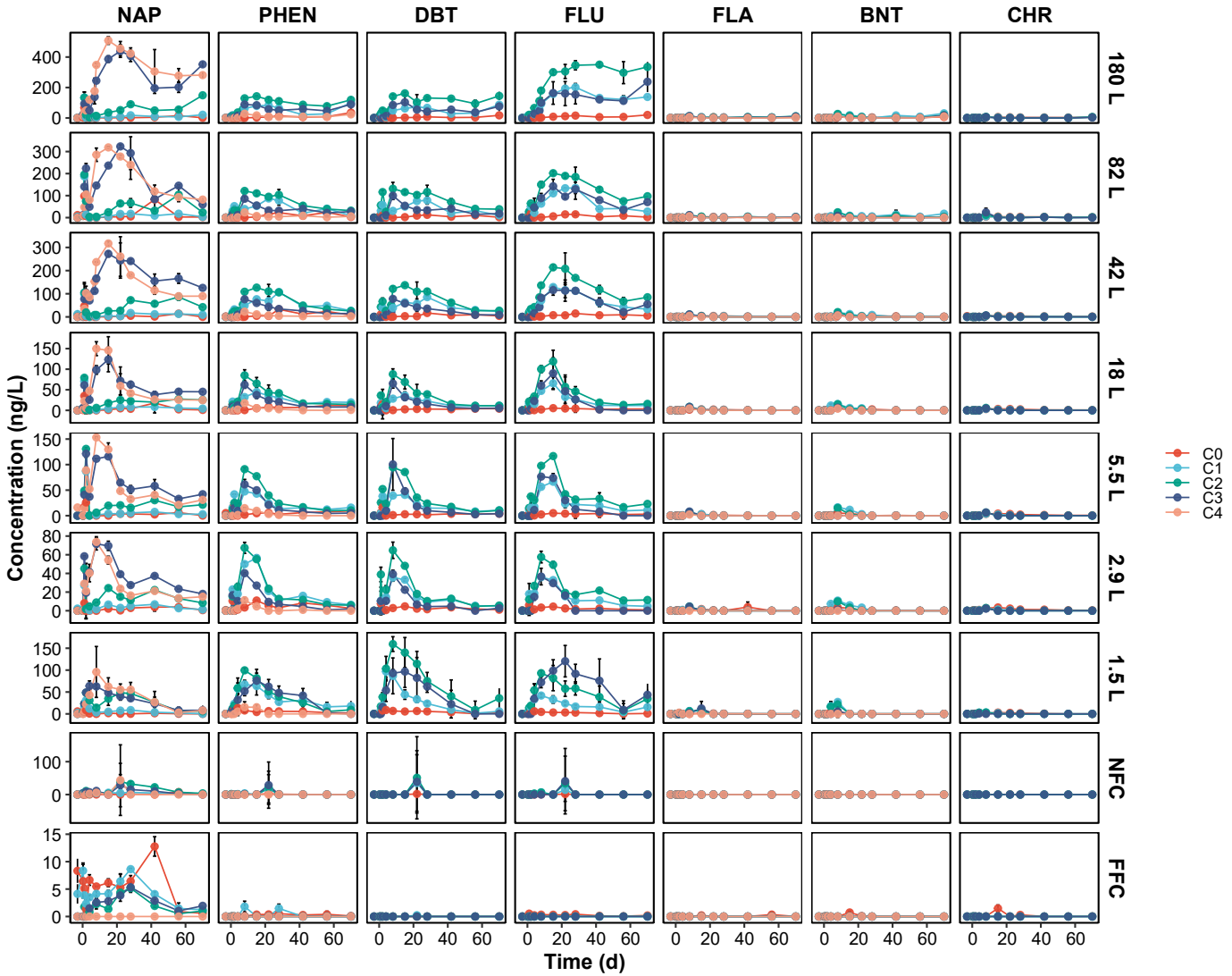

Figure S5. 6. Temporal progression of alkylated PAH concentrations in the water columns of each treatment and control, across each parent PAH group. The error bars represent standard deviation about the mean.

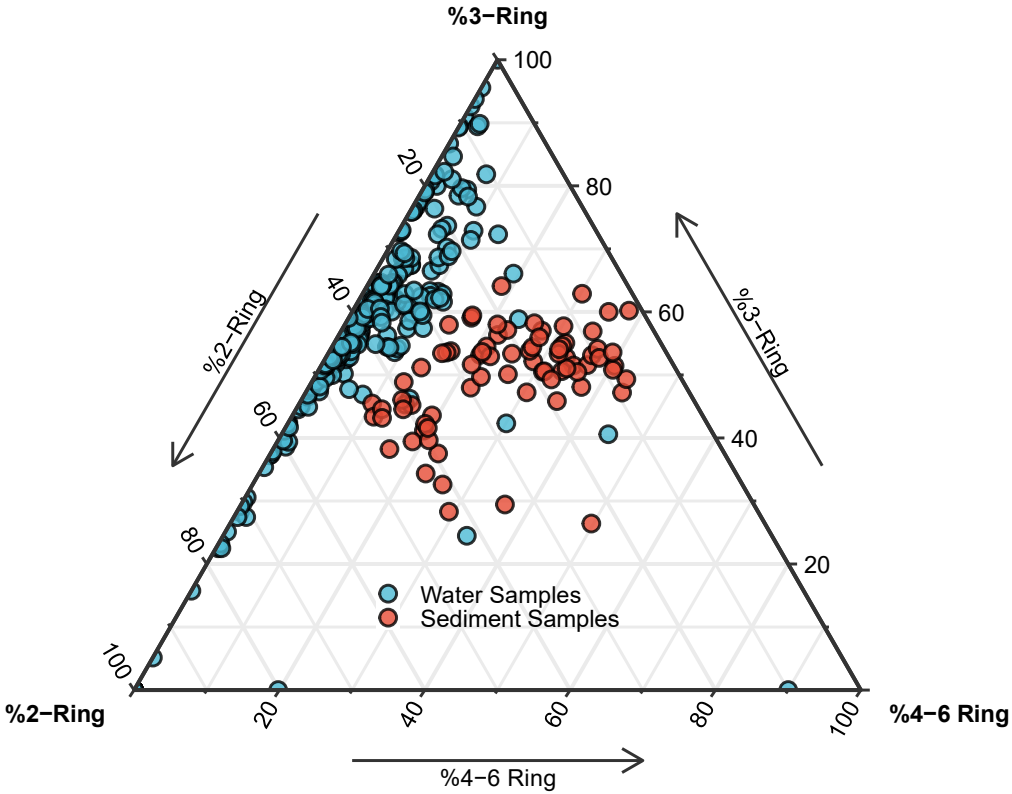

Figure S5. 7. Ternary plot showing the proportions of PAH groups by ring number that make up the ΣPAH46 concentrations in both water and sediment samples.

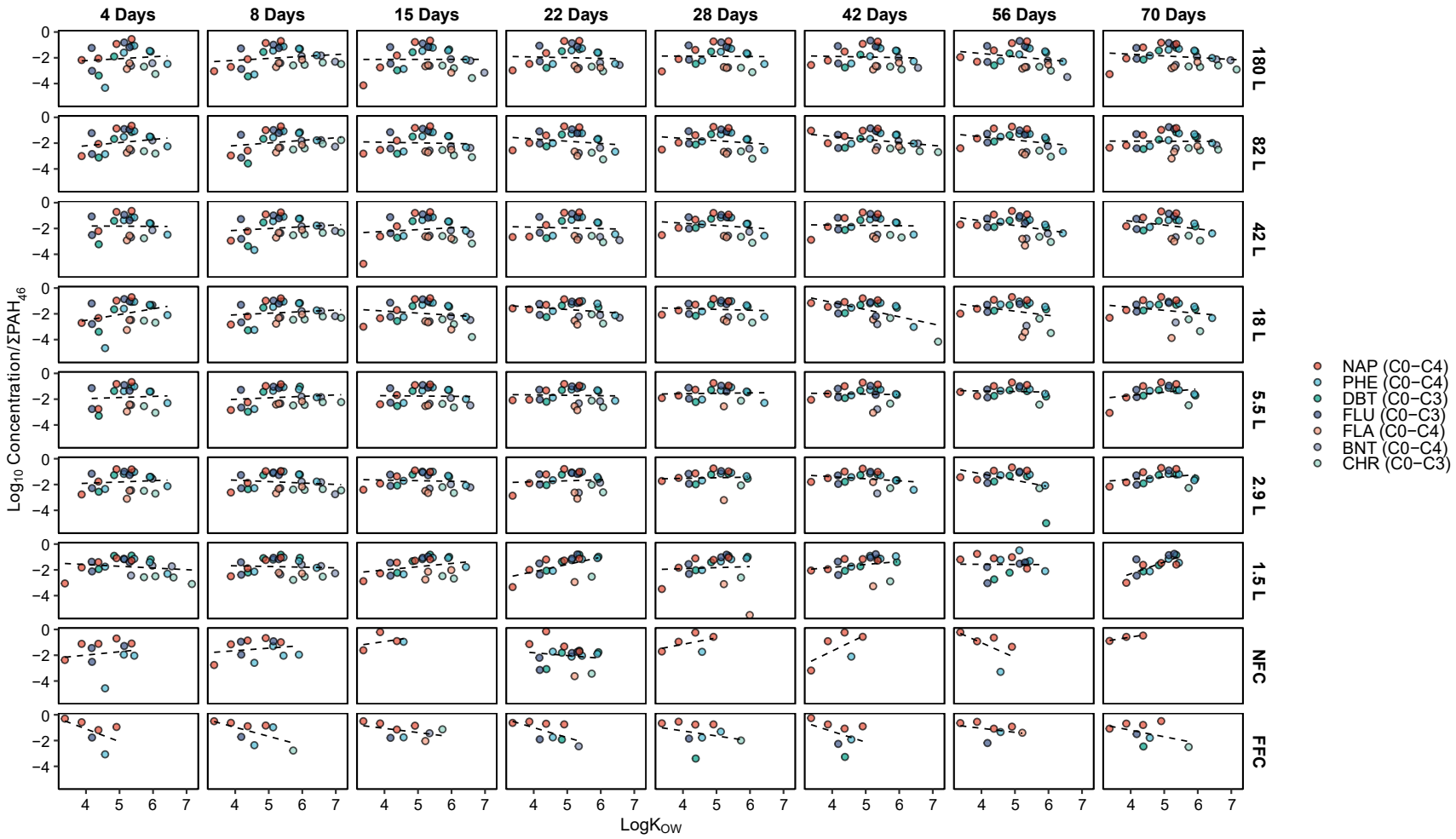

Figure S5. 8. The relationship between water column concentration of individual PAHs and logK_{OW}. The dashed lines represent linear regression outputs. Individual compound concentrations were normalized to the ΣPAH_{46} concentration of each respective sample. Compounds whose concentrations were below MDL were omitted from this analysis.

Table S5. 3. Maximum concentrations of 7 different PAH groups measured in our study compared to other studies using diluted bitumen at similar oil:water ratios.

	Our Study				Ortmann et al. (2020)[a]						Stoyanovich et al. (2019)[b]	
	CLB 1:10000 (18 L)		CLB 1:4600 (42 L)		AWB 1:6400		Synbit 1:6400		WCS 1:6400		CLB 1:8000	
PAH Group	Max Conc (ng/L)	T_{max} (d)	Max Conc (ng/L)	T_{max} (d)	Max Conc (ng/L)	T_{max} (d)	Max Conc (ng/L)	T_{max} (d)	Max Conc (ng/L)	T_{max} (d)	Max Conc (ng/L)	T_{max} (d)
ΣNAP_{C0-C4}	299	8	619	15	1466	2	2125	2	3196	2	1005	4
$\Sigma PHEN_{C0-C4}$	197	8	284	28	26.76	4	2719	10	1974	10	362	4
ΣDBT_{C0-C3}	182	8	293	2	0	0	1550	10	1431	10	89	7
ΣFLU_{C0-C3}	280	15	466	15	130.5	4	1508	10	1021	10	251	4
ΣFLA_{C0-C4}	27.5	8	34.5	8	-	-	-	-	-	-	12	4
ΣBNT_{C0-C4}	45.9	8	61.1	8	12.14	14	1190	10	1058	10	nd	nd
ΣCHR_{C0-C3}	17.3	8	21.2	8	0	0	766	10	444	10	5	4

[a]Ortmann et al. (2020) spilled 3 different types of diluted bitumen (Access Wester Blend; AWB, Synbit, and Western Canadian Select; WCS) into enclosures containing seawater during the summer and sampled the water column for 14 days following the spill.

[b]Stoyanovich et al. (2019) spilled Cold Lake Blend (CLB) into tanks containing freshwater during the summer and samples the water column for 11 days following the spill (Chapter 2)

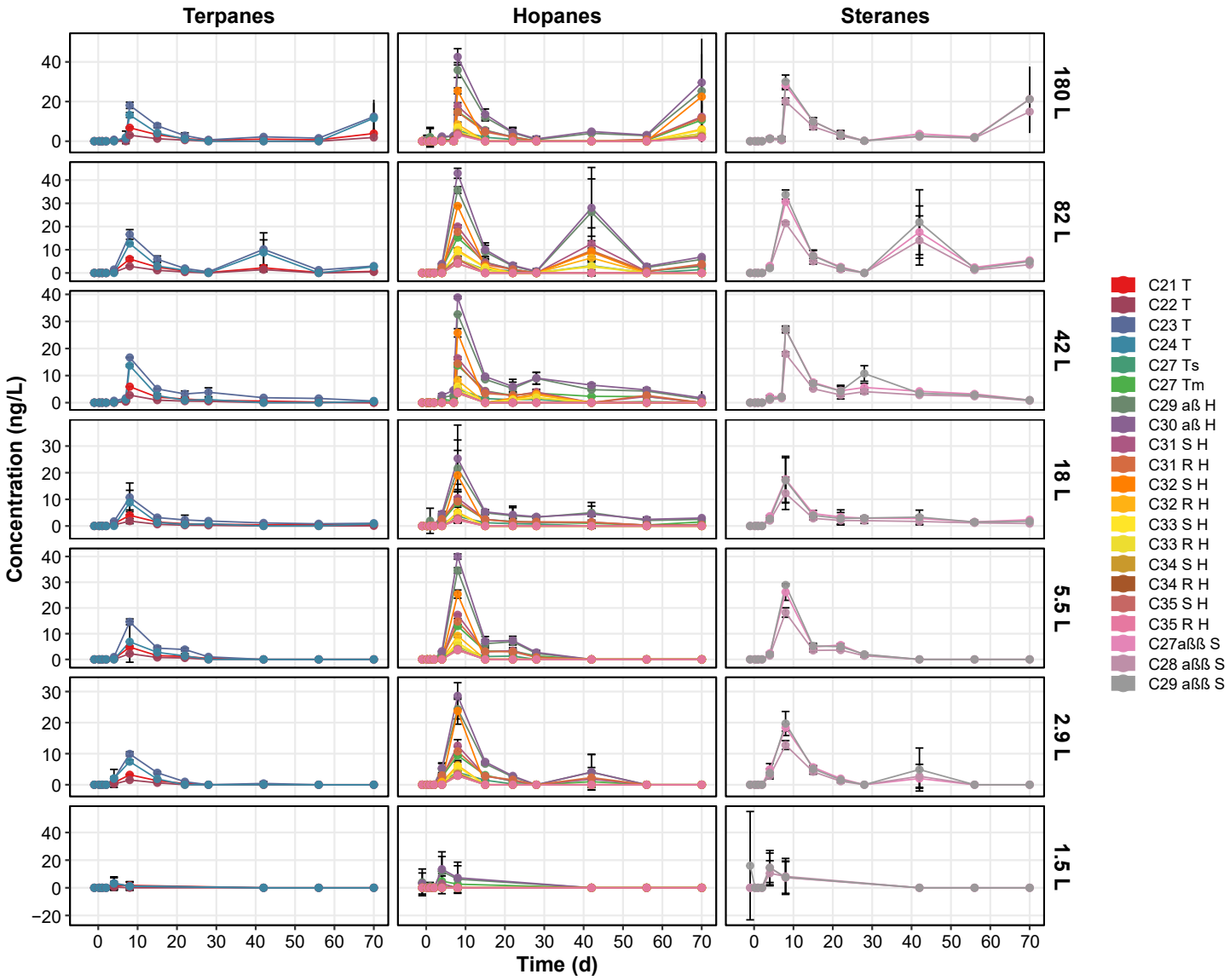

Figure S5. 9. Temporal progression of petroleum biomarker compound concentrations(mean ± standard deviation) in the water column.

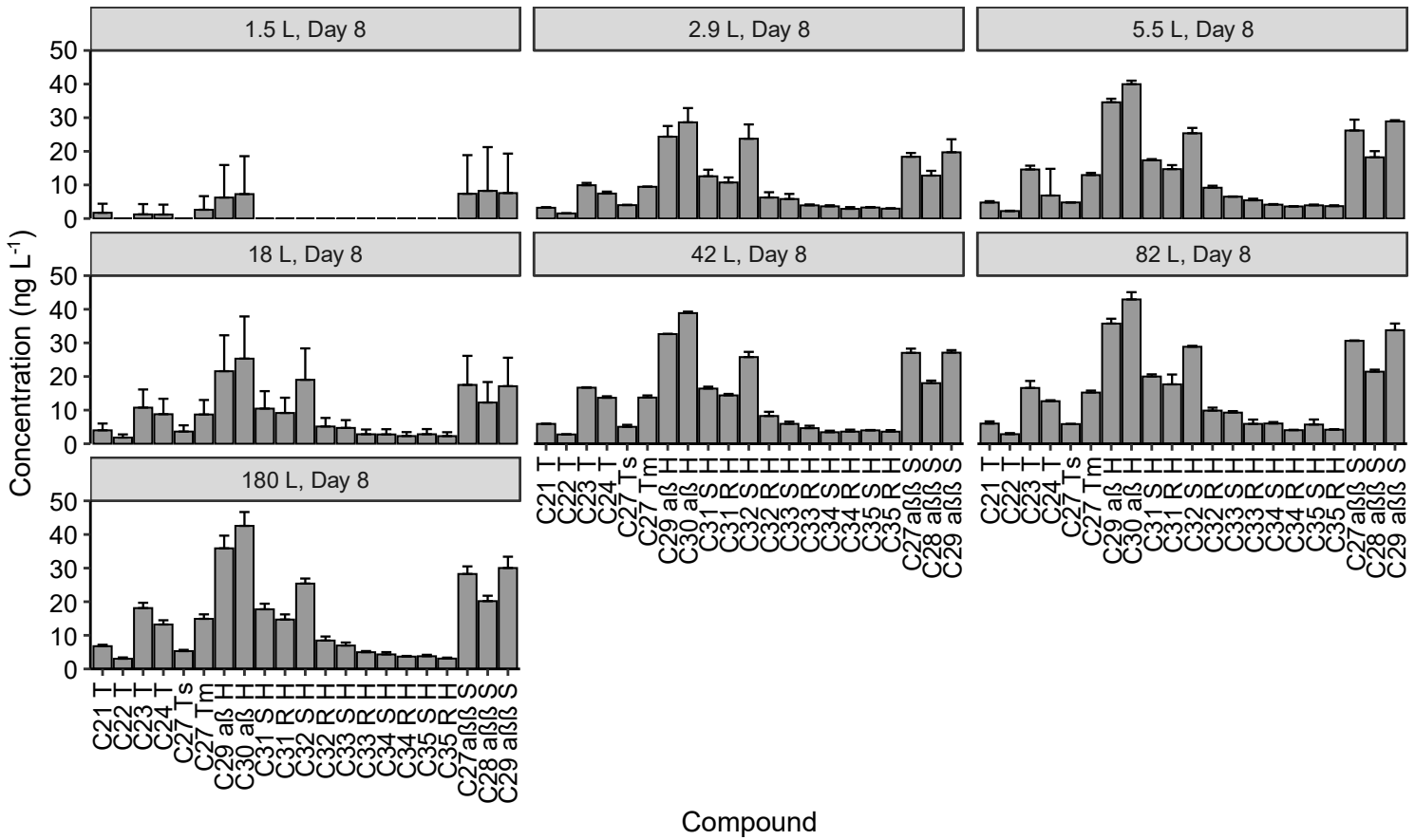

Figure S5. 10. Concentration profiles of petroleum biomarkers in water samples collected on day 8 from each dilbit amended treatment. Error bars represent standard deviation about the mean.

2.2 Hydrocarbons in the Sediments

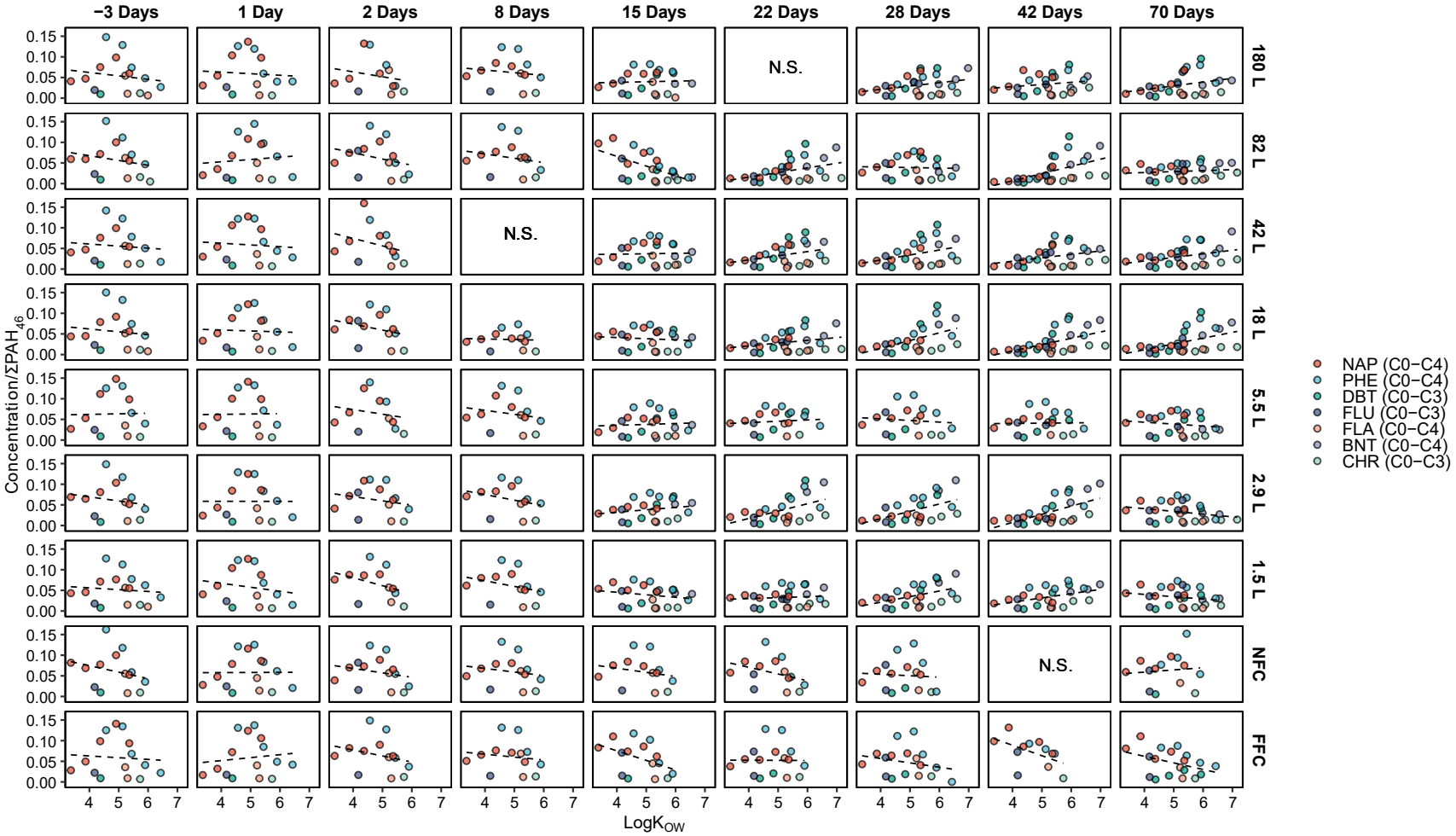

Figure S5. 11. The relationship between sediment concentration of individual PAHs and logK_{OW}. The dashed lines represent linear regression outputs. Individual compound concentrations were normalized to the ΣPAH_{46} concentration of each respective sample. Compounds whose concentrations were below MDL were omitted from this analysis.

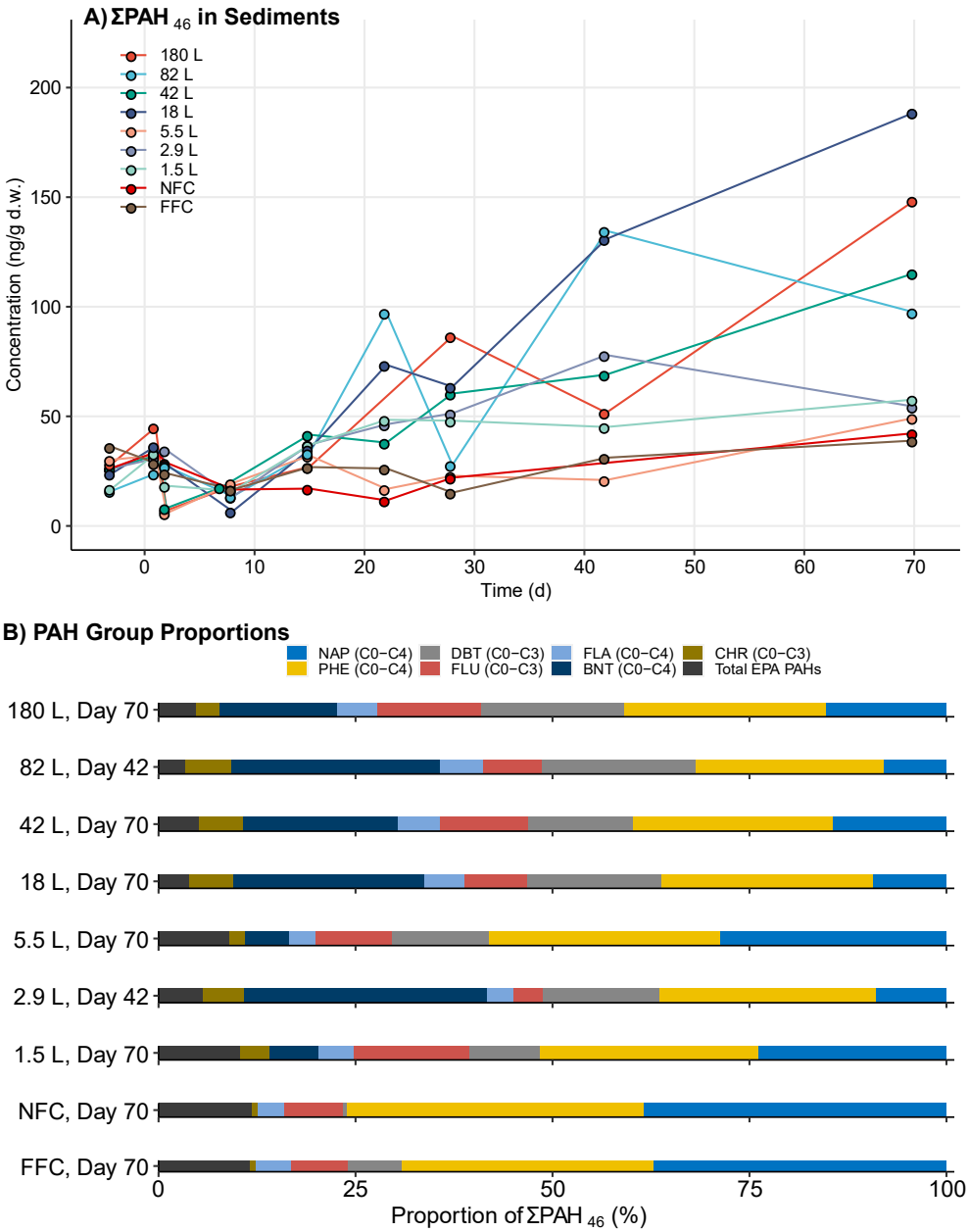

Figure S5. 12. Temporal progression of mean ΣPAH_{46} concentrations in the sediments (A) and the resulting proportions of each PAH group during the period of maximum ΣPAH_{46} concentration in each treatment (B).

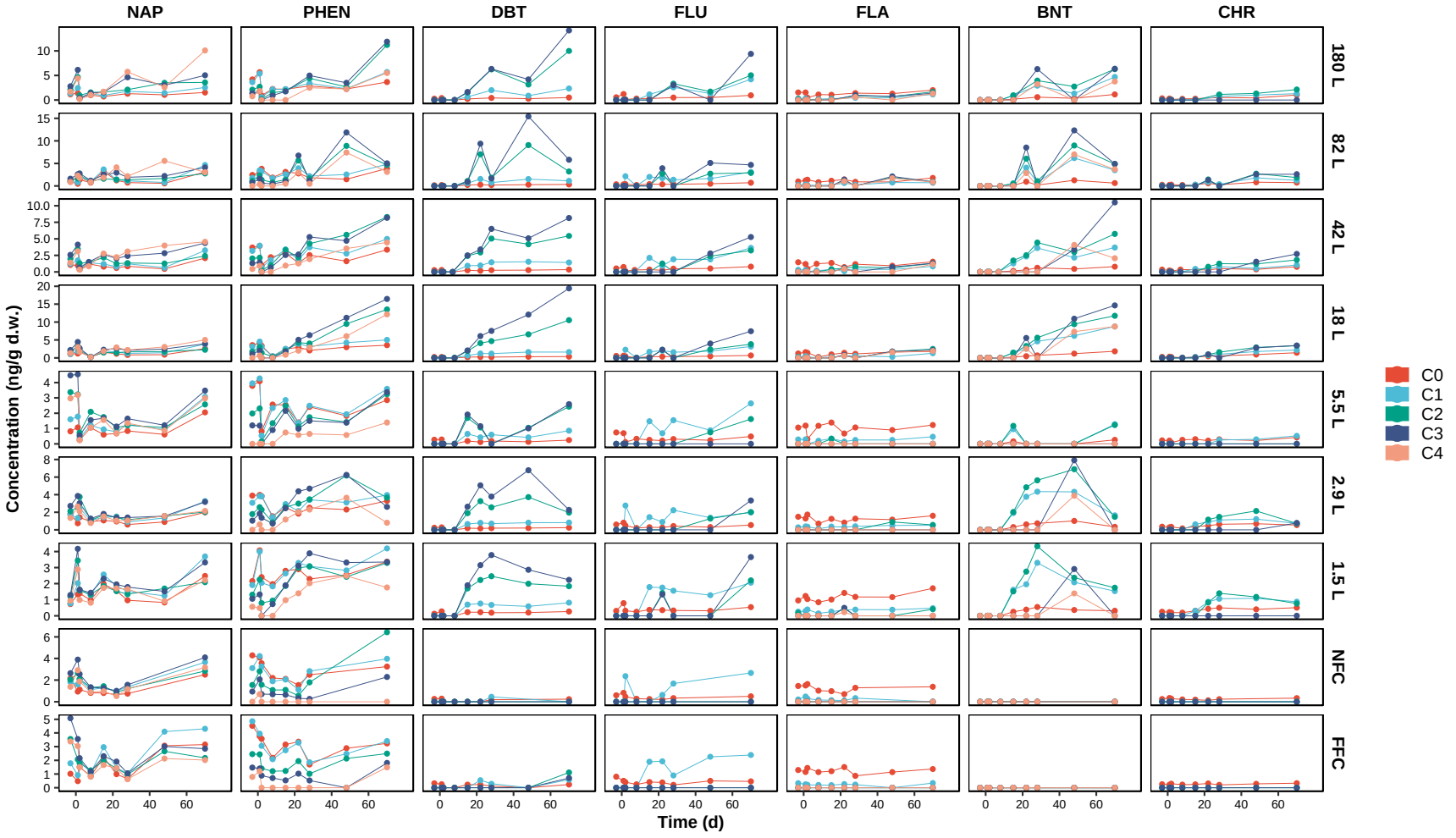

Figure S5. 13. Temporal progression of alkylated PAH concentrations in sediment samples collected from each treatment and control, across each parent PAH group.

Table S5. 4. Comparison between sediment jar and oiled sediment core data.

PAH Group	Jar Sample Max Jar[a]	Oiled Core Sample TB-18-1	TB-18-2	TB-18-3	TB-82-1	TB-82-2	TB-82-3
ΣPAH_{46}	189	14646 (77X)	1696.2 (9X)	587.2 (3X)	379.2 (2X)	4708.6 (25X)	532.3 (3X)
$\Sigma NAP_{C0\text{-}C4}$	22.8	263 (12X)	78.9 (3X)	84.1 (4X)	25.8 (1X)	343.6 (15X)	63.5 (3X)
$\Sigma PHEN_{C0\text{-}C4}$	50.7	4144 (82X)	581.2 (11X)	136.1 (3X)	150.8 (3X)	1240.5 (24X)	145.0 (3X)
$\Sigma DBT_{C0\text{-}C3}$	31.9	3684 (115X)	343.6 (11X)	127.9 (4X)	62.8 (2X)	1016.6 (32X)	115.4 (4X)
$\Sigma FLU_{C0\text{-}C3}$	19.6	929 (47X)	88.7 (5X)	50.8 (3X)	22.5 (1X)	254.1 (13X)	44.8 (2X)
$\Sigma FLA_{C0\text{-}C4}$	9.65	859 (89X)	76.2 (8X)	22.6 (2X)	16.1 (2X)	222.4 (23X)	23.4 (2X)
$\Sigma BNT_{C0\text{-}C4}$	45.8	3760 (82X)	410.9 (9X)	127.4 (3X)	75.7 (2X)	1301.0 (28X)	104.9 (2X)
$\Sigma CHR_{C0\text{-}C3}$	10.5	788 (75X)	87.9 (8X)	25.3 (2X)	15.5 (1X)	249.1 (24X)	25.3 (2X)

[a]The maximum jar values were observed in the 18 L treatment for each PAH group except for $\Sigma FLU_{C0\text{-}C3}$ and $\Sigma NAP_{C0\text{-}C4}$ which were observed in the 180 L treatment, all on day 70.

2.3 Hydrocarbons in the Air

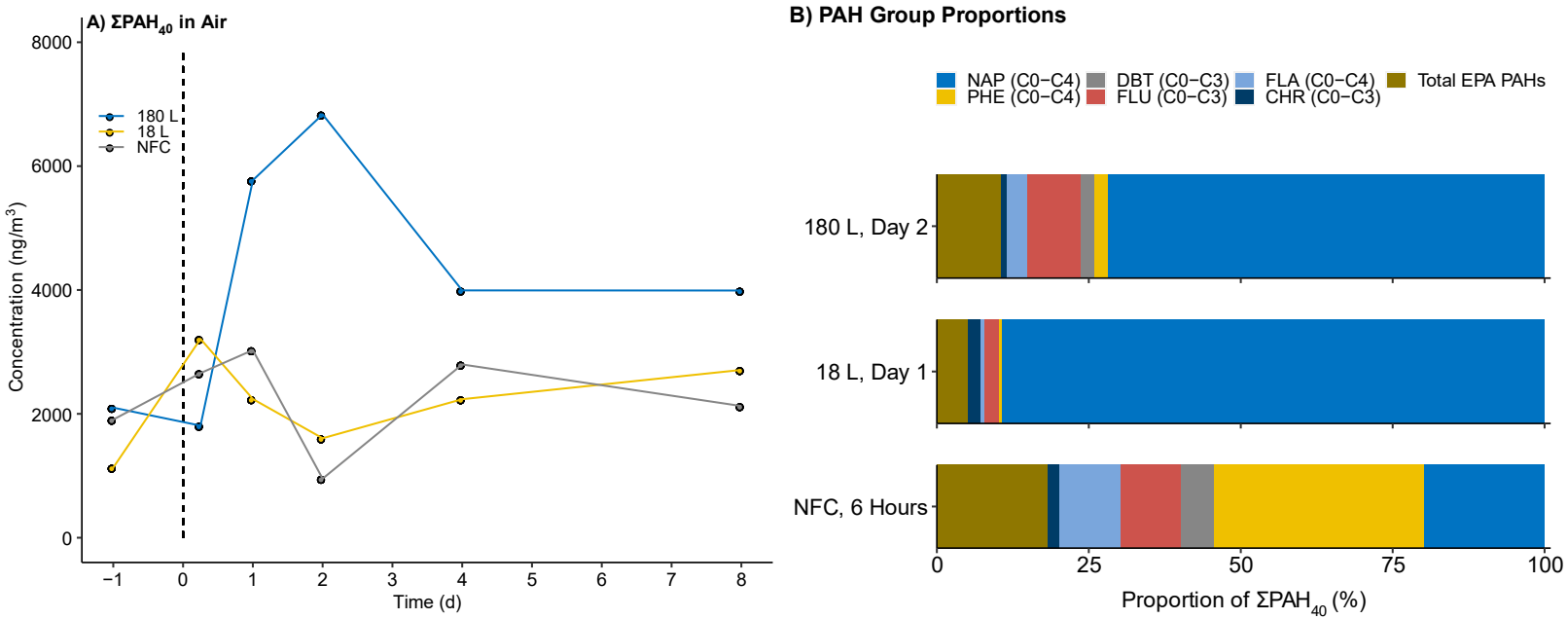

Figure S5. 14. Temporal progression of ΣPAH_{40} concentrations in the sediments (A) and the resulting proportions of each PAH group during the period of maximum ΣPAH_{40} concentration in each treatment (B).

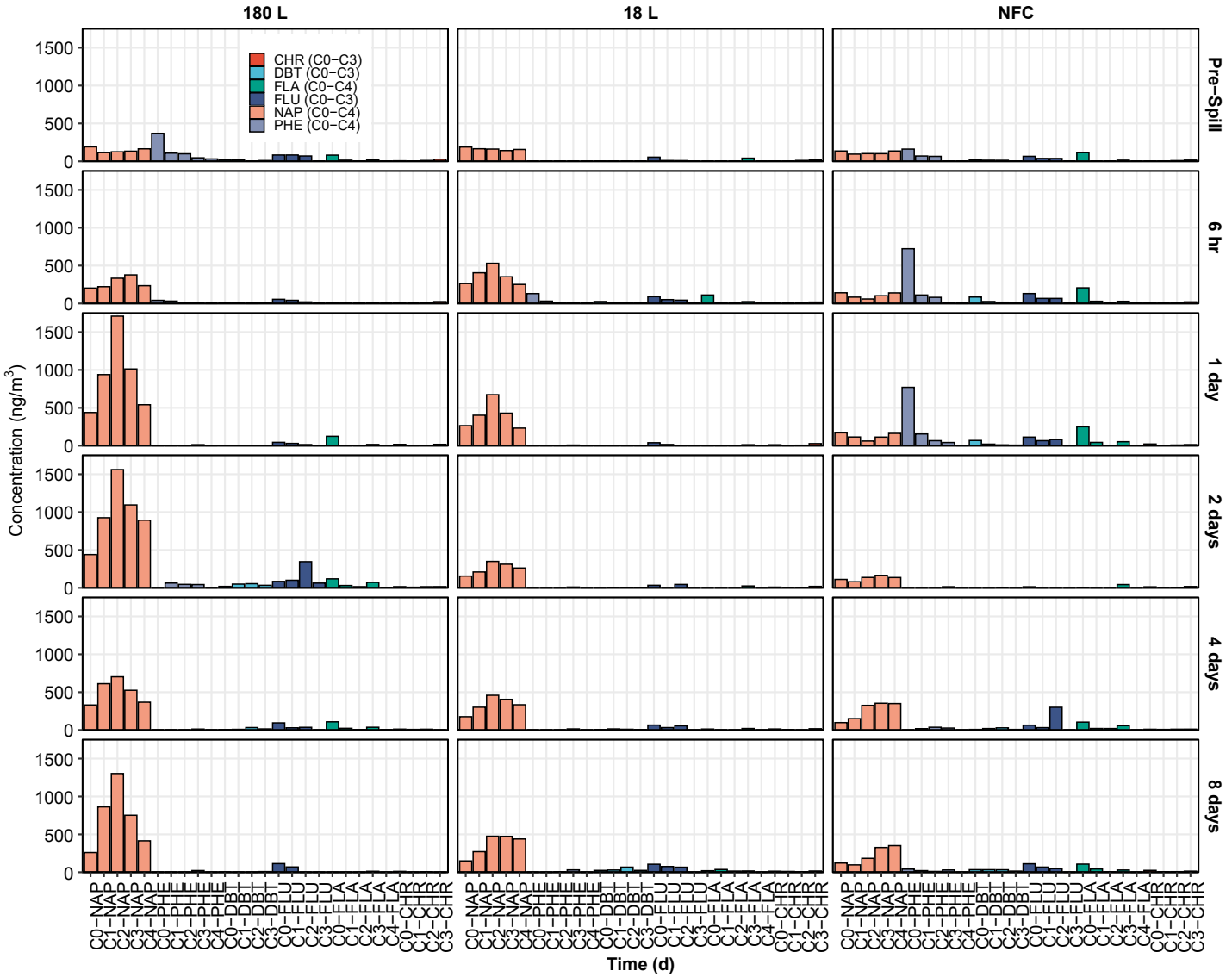

Figure S5. 15. Alkylated PAH profiles of each air sample collected over time during the first 8 days of the study.

2.4 Relationship with Spill Size

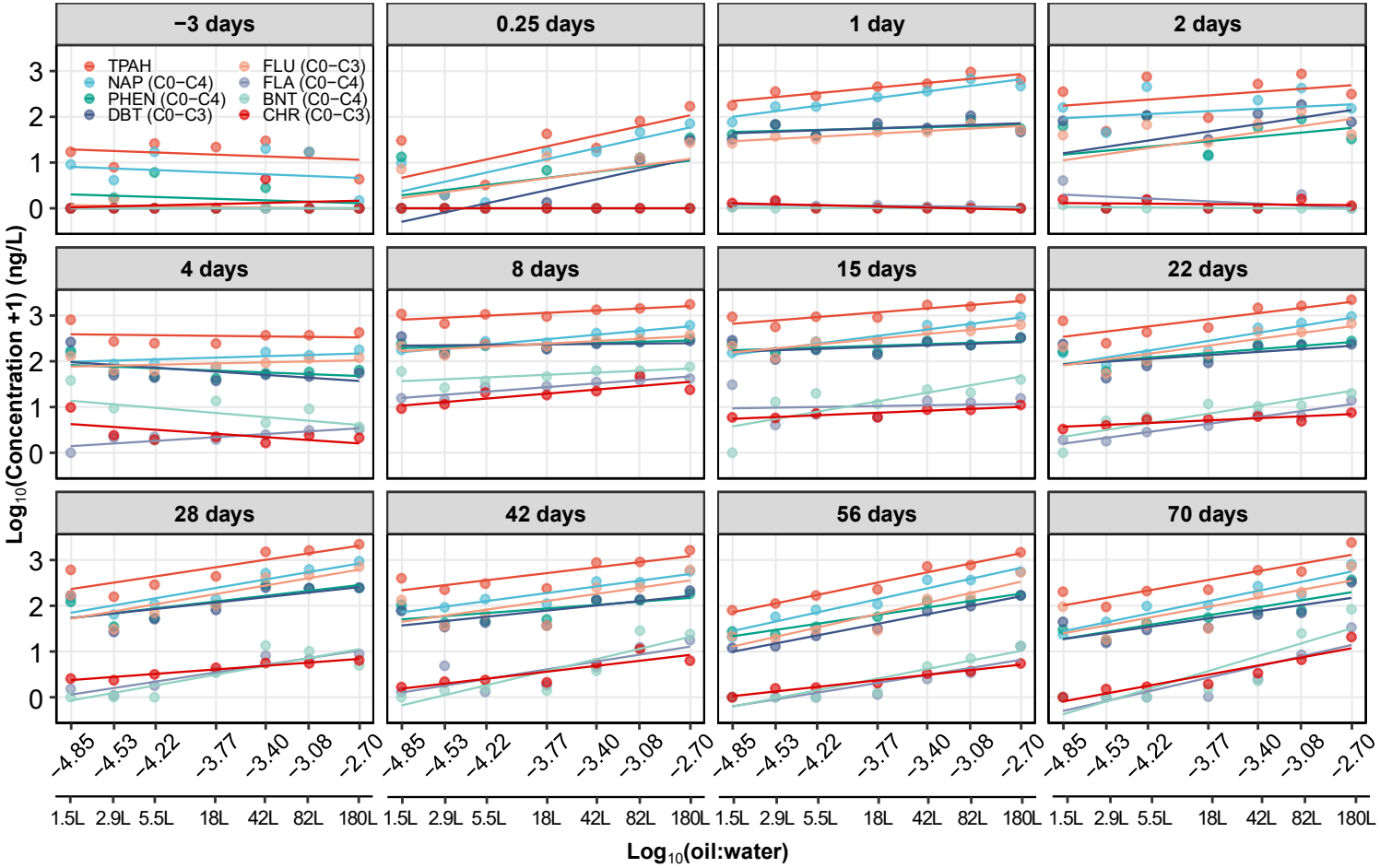

Figure S5. 16. Individual linear regressions comparing concentration in the water column and spill volume at each timepoint for each PAH group. Both axes were logarithmically transformed. To account for cases where concentrations were 0, a constant of 1 was added to each measurement prior to transformation. The controls were excluded from the regressions.

Table S5. 5. Water column regression coefficients obtained by regressing the log_{10} transformed concentration of each respective PAH group against the log_{10} transformed oil:water ratio (alpha = 0.05). Certain compounds remained below detection limit during the earlier timepoints of the study and therefore did not yield sufficient regression coefficients, denoted by "*NA*".

Compound group	Pre-Spill to 8 days						15 to 70 days					
	$Log_{10}[PAH]_i = m * Log_{10}[oil:water] + b$						$Log_{10}[PAH]_i = m * Log_{10}[oil:water] + b$					
	Time	**m**	**b**	**R^2**	***p***	**Sig**	**Time**	**m**	**b**	**R^2**	***p***	**Sig**
ΣPAH_{46}	-3 days	-0.10	0.78	0.07	0.553	no	15 days	0.23	3.94	0.75	0.012	*
NAP (C0-C4)		-0.11	0.36	0.03	0.722	No		0.38	3.98	0.95	0.0002	***
PHEN (C0-C4)		-0.09	-0.13	0.05	0.619	No		0.09	2.69	0.34	0.168	No
DBT (C0-C3)		0.00	0.00	*NA*	*NA*	No		0.10	2.68	0.19	0.322	No
FLU (C0-C3)		-0.04	-0.12	0.17	0.357	No		0.28	3.54	0.79	0.008	*
FLA (C0-C4)		0.00	0.00	*NA*	*NA*	No		0.05	1.19	0.01	0.795	No
BNT (C0-C4)		0.00	0.00	*NA*	*NA*	No		0.51	3.04	0.59	0.045	*
CHR (C0-C3)		0.07	0.35	0.05	0.634	No		0.12	1.33	0.78	0.009	*
ΣPAH_{46}	0.25 days	0.64	3.75	0.50	0.076	No	22 days	0.35	4.26	0.65	0.029	*
NAP (C0-C4)		0.65	3.53	0.62	0.034	*		0.48	4.24	0.84	0.004	**
PHEN (C0-C4)		0.35	1.99	0.18	0.339	No		0.23	3.03	0.53	0.062	No
DBT (C0-C3)		0.64	2.81	0.66	0.027	*		0.19	2.85	0.25	0.256	No
FLU (C0-C3)		0.40	2.16	0.25	0.254	No		0.40	3.84	0.63	0.033	*
FLA (C0-C4)		0.00	0.00	*NA*	*NA*	No		0.40	2.15	0.94	0.0003	***
BNT (C0-C4)		0.00	0.00	*NA*	*NA*	No		0.47	2.62	0.77	0.010	*
CHR (C0-C3)		0.00	0.00	*NA*	*NA*	No		0.13	1.19	0.72	0.015	*
ΣPAH_{46}	1 day	0.27	3.67	*NA*	0.006	*	28 days	0.44	4.50	0.66	0.027	*
NAP (C0-C4)		0.38	3.85	0.89	0.002	**		0.50	4.28	0.79	0.007	*
PHEN (C0-C4)		0.07	2.02	0.24	0.269	No		0.34	3.36	0.56	0.052	No
DBT (C0-C3)		0.10	2.14	0.21	0.304	No		0.31	3.26	0.41	0.123	No
FLU (C0-C3)		0.15	2.22	0.76	0.011	*		0.50	4.14	0.63	0.033	*
FLA (C0-C4)		-0.03	-0.04	0.21	0.303	No		0.45	2.24	0.89	0.001	**

BNT (C0-C4)		-0.01	-0.03	0.35	0.160	No			0.52	2.46	0.70	0.018	*
CHR (C0-C3)		-0.07	-0.21	0.53	0.062	No			0.22	1.42	0.93	0.0004	***
ΣPAH_{46}	2 days	0.21	3.25	0.12	0.442	No		42 days	0.35	4.02	0.67	0.025	*
NAP (C0-C4)		0.14	2.66	0.04	0.661	No			0.39	3.75	0.88	0.002	**
PHEN (C0-C4)		0.27	2.49	0.09	0.509	No			0.22	2.76	0.43	0.107	No
DBT (C0-C3)		0.44	3.33	0.20	0.313	No			0.30	3.03	0.56	0.054	No
FLU (C0-C3)		0.42	3.10	0.23	0.277	No			0.42	3.69	0.50	0.074	No
FLA (C0-C4)		-0.14	-0.36	0.21	0.298	No			0.47	2.37	0.64	0.030	*
BNT (C0-C4)		-0.02	-0.07	0.35	0.160	No			0.70	3.20	0.80	0.007	*
CHR (C0-C3)		-0.02	0.01	0.03	0.720	No			0.34	1.86	0.76	0.011	*
ΣPAH_{46}	4 days	-0.03	2.44	0.02	0.769	No		56 days	0.60	4.77	0.97	0.0001	***
NAP (C0-C4)		0.08	2.40	0.20	0.309	No			0.64	4.57	0.95	0.0002	***
PHEN (C0-C4)		-0.11	1.38	0.19	0.322	No			0.43	3.44	0.94	0.0003	***
DBT (C0-C3)		-0.19	1.05	0.27	0.228	No			0.56	3.73	0.98	0.00002	****
FLU (C0-C3)		0.06	2.20	0.14	0.415	No			0.66	4.31	0.87	0.002	**
FLA (C0-C4)		0.18	1.03	0.72	0.016	No			0.47	2.10	0.79	0.008	*
BNT (C0-C4)		-0.25	-0.06	0.21	0.305	No			0.57	2.54	0.88	0.002	**
CHR (C0-C3)		-0.20	-0.33	0.36	0.157	No			0.32	1.58	0.97	0.00004	****
ΣPAH_{46}	8 days	0.14	3.58	0.63	0.033	*		70 days	0.51	4.50	0.78	0.008	*
NAP (C0-C4)		0.26	3.47	0.92	0.001	**			0.61	4.39	0.90	0.001	**
PHEN (C0-C4)		0.08	2.66	0.50	0.075	No			0.47	3.58	0.80	0.006	*
DBT (C0-C3)		0.03	2.46	0.02	0.736	No			0.42	3.31	0.63	0.033	*
FLU (C0-C3)		0.15	2.96	0.69	0.021	*			0.54	4.00	0.57	0.048	*
FLA (C0-C4)		0.22	2.26	0.87	0.002	**			0.67	2.96	0.77	0.010	*
BNT (C0-C4)		0.13	2.19	0.41	0.122	No			0.87	3.87	0.77	0.009	*
CHR (C0-C3)		0.24	2.20	0.68	0.023	*			0.54	2.53	0.88	0.002	**

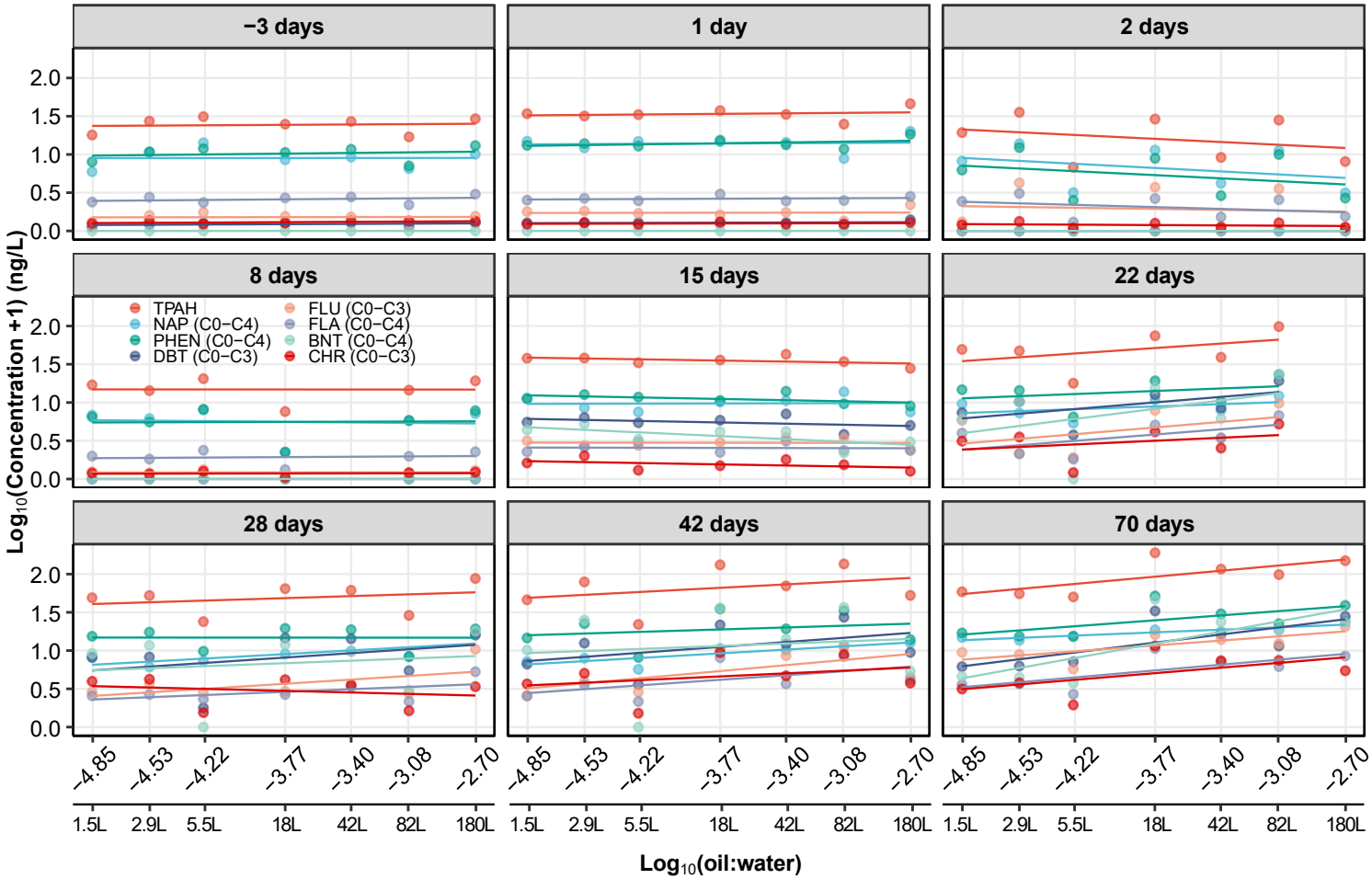

Figure S5. 17. Individual linear regressions comparing concentration in the sediments and spill volume at each timepoint for each PAH group. Both axes were logarithmically transformed. To account for cases where concentrations were 0, a constant of 1 was added to each measurement prior to transformation. The controls were excluded from the regressions.

Table S5. 6. Sediment regression coefficients obtained by regressing the log_{10} transformed concentration of each respective PAH group against the log_{10} transformed oil:water ratio (alpha = 0.05). Certain compounds remained below detection limit during the earlier timepoints of the study and therefore did not yield sufficient regression coefficients, denoted by "*NA*".

Compound group	Pre-Spill to 15 days							22 to 70 days						
	$Log_{10}[PAH]_i = m * Log_{10}[oil:water] + b$							$Log_{10}[PAH]_i = m * Log_{10}[oil:water] + b$						
	Time	**m**	**b**	**R^2**	***p***	**Sig**		**Time**	**m**	**b**	**R^2**	***p***	***Sig***
ΣPAH_{46}	-3 days	0.01	1.44	0.01	0.831	No		22 days	0.16	2.31	0.18	0.404	No
NAP (C0-C4)		0.00	0.96	0.0001	0.985	No			0.08	1.25	0.18	0.407	No
PHEN (C0-C4)		0.02	1.10	0.04	0.676	No			0.09	1.49	0.09	0.555	No
DBT (C0-C3)		0.01	0.12	0.12	0.439	No			0.19	1.73	0.31	0.253	No
FLU (C0-C3)		0.00	0.19	0.002	0.918	No			0.20	1.41	0.20	0.368	No
FLA (C0-C4)		0.02	0.48	0.09	0.517	No			0.18	1.28	0.33	0.230	No
BNT (C0-C4)		0.00	0.00	*NA*	*NA*	No			0.29	2.03	0.18	0.406	No
CHR (C0-C3)		0.01	0.16	0.25	0.252	No			0.11	0.90	0.11	0.524	No
ΣPAH_{46}	1 day	0.02	1.60	0.03	0.698	No		28 days	0.07	1.95	0.08	0.541	No
NAP (C0-C4)		0.01	1.18	0.01	0.876	No			0.13	1.44	0.56	0.052	No
PHEN (C0-C4)		0.03	1.26	0.15	0.389	No			0.00	1.17	0.00002	0.993	No
DBT (C0-C3)		0.01	0.13	0.05	0.619	No			0.16	1.50	0.13	0.419	No
FLU (C0-C3)		0.00	0.25	0.001	0.943	No			0.15	1.12	0.32	0.187	No
FLA (C0-C4)		0.01	0.46	0.04	0.651	No			0.09	0.81	0.31	0.195	No
BNT (C0-C4)		0.00	0.00	*NA*	*NA*	No			0.09	1.16	0.02	0.736	No
CHR (C0-C3)		0.00	0.11	0.05	0.621	No			-0.06	0.26	0.06	0.610	No
ΣPAH_{46}	2 days	-0.11	0.78	0.09	0.520	No		42 days	0.12	2.28	0.12	0.448	No
NAP (C0-C4)		-0.12	0.36	0.12	0.449	No			0.13	1.47	0.70	0.020	*
PHEN (C0-C4)		-0.11	0.30	0.09	0.508	No			0.07	1.54	0.06	0.593	No
DBT (C0-C3)		0.00	0.00	*NA*	*NA*	No			0.17	1.69	0.20	0.308	No
FLU (C0-C3)		-0.03	0.16	0.01	0.843	No			0.21	1.52	0.41	0.124	No

FLA (C0-C4)		-0.06	0.07	0.12	0.451	No			0.16	1.23	0.31	0.193	No
BNT (C0-C4)		0.00	0.00	*NA*	*NA*	No			0.09	1.39	0.01	0.795	No
CHR (C0-C3)		-0.01	0.03	0.07	0.566	No			0.11	1.07	0.10	0.484	No
ΣPAH_{46}	8 days	0.00	1.17	0.00003	0.991	No	70 days		0.21	2.76	0.53	0.063	No
NAP (C0-C4)		-0.02	0.67	0.01	0.874	No			0.09	1.59	0.83	0.004	**
PHEN (C0-C4)		0.01	0.77	0.001	0.958	No			0.17	2.05	0.42	0.114	No
DBT (C0-C3)		0.00	0.00	*NA*	*NA*	No			0.29	2.18	0.55	0.058	No
FLU (C0-C3)		0.00	0.09	0.0002	0.977	No			0.17	1.71	0.54	0.061	No
FLA (C0-C4)		0.01	0.33	0.01	0.822	No			0.20	1.50	0.52	0.068	No
BNT (C0-C4)		0.00	0.00	*NA*	*NA*	No			0.42	2.67	0.56	0.053	No
CHR (C0-C3)		0.00	0.09	0.01	0.847	No			0.19	1.43	0.34	0.171	No
ΣPAH_{46}	15 days	-0.04	1.41	0.24	0.267	No							
NAP (C0-C4)		0.01	1.01	0.002	0.928	No							
PHEN (C0-C4)		-0.04	0.88	0.27	0.237	No							
DBT (C0-C3)		-0.04	0.58	0.16	0.374	No							
FLU (C0-C3)		0.00	0.47	0.001	0.954	No							
FLA (C0-C4)		0.00	0.39	0.003	0.903	No							
BNT (C0-C4)		-0.11	0.16	0.46	0.096	No							
CHR (C0-C3)		-0.04	0.04	0.19	0.335	No							

2.5 Implications for Ecological Exposure

Table S5. 7. CCME guidelines for protection of aquatic life. Only PAHs with available data are presented.

Compound	Water Quality	Sediment Quality	
	Conc (ng/L)	ISQG[a] (ng/g d.w.)	PEL[a] (ng/g d.w.)
2-Methylnaphthalene		20.2	201
Acenaphthene	5800	6.71	88.9
Acenaphthylene	NA	5.87	128
Anthracene	12	46.9	245
Benz(a)anthracene	18	31.7	385
Benzo(a)pyrene	15	31.9	782
Chrysene	NA	57.1	862
Dibenz(a,h)anthracene	NA	6.22	135
Fluoranthene	40	111	2355
Fluorene	3000	21.2	144
Naphthalene	1100	34.6	391
Phenanthrene	400	41.9	515
Pyrene	25	53	875

[a]ISQC: Interim Sediment Quality Guideline
[b]PEL: Probable Effect Level

Supporting References

Ortmann, A.C., Cobanli, S.E., Wohlgeschaffen, G., MacDonald, J., Gladwell, A., Davis, A., Robinson, B., Mason, J., King, T.L., 2020. Measuring the fate of different diluted bitumen products in coastal surface waters. Mar. Pollut. Bull. 153, 111003.

Stoyanovich, S., Yang, Z., Hanson, M., Hollebone, B., Orihel, D., Palace, V., Rodriguez-Gil, J., Faragher, R., Mirnaghi, F., Shah, K., Blais, J., 2019. Simulating a spill of diluted bitumen: Environmental weathering and submergence in a model freshwater system. ET&C. https://doi.org/10.1002/etc.4600

REFERENCES

Achten, C., Andersson, J.T., 2015. Overview of Polycyclic Aromatic Compounds (PAC). Polycycl. Aromat. Compd. 35, 177–186. https://doi.org/10.1080/10406638.2014.994071

Aeppli, C., Carmichael, C.A., Nelson, R.K., Lemkau, K.L., Graham, W.M., Redmond, M.C., Valentine, D.L., Reddy, C.M., 2012. Oil weathering after the Deepwater Horizon disaster led to the formation of oxygenated residues. Environ. Sci. Technol. 46, 8799–8807.

Alderman, S.L., Lin, F., Farrell, A.P., Kennedy, C.J., Gillis, T.E., 2017. Effects of diluted bitumen exposure on juvenile sockeye salmon: from cells to performance. Environ. Toxicol. Chem. 36, 354–360.

Allan, S.E., Smith, B.W., Anderson, K.A., 2012. Impact of the Deepwater Horizon oil spill on bioavailable polycyclic aromatic hydrocarbons in Gulf of Mexico coastal waters. Environ. Sci. Technol. 46, 2033–2039.

Anderson, R.F., Schiff, S.L., Hesslein, R.H., 1987. Determining sediment accumulation and mixing rates using 210Pb, 137Cs, and other tracers: problems due to postdepositional mobility or coring artifacts. Can. J. Fish. Aquat. Sci. 44, s231–s250.

Andersson, J.T., Achten, C., 2015. Time to say goodbye to the 16 EPA PAHs? Toward an up-to-date use of PACs for environmental purposes. Polycycl. Aromat. Compd. 35, 330–354. https://doi.org/10.1080/10406638.2014.991042

Baca, B.J., Getter, C.D., 1985. Freshwater oil spill considerations: protection and cleanup, in: International Oil Spill Conference. American Petroleum Institute, pp. 385–390. https://doi.org/10.7901/2169-3358-1985-1-385

Barron, M.G., Conmy, R.N., Holder, E.L., Meyer, P., Wilson, G.J., Principe, V.E., Willming, M.M., 2018. Toxicity of Cold Lake Blend and Western Canadian Select dilbits to standard aquatic test species. Chemosphere 191, 1–6.

Barron, M.G., Moso, E.M., Conmy, R.N., Meyer, P., Sundaravadivelu, D., 2020. Toxicity of sediment oiled with diluted bitumens to freshwater and estuarine amphipods. Mar. Pollut. Bull. 163, 111941.

Beaty, K.G., 1994. Sediment transport in a small stream following two successive forest fires. Can. J. Fish. Aquat. Sci. 51, 2723–2733.

Bejarano, A.C., Clark, J.R., Coelho, G.M., 2014. Issues and challenges with oil toxicity data and implications for their use in decision making: A quantitative review. Environ. Toxicol. Chem. 33, 732–742.

Bird, G.A., Stephenson, M., Cornett, R.J., 1993. The surface water model for assessing Canada's nuclear fuel waste disposal concept. Waste Manag. 13, 153–170.

Brussaard, C.P., Peperzak, L., Beggah, S., Wick, L.Y., Wuerz, B., Weber, J., Arey, J.S., Van Der Burg, B., Jonas, A., Huisman, J., 2016. Immediate ecotoxicological effects of short-lived oil spills on marine biota. Nat. Commun. 7, 1–11.

CAPP, 2019. 2019 Crude Oil Forecast, Markets and Transportation (No. 2019– 0018). Canadian Association of Petroleum Producers (CAPP), Calgary, AB.

Charrié-Duhaut, A., Lemoine, S., Adam, P., Connan, J., Albrecht, P., 2000. Abiotic oxidation of petroleum bitumens under natural conditions. Org. Geochem. 31, 977–1003.

Crosby, S., Fay, R., Groark, C., Smith, J.R., Sullivan, T., Pavia, R., Shigenaka, G., 2013. Transporting Alberta oil sands products: defining the issues and assessing the risks (No. NOAA Technical Memorandum NOS OR&R 43). U.S. Dept. of Commerce, Seattle, WA: Emergency Response Division, NOAA.

Crusius, J., Anderson, R.F., 1991. Core compression and surficial sediment loss of lake sediments of high porosity caused by gravity coring. Limnol. Oceanogr. 36, 1021–1030.

Debruyn, A.M., Wernick, B.G., Stefura, C., McDonald, B.G., Rudolph, B.-L., Patterson, L., Chapman, P.M., 2007. In situ experimental assessment of lake whitefish development following a freshwater oil spill. Environ. Sci. Technol. 41, 6983–6989. https://doi.org/10.1021/es0709425

Durham, R.W., Joshi, S., 1984. Lead–210 Dating of Sediments From Some Northern Ontario Lakes, in: Developments in Palaeontology and Stratigraphy. Elsevier, pp. 75–85.

Fingas, M., 2015. Review of The Properties and Behaviour of Diluted Bitumen, in: Proceeding of the 39th Arctic and Marine Oil-Spill Program Technical Seminar. Environment and Climate Change Canada, Vancouver, B.C., Canada, pp. 470–494.

Fingas, M., Fieldhouse, B., 2009. Studies on crude oil and petroleum product emulsions: Water resolution and rheology. Colloids Surf. Physicochem. Eng. Asp. 333, 67–81.

Fitzpatrick, F., Bejarano, A., Michel, J., Williams, L., 2012. Net Environmental Benefit Analysis (NEBA) Relative Risk Ranking Conceptual Design: Kalamazoo River System, Enbridge Line 6B MP 608 Marshall, MI Pipeline Release. U.S. Geological Survey, Reston, Virginia.

Fitzpatrick, F.A., Boufadel, M.C., Johnson, R., Lee, K.W., Graan, T.P., Bejarano, A.C., Zhu, Z., Waterman, D., Capone, D.M., Hayter, E., 2015. Oil-particle interactions and submergence from crude oil spills in marine and freshwater environments: Review of the science and future research needs (No. 2015–1076). US Geological Survey.

Gros, J., Nabi, D., Würz, B., Wick, L.Y., Brussaard, C.P., Huisman, J., van der Meer, J.R., Reddy, C.M., Arey, J.S., 2014. First day of an oil spill on the open sea: Early mass transfers of hydrocarbons to air and water. Environ. Sci. Technol. 48, 9400–9411. https://doi.org/10.1021/es502437e

Husky Energy Inc, 2016. North Saskatchewan River Water Source Risk Assessment Report.

Jones, D., Scarlett, A.G., West, C.E., Rowland, S.J., 2011. Toxicity of individual naphthenic acids to Vibrio fischeri. Environ. Sci. Technol. 45, 9776–9782.

Kennon, M.E., Bouldin, J.L., 2015. Aquatic Effects of a Localized Oil Spill on Lake Conway, AR and Its Tributaries. J. Ark. Acad. Sci. 69, 60–67.

King, T.L., Robinson, B., Lee, K., Li, H., Boufadel, M.C., Clyburne, J.A., 2019. Seasonal Effect Data on Monocyclic Aromatics Dissolution from Surface Spills of Bitumen Blends: Implications for Environmental Risk Assessments, in: Proceedings of the Forty-Second AMOP Technical Seminar. Environment and Climate Change Canada, Ottawa, ON, Canada, pp. 773–790.

Lam, V., Li, G., Song, C., Chen, J., Fairbridge, C., Hui, R., Zhang, J., 2012. A review of electrochemical desulfurization technologies for fossil fuels. Fuel Process. Technol. 98, 30–38.
Lee, K. (chair), Boufadel, M., Chen, B., Foght, J., Hodson, P., Swanson, S., Venosa, A., 2015. Expert Panel Report on the Behaviour and Environmental Impacts of Crude Oil Released into Aqueous Environments (No. ISBN: 978-1-928140-02-3). Royal Society of Canada, Ottawa, ON, Canada.
Lee, K., Prince, R.C., Greer, C.W., Doe, K.G., Wilson, J.E.H., Cobanli, S.E., Wohlgeschaffen, G.D., Alroumi, D., King, T., Tremblay, G.H., 2003. Composition and toxicity of residual Bunker C fuel oil in intertidal sediments after 30 years. Spill Sci. Technol. Bull. 8, 187–199.
Madison, B.N., Hodson, P.V., Langlois, V.S., 2017. Cold Lake Blend diluted bitumen toxicity to the early development of Japanese medaka. Environ. Pollut. 225, 579–586.
Marvanová, S., Vondrácek, J., Pěnččíková, K., Trilecová, L., Krčmářř, P., Topinka, J., Nováková, Z., Milcová, A., Machala, M., 2008. Toxic effects of methylated benz [a] anthracenes in liver cells. Chem. Res. Toxicol. 21, 503–512.
Mössner, S.G., Wise, S.A., 1999. Determination of polycyclic aromatic sulfur heterocycles in fossil fuel-related samples. Anal. Chem. 71, 58–69.
Murphy, B.L., Morrison, R.D., 2014. Introduction to environmental forensics. Academic Press.
NASEM, 2016. Spills of Diluted Bitumen from Pipelines: A Comparative Study of Environmental Fate, Effects, and Response (No. ISBN: 978-0-309-38010-2). National Academies of Sciences, Engineering and Medicine (NASEM), Washington, DC.
NEB, 2017. Incident Data. National Energy Board. Government of Canada, Calgary, AB.
Neff, J.M., Stubblefield, W.A., 1995. Chemical and toxicological evaluation of water quality following the Exxon Valdez oil spill, in: Exxon Valdez Oil Spill: Fate and Effects in Alaskan Waters. ASTM International.
Ortmann, A.C., Cobanli, S.E., Wohlgeschaffen, G., MacDonald, J., Gladwell, A., Davis, A., Robinson, B., Mason, J., King, T.L., 2020. Measuring the fate of different diluted bitumen products in coastal surface waters. Mar. Pollut. Bull. 153, 111003.
Owens, E.H., Taylor, E., Marty, R., Little, D.I., 1993. An inland oil spill response manual to minimize adverse environmental impacts, in: International Oil Spill Conference. American Petroleum Institute, pp. 105–109.
Philibert, D.A., Philibert, C.P., Lewis, C., Tierney, K.B., 2016. Comparison of diluted bitumen (dilbit) and conventional crude oil toxicity to developing zebrafish. Environ. Sci. Technol. 50, 6091–6098.
Reddy, C.M., Quinn, J.G., 2001. The North Cape oil spill: hydrocarbons in Rhode Island coastal waters and Point Judith pond. Mar. Environ. Res. 52, 445–461.
Rodriguez-Gil, J.L., Stoyanovich, S., Hanson, M.L., Hollebone, B., Orihel, D.M., Palace, V., Faragher, R., Mirnaghi, F.S., Shah, K., Yang, Z., 2021. Simulating diluted bitumen spills in boreal lake limnocorrals-Part 1: Experimental design and

responses of hydrocarbons, metals, and water quality parameters. Sci. Total Environ. 148537.
Shah, K., Watson, K., Hollebone, B., Yang, Z., Lambert, P., Faragher, R., Aljawahari, M., Dey, D., Mirnaghi, F., Stoyanovich, S., Blais, J.M., 2019. The BOREAL Project: The Design and Execution of a Controlled Oil Spill Study in a Canadian Freshwater Lake, in: Proceedings of the Forty-Second AMOP Technical Seminar. Environment and Climate Change Canada, Ottawa, ON, Canada, pp. 276–294.
Stantec, 2012. Summary of Clean up and Effects of the 2007 Spill of Oil from Trans Mountain Pipeline to Burrard Inlet (No. Project No. 1231-10505).
Stoyanovich, S., Rodríguez-Gil, J.R., Hanson, M., Hollebone, B.P., Orihel, D.M., Palace, V., Faragher, R., Mirnaghi, F.S., Shah, K., Yang, Z., 2021. Simulating diluted bitumen spills in boreal lake limnocorrals-Part 2: Factors affecting the physical characteristics and submergence of diluted bitumen. Sci. Total Environ. 148580.
Stoyanovich, S., Yang, Z., Hanson, M., Hollebone, B., Orihel, D., Palace, V., Rodriguez-Gil, J., Faragher, R., Mirnaghi, F., Shah, K., Blais, J., 2019. Simulating a spill of diluted bitumen: Environmental weathering and submergence in a model freshwater system. ET&C. https://doi.org/10.1002/etc.4600
Tarr, M.A., Zito, P., Overton, E.B., Olson, G.M., Adhikari, P.L., Reddy, C.M., 2016. Weathering of oil spilled in the marine environment. Oceanography 29, 126–135. https://doi.org/10.5670/oceanog.2016.77
Tidwell, L.G., Allan, S.E., O'Connell, S.G., Hobbie, K.A., Smith, B.W., Anderson, K.A., 2016. PAH and OPAH flux during the deepwater horizon incident. Environ. Sci. Technol. 50, 7489–7497.
Turcotte, D., Akhtar, P., Bowerman, M., Kiparissis, Y., Brown, R.S., Hodson, P.V., 2011. Measuring the toxicity of alkyl-phenanthrenes to early life stages of medaka (Oryzias latipes) using partition-controlled delivery. Environ. Toxicol. Chem. 30, 487–495.
US EPA, 2013. Dredging Begins on Kalamazoo River, Enbridge Oil Spill, Marshall, Michigan. U.S. Environmental Protection Agency (US EPA).
USDOT, 2017. Hazardous Liquid Accident Data, 2010 - 2017, In: Pipeline and Hazardous Materials Safety Administration, ed. Pipeline Data and Statistics. Washington, DC: U.S. Department of Transportation,.
Van Hamme, J.D., Singh, A., Ward, O.P., 2003. Recent advances in petroleum microbiology. Microbiol. Mol. Biol. Rev. 67, 503–549.
Vendrame, R., Braga, R.S., Takahata, Y., Galvao, D.S., 1999. Structure- activity relationship studies of carcinogenic activity of polycyclic aromatic hydrocarbons using calculated molecular descriptors with principal component analysis and neural network methods. J. Chem. Inf. Comput. Sci. 39, 1094–1104.
Yang, Z., Hua, Y., Mirnaghi, F., Hollebone, B.P., Jackman, P., Brown, C.E., Yang, C., Shah, K., Landriault, M., Chan, B., 2018. Effect of evaporative weathering and oil-sediment interaction on the fate and behavior of diluted bitumen in marine environments. Part 2. The water accommodated and particle-laden hydrocarbon species and toxicity of the aqueous phase. Chemosphere 191, 145–155. https://doi.org/10.1016/j.chemosphere.2017.10.033

Yang, Z., Shah, K., Laforest, S., Hollebone, B.P., Situ, J., Crevier, C., Lambert, P., Brown, C.E., Yang, C., 2020. Occurrence and weathering of petroleum hydrocarbons deposited on the shoreline of the North Saskatchewan River from the 2016 Husky oil spill. Environ. Pollut. 258, 113769.

CHAPTER 6: EARLY MASS TRANSFER OF MONOCYCLICS TO WATER FOLLOWING DILUTED BITUMEN SPILLS IN FRESHWATER LIMNOCORRALS

Stoyanovich, S[a]., Saunders, L[a]., Tugulea, A.M[b]., Hnatiw, J[b]., Strathern, R[b]., Hanson, M[c]., Hollebone, B.P[d]., Orihel, D. M[e]., Palace, V[f]., Rodriguez-Gil, JR[a]., Blais, J.M[a*].

[a] Department of Biology, University of Ottawa, Ottawa, Ontario, Canada

[b] Exposure and Biomonitoring Division Health Canada, Ottawa, Ontario, Canada

[c] Department of Environment and Geography, University of Manitoba, Winnipeg, Manitoba, Canada.

[d] Emergencies Science and Technology Section, Environment and Climate Change Canada, Ottawa, Ontario, Canada

[e] Department of Biology and School of Environmental Studies, Queen's University, Kingston, Ontario, Canada

[f] International Institute for Sustainable Development Experimental Lakes Area, Winnipeg, Manitoba, Canada

*Corresponding Author: Jules Blais (jules.blais@uottawa.ca)

STATEMENT OF CONTRIBUTIONS

Stoyanovich, S: conceptualization, writing, formal analysis, analytical, field work
Saunders, L: Model framework, writing, review
Tugulea, A: Analytical method
Hnatiw, J: Analytical method
Strathern, R: Analytical method
Hanson, M: reviewing, funding acquisition
Hollebone, B: reviewing, funding acquisition
Orihel, D: reviewing, funding acquisition
Palace, V: reviewing, funding acquisition
Rodriguez-Gil, J: reviewing
Blais, J: supervision, reviewing, funding acquisition, conceptualization, corresponding author

This chapter was prepared for submission to the journal: *Environmental Science and Technology*

ABSTRACT

During the initial days of a diluted bitumen (dilbit) spill, the monocyclic BTEX compounds partition rapidly into the air and water through evaporation and dissolution. The ability to accurately characterize these processes are necessary for assessing exposures, estimating damages, and conducting a mass balance. We investigated these processes following a series of experimental dilbit spills into 10 m diameter limnocorrals installed in a Boreal lake in Northwestern Ontario. We conducted seven individual dilbit spills, ranging in volume from 1.5 to 180 L, resulting in oil-to-water ratios between 1:71 000 (v/v, %) and 1:500 (v/v, %). We report on the concentrations of BTEX in the water column over the first 4 days of the spills. BTEX compounds reached maximum concentrations in the water columns between 10 – 24 h post release and subsequently decreased to below method detection limits after 96 h. We developed a mass transfer model, parametrized based on physical-chemical properties of the individual BTEX compounds and environmental conditions. The model accurately predicted the fractionation of BTEX from the dilbit slick into the water column and the resulting temporal dissolution trends. This experiment allowed for important field evaluation of the model at a variety of different spill sizes. This is the first report on the dissolution trends of BTEX following large-scale experimental dilbit spills in natural freshwater systems.

1 INTRODUCTION

Canada's bitumen is a semi-liquid form of crude oil that is too dense and viscous to flow in pipelines, requiring dilution to facilitate its transport (Government of Canada, 2013). A commonly employed solution to this problem involves the blending of bitumen with a lighter product, such as natural gas condensates (Lee et al., 2015), which decreases the density and viscosity of the oil. Condensates contain primarily low molecular weight volatile hydrocarbons, which include some of the most toxic aromatic hydrocarbons like benzene, toluene, ethylbenzene, and *o,m,p*-xylenes, collectively termed BTEX (Fingas, 2015a; King et al., 2017). This newly formed product, referred to as diluted bitumen (dilbit), can contain between 0.6–2.0 % w/w BTEX (King et al., 2017).

Following a spill, a series of physical weathering processes alter dilbit's physical and chemical properties (NRC, 2003). Evaporation tends to dominate the early weathering of oil, affecting compounds with boiling points below that of *n*-hexadecane (*n*-C_{16}) (Lee et al., 2015). For lighter oils, evaporation can remove up to 75% of the oils initial volume, medium crude oils by up to 40%, and heavy residual oils by up to 5% (Fingas, 1997). In contrast, dissolution has a minimal effect on the overall oil mass balance following the early days of a spill (Fingas, 2015a; Harrison et al., 1975). Studies with crude oil indicate that less than 1% of oil constituents enter the water column via dissolution (Cohen et al., 1980). Although only a small proportion of oil constituents enter the water column, dissolution is still a significant process from an ecotoxicological standpoint, as several of the more water-soluble components of crude oils may be toxic to aquatic species (Madison et al., 2017; McDonnell et al., 2019; Philibert et al., 2016).

The monocyclic BTEX compounds are the most water soluble fraction of crude oils (Fayemiwo et al., 2017) and are on the US EPA's list of toxic priority pollutants as they are known to be acutely toxic to aquatic organisms (US-EPA, 2014). A recent laboratory exposure study by Philibert et al., (2016) revealed that following spills of condensate bitumen blends, BTEX is a more suitable predictor of lethality and malformation in early life stages of zebrafish compared to the larger aromatics. Despite reports of toxicity of BTEX in diluted bitumen in laboratory studies, there are limited field data that evaluate the dissolution of BTEX in the water column following actual spill events. This lack of data is likely because spills are unexpected, and researchers often arrive too late to observe these processes immediately (i.e., within hours) following a spill. Recently, work by Ortmann et al. (2020) has shown that ΣBTEX concentrations in water following experimental dilbits spills ranged from 10-70 μg L^{-1}, approximately three orders of magnitude lower than concentrations that cause toxicity in zebrafish (Philibert et al., 2016). This comparison highlights the importance of characterizing ΣBTEX dynamics in the water column following natural dilbit spill scenarios.

Several predictive models have been developed to characterize the fate of petrogenic (oil-derived) hydrocarbons following crude oil spills (Arey et al., 2007a, 2007b; Chao et al., 2001; Daling and StrØm, 1999; Fingas, 1997; Gros et al., 2014; Guo and Wang, 2009; Harrison et al., 1975; Lemkau, 2012; Luk and Kuan, 1993; Riazi and Edalat, 1996; Stiver et al., 1989). Some of these models consider the oil as a single component (Chao et al., 2001; Daling and StrØm, 1999; Fingas, 1997; Guo and Wang, 2009), some divide the oil into smaller pseudo-components (Harrison et al., 1975; Luk and Kuan, 1993; Riazi and Edalat, 1996), and others consider the fate of individual

hydrocarbons on a compound-specific basis (Arey et al., 2007a, 2007b; Gros et al., 2014; Lemkau, 2012; Stiver et al., 1989). More recently, models that employ a mass transfer approach have successfully predicted both long-term (Arey et al., 2007a; Lemkau, 2012) and short-term (Gros et al., 2014) partitioning behaviour of hydrocarbons into the air and water following oil spills at sea. While the latter approach has proven useful, there are currently few published studies modelling the early evaporation and dissolution dynamics of monoaromatic compounds, such as BTEX, following a dilbit spill in freshwater.

Here, we report the fate of BTEX chemicals in a series of controlled dilbit spill experiments in limnocorrals installed in a boreal lake in northwestern Ontario. This study is part of the BOREAL project (Boreal Lake Oil Release Experiments by Additions to Limnocorrals), a multi-phase program to examine the fate, behaviour, and impacts of dilbit spills in freshwater environments (Rodriguez-Gil et al., 2021; Stoyanovich et al., 2021). With this study, we aim to provide novel information on the immediate behaviour of BTEX after dilbit spills occurring under natural environmental conditions typical of a boreal shield lake. We present detailed BTEX compositional analysis of the water column during the first 4 days after release and compare the field measurements to a transport model developed to describe the evaporation and dissolution of BTEX from dilbit.

2 MATERIALS AND METHODS

2.1. Simulated Dilbit Spills

We conducted this study at the International Institute for Sustainable Development – Experimental Lakes Area (IISD-ELA), near Kenora, Ontario (Canada) between June 20 – August 29, 2018. We installed nine limnocorrals in a ~ 2-m deep littoral zone on the northern shore of Lake 260, a clear oligotrophic lake 32.8 ha in area with a maximum depth of 15.7 m and an approximate water volume of 1 975 000 m^3. Limnocorrals consist of a 10 m diameter floating ring to which we attached a high-density polyethylene (HDPE) cylindrical membrane extending down to the sediments. We used sandbags to seal the plastic membrane to the lake bottom. We simulated a total of seven individual dilbit spills at volumes: 1.5, 2.9, 5.5, 18, 42, 82, or 180 L. The remaining two limnocorrals served as controls, one far-field and one near field. The dilbit used in this study was Cold Lake Winter Blend (CLWB), the physical and chemical properties for which can be found in SI Table S6.1. A detailed overview of the experimental set up and rationale for the spill volume is described by Rodriguez-Gil et al. (2021) and the dilbit addition process is given by Shah et al (2019).

2.2. Analysis of Water Samples

We collected water samples for BTEX analysis at 1 h, 6 h, 10 h, 24 h, 48 h, and 96 h following dilbit additions. Briefly, a 60 mL pre-cleaned amber glass vial was uncapped under water and allowed to fill completely and was then re-capped. All sampling for BTEX was carried out just the below the water's surface in an oil-free partition area of the limnocorral at an approximate depth of 0.25 m. All vials were stored in the dark at -4°C within an hour of collection. After the final samples were collected 96

h post dilbit release, all samples were shipped to a Health Canada (HC) laboratory in Ottawa, ON.

BTEX compounds were extracted from collected water samples using 100 μm solid phase microextraction (SPME) polydimethylsiloxane (PDMS) fibers and analyzed on a GC-MS (Bruker 450/300 GC-MS from Bruker LTD, Freemont CA). Detailed analysis methods description has been given in Supporting Information.

2.3. Diluted bitumen-water mass transfer model

The model framework describes a CLWB dilbit spill onto the water's surface experimental limnocorrals. We assumed the loss of BTEX components from the dilbit slick due to evaporation and dissolution, which were described by the "two-film" mass transfer model (Liss and Slater, 1974; Schwarzenbach et al., 2003). Reactive losses via photodegradation and biodegradation were assumed negligible. The model was then built based on the individual BTEX compounds known or estimated physical and chemical properties (SI Table S6.4) and treatment specific parameters (SI Table S6.5).

2.3.1. Loss of BTEX from diluted bitumen

The removal of BTEX components from the dilbit slick is controlled by diffusion from the dilbit phase to the air and water phases through evaporation or dissolution, respectively. Equation 1 describes the first order loss in the concentration of the analyte from bulk dilbit as:

$$\frac{dC_{i,O}}{dt} = -k_{i,OT} \times C_{i,O} \qquad (1)$$

where $C_{i,O}$ is the concentration of compound *i* in dilbit (μg kg^{-1}) and $k_{i,OT}$ the total elimination rate constant for compound *i* in the oil slick (d^{-1}). The $k_{i,OT}$ represents the

sum of competing processes of evaporation ($k_{i,OE}$; d^{-1}) and entry to the water column ($k_{i,OW}$; d^{-1}).

$$k_{i,OT} = k_{i,OE} + k_{i,OW} \quad (2)$$

We used a similar approach as Arey et al. (2007a) and Gros et al. (2014) to estimate the values of $k_{i,OE}$ and $k_{i,OW}$ using a "two-film" mass transfer model (Liss and Slater, 1974; Schwarzenbach et al., 2003):

$$k_{i,OE} = \frac{D_{i,air} K_{i,AO}}{\delta_{oil} \delta_{air}} \quad (3)$$

$$k_{i,OW} = \frac{D_{i,water} K_{i,WO}}{\delta_{oil} \delta_{water}} \quad (4)$$

where δ_{oil}, δ_{air}, and δ_{water} is the boundary layer thicknesses (m) for oil, air, and water respectively. The $D_{i,air}$ and $D_{i,water}$ are the diffusivities of compound *i* (m^2 d^{-1}) in air and water, respectively. The $K_{i,AO}$ and $K_{i,WO}$ are air-oil and water-oil partition coefficients (unitless).

We calculated δ_{air} (0.68 cm) and δ_{water} (0.068 cm) from mass transfer coefficients for sulfur hexafluoride measured in each limnocorral (Saunders et al., In Prep) from Equation S1. The $D_{i,air}$ and $D_{i,water}$ were estimated from molecular weight (Schwarzenbach et al., 2003). The $K_{i,AO}$ and $K_{i,WO}$ were estimated from Raoult's Law as (Arey et al. 2007):

$$K_{i,AO} = \frac{P_i^L V_{oil}}{RT} \quad (5)$$

$$K_{i,WO} = C_i^{sat} V_{oil} \quad (6)$$

where P_i^L (Pa) is the vapor pressure of compound *i*, C_i^{sat} is the water solubility of compound *i (mol* m^{-3}*)*, V_{oil} is the molar volume of the dilbit mixture (L mol^{-1}), R is the molar gas constant (8.314 J mol^{-1} K^{-1}), and T is the oil temperature which was assumed

to be equal to the temperature of air (294 K). The P_i^L was corrected for oil temperature using the van't Hoff equation (Equation S2). The V_{oil} was calculated using Equation S3 in the Supporting Information.

We calculated the slick thickness, $\delta_{oil,}$ from the volume of dilbit added on day 0 (V_O; m^3) and the average surface area of the slicks (A_O; m^2) during the first 4 days estimated from aerial drone photographs using *ImageJ* (ver 1.50) software. We assumed that slick thickness was uniform during the 4-day study period. Additionally, we also evaluated the model sensitivity of δ_{oil}, by running the model at range of possible thicknesses. This assessment is discussed further in the sensitivity analysis section.

2.3.2. Uptake and elimination of BTEX from water

Chemical uptake and elimination of BTEX in water is described as:

$$\frac{dC_{i,W}}{dt} = k_{i,OW} \times C_{i,O} - k_{i,WT} \times C_{i,W} \quad (7)$$

where $k_{i,OW}$ the rate constant for oil to water dissolution of compound *i* (d^{-1}), $k_{i,WT}$ is the total elimination rate constant of compound *i* in the water column (d^{-1}), $C_{i,O}$ and $C_{i,W}$ are the concentration of compound *i* in the oil (μg g^{-1}) and water column (μg L^{-1}), respectively.

The $k_{i,WT}$ is the sum of all loss processes in the water column and includes volatilization from water to air ($k_{i,WE}$; d^{-1}), diffusion from water to sediment ($k_{i,WS}$; d^{-1}), transformation in water ($k_{i,WR}$; d^{-1}), diffusion from water to oil ($k_{i,WO}$; d^{-1}), and loss from the limnocorral to the surrounding lake ($k_{i,WL}$; d^{-1}):

$$k_{i,WT} = k_{i,WE} + k_{i,WS} + k_{i,WO} + k_{i,WR} + k_{i,WL} \quad (8)$$

The equations used to calculate $k_{i,WE}$, $k_{i,WR}$, $k_{i,WO}$, and $k_{i,WL}$ are described in Section 1.3 of the Supporting information.

This model is developed to run a Euler-type numerical integration to produce time-series concentrations in the dilbit slick (Equation 1) and water column (Equation 7) throughout the specified time window. To match the experimental sampling period, we ran the model for 4 days, updating the different equations at 1000-time steps, or every 5 minutes and 45 seconds (SI Table S6.6). The initial mass of individual BTEX components in the oil slick were assumed to be equal to the concentration in the fresh dilbit (μg g^{-1}) multiplied by the mass of dilbit added (g). The initial mass of individual BTEX components in the water column was set equal to 0 μg. The ordinary differential equations were solved suing the *ode* function available under the *deSolve* package (Soetaert et al., 2020) available in R (v.3.6.3).

2.4. Model Evaluation

To test the model, we compared the model predicted concentrations to the observed concentrations in water at each time point (n=5) for each individual BTEX compound and for ΣBTEX. The mean model bias (MB) was derived on both a compound- and treatment-specific basis as (Alava et al., 2012; Gobas et al., 2018):

$$MB_{i,j} = 10^{\left(\sum_{i=1}^{n} \frac{\left[log\left(C_{p,i,j}/C_{o,i,j}\right)\right]}{n}\right)} \quad (9)$$

where $MB_{i,j}$ is the geometric mean (assuming log normal distribution of predicted and observed concentrations) of the ratio of predicted and observed concentrations for all compounds, *i,* in treatments, *j.* Time 0 values were omitted from this analysis and concentrations of 0 (i.e., non-detects) in experimental data were replaced by the method detection limit divided by two (SI Table S6.2). If the MB is greater than 1, then the model overpredicts the observed concentrations by a factor equal to the MB value. If the MB is

less than 1, then the model underpredicts the observed concentrations by a factor equal to the MB value. A perfect model would have a MB value of 1.

We performed a sensitivity analysis to determine the impact of error in the model's state variables on the predicted water column concentrations. The parameters explored in this exercise were boundary layer thicknesses (air, water, and oil), diffusivities ($D_{i,air}$ and $D_{i,water}$), oil temperature, water solubility, vapor pressure, and oil properties (oil molar volume and density). Varying the parameters by +/- 10%, a commonly used range for sensitivity analysis (Alava et al., 2012; Lemkau, 2012), enabled the identification of parameters that are the most important to accurately describe in future models. Sensitive variables have a large impact on model outcome from just a small change. This analysis involved changing each model variable (*I*) by a fixed amount (Δ*I*) and then monitoring the change (Δ*O)* in the outcome variable (*O)* to determine the variable's sensitivity, *S* (Alava et al., 2012; Gobas and Arnot, 2010):

$$S = \left(\frac{(\Delta O/O)}{(\Delta I/I)}\right) \quad (10)$$

In this case, the model outcome studied was the predicted maximum ΣBTEX concentration in the water column.

Considering the high degree of uncertainty associated with slick thickness (δ_{oil}) calculations, a variation of only 10% as discussed above is likely not enough to capture the true uncertainty in the results. We therefore included an additional sensitivity analysis with a broader range of variation. We adjusted the average slick thickness by a factor of 10 in both directions (upper limit = δ_{oil}*10, lower limit = δ_{oil}/10) to establish a range of possible thickness values (SI Table S6.7). We then set up 50 equidistant points

within these ranges and ran the simulation, each time using a new value for δ_{oil} and assessed how the model output changed using equation 10.

We did not conduct any formal uncertainty analysis based on model input variability because we assumed that the most influential uncertainties arose from estimating oil slick thickness (as discussed above).

3 RESULTS AND DISCUSSION

3.1. Temporal progression of BTEX in water column

The concentration of ΣBTEX in water increased rapidly in each treatment, reaching maximum concentrations between 1.9 and 108 µg L^{-1} after 10 hours in all treatments except in the 180 and 1.5 L treatments, which reached maximum concentrations after 24 and 6 hours, respectively (Figure 6.1A). Across all treatments, benzene made up the highest proportion of BTEX in water (41 – 61 %), followed by toluene (18 – 43 %), *o,m,p*-xylenes (10 – 19 %), and ethylbenzene (0.8 – 2.4 %) (SI Figure S6.3). These differences are likely due to compound specific water solubilities, which progress in the following order: benzene (1780 mg L^{-1}) > toluene (515 mg L^{-1}) > *o,m,p*-xylenes (160 – 220 mg L^{-1}) > ethylbenzene (152 mg L^{-1}) (SI Table S6.3). ΣBTEX concentrations then decreased for the remainder of the sampling period, approaching the detection limit at 96 h post-addition in all treatments except for 180 L, which was still at 49 µg L^{-1} after 96 h. Benzene reached highest concentrations in water, ranging between 0.79 – 54.1 µg L^{-1} across all treatments (Figure 6.1B), followed by toluene (0.42 – 45.1 µg L^{-1}, Figure 6.1C), *o,m,p*-xylenes (0.28 – 11.2 µg L^{-1}, Figure 6.1E), and ethylbenzene (0.045 – 2.02 µg L^{-1}, Figure 6.1D). The only compound to have surpassed

the CCME water quality guideline for protection of aquatic life was toluene (interim guideline of 2 µg L^{-1}). However this guideline value is based on a 27 day LC_{50} for rainbow trout (Black et al., 1982). Considering toluene concentrations were below detection after just 96 hours suggests there may be low risk of chronic toxicity at the observed concentrations.

The regression design used here allows us to determine how well dilbit spill size (oil:water ratio) can predict BTEX concentrations in the water column using simple linear regression similar to previous work by Stoyanovich et al. (In Prep). A significantly positive slope would indicate that as the ratio of dilbit to water increases, the concentrations of BTEX in the water column will increase. SI Figure S6.4 highlights the dynamics of concentration change across spill volumes, specifically the linearity of the relationship between BTEX concentrations and oil:water ratios. We observed a significant positive relationship emerge at the majority of timepoints from 10 h post dilbit release and onwards for benzene, toluene, ethylbenzene, o,*m,p*-xylenes, and ΣBTEX (SI Figure S6.4 & Table S6.8). This positive relationship persisted until the final sampling timepoint (96 h) for benzene and ΣBTEX, whereas by the 96 h timepoint the remaining compounds had already decreased to below method detection limits.

We can relate the maximum BTEX mass detected in the water to the amount that was actually released in each spill by considering the mass of CLWB added, the BTEX content of the added oil, and the estimated water volumes of the limnocorrals. Interestingly, the percentage of ΣBTEX dissolution ranged from 0.56 – 1.32 % across all treatments. For individual compounds; benzene, toluene, ethylbenzene, and *o,m,p*-xylenes, the fraction of chemical dissolved in the water column ranged between 2.1 –

4.2 %, 0.4 – 1.2 %, 0.2 – 0.9 %, and 0.1 – 0.4%, respectively, across all treatments (SI Table S6.3). This indicates that dissolution is only a minor loss process when considering the fate of monocyclics following a dilbit spill. These monocyclic dissolution percentages are similar to those reported by King et al., (2019) for ΣBTEX (1.8 – 3.9%) following the natural weathering of bitumen blends on water in floating microcosms.

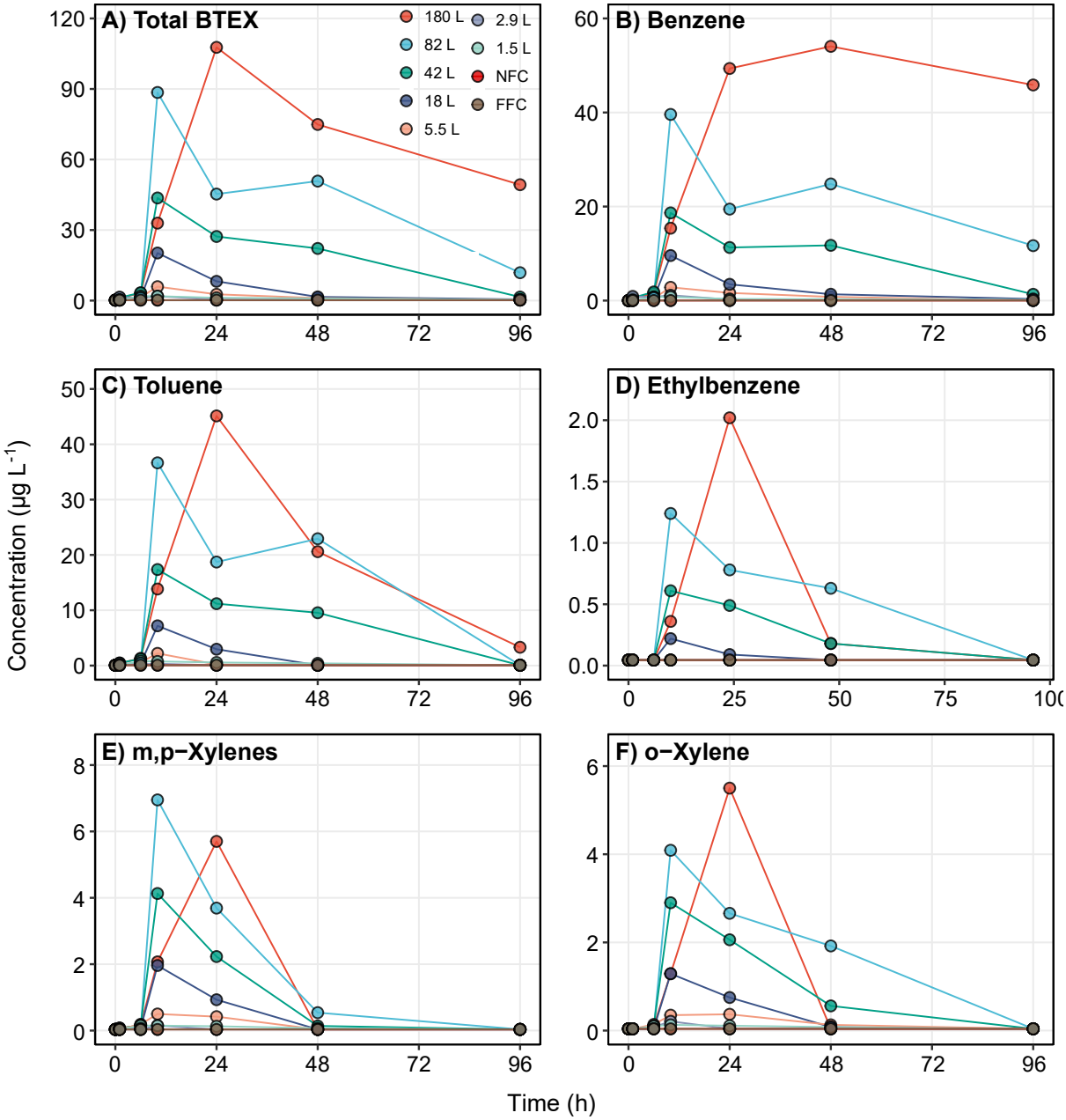

Figure 6. 1. (A) ΣBTEX, (B) benzene, (C) toluene, (D) ethylbenzene, and (E) *o,m,p*-xylenes over time

The observed BTEX depletion is likely due primarily to evaporation across the water – air interface (Fingas, 2015b). Transfer from the water column to the atmosphere would be restricted by the presence of the oil slick, as suggested in a previous publication by Stoyanovich et al., (2019). For example, the average slick surface area during the first 4 days of the study was roughly 2.4 – 25.5X greater in the 180 L treatment compared to the remainder of the treatments. This inherently decreases the amount of open water – air interface in the two highest treatments and may explain why ΣBTEX concentrations did not return to baseline concentrations after 96 hours.

A comparison between past dilbit studies that measure BTEX in the water column and the present study can be found in SI Table S6.10. Witt Obrien's et al. (2013) measured ΣBTEX dissolution over 9 days following experimental spills of CLWB and AWB into large freshwater tanks (1490 – 66 000 L) under varying wind and wave conditions. The researchers measured maximum ΣBTEX concentrations between 900 – 3000 μg L^{-1}, roughly 9 – 30X higher than maximum values observed in our study. The oil:water ratios used by Witt Obrien's ranged from 1:446 to 1:118 and produced slick thicknesses of 10 mm. King et al. (2019) modelled the dissolution of ΣBTEX over 8 days following experimental spills of AWB, WCS, and Synbit into a circular flume tank containing seawater (1300 L) under spring and summer conditions (wave currents of 21 cm/s). At an oil:water ratio of 1:5000, the maximum ΣBTEX concentrations ranged from approximately 20 – 60 μg L^{-1} across all dilbit types, reached between 8 hours and 2 days posttreatment, similar to maximum values observed in our study. Finally, Ortmann et al. (2020) reported ΣBTEX concentrations in the water column over 14 days following

spills of AWB, WCS, and Synbit into flume tank enclosures (~250 L) filled with natural seawater during the spring, summer, and autumn. At an oil:water ratio of 1:8600, the maximum ΣBTEX concentrations ranged from 5 – 64 μg L^{-1}, all of which were reached 1 day after the spill and were within the range of concentrations observed in our study.

Several factors can influence the dissolution of water-soluble hydrocarbons from an oil slick into the water column. First, the BTEX content of the source oil. CLWB, AWB, WCS, and Synbit are made up of 0.89, 1.96, 0.56, and 0.87% BTEX, respectively (King et al. 2019). Since the dilbits are all slightly different in chemical composition, accurate comparisons are difficult to discern. Second, the oil:water ratio selected is directly proportional to the measured hydrocarbon concentrations in the water column (Chapter 5). For example, the oil:water ratios used by Witt Obrien et al. (2013) were approximately 4- to 600-fold higher than those used in the present study, and these differences are reflected in the maximum BTEX concentrations observed in either study. Finally, the thickness of the dilbit slick is a very important factor. Gros et al. (2014) note that thicker oil slicks would produce higher hydrocarbon concentrations within the water column due to the larger load of oil mass per area.

3.2. Modelled dissolution and evaporation rates of BTEX

Evaporation rate constants (Equation 3) ranged between 27–436 d^{-1} for benzene, 7–114 d^{-1} for toluene, 2.1–34 d^{-1} for ethylbenzene, and 1.9–31.0 d^{-1} for *o,m,p*-xylenes, across all treatments (SI Table S6.11). The model-derived dissolution rate constants (Equation 4) ranged from 0.2–3.3 d^{-1} for benzene, 0.04–0.7 d^{-1} for toluene, 0.01–0.2 d^{-1} for ethylbenzene, 0.01–0.2 d^{-1} for *o,m,p*-xylenes, across all treatments (SI Table S6.11). Linear regression results showed no significant relationship between either the

evaporation or dissolution rates and the oil:water ratio, suggesting that the magnitude of the rates does not depend on the volume of dilbit spilled. This finding was consistent with the findings from Chapter 4 where we found no significant relationship between empirical total loss rate constants for PAHs to spill volume.

3.3. Model Performance

The modelled water column concentrations of ΣBTEX (Figure 6.2) were in good agreement with observed concentrations. Between 29 – 86% of predicted ΣBTEX concentrations were within three-fold of observed concentrations, when matched by timepoint (SI Figure S6.6). The mean model bias (MB) values and their associated 95% confidence intervals (CI) for each individual compound in each treatment can be found in SI Table S6.12. The mean MB for ΣBTEX ranged from 0.9 (-0.7 – 2.5) to 3.7 (-0.3 – 7.6) across all treatments. The model slightly under predicted ΣBTEX concentration in the 1.5 L treatment, and over predicted in all the other treatments. As for individual BTEX compounds, the model was in good agreement with observed concentrations for toluene and ethylbenzene, but tended to underpredict benzene concentrations and overpredict *o,m,p*-xylene concentrations (SI Figure S6.5). Between 14 – 57% (benzene), 29 – 71% (toluene), 14 – 86% (ethylbenzene), and 0 – 71% (*o,m,p*-xylenes) of predicted concentrations, across all treatments, were within three-fold of observed concentrations when matched by timepoint (SI Figure S6.6). The mean MB values (95% CI) for the benzene in the water column (n = 6) ranged from 0.5 (-3.1 – 4.1) to 1.6 (-6.5 – 9.8) across all treatments. For benzene, the mean MB were close to 1.0 indicating no systematic over- or under- prediction in the water column. The mean MB values (95% CI) for the toluene in the water column (n = 6) ranged from 0.9 (-1.4 – 3.2) to 7.8 (2.0 –

13.6) across all treatments. For toluene, the model tended to underpredict in the 1.5 L treatment, but over predict in all other treatments. The mean MB values (95% CI) for the ethylbenzene in the water column (n = 6) ranged from 0.4 (-0.8 – 1.6) to 9.8 (7.0 – 12.5) across all treatments. For ethylbenzene, the model underpredicted in the 1.5 and 2.9 L treatments and overpredicted in the remaining treatments. Finally, the mean MB values (95% CI) for the *o,m,p*-xylenes in the water column (n = 6) ranged from 1.9 (0.8 – 2.9) to 57.7 (-52.2 – 63.2) across all treatments. For *o,m,p*-xylenes, the model slightly over predicted concentrations in the 1.5 L treatment, and vastly over predicted concentrations in the remaining treatments (MB>5). Overall, the model tended to overpredict when all timepoints are considered (SI Figure S6.6), however, water samples were limited to single samples (i.e., no replicates) and therefore error in the concentrations could not be quantified. It is important to note that the mean MB values are averaged across all sampled timepoints (n=6) and when examining Figure 6.2 and Figure S6.5, we observe that most of the over estimation occurred during the latter time points (>24 h), suggesting that our model may underestimate the overall loss of BTEX from the water column. Although our study considered several potential pathways for BTEX loss (i.e., evaporation, diffusion, reabsorption, reaction, leakage), possible errors with respect to the specification of these rate constants may explain apparent discrepancies between observed and modelled concentrations in the water column. It is also possible that there are other loss processes in the water column that are not considered in the model. One factor that was not explored in the model was the influence of asphaltenes and resins migrating to the dilbit-water interface, forming a

barrier to further dissolution of more water-soluble compounds (Fingas et al., 1996; Lee et al., 2015).

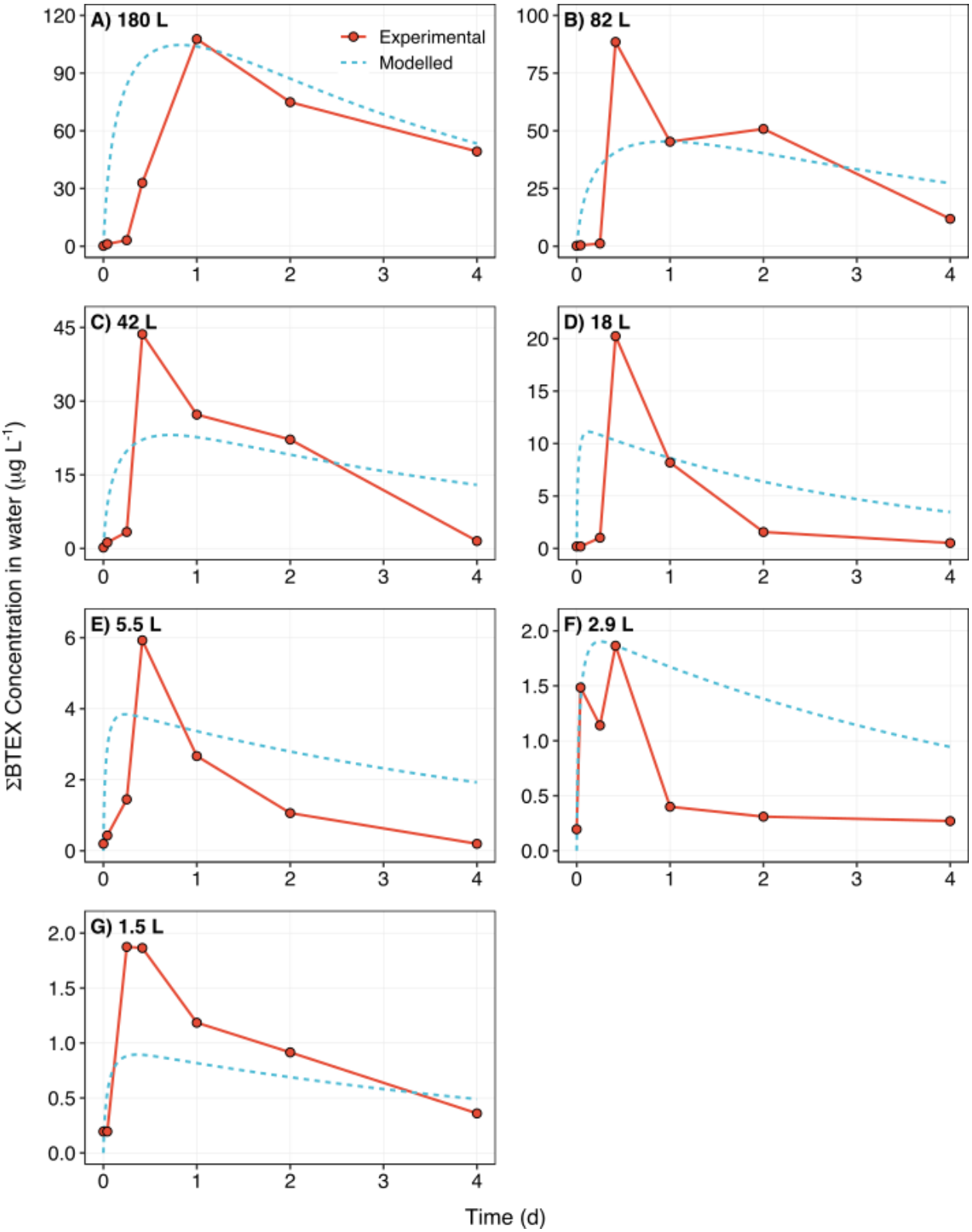

Figure 6. 2. Predicted and observed ΣBTEX concentrations in the water column of each treatment over time.

Figure 6.3 summarizes the mass transfer model calibration as evaluated against the observed maximum concentrations of individual BTEX compounds and ΣBTEX. The combined goodness of fit test for all BTEX compounds and treatments yielded the following relationship:

$$LogC_{BTEX(obs)} = 0.97 \pm 0.070 LogC_{BTEX(pred)} + 0.14 \pm 0.066;\ R^2 = 0.86,\ p<0.0005$$

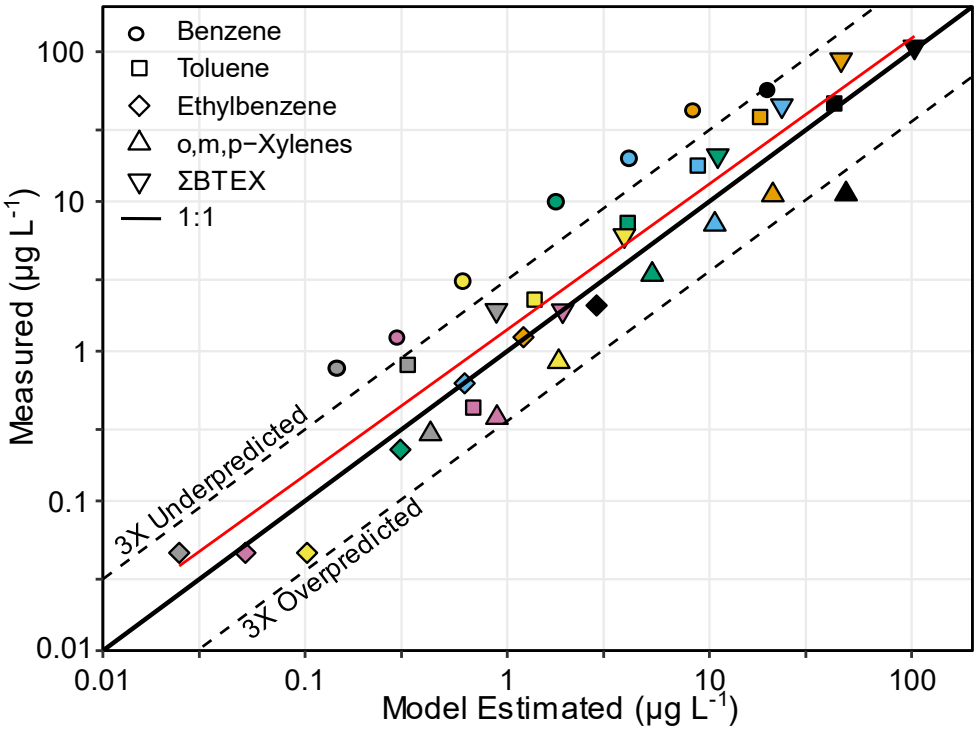

Figure 6. 3. Relationship between the measured and model estimated maximum concentration of individual BTEX compounds and ΣBTEX measured over time in each treatment. The red line represents the overall goodness of fit for all BTEX compounds and treatments. 180 L treatment = black; 82 L treatment = orange; 42 L treatment = blue; 18 L treatment = green; 5.5 L treatment = yellow; 2.9 L treatment = pink; and 1.5 L treatment = gray.

The mass transfer model was able to predict maximum water column concentrations of benzene with 13 – 27 % accuracy, toluene with 38 – 92 % accuracy, ethylbenzene with 67 – 100 % accuracy, *o,m,p*-xylenes with 24 – 75 % accuracy, and ΣBTEX with 47 – 100 % accuracy, across all treatments. Further, model estimated

maximum concentrations observed in the water column are shown to be within a factor of three to observed concentrations in all cases except benzene in the 1.5, 2.9, 5.5, 18, 42, and 82 L treatments, and *o,m,p*-xylenes in the 180 L treatment (Figure 6.3).

Based on model outputs, it is likely that we are overpredicting the evaporation rate constant ($k_{i,OE}$; d^{-1}) for benzene, whose model predicted evaporative half-lives are between 0.1 – 1.6 min, across each treatment. Therefore, within minutes of the spill, the model predicts there is no benzene remaining in the slick, and all dissolution would cease. The magnitude of the evaporation rate constant is directly proportional to the compounds theoretical vapor pressure, and benzene has a vapor pressure that is 3 – 11X greater than the remaining BTEX compounds (Mackay et al., 2006). It is possible that this model is not optimized for a compound as volatile as benzene.

3.4. Simulated Mass Balance for BTEX

According to the model, between 0 – 7.4% of the ΣBTEX remained in the slicks, 92.1 – 99.5% was evaporated, and 0.5 – 0.6% was dissolved after just 24 h post oil release. The model predictions after 96 h (0 – 0.03%, 99.6 – 99.8%, and 0.2 – 0.4%, respectively) suggest that virtually all of the BTEX has been removed from the dilbit slicks, and the majority has evaporated into the air, with less than 1% entering the water column. These predictions coincide with water column mass apportionments observed in experimental data, where 0.1 – 0.9% of ΣBTEX was dissolved on day 1 and 0.03 – 0.3% of ΣBTEX was dissolved on day 4, across all treatments. Our model estimates were significantly lower than those of Gros et al. (2014) who developed a mass transfer model to study the mass of oil lost to evaporation and dissolution during the initial days following the release of 4.3 m^3 Norwegian grane crude oil at sea. Their model predicts

benzene and toluene become 13% and 5% dissolved, respectively. Our results suggest that following simulated dilbit spills under realistic environmental conditions, the risk of BTEX contamination and toxicity within the water column is low. With the majority of the monoaromatics entering the atmosphere, inhalation exposure is expected to be the main concern for spill responders, which may result in acute or chronic effects (NASEM, 2016). Our results stress the importance of monitoring airborne volatiles during the initial stages of dilbit spill clean-up.

3.5. Sensitivity Analysis

Supporting information Table S6.13 illustrates the sensitivity of the state variables of the model. Oil temperature had the greatest overall effect on the model estimates, resulting in an average decrease of 17% of the maximum predicted ΣBTEX concentration in water when oil temperature was increased by 10%, across all treatments (SI Table S6.14). Other influential parameters were the air and water-film thicknesses, diffusivities in air and water, vapor pressure, and water solubility. These parameters are used directly to calculate evaporation ($k_{i,OE}$; Equation 3) and dissolution rates ($k_{i,OW}$; Equation 4) in this model. In any instance where the evaporation rates decrease, this resulted in more compounds remaining in the slick for dissolution, resulting in an increased concentration of BTEX in the water column, and vice versa.

Varying oil slick thickness by +/- 10% did not have a drastic impact on the overall model outcome in this study. These findings contrast previous studies (Arey et al., 2007a; Gros et al., 2014; Lemkau, 2012; Yarranton et al., 2015), where slick thickness has been shown to cause differences in weathering rates. Aside from methods to remotely measure oil slick thickness, such as microwave radiometry and time of

acoustic travel, there are no established methods to accurately measure oil slick thickness in the field (Fingas, 2018). In this study we determined thickness using similar methods as Arey et al. (2007a) and Gros et al. (2014), by dividing the volume of dilbit spilled (m^3) by the observed surface area of the slicks (m^2). However, there is a large degree of uncertainty in both estimated volume and area measurements, especially as weathering proceeds. As water becomes entrained in the oil slick, the effective volume of the spill will increase (Fingas, 2018; Fingas and Fieldhouse, 2004). Areas of interspersed water and sheen can make it difficult to identify clear slick borders when estimating surface area. Heavy oils, such as dilbit, do not form a consistent homogeneous slick and are instead thicker at the center and thinner towards the edges (Hollinger and Mennella, 1973). Finally, our surface area estimates were estimated from aerial photographs taken once daily during the first 4 days of the experiment, representative of single timepoints. Our previous work has shown that the distribution of the dilbit slicks were highly dependent on wind speed therefore the slick thickness likely changed throughout the days. Because of these factors, a sensitivity analysis where slick thickness is only varied by 10% is likely not enough to capture the range of possible slick thicknesses that would occur under the given spill scenarios.

When slick thickness was increased by 90%, the maximum predicted ΣBTEX concentration in the water decreased by 22 – 46% across all treatments (Figure 6.4, SI Table S6.15 & S6.16). In contrast, decreasing the slick thickness by 90% resulted in an increase of predicted ΣBTEX concentration by 4 – 8% in the 42, 82, and 180 L treatments, and a 4 – 18% decrease in the 1.5, 2.9, 5.5, and 18 L treatments. Variation in slick thickness affects the $k_{i,OE}$ (Equation 3), $k_{i,OW}$ (Equation 4), and $k_{i,WO}$ (Equation

S6). As the slicks become thicker, both the oil evaporation rate ($k_{i,OE}$) and dissolution rate ($k_{i,OW}$) decrease, resulting in BTEX remaining in the dilbit slick for longer periods of time. Further, since the oil reabsorption rate ($k_{i,WO}$) is related to $k_{i,OW}$, and $k_{i,WO}$ contributes to the total loss from water ($k_{i,WT}$; d^{-1}), we observe the BTEX remaining in the water column for longer periods of time. For example, the base model for benzene in the 180 L treatment had an oil slick thickness value of 0.0034 m and resulting evaporation, dissolution, and water-oil diffusion rates of 310, 0.2, and 0.09 d^{-1}, respectively. When we ran the simulation with a slick thickness of 0.034 m (+90%), the resulting rates for benzene decreased by an order of magnitude to 31, 0.02, and 0.009 d^{-1}, respectively, and these trends were consistent for each compound across each treatment. Since oil slick thickness is such a difficult parameter to accurately define, and slick thickness can vary from 2 μm to 20 mm (Fingas, 2018), future models should be run at a variety of possible thickness values to capture a wider range of potential model outcome values.

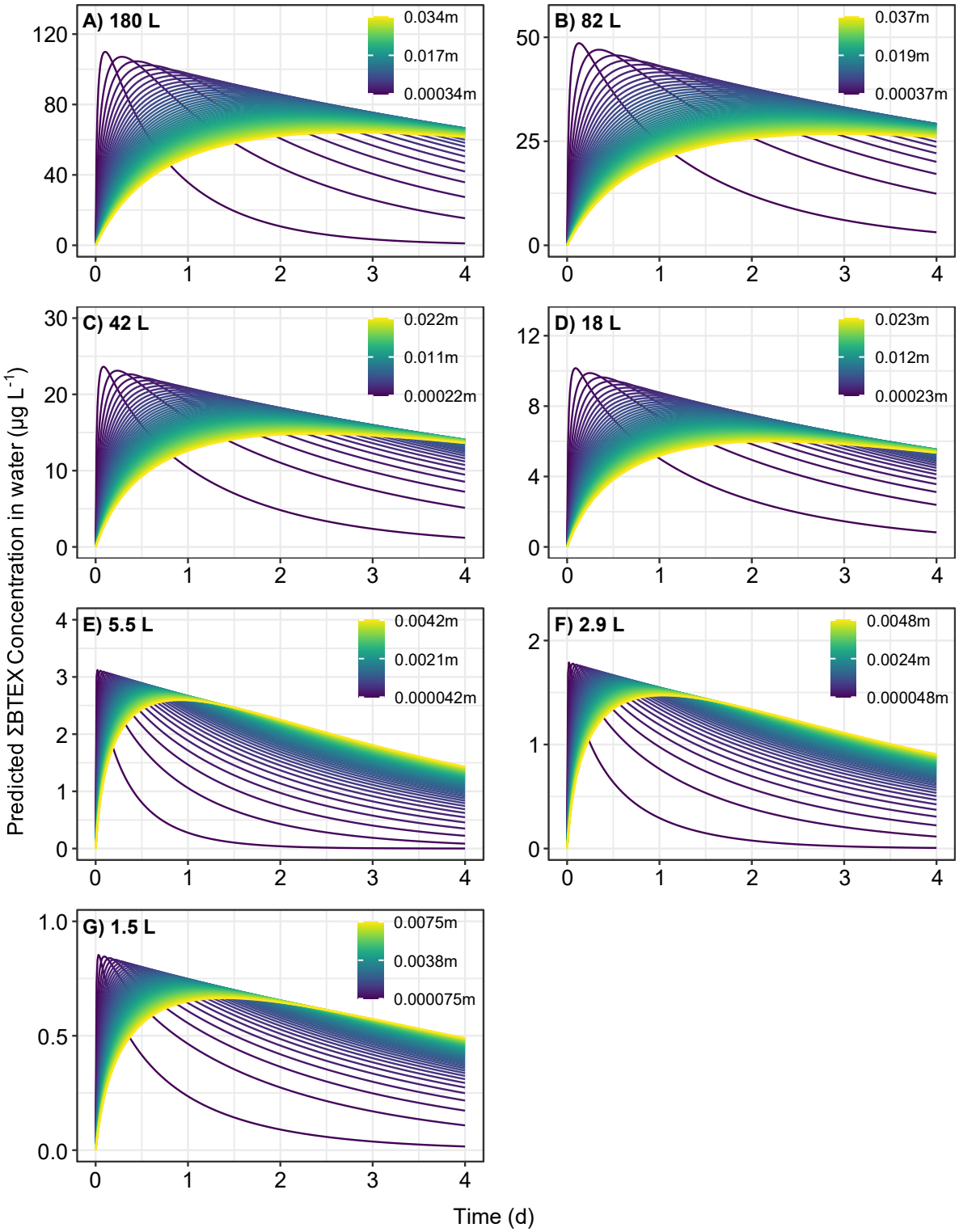

Figure 6. 4. Predicted ΣBTEX concentrations in the water column in each treatment at different dilbit slick thickness values, varied at +/- 90% of base model values. Base model values include: 180 L = 0.0034 m; 82 L = 0.0037 m; 42 L = 0.00022 m; 18 L = 0.00023 m; 5.5 L = 0.00042 m; 2.9 L = 0.00048 m; 1.5 L = 0.00075 m.

3.6. Implications and Limitations

This is the first attempt to model the mass transfer of BTEX in dilbit slicks and to compare the model outputs to real-time field observations. Our results suggest that the concentrations of BTEX in water did not exceed any water quality guidelines or toxicity thresholds for protection of aquatic life. However, the early fluxes of BTEX into the air (>90%) may be of concern to populations downwind from a spill and to first responders on site to manage the oil recovery, as they would be at risk of inhalation exposure (Middlebrook et al., 2012).

Our model has proven applicable to a wide range of dilbit spill sizes, ranging in oil:water ratios of 1:71 000 to 1:500 (v/v). Since the model is regulated entirely by compound specific physical-chemical properties and ambient environmental conditions, it will be useful to infer the behaviour of BTEX under different environmental conditions (i.e., temperature, wind, water column) and spill scenarios. At lower temperatures, evaporation and dissolution are expected to be slower compared to higher temperatures. Furthermore, colder temperatures would result in lower chemical volatility (Schwarzenbach et al., 2003), which would in turn decrease the air-oil partition coefficients and thereby the evaporation rates. As noted by Gros et al. (2014), decreasing temperature also decreases water solubility, but to a lesser extent than vapor pressure. Thus, colder weather conditions, such as a spill in the winter months, would produce greater concentrations of BTEX in the water column compared to a summer spill. This has been shown empirically via tank-based studies by Ortmann et al. (2020).

As with any model, limitations do exist. The molecular diffusion of compounds through the dilbit slick was not considered in this study as this process is thought to be most important in water-in-oil emulsions (Irvine et al., 1999; Wang and Stout, 2007), which were not observed in the first 4 days of our study. Regardless, an oil slick diffusion term should be included in future models, especially those that aim to predict mass transfer over a longer period of time, at which point the formation of emulsions may become important. Arey et al. (2007a) incorporated an oil-slick diffusion term, D_{oil}, in their mass transfer model and noted that that oil-phase diffusion is likely important for volatile hydrocarbons under higher oil loadings (large δ_{oil}) and low temperature (higher viscosity). However, the authors noted that no accepted method exists to derive values for D_{oil}, and the added effort to parameterize a rudimentary equation for D_{oil} is not worthwhile compared to a simpler approach of simply omitting this term. Evaporation and dissolution were the only two loss processes considered to act upon the dilbit slick in this study. While these are the most pertinent processes to consider when modeling over short periods of time, future models looking to include a wider range of hydrocarbons over a longer simulation period must consider other weathering processes such as dispersion, biodegradation, and photooxidation. Our model is optimized for the initial days of a dilbit spill under summer conditions and is therefore not adaptable for longer time periods where seasonal or diurnal variation would be present. Finally, our model does not take into consideration rain or wave activity, which could force small droplets of dilbit into the water column through dispersion (Lee et al., 2015; NASEM, 2016), increasing the surface area to volume ratio of the dilbit and the rate of hydrocarbon dissolution (Lee et al., 2015).

The mass transfer model developed here accurately predicted dissolution trends that act on BTEX compounds immediately following a dilbit spill in freshwater. The base model tended to over predict water column concentration when averaged across all sampling timepoints. Overall, maximum concentrations of ΣBTEX in the water column were predicted with 47 – 100% accuracy to observed values. Sensitivity analysis suggests accurately constraining parameters including water and air-film thickness, oil temperature, diffusivities in water and air, saturation concentrations, and vapor pressures would enable more accurate modelling. Furthermore, testing the model across a wider range of potential oil slick thicknesses could improve model performance in future applications.

ACKNOWLEDGEMENTS

Funding for the present study was provided by a Natural Sciences and Engineering Research Council Strategic Partnership Grant (STPGP 493786-16 awarded to J.M. Blais, M. Hanson, and D.M. Orihel), a grant under the Oceans Protection Program, in-kind contributions from Environment and Climate Change Canada (ECCC) and Health Canada (HC), and in-kind support from the IISD-Experimental Lakes Area. A special thank you to J. Séguin, T. Black, J. Cederwall, L. Timlick, S. Patterson, J. Mason, D. Denton, H. Kosichek, K. Watson, and D. Dey for their contributions to the project.

SUPPORTING INFORMATION

1. Supporting Methodology

1.1 CLWB Properties

Table S6. 1. Physical Properties of fresh, unweathered Cold Lake Winter Blend (CLWB) dilbit

Measurement	Value
Density at 15°C (g mL^{-1})	0.9215
Density at 0 °C (g mL^{-1})	0.932
API Gravity	21.5
Viscosity at 15 °C (mPa·S)	181
Viscosity at 0 °C (mPa·S)	547
Flash Point (°C)	-6
Pour Point (°C)	-43
Sulfur Content (%)	3.3
Benzene (μg g^{-1})	1469
Toluene (μg g^{-1})	4146
Ethylbenzene (μg g^{-1})	410
o,m,p-Xylenes (μg g^{-1})	4924

1.2 Analytical

1.2.1 Sample Storage

We collected travel blanks during sampling period throughout the initial 96 h of the spills. All collected water samples were kept in coolers, with ice packs, maintaining temperatures below 10 C and above freezing during shipping. All samples were analyzed immediately upon arrival at the receiving laboratory.

1.2.2 Analytical Standards

A 200 μg mL^{-1} standard mix of BTEX compounds containing benzene (CAS# 71-43-2), toluene (CAS# 108-88-3), ethylbenzene (CAS# 100-41-4), *o*-xylene (CAS# 95-47-6), *m*-xylene (CAS# 108-38-3), and *p*-xylene (CAS# 106-42-3) was obtained from

Restek Corporation (110 Benner Circle, Bellefonte, PA, 16823). Individual deuterated isotopic standards of *d*6-benzene, *d*8-toluene, *d*10-ethylbenzene, *d*10-*o*-xylene, and *d*10-*p*-xylene were purchased from Cambridge Isotope Laboratory (50 Frontage Road, Andover, MA, 01810-54130). A high spiking standard consisting of 4 mg L^{-1} BTEX mix in 99.9% LC-grade methanol from Omnisolve (4710 Sweden Rd., Charlotte, NC, 28224) and a low spiking standard consisting of 0.5 mg L^{-1} BTEX mix and 99.9% methanol. Further, the isotopic spiking standard was prepared by mixing 1 mg L^{-1} of deuterated BTEX in 99.9% methanol.

1.2.3 Vials, columns, and fibers

20 mL solid phase microextraction (SPME) vials, polydimethylsiloxane (PDMS) 100 µm fibers, and magnetic caps were purchased from Supelco (485F US Highway One South, Suite 210, Iselin, NJ). Finally, The DB-5 30m x 0.32ID x 1µm film column was purchased from J&W Scientific, Agilent Technologies (5301 Stevens Creek Blvd. Santa Clara, CA, 95051).

1.2.4 Calibration Curve

Daily calibration curves (Figure S6.1) were prepared by adding 1.2 g of sodium chloride (NaCl) and 12 mL of lake water (collected from the study site 6 weeks prior to the dilbit addition) to 20 mL SPME vials and capped immediately. The standard mix and isotopic standards were added to each vial so as to have a calibration curve ranging in concentration from 0.1 to 10 µg/L with an isotopic standard concentration of 2 µg/L. Vials were capped immediately after each addition and vortexed after all standard/isotopic additions were completed.

a) 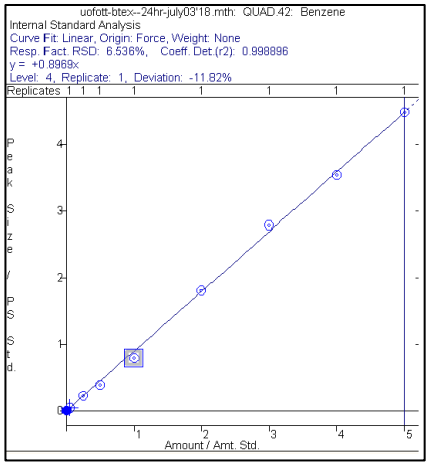

b) 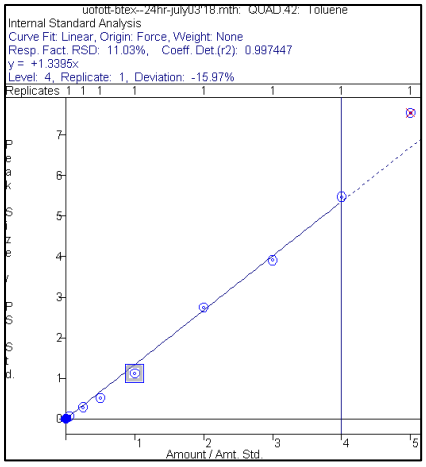

Figure S6. 1. Example of calibration curves for benzene (a) and toluene (b) used for the 24-hour time interval samples.

1.2.5 Analytical Instrumentation

We determined BTEX concentrations on an Bruker 450/300 GC-MS triple quadrapole from Bruker LTD, (2859 Bayview Dr, Fremont, CA 94538) equipped with a CombiPAL autosampler (CTC Analytics AG, Zwingen, CH). We performed chemical separation using an Agilent DB-5MS Column (30m x 0.25mm x 1.0 µm film thickness) under a constant column flow of UHP Helium carrier gas at 1.2 ml/min with UHP Helium. The CombiPAL autosampler was configured at an agitator temperature of 33°C, an extraction speed of 500 rpm, an extraction time of 15 minutes, a desorption temperature of 240°C, and a desorption time of 1 minute. The temperature program used for BTEX determination was 40°C for 0.5 min, ramp at 4°C/min to 110°C with no hold, then ramped at 20°C/min to 200°C and held for 3.5 min. The MS had a source temperature of 200°C, a transfer line temperature of 240°C, an electron energy of -70eV, a filament current of 50 µA, and a select ion monitoring (SIM) mode between 50 – 300 *m/z*.

1.2.6 Quality Assurance and Control

Calibration curves were run every day. A QC verification sample, prepared identically with the 2 µg/L calibration curve point, was run every 10th sample. A blank fiber, blank lake water, and blank lake water spiked with isotopic-BTEX standard were included in every analytical run.

Table S6. 2. Method detection limits (MDLs) for each BTEX compounds

Compound	MDL (μg/L)	Dynamic Range (μg/L)	Mean % Recovery
Benzene	0.03	0.1 – 10.0	94.0 ± 7.7
Toluene	0.12	0.1 – 8.0	86.0 ± 6.2
Ethylbenzene	0.09	0.1 – 2.0	98.5 ± 11.7
m,p-Xylene	0.07	0.1 – 2.0	93.2 ± 13.0
o-Xylene	0.08	0.1 – 2.0	98.0 ± 10.5

1.2.7 Analyte Quantification

Analyte quantification (Figure S6.2) was performed using calibration curves prepared in ELA water. All samples were adjusted for recovery using isotope-labelled internal standards.

Table S6. 3. Retention time (RT), identification and confirmation ions of analytes

Compound	RT (min)	Quant Ion (*m/z*)	Ref Ion (*m/z*)	Labelled Std (*m/z*)
Benzene	5.2	78	77	84
Toluene	9.5	91	92	98
Ethylbenzene	13.6	91	106	98
m,p-Xylene	14.0	91	106	98
o-Xylene	15.0	91	106	98

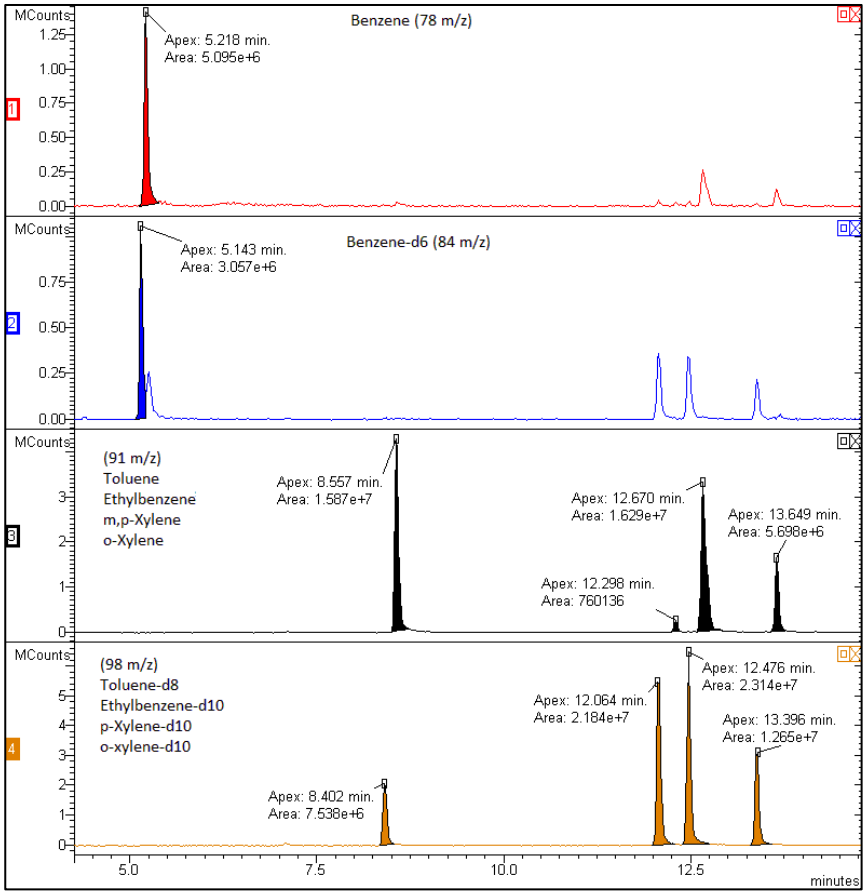

Figure S6. 2. Example of chromatogram of a water sample collected from the 18 L treatment at the 24 h sampling timepoint.

1.3 Mass Transfer Model

1.3.1 Calculation of parameters to estimate the loss of BTEX from diluted bitumen

Calculation of δ_{air} and δ_{water}

The air and water boundary layer thicknesses, δ_{air} and δ_{water}, were estimated from "overall" mass transfer coefficients for sulfur hexafluoride (SF_6) measured in the control limnocorrals (those receiving no dilbit) during the dilbit spill study (Saunders et al. In Prep). Because SF_6 is water-phase resistance controlled, the water boundary layer thickness (δ_{water}) can be estimated from mass transfer coefficients of SF_6 ($v_{E,SF6}$) as:

$$v_{e,SF6} = D_{SF6}/\delta_{water} \quad \text{(S1)}$$

where $D_{SF6,W}$ is the molecular diffusivity of SF_6 in water (6.78×10^{-5} m^2 d^{-1}). The $D_{SF6,W}$ was estimated from molecular weight according to Schwarzenbach et al. (2003) and the measured $v_{E,SF6}$ is 0.10 m d^{-1} (Saunders et al. In Prep). Rearrangement of Equation S1 calculates a δ_{water} of 0.00068 m. The δ_{air} was estimated from δ_{water} as $10\times\delta_{water}$ = 0.0068 m.

1.3.2 Temperature correction of vapour pressure.

The P_i^L was corrected for temperature using the van't Hoff equation as given by Arey et al. (2007):

$$P_i^L(\mathrm{T}) = P_i^L(T_{ref})exp\left[-\frac{\Delta_{vap}H_i}{R}\left(\frac{1}{T}-\frac{1}{T_{ref}}\right)\right] \quad \text{(S2)}$$

where T_{ref} is the reference temperature (298 K), $\Delta_{vap}H_i$ is the enthalpy of vaporization of compound *I* (KJ mol^{-1}; Table S3)

1.3.3 Calculation of oil molar volume

The oil molar volume (V_{oil}) of CLWB was estimated as (Arey et al 2007):

$$V_{oil}(t) = \frac{\sum_{i=1}^{N}(M_i(t)*MW_i)}{\sum_{i=1}^{N}(M_i(t)*\rho_{oil}(t))} \quad \text{(S3)}$$

where $V_{oil}(t)$ is the average molar volume (L mol^{-1}) for compounds within the studied range, $\rho_{oil}(t)$ is the density of the oil (kg m^{-3}), and $M_i(t)$ is the mass (kg) of compound *i* at time *t*, and N is the number of compounds analyzed (110). Conceivably V_{oil} would change with time as the dilbit weathers, however since the model was not sensitive to changes in V_{oil}, it remained constant.

1.3.4 Derivation of elimination rate constants for BTEX in water

The rate constant for evaporation from water ($k_{i,WE}$; d^{-1}) was estimated as (Gobas et al. 2018):

$$k_{WE} = \frac{SA_w f_{DW} v_E}{V_W} \quad \text{(S4)}$$

where SA_w is the surface area of open-water (m^2), f_{DW} is the fraction of dissolved component (unitless), v_E is the volatilization mass transfer coefficient ($m\ d^{-1}$), and V_W is the water volume (m^3).

The rate constant for water to sediment diffusion (k_{WS}; d^{-1}) was calculated as (Gobas et al. 2018):

$$k_{WS} = SA_S v_D \frac{f_{DW}}{V_W} \quad \text{(S5)}$$

where SA_S is the surface area of the sediments (m^2), v_D is the sediment-water diffusion mass transfer coefficient ($m\ d^{-1}$), f_{DW} is the fraction of chemical freely dissolved in the water (unitless), and V_W is the water volume. The reaction/transformation rate constant, (k_{WR}; d^{-1}), was estimated using the BIOHCWin program (Howard et al., 2005) given in EPISuite (US EPA 2012)

The rate constant for water to oil diffusion (k_{WO}; d^{-1}) was estimated from $k_{i,OW}$ as:

$$k_{WO} = \frac{k_{i,ow} V_O}{K_{i,WO} V_W} \quad \text{(S6)}$$

where k_{OW} (d^{-1}) is the dissolution rate constant (d^{-1}), V_O is the volume of spilled diluted bitumen (m^3), $K_{i,WO}$ is the water-oil partition coefficient (unitless; Equation 8), and V_W is the water volume (m^3).

Finally, any loss of chemical from the limnocorrals due to leaks was accounted for from estimated water residence times which were determined by spiking each

limnocorral with tritiated water at the beginning of the experiment and tracking the change in tritium concentration over time (Rodriguez-Gil et al., 2021).

The model assumes an instantaneous release of diluted bitumen onto the water's surface of the limnocorrals forming a uniform, well-mixed layer of dilbit. The surface areas of the individual slicks were assumed to be equal to the average surface area measured over the first 4 days of the experiment.

1.3.5 Derivation of elimination rate constants for BTEX in water

Table S6. 4. Compound specific chemical properties and calculated input parameters included in the mass transfer model

Parameter	Symbol	Benzene	Toluene	Ethylbenzene	*o,m,p*-xylenes[a]	Equation/Source/Reference
Molecular Weight ($g\ mol^{-1}$)	MW	78.112	92.139	106.165	106.165	(Mackay et al., 2006)
Water Solubility ($mg\ L^{-1}$)	C^{sat}	1780	531	161	183	(Lide, 2004)
Henry's Law Constant ($Pa\ m^3\ mol^{-1}$)	H	557	660	843	657	(Lide, 2004)
Liquid vapor pressure at 20ºC (Pa)	P^L		2930	930	780	(Van Agteren et al., 1998)
Enthalpy of vaporization at 25ºC ($kJ\ mol^{-1}$)	ΔH_{vap}	33.843	37.99	42.25	42.79	(Mackay et al., 2006)
Octanol – water partition coefficient (unitless)	Log K_{OW}	2.13	2.73	3.15	3.16	(Lide, 2004)
Organic carbon – water partition coefficient ($L\ KgOC^{-1}$)	K_{OC}	59	182	363	386	$K_{OC} = 0.35*K_{OW}$
Air – water partition coefficient (unitless)	K_{AW}	0.2256	0.2754	0.3592	0.2455	$K_{AW} = H/(8.314*[273+T_W])$
Diffusivity in air at 25ºC and 1 atm ($cm^2\ d^{-1}$)	D_{air}	334.8	298.44	272.16	272.16	(EPA, 2016)
Diffusivity in water at 25ºC and 1 atm ($cm^2\ d^{-1}$)	D_{water}	0.03708	0.03276	0.029628	0.029628	(EPA, 2016)
Fraction of freely dissolved chemical in water (unitless)	f_{DW}	1	1	1	1	$f_{DW} =1/(1+(C_{POC}*0.35*OC_{PW}*K_{OC}/d_{PW})$
Fraction of free chemical in sediment (unitless)	f_{DS}	0.9698	0.8983	0.7623	0.7363	$f_{DS} =1/(1+(C_{POC}*0.35*OC_{PW}*K_{OC}/d_{PW})$
Air-oil partition coefficient (unitless)	K_{AO}	0.0009	0.0003	0.0001	0.0001	$K_{AO} = P^L*V_{oil}/RT$
Water-oil partition coefficient (unitless)	K_{WO}	0.0047	0.0012	0.0003	0.0004	$K_{WO} = V_{oil}*C^{sat}$
Liquid density at 20ºC ($g\ cm^{-3}$)	ρ^L	0.8765	0.8669	0.8670	0.8752	(Mackay et al., 2006)
Molar volume ($m^3\ mol^{-1}$)	V_i	$8.9x10^{-5}$	$1.1x10^{-3}$	$1.2x10^{-4}$	$1.2x10^{-4}$	$V_i = MW/\rho_i^L$
Molecular radius (m)	r_i	$3.3x10^{10}$	$3.3x10^{10}$	$3.3x10^{10}$	$33.3x10^{10}$	$r_i = (3V_i/4\pi N_a)^{1/3}$

Table S6. 5. Treatment/limnocorral specific environmental inputs used in mass transfer model.

Environmental Inputs	Symbol	1.5 L	2.9L	5.5 L	18 L	42 L	82 L	180 L	Equation/Source/Reference
Water surface area (m^2)	A_W	75	75	75	75	75	75	75	Measured
Water volume (m^3)	V_W	105.9	99.9	95.5	109.0	108.6	99.5	105.9	(Rodriguez-Gil et al. In Prep)
Dilbit Volume (m^3)	V_o	0.0015	0.0029	0.0055	0.018	0.042	0.082	0.0015	Measured
Slick surface Area (m^2)	A_o	2	6	13	8	19	22	53	Measured
Slick thickness (m)	δ_{Oil}	0.00075	0.00048	0.00042	0.00225	0.0022	0.0037	0.0034	$\delta_{Oil} = V_o/A_o$
Water-film thickness (m)	δ_{Water}	0.00068	0.00068	0.00068	0.00068	0.00068	0.00068	0.00068	$\delta_{Water} = v_{E,\ SF6}/D_{SF6}$ (Saunders et al., In Prep)
Air-film thickness (m)	δ_{Air}	0.0068	0.0068	0.0068	0.0068	0.0068	0.0068	0.0068	$\delta_{Air} = 10^* \delta_{Water}$
Molar Volume (L mol^{-1})	V_{Oil}	0.206	0.206	0.206	0.206	0.206	0.206	0.206	$V_{Oil} = \Sigma(M_i^*MW_i)/ \Sigma(M_i^* \rho)$
Volatilization mass transfer coefficient (m d^{-1})	v_E	0.0091	0.0062	0.0060	0.0068	0.0036	0.0062	0.0031	(Saunders et al. In Prep)
Sediment-water diffusion mass transfer coefficient (m d^{-1})	v_d	0.0096	0.0096	0.0096	0.0096	0.0096	0.0096	0.0096	(Gobas et al. 2018)
Water temperature (ºC)	T_W	24	24	24	24	24	24	24	Measured
Air temperature (ºC)	T_A	21	21	21	21	21	21	21	Measured
Concentration of DOC in water (kg L^{-1})	C_{DOC}	$5.1x10^{-6}$	$6.2x10^{-6}$	$4.9x10^{-6}$	$4.9x10^{-6}$	$4.9x10^{-6}$	$4.7x10^{-6}$	$4.7x10^{-6}$	Measured
Concentration of solids in sediment (kg L^{-1})	C_{SS}	1.51	1.51	1.51	1.51	1.51	1.51	1.51	(Gobas et al. 2018)
Density of suspended solids (kg L^{-1})	d_{PW}	2.4	2.4	2.4	2.4	2.4	2.4	2.4	(Gobas et al. 2018)
Density of sediment solids (kg L^{-1})	d_{SS}	2.4	2.4	2.4	2.4	2.4	2.4	2.4	(Gobas et al. 2018)
Organic carbon content of suspended solids (unitless)	OC_{PW}	0.04	0.04	0.04	0.04	0.04	0.04	0.04	(Gobas et al. 2018)
Organic carbon content of bottom sediment (unitless)	OC_{SS}	0.003	0.003	0.003	0.003	0.003	0.003	0.003	Measured
Density of organic carbon (kg L^{-1})	d_{OC}	1	1	1	1	1	1	1	(Gobas et al. 2018)
Sediment surface area (m^2)	A_S	75	75	75	75	75	75	75	Measured
Volume of sediment (m^3)	V_S	3.4	3.4	3.4	3.4	3.4	3.4	3.4	Measured

Table S6. 6. Equations and variables used to calculate rate constants and condition in which ordinary differential equations were integrated

Rate Constants	**Equation/Variable/Source**
Oil-to-water transfer (k_{OW}; d^{-1})	$K_{OT} = k_{OW} + k_{OE}$
Evaporation from oil (k_{OE}; d^{-1})	$k_{OW} = ([D_{water}*K_{WO}]/[\delta_{oil}* \delta_{water}])$[a]
Total elimination from oil (k_{OT}; d^{-1})	$K_{OE} = ([D_{air}*K_{AO}]/[\delta_{oil}* \delta_{air}])$[b]
Evaporation from water (k_{WE}; d^{-1})	$k_{WE} = ([SA_W*f_{DW}*v_e]/V_W)$[c]
Reabsorption in oil (k_{WO}; d^{-1})	$k_{WO} = (k_{OW}*V_o)/(K_{WO}*V_w)$[d]
Reaction (k_{WR}; d^{-1})	BIOHCWin (Howard et al., 2005) in EPISuite (US EPA 2012)
Diffusion to sediments (k_{WS}; d^{-1})	$k_{WS} = A_S*v_d*(f_{DW}/V_w)$
Water leakage (k_{WL}; d^{-1})	*(Rodriguez-Gil et al. In Prep)*
Total elimination from water (k_{WT}; d^{-1})	$K_{WT} = k_{WE} + k_{WO} + k_{WR} + k_{WS} + k_{WL}$
Integration	**Equation**
Change in chemical mass in dilbit that occurs over the time step dt.	dM_O
Change in chemical mass in water that occurs over the time step dt.	dM_W
Mass (g) of chemical *i* in oil at the previous time step (t – dt)	$M_{i,O}$ (t-1)
Mass (g) of chemical *i* in water at the previous time step (t – dt)	$M_{i,W}$ (t-1)
Time range (d)	0 to 4
Number of timepoints	1000
Time step (s)	345
Mass (g) of chemical *i* in oil at time *t*	$M_{i,O}$ (t) = $M_{i,O}$ (t-1)+ dM_O
Mass (g) of chemical *i* in water at time *t*	$M_{i,W}$ (t) = $M_{i,W}$ (t-1)+ dM_W

Table S6. 7. Oil slick thickness sensitivity analysis parameters

Treatment	Dilbit volume (m^3) at *t*=0	Average slick area (m^2) measured over 4 d	Base Model δ_{oil} values (m)	Lower limit (δ_{oil}/10, m) +% variation from base model	Upper limit (δ_{oil} ∗10, m) -% variation from base model
1.5 L	0.0015	2	0.00075	0.000075 (+90%)	0.0075 (-90%)
2.9 L	0.0029	6	0.00048	0.000048 (+90%)	0.0048 (-90%)
5.5 L	0.0055	13	0.00042	0.000042 (+90%)	0.0042 (-90%)
18 L	0.018	8	0.00225	0.000225 (+90%)	0.0225 (-90%)
42 L	0.042	19	0.0022	0.00022 (+90%)	0.022 (-90%)
82 L	0.082	22	0.0037	0.00037 (+90%)	0.037 (-90%)
180 L	0.18	53	0.0034	0.00034 (+90%)	0.34 -90%)

2. Supporting Results

2.1 Time Series BTEX Analysis

Table S6. 8. Raw time series water column concentrations of BTEX compounds. Values of 0 represent occurrences where concentrations were below MDL

Limnocorral	Time (h)	Benzene (μg/L)	Toluene (μg/L)	Ethylbenzene (μg/L)	*o,m,p*-Xylenes (μg/L)
180 L	0	0	0	0	0
	1	0.56	0.43	0	0.07
	6	1.52	1.31	0	0.26
	10	15.39	13.84	0.36	3.36
	24	49.36	45.13	2.02	11.2
	48	54.06	20.59	0.18	0
	96	45.85	3.31	0	0
82 L	0	0	0	0	0
	1	0.17	0.12	0	0
	6	0.59	0.46	0	0
	10	39.59	36.65	1.24	11.04
	24	19.45	18.72	0.78	6.35
	48	24.8	22.93	0.63	2.46
	96	11.68	0	0	0
42 L	0	0	0	0	0
	1	0.59	0.48	0	0.07
	6	1.84	1.21	0	0.27
	10	18.65	17.36	0.61	7.03
	24	11.29	11.19	0.49	4.29
	48	11.75	9.55	0.18	0.7
	96	1.34	0	0	0
18 L	0	0	0	0	0
	1	0	0	0	0
	6	0.5	0.37	0	0.07
	10	9.58	7.19	0.22	3.25
	24	3.46	2.96	0.09	1.68
	48	1.35	0	0	0.08
	96	0.34	0	0	0
5.5 L	0	0	0	0	0
	1	0.13	0.18	0	0
	6	0.49	0.58	0	0.33
	10	2.82	2.21	0	0.85
	24	1.63	0.2	0	0.79
	48	0.79	0	0	0.13
	96	0	0	0	0
2.9 L	0	0	0	0	0
	1	0.9	0.42	0	0.08
	6	0.76	0.22	0	0.08
	10	1.13	0.33	0	0.36
	24	0.22	0	0	0
	48	0.13	0	0	0
	96	0.09	0	0	0
1.5 L	0	0	0	0	0
	1	0	0	0	0
	6	0.77	0.81	0	0.25
	10	0.79	0.75	0	0.28
	24	0.34	0.56	0	0.24
	48	0.31	0.41	0	0.15
	96	0.18	0	0	0

[α]Values reported as zero (0) represent non-detects (concentrations below MDLs) (Table S6.2)

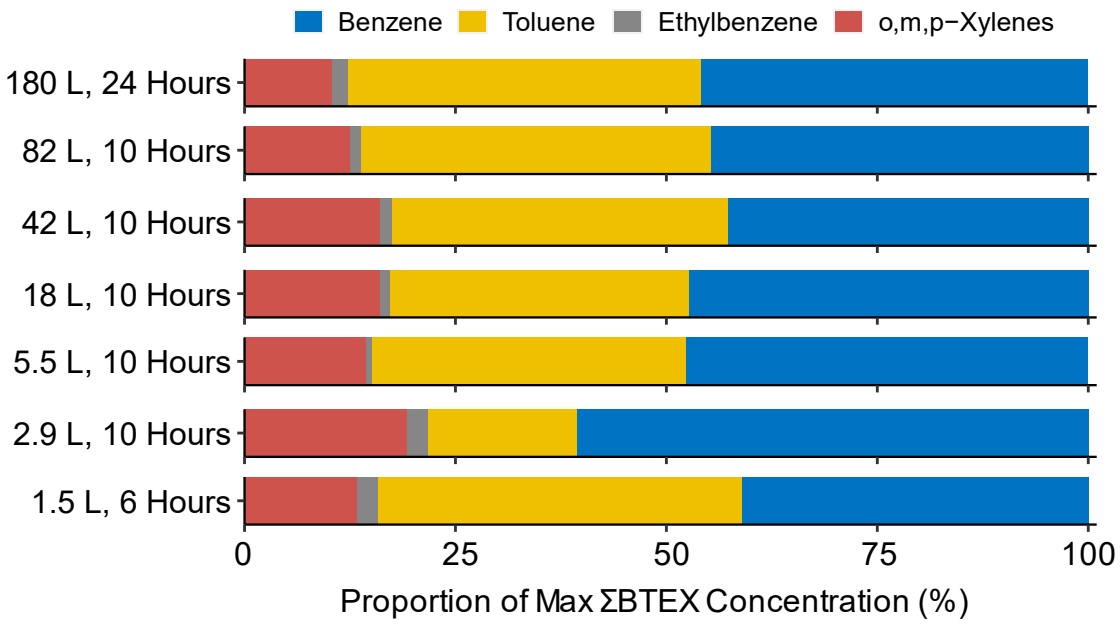

Figure S6. 3. The proportion of each individual BTEX compound that makes up the maximum ΣBTEX concentration observed in each treatment. The y-axis represents each treatment and the timepoint in which the maximum ΣBTEX concentration was observed during the study.

2.2 Regression Analysis

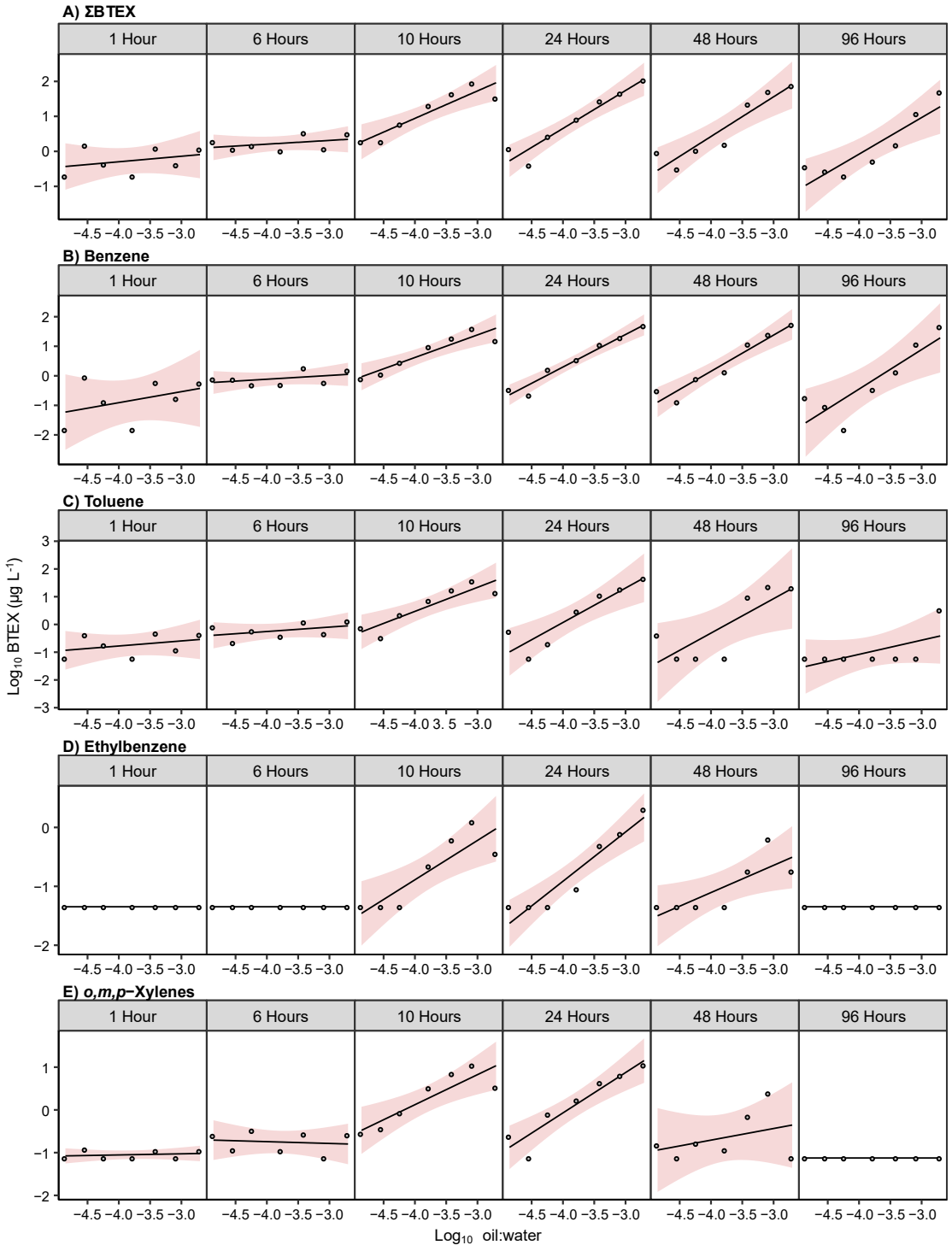

Figure S6. 4. Individual linear regressions of log transformed BTEX in the water column against log transformed oil:water (v/v) ratios.

Table S6. 9. Coefficients and significance of regressions in Figure S6.2.
$Log_{10}[C] = m*log_{10}[oil:water] + b$

Time	Compound	m	b	R^2	*p*	Sig
1 Hour	BTEX	0.16	0.33	0.11	0.47	No
6 Hours		0.11	0.63	0.16	0.38	No
10 Hours		0.78	4.08	0.84	0.003	Yes
24 Hours		1.08	4.99	0.92	0.001	Yes
48 Hours		1.13	4.96	0.87	0.002	Yes
96 Hours		1.04	4.10	0.81	0.01	Yes
1 Hour	Benzene	0.37	0.58	0.16	0.38	No
6 Hours		0.13	0.39	0.19	0.33	No
10 Hours		0.77	3.68	0.86	0.003	Yes
24 Hours		1.10	4.70	0.96	0.0001	Yes
48 Hours		1.23	5.06	0.93	0.0005	Yes
96 Hours		1.34	4.90	0.75	0.01	Yes
1 Hour	Toluene	0.18	-0.05	0.13	0.43	No
6 Hours		0.16	0.38	0.20	0.32	No
10 Hours		0.87	3.93	0.81	0.01	Yes
24 Hours		1.24	5.04	0.82	0.005	Yes
48 Hours		1.24	4.65	0.63	0.03	Yes
96 Hours		0.51	0.97	0.37	0.14	No
1 Hour	Ethylbenzene	0.00	-1.35	0.52	0.14	No
6 Hours		0.00	-1.35	0.52	0.14	No
10 Hours		0.67	1.79	0.77	0.01	Yes
24 Hours		0.84	2.43	0.91	0.001	Yes
48 Hours		0.46	0.74	0.64	0.03	Yes
96 Hours		0.00	-1.35	0.52	0.14	No
1 Hour	*o,m,p*-Xylenes	0.03	-0.95	0.05	0.65	No
6 Hours		-0.04	-0.91	0.02	0.77	No
10 Hours		0.70	2.9	0.78	0.0084	Yes
24 Hours		0.94	3.7	0.88	0.0017	Yes
48 Hours		0.27	0.38	0.14	0.40	No
96 Hours		NA	-1.1	NA	NA	NA

Table S6. 10. Comparison between the present study and other tank studies using dilbit blends under various conditions and oil:water ratios

Dilbit Type	Oil:Water (v/v)	Initial slick thickness (mm)[a]	Conditions	Max ΣBTEX (μg L^{-1})	T_{max}	Reference
CLWB	1:500 1:1200 1:2500 1:5900 1:17000 1:34000 1:71000	2.5 1.1 0.6 0.3 0.08 0.04 0.02	Summer	108 89 44 20 6 1.9 1.9	1 d 10 h 10 h 10 h 10 h 10 h 6 h	Present Study
CLWB AWB	1:446 1:118 1:118 1:180 1:180 1:180	11.71 10.1 10.1 10.68 10.80 10.68	Static[b] Mild[c] Moderate[d] Static Mild Moderate	900 1200 3000 924 1500 1700	6 d 2 d 4 h 8 d 2 d 4 h	(Witt O'Briens et al., 2013)
AWB WCS Synbit	1:5000 1:5000 1:5000	~1.1 ~1.1 ~1.1	Spring Summer Spring Summer Spring Summer	~100 ~100 ~60 ~20 ~20 ~20	2 d 1 d 2 d 8 h 1 d 8 h	(King et al., 2019)
AWB WCS Synbit	1:8600 1:8600 1:8600	~0.03 ~0.03 ~0.03	Spring Summer Autumn Spring Summer Autumn Spring Summer Autumn	64 39 41 20 11 16 10 2 5	1 d 1 d 1 d 1 d 1 d 1 d 1 d 1 d 1 d	(Ortmann et al., 2020)

[a]Slick thickness values were provided by Witt Obrien's et al. (2013), otherwise they were estimated based on the volume of dilbit added, and the dimensions of the test tank/enclosure (0.011m^2 x 21 rings = 0.23m^2 for King et al. (2019) and 1.25m x 0.97x = 1.2m^2 for Ortmann et al. (2020))
[b]Static- no agitation
[c]Mild- average wavelets height of approximately 2 – 4 cm and average wind speed of 2.23 m/s
[d]Moderate- average wavelets height of approximately 5 – 7 cm and average wind speed of 4.5 m/s

2.3 Mass Transfer Model

Table S6. 11. Rate constants for individual BTEX components used in the mass transfer model

180 L Treatment					
Rate constants	**Benzene**	**Toluene**	**Ethylbenzene**	***o,m,p*-Xylenes**	**Equation/Reference**
DILBIT SLICK					
Oil-to-water transfer (k_{OW}; 1/d)	0.221	0.048	0.011	0.015	$k_{OW} = ([D_{water}*K_{WO}]/[\delta_{oil}* \delta_{water}])$
Evaporation from oil (k_{OE}; 1/d)	28.856	7.582	2.259	2.048	$k_{OE} = ([D_{air}*K_{AO}]/[\delta_{oil}* \delta_{air}])$
Total elimination from oil (k_{OT}; 1/d)	29.076	7.630	2.270	0.031	$k_{OT} = k_{OW} + k_{OE}$
WATER COLUMN					
Evaporation from water (k_{WE}; 1/d)	0.006	0.006	0.006	0.006	$k_{WE} = ([SA_W*f_{DW}*v_e]/V_W)$
Reabsorption in oil (k_{WO}; 1/d)	0.093	0.082	0.075	0.075	$k_{WO} = (k_{OW}*V_o)/(K_{WO}*V_w)$
Reaction (k_{WR}; 1/d)	0.152	0.154	0.139	0.156	EPIsuite
Diffusion to sediments (k_{WS}; 1/d)	0.007	0.007	0.007	0.007	$k_{WS} = A_S*v_d*(f_{DW}/V_w)$
Water leakage (k_{WL}; 1/d)	0.005	0.005	0.005	0.005	*(Rodriguez-Gil et al. In Prep)*
Total elimination from water (k_{WT}; 1/d)	0.263	0.254	0.231	0.248	$K_{WT} = k_{WE} + k_{WO} + k_{WR} + k_{WS} + k_{WL}$
82 L Treatment					
Rate constants	**Benzene**	**Toluene**	**Ethylbenzene**	***o,m,p*-Xylenes**	**Equation/Reference**
DILBIT SLICK					
Oil-to-water transfer (k_{OW}; 1/d)	0.203	0.044	0.010	0.014	$k_{OW} = ([D_{water}*K_{WO}]/[\delta_{oil}* \delta_{water}])$
Evaporation from oil (k_{OE}; 1/d)	26.516	6.967	2.076	1.882	$k_{OE} = ([D_{air}*K_{AO}]/[\delta_{oil}* \delta_{air}])$
Total elimination from oil (k_{OT}; 1/d)	26.719	7.011	2.086	0.028	$k_{OT} = k_{OW} + k_{OE}$
WATER COLUMN					
Evaporation from water (k_{WE}; 1/d)	0.005	0.005	0.005	0.005	$k_{WE} = ([SA_W*f_{DW}*v_e]/V_W)$
Reabsorption in oil (k_{WO}; 1/d)	0.036	0.032	0.029	0.029	$k_{WO} = (k_{OW}*V_o)/(K_{WO}*V_w)$

Reaction (k_{WR}; 1/d)	0.152	0.154	0.139	0.156	EPIsuite
Diffusion to sediments (k_{WS}; 1/d)	0.007	0.007	0.007	0.007	$k_{WS} = A_S * v_d * (f_{DW}/V_w)$
Water leakage (k_{WL}; 1/d)	0.005	0.005	0.005	0.005	*(Rodriguez-Gil et al. In Prep)*
Total elimination from water (k_{WT}; 1/d)	0.206	0.204	0.185	0.202	$K_{WT} = k_{WE} + k_{WO} + k_{WR} + k_{WS} + k_{WL}$
42 L Treatment					
Rate constants	**Benzene**	**Toluene**	**Ethylbenzene**	***o,m,p*-Xylenes**	**Equation/Reference**
DILBIT SLICK					
Oil-to-water transfer (k_{OW}; 1/d)	0.341	0.074	0.017	0.024	$k_{OW} = ([D_{water} * K_{WO}]/[\delta_{oil} * \delta_{water}])$
Evaporation from oil (k_{OE}; 1/d)	44.595	11.717	3.491	3.166	$k_{OE} = ([D_{air} * K_{AO}]/[\delta_{oil} * \delta_{air}])$
Total elimination from oil (k_{OT}; 1/d)	44.936	11.791	3.508	0.047	$k_{OT} = k_{OW} + k_{OE}$
WATER COLUMN					
Evaporation from water (k_{WE}; 1/d)	0.005	0.005	0.005	0.005	$k_{WE} = ([SA_W * f_{DW} * v_e]/V_W)$
Reabsorption in oil (k_{WO}; 1/d)	0.029	0.025	0.023	0.023	$k_{WO} = (k_{OW} * V_o)/(K_{WO} * V_w)$
Reaction (k_{WR}; 1/d)	0.152	0.154	0.139	0.156	EPIsuite
Diffusion to sediments (k_{WS}; 1/d)	0.008	0.008	0.008	0.008	$k_{WS} = A_S * v_d * (f_{DW}/V_w)$
Water leakage (k_{WL}; 1/d)	0.004	0.004	0.004	0.004	*(Rodriguez-Gil et al. In Prep)*
Total elimination from water (k_{WT}; 1/d)	0.197	0.196	0.178	0.195	$K_{WT} = k_{WE} + k_{WO} + k_{WR} + k_{WS} + k_{WL}$
18 L Treatment					
Rate constants	**Benzene**	**Toluene**	**Ethylbenzene**	***o,m,p*-Xylenes**	**Equation/Reference**
DILBIT SLICK					
Oil-to-water transfer (k_{OW}; 1/d)	3.336	0.726	0.168	0.231	$k_{OW} = ([D_{water} * K_{WO}]/[\delta_{oil} * \delta_{water}])$
Evaporation from oil (k_{OE}; 1/d)	436.041	114.567	34.133	30.955	$k_{OE} = ([D_{air} * K_{AO}]/[\delta_{oil} * \delta_{air}])$
Total elimination from oil (k_{OT}; 1/d)	439.377	115.293	34.301	0.461	$k_{OT} = k_{OW} + k_{OE}$
WATER COLUMN					
Evaporation from water (k_{WE}; 1/d)	0.005	0.005	0.005	0.005	$k_{WE} = ([SA_W * f_{DW} * v_e]/V_W)^c$

Reabsorption in oil (k_{WO}; 1/d)	0.120	0.106	0.096	0.096	$k_{WO} = (k_{OW}*V_o)/(K_{WO}*V_w)$
Reaction (k_{WR}; 1/d)	0.152	0.154	0.139	0.156	EPIsuite
Diffusion to sediments (k_{WS}; 1/d)	0.007	0.007	0.007	0.007	$k_{WS} = A_S*v_d*(f_{DW}/V_w)$
Water leakage (k_{WL}; 1/d)	0.035	0.035	0.035	0.035	*(Rodriguez-Gil et al. In Prep)*
Total elimination from water (k_{WT}; 1/d)	0.318	0.306	0.281	0.298	$K_{WT} = k_{WE} + k_{WO} + k_{WR} + k_{WS} + k_{WL}$
5.5 L Treatment					
Rate constants	**Benzene**	**Toluene**	**Ethylbenzene**	***o,m,p*-Xylenes**	**Equation/Reference**
Oil-to-water transfer (k_{OW}; 1/d)	1.787	0.389	0.090	0.123	$k_{OW} = ([D_{water}*K_{WO}]/[\delta_{oil}* \delta_{water}])$
Evaporation from oil (k_{OE}; 1/d)	233.593	61.375	18.286	16.583	$k_{OE} = ([D_{air}*K_{AO}]/[\delta_{oil}* \delta_{air}])$
Total elimination from oil (k_{OT}; 1/d)	235.381	61.764	18.376	0.247	$k_{OT} = k_{OW} + k_{OE}$
WATER COLUMN					
Evaporation from water (k_{WE}; 1/d)	0.002	0.002	0.002	0.002	$k_{WE} = ([SA_W*f_{DW}*v_e]/V_W)$
Reabsorption in oil (k_{WO}; 1/d)	0.022	0.020	0.018	0.018	$k_{WO} = (k_{OW}*V_o)/(K_{WO}*V_w)$
Reaction (k_{WR}; 1/d)	0.152	0.154	0.139	0.156	EPIsuite
Diffusion to sediments (k_{WS}; 1/d)	0.007	0.007	0.007	0.007	$k_{WS} = A_S*v_d*(f_{DW}/V_w)$
Water leakage (k_{WL}; 1/d)	0.004	0.004	0.004	0.004	*(Rodriguez-Gil et al. In Prep)*
Total elimination from water (k_{WT}; 1/d)	0.187	0.187	0.170	0.187	$K_{WT} = k_{WE} + k_{WO} + k_{WR} + k_{WS} + k_{WL}$
2.9 L Treatment					
Rate constants	**Benzene**	**Toluene**	**Ethylbenzene**	***o,m,p*-Xylenes**	**Equation/Reference**
DILBIT SLICK					
Oil-to-water transfer (k_{OW}; 1/d)	1.564	0.340	0.079	0.108	$k_{OW} = ([D_{water}*K_{WO}]/[\delta_{oil}* \delta_{water}])$
Evaporation from oil (k_{OE}; 1/d)	204.394	53.703	16.000	14.510	$k_{OE} = ([D_{air}*K_{AO}]/[\delta_{oil}* \delta_{air}])$
Total elimination from oil (k_{OT}; 1/d)	205.958	54.044	16.079	0.216	$k_{OT} = k_{OW} + k_{OE}$
WATER COLUMN					

Evaporation from water (k_{WE}; 1/d)	0.005	0.005	0.005	0.005	$k_{WE} = ([SA_W * f_{DW} * v_e]/V_W)$
Reabsorption in oil (k_{WO}; 1/d)	0.010	0.009	0.008	0.008	$k_{WO} = (k_{OW} * V_o)/(K_{WO} * V_w)$
Reaction (k_{WR}; 1/d)	0.152	0.154	0.139	0.156	EPIsuite
Diffusion to sediments (k_{WS}; 1/d)	0.007	0.007	0.007	0.007	$k_{WS} = A_S * v_d * (f_{DW}/V_w)$
Water leakage (k_{WL}; 1/d)	0.016	0.016	0.016	0.016	*(Rodriguez-Gil et al. In Prep)*
Total elimination from water (k_{WT}; 1/d)	0.190	0.191	0.175	0.192	$K_{WT} = k_{WE} + k_{WO} + k_{WR} + k_{WS} + k_{WL}$
1.5 L Treatment					
Rate constants	**Benzene**	**Toluene**	**Ethylbenzene**	***o,m,p*-Xylenes**	**Equation/Reference**
DILBIT SLICK					
Oil-to-water transfer (k_{OW}; 1/d)	1.001	0.218	0.050	0.069	$k_{OW} = ([D_{water} * K_{WO}]/[\delta_{oil} * \delta_{water}])$
Evaporation from oil (k_{OE}; 1/d)	130.812	34.370	10.240	9.286	$k_{OE} = ([D_{air} * K_{AO}]/[\delta_{oil} * \delta_{air}])$
Total elimination from oil (k_{OT}; 1/d)	131.813	34.588	10.290	0.138	$k_{OT} = k_{OW} + k_{OE}$
WATER COLUMN					
Evaporation from water (k_{WE}; 1/d)	0.002	0.002	0.002	0.002	$k_{WE} = ([SA_W * f_{DW} * v_e]/V_W)$
Reabsorption in oil (k_{WO}; 1/d)	0.003	0.003	0.002	0.002	$k_{WO} = (k_{OW} * V_o)/(K_{WO} * V_w)$
Reaction (k_{WR}; 1/d)	0.152	0.154	0.139	0.156	EPIsuite
Diffusion to sediments (k_{WS}; 1/d)	0.008	0.008	0.008	0.008	$k_{WS} = A_S * v_d * (f_{DW}/V_w)$
Water leakage (k_{WL}; 1/d)	0.003	0.003	0.003	0.003	*(Rodriguez-Gil et al. In Prep)*
Total elimination from water (k_{WT}; 1/d)	0.169	0.170	0.155	0.172	$K_{WT} = k_{WE} + k_{WO} + k_{WR} + k_{WS} + k_{WL}$

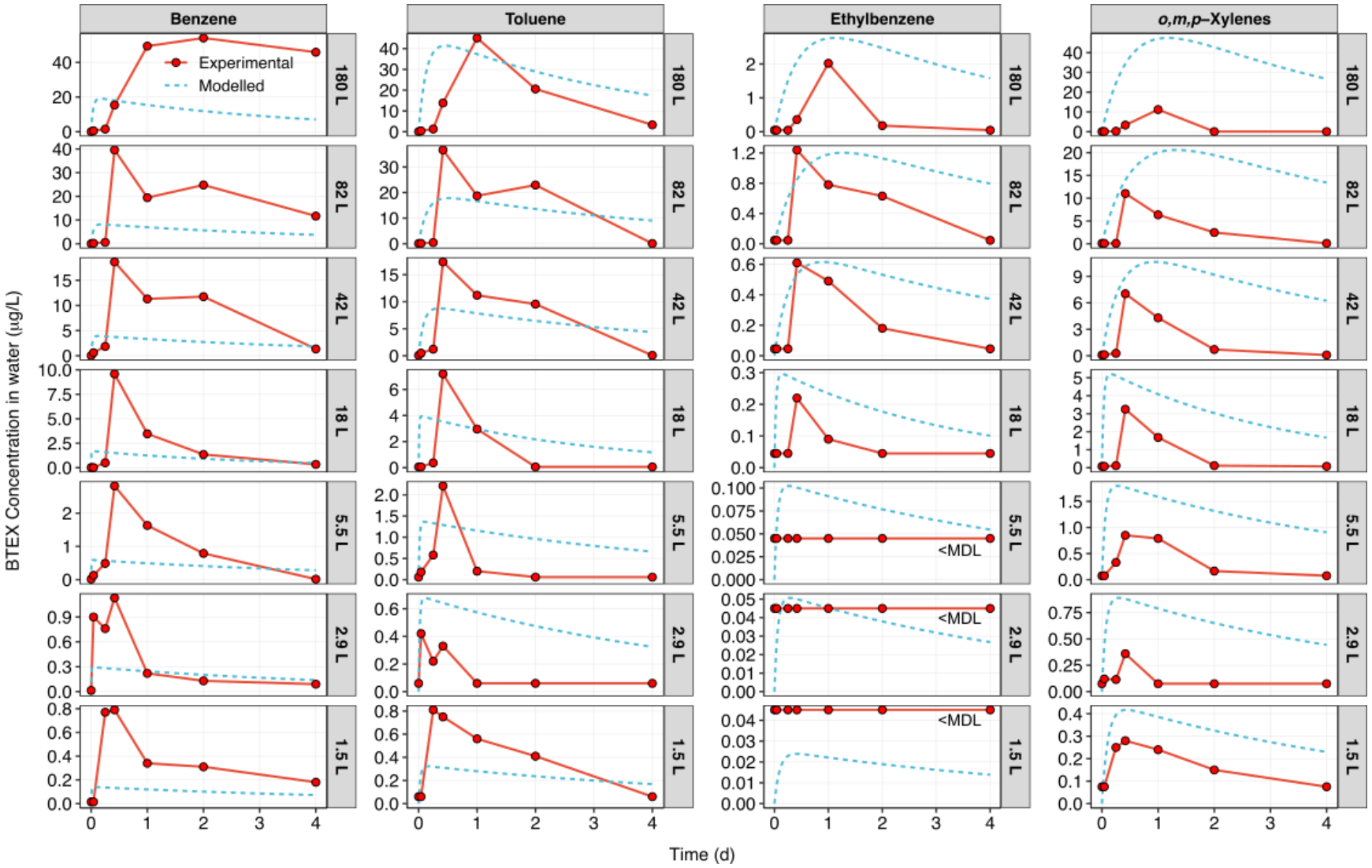

Figure S6. 5. Predicted and observed water column concentrations of benzene, toluene, ethylbenzene, and *o,m,p*-xylenes over time in each treatment. Observed ethylbenzene concentrations were below MDL in the 5.5, 2.9, and 1.5 L treatments and were replaced by the respective MDL value divided by 2.

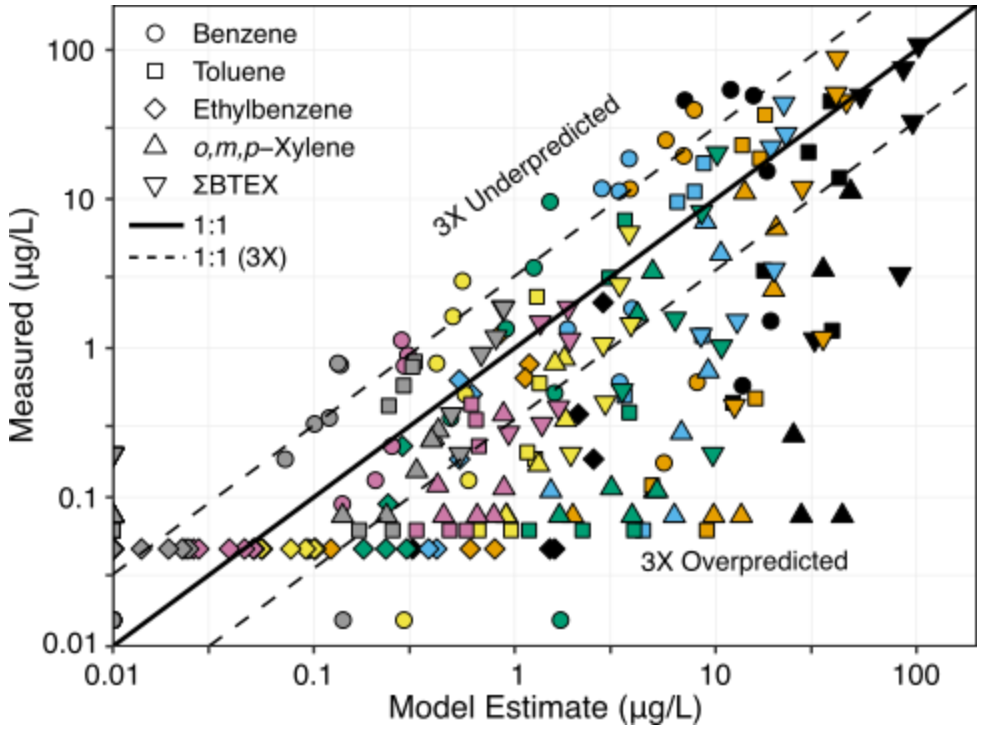

Figure S6. 6. Relationship between the measured and model estimated concentrations of individual BTEX compounds and ΣBTEX measured over time in each treatment. 180 L treatment = black; 82 L treatment = orange; 42 L treatment = blue; 18 L treatment = green; 5.5 L treatment = yellow; 2.9 L treatment = pink; and 1.5 L treatment = gray.

Table S6. 12. Mean model bias (MB) and 95% confidence intervals for each BTEX compound and ΣBTEX

Treatment	Benzene	Toluene	Ethylbenzene	*o,m,p*-Xylenes	ΣBTEX
180 L	1.2 (-5.7 - 8.2)	5.0 (1.4 - 8.5)	9.8 (7.0 - 12.5)	57.7 (52.2 - 63.2)	3.7 (-0.3 - 7.6)
82 L	1.1 (-6.7 - 9.0)	6.1 (-4.1 - 16.3)	3.3 (0.4 - 6.1)	16.4 (10.4 - 22.3)	3.0 (-2.1 - 8.1)
42 L	0.8 (-2.4 - 4.0)	3.1 (-2.6 - 8.8)	2.8 (0.7 - 4.9)	10.3 (6.6 - 14)	2.2 (-0.6 - 5.1)
18 L	1.6 (-6.5 - 9.8)	7.8 (2.0 - 13.6)	3.1 (1.7 - 4.6)	13.1 (9.4 - 16.8)	4.4 (0.2 - 8.6)
5.5 L	1.2 (-3.4 - 5.8)	4.6 (1.9 - 7.3)	1.7 (0.7 - 2.8)	5.5 (3.7 - 7.3)	2.6 (0.4 - 4.9)
2.9 L	0.7 (-1.2 - 2.5)	3.9 (2.2 - 5.6)	0.8 (-0.2 - 1.9)	5.7 (4.3 - 7.1)	2.1 (0.5 - 3.8)
1.5 L	0.5 (-3.1 - 4.1)	0.9 (-1.4 - 3.2)	0.4 (-0.8 - 1.6)	1.9 (0.8 - 2.9)	0.9 (-0.7 - 2.5)

Table S6. 13. Sensitivity (S) of state variables on the maximum ΣBTEX concentration in the water column.

Parameter	Variation Applied	Sensitivity (*S*)						
		180 L	**82 L**	**42 L**	**18 L**	**5.5 L**	**2.9 L**	**1.5 L**
Oil slick thickness (δ_{oil})	+ 10%	-0.1	-0.03	-0.09	-0.04	-0.05	-0.02	-0.12
	- 10%	-0.11	-0.03	-0.1	-0.04	-0.05	-0.02	-0.13
Water-film thickness (δ_{water})	+ 10%	-0.86	-0.9	-0.89	-0.9	-0.9	-0.89	-0.8
	- 10%	-1.04	-1.1	-1.09	-1.1	-1.1	-1.09	-1.08
Air-film thickness (δ_{air})	+ 10%	0.83	0.95	0.88	0.95	0.94	0.96	0.84
	- 10%	0.85	0.96	0.89	0.96	0.95	0.96	0.86
Oil Temperature (T_o)	+ 10%	-1.61	-1.82	-1.7	-1.82	-1.8	-1.83	-1.63
	- 10%	0.06	0.09	0.07	0.09	0.08	0.09	0.06
Oil Density (ρ_o)	+ 10%	-0.15	-0.04	-0.11	-0.04	-0.05	-0.03	-0.14
	- 10%	-0.16	-0.04	-0.11	-0.04	-0.05	-0.03	-0.15
Diffusivity in air ($D_{i,air}$)	+ 10%	-0.77	-0.87	-0.81	-0.87	-0.86	-0.88	-0.78
	- 10%	-0.92	-1.06	-0.97	-1.05	-1.04	-1.06	-0.93
Diffusivity in water ($D_{i,water}$)	+ 10%	0.94	0.99	0.98	0.99	0.99	0.98	0.97
	- 10%	0.95	0.99	0.98	0.99	0.99	0.98	0.97
Molar Volume (V_{oil})	+ 10%	0.15	0.03	0.1	0.04	0.05	0.03	0.14
	- 10%	0.17	0.04	0.12	0.04	0.06	0.04	0.16
Saturation Concentration (C_i^{SAT})	+ 10%	0.99	0.99	0.99	0.99	0.99	0.99	0.99
	- 10%	0.99	0.99	0.99	0.99	0.99	0.99	0.99
Vapor Pressure (P_i^L)	+ 10%	-0.77	-0.87	-0.81	-0.87	-0.86	-0.88	-0.78
	- 10%	-0.92	-1.06	-0.97	-1.05	-1.04	-1.06	-0.93

Table S6. 14. The resulting change in maximum ΣBTEX concentration in the water column that result from changing the value of the state variables by +/- 10%.

Parameter	Variation Applied	% change in max ΣBTEX predicted in Water Column						
		180 L	82 L	42 L	18 L	5.5 L	2.9 L	1.5 L
Oil slick thickness (δ_{oil})	+ 10%	-1.04	-1.21	-0.94	-0.22	-0.32	-0.39	-0.50
	- 10%	1.09	1.28	0.99	0.22	0.33	0.40	0.52
Water-film thickness (δ_{water})	+ 10%	8.27	8.37	8.75	9.56	9.53	9.48	9.37
	- 10%	-8.48	-8.57	-8.92	-9.64	-9.60	-9.56	-9.47
Air-film thickness (δ_{air})	+ 10%	-8.62	-8.85	-8.92	-8.94	-9.00	-9.02	-9.03
	- 10%	10.42	10.76	10.86	10.89	10.98	11.01	11.02
Oil Temperature (T_o)	+ 10%	-16.12	-16.30	-16.97	-18.29	-18.24	-18.16	-17.98
	- 10%	-0.59	-0.62	-0.70	-0.87	-0.86	-0.85	-0.83
Oil Density (ρ_o)	+ 10%	-1.49	-1.40	-1.05	-0.32	-0.35	-0.39	-0.50
	- 10%	1.60	1.50	1.11	0.33	0.37	0.41	0.52
Diffusivity in air ($D_{i,air}$)	+ 10%	-7.70	-7.79	-8.10	-8.76	-8.73	-8.69	-8.60
	- 10%	9.17	9.29	9.72	10.62	10.58	10.53	10.40
Diffusivity in water ($D_{i,water}$)	+ 10%	9.39	9.68	9.78	9.80	9.88	9.91	9.92
	- 10%	-9.49	-9.74	-9.82	-9.84	-9.91	-9.92	-9.93
Molar Volume (V_{oil})	+ 10%	1.48	1.38	1.03	0.31	0.34	0.38	0.48
	- 10%	-1.68	-1.58	-1.19	-0.37	-0.40	-0.45	-0.56
Saturation Concentration (C_i^{SAT})	+ 10%	9.94	9.94	9.93	9.93	9.93	9.93	9.93
	- 10%	-9.95	-9.95	-9.95	-9.94	-9.94	-9.94	-9.94
Vapor Pressure (P_i^L)	+ 10%	-7.70	-7.79	-8.10	-8.76	-8.73	-8.69	-8.60
	- 10%	9.17	9.29	9.72	10.62	10.58	10.53	10.40

Table S6. 15. Sensitivity (S) of oil slick thickness on the maximum ΣBTEX concentration in the water column.

Parameter	Variation Applied	Sensitivity (*S*)						
		180 L	82 L	42 L	18 L	5.5 L	2.9 L	1.5 L
Oil slick thickness (δ_{oil})	+ 90%	0.42	0.45	0.39	0.51	0.35	0.24	0.28
	- 90%	0.075	0.094	0.040	-0.085	-0.198	-0.054	-0.039

Table S6. 16. The resulting change in maximum ΣBTEX concentration in the water column that result from changing the oil slick thickness by +/- 90%.

Parameter	Variation Applied	% change in max ΣBTEX predicted in Water Column						
		180 L	82 L	42 L	18 L	5.5 L	2.9 L	1.5 L
Oil slick thickness (δ_{oil})	+ 90%	-37.84	-40.31	-34.98	-45.55	-31.73	-21.72	-24.87
	- 90%	6.73	8.45	3.59	-7.67	-17.83	-4.82	-3.47

Supporting References

EPA, 2016. EPA On-line Tools for Site Assessment Calculation. Environmental Protection Agency, Ecosystems Research, Athens, GA.

Gobas, F.A., Lai, H.-F., Mackay, D., Padilla, L.E., Goetz, A., Jackson, S.H., 2018. AGRO-2014: A time dependent model for assessing the fate and food-web bioaccumulation of organic pesticides in farm ponds: Model testing and performance analysis. Science of The Total Environment 639, 1324–1333. https://doi.org/10.1016/j.scitotenv.2018.05.115

Howard, P., Meylan, W., Aronson, D., Stiteler, W., Tunkel, J., Comber, M., Parkerton, T.F., 2005. A new biodegradation prediction model specific to petroleum hydrocarbons. Environmental Toxicology and Chemistry: An International Journal 24, 1847–1860.

King, T.L., Robinson, B., Lee, K., Li, H., Boufadel, M.C., Clyburne, J.A., 2019. Seasonal Effect Data on Monocyclic Aromatics Dissolution from Surface Spills of Bitumen Blends: Implications for Environmental Risk Assessments, in: Proceedings of the Forty-Second AMOP Technical Seminar. Environment and Climate Change Canada, Ottawa, ON, Canada, pp. 773–790.

Lide, D.R., 2004. CRC handbook of chemistry and physics. CRC press.

Mackay, D., Shiu, W.-Y., Ma, K.-C., Lee, S.C., 2006. Handbook of physical-chemical properties and environmental fate for organic chemicals. CRC press.

Ortmann, A.C., Cobanli, S.E., Wohlgeschaffen, G., MacDonald, J., Gladwell, A., Davis, A., Robinson, B., Mason, J., King, T.L., 2020. Measuring the fate of different diluted bitumen products in coastal surface waters. Marine Pollution Bulletin 153, 111003.

Rodriguez-Gil, J.L., Stoyanovich, S., Hanson, M.L., Hollebone, B., Orihel, D.M., Palace, V., Faragher, R., Mirnaghi, F.S., Shah, K., Yang, Z., 2021. Simulating diluted bitumen spills in boreal lake limnocorrals-Part 1: Experimental design and responses of hydrocarbons, metals, and water quality parameters. Science of The Total Environment 148537.

US Environmental Protection Agency, 2012. Estimation Programs Interface Suite for Microsoft Windows, Ver 4.11 [WWW Document]. URL https://www.epa.gov/tsca-screening-tools/epi-suitetm-estimation-program-interface (accessed 4.3.21).

Witt O'Briens, Polaris Applied Sciences, Western Canada Marine Response Corporation, 2013. A study of fate and behavior of diluted bitumen oils in marine waters: Dilbit Experiments, Trans Mountain Pipeline ULC.

REFERENCES

Alava, J.J., Ross, P.S., Lachmuth, C., Ford, J.K., Hickie, B.E., Gobas, F.A., 2012. Habitat-based PCB environmental quality criteria for the protection of endangered killer whales (Orcinus orca). Environmental science & technology 46, 12655–12663.

Arey, J.S., Nelson, R.K., Plata, D.L., Reddy, C.M., 2007a. Disentangling oil weathering using GCxGC. 2. Mass transfer calculations. Environmental science & technology 41, 5747–5755.

Arey, J.S., Nelson, R.K., Reddy, C.M., 2007b. Disentangling oil weathering using GCxGC. 1. Chromatogram analysis. Environmental science & technology 41, 5738–5746.

Black, J.A., Birge, W.J., McDonnell, W.E., Westerman, A.G., Ramey, B.A., Bruser, D.M., 1982. The aquatic toxicity of organic compounds to embryo-larval stages of fish and amphibians.

Chao, X., Shankar, N.J., Cheong, H.F., 2001. Two-and three-dimensional oil spill model for coastal waters. Ocean engineering 28, 1557–1573.

Cohen, Y., Mackay, D., Shiu, W.Y., 1980. Mass transfer rates between oil slicks and water. The Canadian journal of chemical engineering 58, 569–575.

Daling, P.S., StrØm, T., 1999. Weathering of oils at sea: model/field data comparisons. Spill Science & Technology Bulletin 5, 63–74.

Fayemiwo, O.M., Daramola, M.O., Moothi, K., 2017. BTEX compounds in water–future trends and directions for water treatment. Water Sa 43, 602–613.

Fingas, M., 2018. The challenges of remotely measuring oil slick thickness. Remote sensing 10, 319.

Fingas, M., 2015a. Review of The Properties and Behaviour of Diluted Bitumen, in: Proceeding of the 39th Arctic and Marine Oil-Spill Program Technical Seminar. Environment and Climate Change Canada, Vancouver, B.C., Canada, pp. 470–494.

Fingas, M., 2015b. Oil and Petroleum Evaporation, in: Handbook of Oil Spill Science and Technology. Wiley Online Library, pp. 205–223.

Fingas, M., Fieldhouse, B., 2004. Formation of water-in-oil emulsions and application to oil spill modelling. Journal of Hazardous Materials 107, 37–50. http://dx.doi.org/10.1016/j.jhazmat.2003.11.008

Fingas, M.F., 1997. Studies on the evaporation of crude oil and petroleum products: I. The relationship between evaporation rate and time. Journal of hazardous materials 56, 227–236.

Fingas, M.F., Fieldhouse, B., Mullin, J., 1996. Studies of water-in-oil emulsions: The role of asphaltenes and resins, in: ARCTIC AND MARINE OILSPILL PROGRAM TECHNICAL SEMINAR. MINISTRY OF SUPPLY AND SERVICES, CANADA, pp. 73–88.

Gobas, F.A., Arnot, J.A., 2010. Food web bioaccumulation model for polychlorinated biphenyls in San Francisco Bay, California, USA. Environmental Toxicology and Chemistry 29, 1385–1395.

Gobas, F.A., Lai, H.-F., Mackay, D., Padilla, L.E., Goetz, A., Jackson, S.H., 2018. AGRO-2014: A time dependent model for assessing the fate and food-web

bioaccumulation of organic pesticides in farm ponds: Model testing and performance analysis. Science of The Total Environment 639, 1324–1333. https://doi.org/10.1016/j.scitotenv.2018.05.115
Government of Canada, 2013. Properties, composition and marine spill behaviour, fate and transport of two diluted bitumen products from the Canadian oil sands (No. ISBN 987-1-100-23004-7), Federal Government Technical Report.
Gros, J., Nabi, D., Würz, B., Wick, L.Y., Brussaard, C.P., Huisman, J., van der Meer, J.R., Reddy, C.M., Arey, J.S., 2014. First day of an oil spill on the open sea: Early mass transfers of hydrocarbons to air and water. Environmental science & technology 48, 9400–9411. https://doi.org/10.1021/es502437e
Guo, W.J., Wang, Y.X., 2009. A numerical oil spill model based on a hybrid method. Marine pollution bulletin 58, 726–734.
Harrison, W., Winnik, M.A., Kwong, P.T., Mackay, D., 1975. Crude oil spills. Disappearance of aromatic and aliphatic components from small sea-surface slicks. Environmental Science & Technology 9, 231–234. https://doi.org/10.1021/es60101a006
Hollinger, J.P., Mennella, R.A., 1973. Oil spills: Measurements of their distributions and volumes by multifrequency microwave radiometry. Science 181, 54–56.
Irvine, G.V., Mann, D.H., Short, J.W., 1999. Multi-year persistence of oil mousse on high energy beaches distant from the Exxon Valdez spill origin. Marine Pollution Bulletin 38, 572–584.
King, T., Mason, J., Thamer, P., Wohlgeschaffen, G., Lee, K., Clyburne, J.A., 2017. Composition of bitumen blends relevant to ecological impacts and spill response, in: Proceedings of the Fortieth AMOP Technical Seminar. Environment and Climate Change Canada, Ottawa, ON, Calgary AB. pp. 463–475.
King, T.L., Robinson, B., Lee, K., Li, H., Boufadel, M.C., Clyburne, J.A., 2019. Seasonal Effect Data on Monocyclic Aromatics Dissolution from Surface Spills of Bitumen Blends: Implications for Environmental Risk Assessments, in: Proceedings of the Forty-Second AMOP Technical Seminar. Environment and Climate Change Canada, Ottawa, ON, Canada, pp. 773–790.
Lee, K. (chair), Boufadel, M., Chen, B., Foght, J., Hodson, P., Swanson, S., Venosa, A., 2015. Expert Panel Report on the Behaviour and Environmental Impacts of Crude Oil Released into Aqueous Environments (No. ISBN: 978-1-928140-02-3). Royal Society of Canada, Ottawa, ON, Canada.
Lemkau, K.L., 2012. Comprehensive study of a heavy fuel oil spill: Modeling and analytical approaches to understanding environmental weathering (PhD Thesis). Massachusetts Institute of Technology.
Liss, P.S., Slater, P.G., 1974. Flux of gases across the air-sea interface. Nature 247, 181–184.
Luk, G.K., Kuan, H.F., 1993. Modelling the behaviour of oil spills in natural waters. Canadian Journal of Civil Engineering 20, 210–219.
Mackay, D., Shiu, W.-Y., Ma, K.-C., Lee, S.C., 2006. Handbook of physical-chemical properties and environmental fate for organic chemicals. CRC press.
Madison, B.N., Hodson, P.V., Langlois, V.S., 2017. Cold Lake Blend diluted bitumen toxicity to the early development of Japanese medaka. Environmental Pollution 225, 579–586.

McDonnell, D., Madison, B.N., Baillon, L., Wallace, S.J., Brown, S.R., Hodson, P.V., Langlois, V.S., 2019. Comparative toxicity of two diluted bitumens to developing yellow perch (Perca flavescens). Science of The Total Environment 655, 977–985.
Middlebrook, A.M., Murphy, D.M., Ahmadov, R., Atlas, E.L., Bahreini, R., Blake, D.R., Brioude, J., De Gouw, J.A., Fehsenfeld, F.C., Frost, G.J., 2012. Air quality implications of the Deepwater Horizon oil spill. Proceedings of the National Academy of Sciences 109, 20280–20285.
NASEM, 2016. Spills of Diluted Bitumen from Pipelines: A Comparative Study of Environmental Fate, Effects, and Response (No. ISBN: 978-0-309-38010-2). National Academies of Sciences, Engineering and Medicine (NASEM), Washington, DC.
NRC, 2003. Oil in the sea III: inputs, fates, and effects. National Academies Press (US).
Ortmann, A.C., Cobanli, S.E., Wohlgeschaffen, G., MacDonald, J., Gladwell, A., Davis, A., Robinson, B., Mason, J., King, T.L., 2020. Measuring the fate of different diluted bitumen products in coastal surface waters. Marine Pollution Bulletin 153, 111003.
Philibert, D.A., Philibert, C.P., Lewis, C., Tierney, K.B., 2016. Comparison of diluted bitumen (dilbit) and conventional crude oil toxicity to developing zebrafish. Environmental science & technology 50, 6091–6098.
Riazi, M.R., Edalat, M., 1996. Prediction of the rate of oil removal from seawater by evaporation and dissolution. Journal of Petroleum Science and Engineering 16, 291–300.
Rodriguez-Gil, J.L., Stoyanovich, S., Hanson, M.L., Hollebone, B., Orihel, D.M., Palace, V., Faragher, R., Mirnaghi, F.S., Shah, K., Yang, Z., 2021. Simulating diluted bitumen spills in boreal lake limnocorrals-Part 1: Experimental design and responses of hydrocarbons, metals, and water quality parameters. Science of The Total Environment 148537.
Saunders, L., Rodriguez-Gil, J.L., Stoyanovich, S., kimpe, L., Hanson, M., Hollebone, B., Orihel, D., Palace, V., Blais, J., In Prep. Air-water mass-transfer of sulfur hexafluoride in field studies with spilled diluted bitumen.
Schwarzenbach, R.P., Gschwend, P.M., Imboden, D.M., 2003. Environmental Organic Chemistry, 2nd ed. ed. John Wiley & Sons.
Shah, K., Watson, K., Hollebone, B., Yang, Z., Lambert, P., Faragher, R., Aljawahari, M., Dey, D., Mirnaghi, F., Stoyanovich, S., Blais, J.M., 2019. The BOREAL Project: The Design and Execution of a Controlled Oil Spill Study in a Canadian Freshwater Lake, in: Proceedings of the Forty-Second AMOP Technical Seminar. Environment and Climate Change Canada, Ottawa, ON, Canada, pp. 276–294.
Soetaert, K., Petzoldt, T., Setzer, R.W., Petzoldt, M.T., 2020. Package 'deSolve.' Solving Initial Value Differential Equations, 2010d. deSolve vignette-R package version 1.
Stiver, W., Shiu, W.Y., Mackay, D., 1989. Evaporation times and rates of specific hydrocarbons in oil spills. Environmental science & technology 23, 101–105.
Stoyanovich, S., Rodríguez-Gil, J.R., Hanson, M., Hollebone, B.P., Orihel, D.M., Palace, V., Faragher, R., Mirnaghi, F.S., Shah, K., Yang, Z., 2021. Simulating diluted

bitumen spills in boreal lake limnocorrals-Part 2: Factors affecting the physical characteristics and submergence of diluted bitumen. Science of The Total Environment 148580.
Stoyanovich, S., Yang, Z., Hanson, M., Hollebone, B.P., Orihel, D.M., Palace, V., Rodriguez-Gil, J.R., Faragher, R., Mirnaghi, F.S., Shah, K., 2019. Simulating a spill of diluted bitumen: Environmental weathering and submergence in a model freshwater system. Environmental toxicology and chemistry.
US-EPA, 2014. Priority Pollutants List.
Wang, Z., Stout, S.A., 2007. Chemical fingerprinting of spilled or discharged petroleum—methods and factors affecting petroleum fingerprints in the environment, Oil spill environmental forensics: fingerprinting and source identification. Elsevier Publishing Company: Boston, MA, USA.
Witt O'Briens, Polaris Applied Sciences, Western Canada Marine Response Corporation, 2013. A study of fate and behavior of diluted bitumen oils in marine waters: Dilbit Experiments, Trans Mountain Pipeline ULC.
Yarranton, H., Motahhari, H.R., Schoeggl, F., Zhou, J.Z., 2015. Evaporative Weathering of Diluted Bitumen Films. Journal of Canadian Petroleum Technology 54, 223–244. https://doi.org/10.2118/174557-PA

CHAPTER 7: GENERAL CONCLUSIONS AND IMPLICATIONS

STUDY OUTCOMES

CHAPTER 2

The objective of Chapter 2 was to offer an assessment of dilbit's fate following exposure to natural lake water and sediment to simulate a Boreal shield environment. We used a land-based mesocosm approach to conduct 2 individual dilbit spills at oil:water ratios of 1:8000 and 1:800 (v/v) and track the changes in physical and chemical properties of both the dilbit slick and the water column for 11 days. We examined the changing density, viscosity, and water content of the dilbit, as well as the loss of petroleum hydrocarbons over time as it weathered. To complement the changes in dilbit composition, we also tracked the petroleum hydrocarbon concentrations in the water column over time. In the first 24 hours of the experiment, volatile hydrocarbons quickly evaporated from the dilbit, resulting in increased dilbit density and viscosity. Both density and viscosity are important properties that can severely impact the efficiency of spill clean-up techniques. The density of the dilbit exceeded 1 g mL^{-1} and its viscosity exceed 1 000 000 mPa·s. These drastic physical and chemical changes ultimately led to dilbit's submergence after 8 days. We also detected rapid accumulation of PAHs in the water columns of both treatments, with accumulation trends following: NAP>PHEN>FLU=DBT>FLA=BNT=CHR. This study provided new information on the environmental fate and behaviour of dilbit specific to freshwater environments, specifically offering early insights into dilbits potential for submergence following a spill

in freshwater. This work served as a pilot study and provided baseline information that was used to inform the design of Chapters 3, 4, 5, and 6.

CHAPTER 3

The objective of Chapter 3 was to report the physical and chemical characteristics, fate, and behaviour of the dilbit during experimental dilbit spills into in-lake limnocorrals lasting 70 days. This chapter focused on qualitative observations of spreading, dispersion, and sinking patterns as well as physical weathering. We conducted a total of 7 individual dilbit spills with oil:water ratios ranging from 1:71 000 to 1:500 (v/v) and allowed the dilbit slicks to weather for a total of 70 days. Similar to Chapter 2, the dilbit's density and viscosity increased over time, exceeding > 1 g mL^{-1} and > 5 000 000 mPa s, respectively. One of the main drivers for the observed increases in density and viscosity was the loss of LMW hydrocarbons (<C_{16}), which decreased by >80% over time across treatments. Ultimately, dilbit sank to the bottom sediments in all treatments, and the time to sinking was positively correlated with spill volume. The lowest dilbit treatment began to sink on day 12, whereas the highest dilbit treatment sank on day 31. While evaporation is thought to be the main driver of density increase and ultimately submergence, other factors such as wind and rain likely played a role. Building on the findings from Chapter 2, this study is, to our knowledge, the first to document complete dilbit submergence following an *in*-situ spill in a freshwater lake. These findings provide further evidence of dilbit's propensity to sink in freshwater under realistic boreal lake conditions.

CHAPTER 4

The objective of Chapter 4 was to expand on the findings of Chapter 3 and focus on the chemical changes in the dilbit slicks over the course of the 70-day limnocorral study. We collected floating dilbit slick samples at multiple time points from each treatment, allowing us to track temporal changes in hydrocarbon composition characteristic of different weathering processes. Our focus was on individual *n*-alkanes, PAHs, and petroleum biomarkers. Depletion rate constants of *n*-alkanes and PAHs ranged from 0.00091 to 0.41 d^{-1} and 0.00075 to 0.38 d^{-1}, respectively. The majority of petroleum biomarkers experienced no significant depletion over time, indicative of their recalcitrance. For individual *n*-alkanes and polycyclic aromatic hydrocarbons (PAHs), depletion rate constants decreased exponentially with increasing molecular weight. We observed no apparent relationship between an individual analyte's depletion rate constant and spill volume, suggesting that the size of the dilbit spill had no effect on the depletion rate of hydrocarbons. The depletion rates obtained in our study were much lower than dilbit weathering studies conducted in a laboratory setting. We also found that diagnostic ratios developed from n-alkanes and PAHs (e.g., LMW/HMW, *n*-C_{17}/pris, *n*-C_{18}/phy, $C_{1+2}N/C_{3+4}N$, C_2N/C_2F, C_3N/C_3F, C_1P/C_1C, C_1F+C_2F/C_3F, C_3C/C_0C, C_3P/C_3C, C_4Fl/C_0Fl) indicated that evaporation, dissolution, and photooxidation were all acting on the dilbit slicks, whereas biodegradation was not a significant factor during the study timeline. This was likely due to the low abundances of hydrocarbon degrading microbes present in this pristine boreal lake.

CHAPTER 5

The objective of Chapter 5 was to describe the quantity and distribution of polycyclic aromatic hydrocarbons (PAHs) in the water columns, sediments, and air following the same simulated dilbit spills as described in Chapters 3 and 4. With our unique experimental design, we were able to begin collecting paired dilbit slick, water column, air, and sediment samples immediately following the spills (earliest sample 6 h post spill) and we continued to collect samples over a period of 70 days. This enabled us to describe both the short- and long-term behaviour of these compounds as they partition from the dilbit slick to the air, water, and sediments of the limnocorrals. Furthermore, we were able to show that concentrations of PAHs in the water column were directly proportional to the oil:water ratio, meaning that the more dilbit that is spilled, the more contaminated the water column will become. Our results suggest that <10% of the spilled PAHs end up in the water and/or sediments, with the majority accumulating in the sediments. Of the PAHs that actually ended up in the water column, concentrations remained below levels that would be toxic to aquatic biota. These findings were also mirrored in the majority of sediment samples. However, our mass balance did not consider PAHs that accumulated in the sediments due to the physical oiling following dilbit submergence. In these instances, sediment PAH concentrations were elevated to the point where they could cause long term toxicological effects to aquatic biota based on emerging dilbit-laden sediment toxicity tests in the literature. These results highlighted the importance of considering the potential for dilbit to submerge in all future risk assessments, as this is no longer a theory, but a reality, especially in freshwater environments.

CHAPTER 6

The final Chapter in this thesis aimed to characterize the dissolution dynamics of the highly toxic BTEX compounds following experimental dilbit spills. With these experimental results in hand, we then attempted to apply a mass transfer model to accurately predict what we observed in the field, based entirely on the physical and chemical properties of the compounds and our given spill scenarios. Dissolution and evaporation are two of the most challenging weathering processes to characterize after a spill. Consistent with previous studies, these two processes removed virtually all of the BTEX compounds from the slicks within the initial days of the spills and the physiochemical mass transfer model developed in this chapter was able to accurately predict these losses. We also found that a variety of parameters, such as air and water film thicknesses, diffusivities, oil temperature, saturation concentrations, vapor pressures, and oil slick thickness all had a strong influence on the overall model outcome. Mass transfer models such as this could be used to explore hypothetical spills under different environmental conditions not explored in this study, such as winter conditions, larger bodies of water, or marine settings, all of which will likely experience a dilbit spill over the coming decades. Further, a formal error propagation analysis would be desirable including a comprehensive Monte Carlo simulation to provide confidence in estimates of model uncertainty.

GENERAL CONCLUSIONS

Diluted bitumen has the propensity to sink under calm freshwater conditions

The first well-documented case of mass dilbit submergence was reported following the Kalamazoo River Spill in 2010. In this case**,** flooding increased the turbulence and suspended sediments in the river, thus promoting oil-sediment aggregates (OSA's), which was thought to be one of the main drivers of observed submergence in the Kalamazoo River spill (Fitzpatrick et al., 2015). Since then, studies have begun to describe the propensity for dilbit to sink under laboratory settings (Hua et al., 2018; Waterman and Garcia, 2015). However, in nearly all of these instances, researchers have suggested a variety of physical factors need to be present including high suspended sediment loads in the water column and some source of energy such as breaking waves or strong currents. Our studies, presented in Chapters 2 and 3, are the first to demonstrate that dilbit can sink under quiescent conditions and low suspended sediment loads typical of a boreal freshwater lake. This implies that weathering alone, without the interaction with suspended sediments, was enough to increase the density of the dilbit past the density of freshwater and cause complete submergence - something that has not been shown before.

Sediments are the ultimate sink for diluted bitumen in a freshwater lake

On a mass balance basis, we see roughly 14 – 23% losses of dilbit to the air occurring within the first 2 days (see Appendix A for calculations) of the spills which then slows for the remainder of the study (Figure 7.1). Considering dilbits are typically 20 – 30% diluent (Crosby et al., 2013), this is likely the majority of the volatile diluent portion evaporating off. As the experimental spills progress and environmental weathering

continues, we begin to see the sediment becoming a dominant sink for the dilbit between days 12 – 31 (Figure 7.1). By the end of the study timelines for each treatment, roughly 20 – 24% of the dilbit had evaporated, 0 % remained on the water's surface, and 76 – 80% had submerged (Table 7.1).

Table 7. 1. Mass balance estimates on the final day of sampling for each individual treatment.

Treatment	Amount Added (Kg)	Time (d)[a]	Percent Evaporated (%)[b]	Percent remaining on surface (%)[c]	Percent submerged to sediment (%)
1.5 L	1.34	19	20.7	0	79.3
2.9 L	2.65	22	19.8	0	80.2
5.5 L	5.09	25	21.7	0	78.4
18 L	16.7	28	23.2	0	77.7
42 L	39.1	43	22.1	0	77.9
82 L	75.5	61	23.6	0	76.4
180 L	165.8	77	22.3	0	77.8

[a]This time represents the point in which no more dilbit was visible on the water's surface (i.e., complete submergence as per Chapter 3)
[b]Dilbit samples were not collected at these specific timepoints, therefore the percent evaporated was assumed to be equal to the nearest timepoint of sample collection
[c]At the timelines presented, no visible surface slick was present (i.e., 0%)

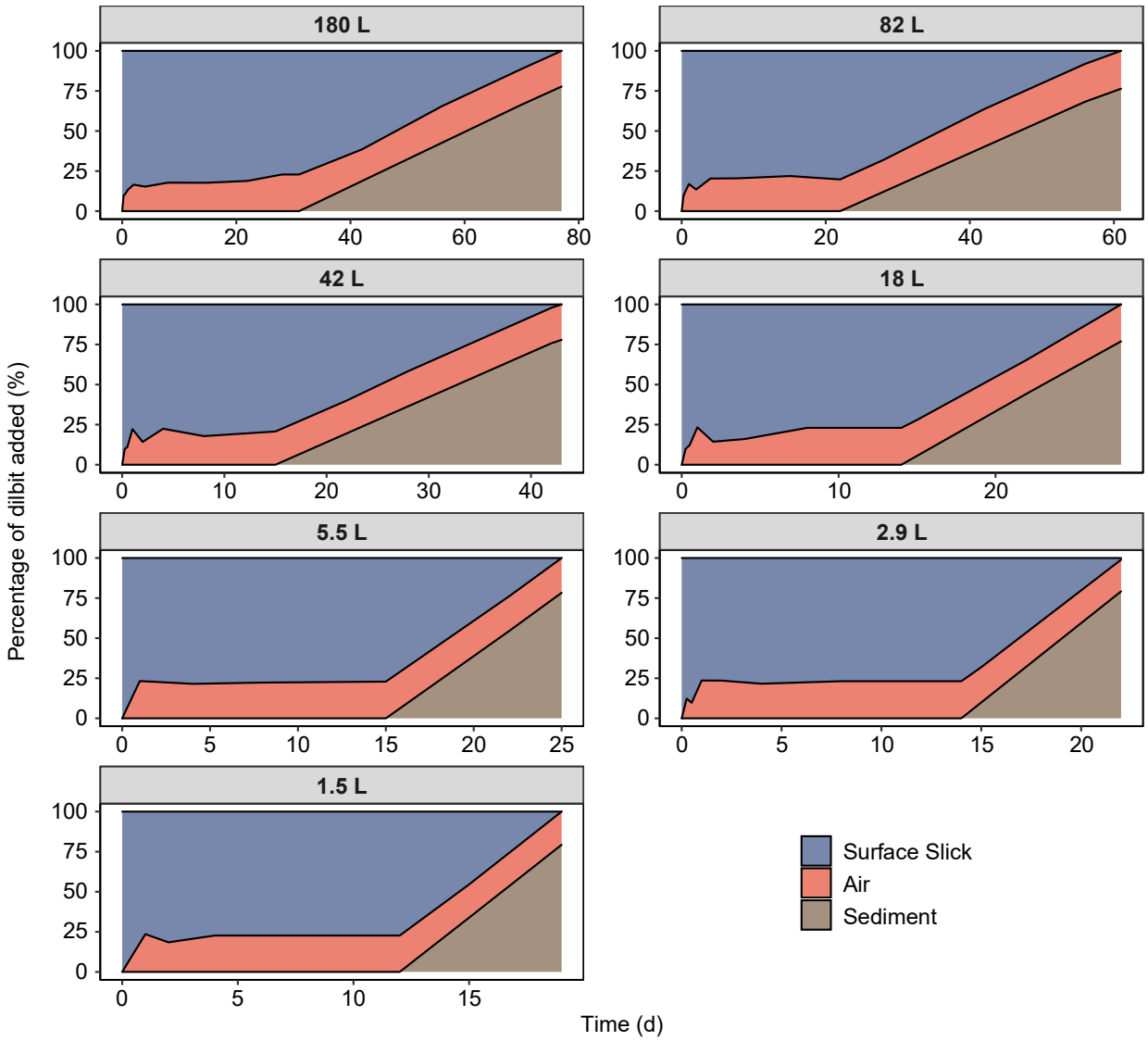

Figure 7. 1. Environmental mass balance of spilled dilbit in each treatment demonstrating the percentage of dilbit that evaporated, remained floating, and submerged to the sediments over time.

Unlike ultra-light crude oil products which can lose nearly 75% to evaporation (Lee et al., 2015), our findings suggest that dilbit will lose <30%, leaving behind more oil that can sink to the sediments. Here we highlight that overall, the ultimate sink for dilbit that is left unattended to for an extended period of time is submergence. These findings stress the need for rapid spill response and the development of non-invasive techniques to recover sunken dilbit in sensitive freshwater sites such as Boreal lakes.

Evaporation, dissolution, and photooxidation are prominent weathering processes in freshwater while biodegradation is not

Characterizing the fate of dilbit when spilled and the affect of environmental processes on spills is crucial to developing response efforts and assisting in recovery strategies. This work focused on four primary weathering processes: evaporation, dissolution, photooxidation, and biodegradation. Although evaporation and dissolution are the most challenging weathering processes to disentangle since they often affect the same set of compounds, our results from Chapters 4 and 5 provide support for both. We also showed that photooxidation is likely an active process under these spill scenarios, targeting the larger, more alkylated PAH compounds. In contrast, limited evidence from this thesis supports the presence of biodegradation following the spills. This suggests that although bioremediation is a proven technique for spill management in marine systems, it may not be a viable option in pristine freshwater lakes such as those located in the Boreal shield of Canada.

The biodegradation of any type of crude oil requires competent hydrocarbon degrading microbes. Areas that are constantly exposed to oil spills or natural oil seeps, such as the Gulf of Mexico, will have established populations of hydrocarbon degraders that can begin to act upon a spill immediately (Lee et al., 2015). While hydrocarbon degraders are ubiquitous, they are likely present in pristine environments, such as a boreal lake, in very low numbers (Atlas, 1981; Ron and Rosenberg, 2014). Our assessment of different biotic and abiotic weathering processes in Chapter 4 suggested that biodegradation played a limited role in the depletion of hydrocarbons within the dilbit slick. However, our timeline may have not been long enough to truly capture these processes. Therefore, future research should focus on expanding the timelines of these

experimental spills from days to years in order to assess the potential for long term biodegradation under pristine freshwater conditions.

Benefits of a regression design- outcomes linked to spill size

Historically, replicated experimental design incorporating an analysis of variance (ANOVA) approach has been widely used for mesocosm or limnocorral type studies (Crossland and Wolff, 1985; Dewey, 1986; Giddings et al., 1984; Kaushik et al., 1985; Stephenson et al., 1986). While the replication of an ANOVA design provides a degree of statistical confidence, it only allows for limited qualitative conclusions and predictions (Liber et al., 1992). In contrast, regression-based designs provide us with quantitative information that can be used to describe the relationship between a response variable and a continuous independent variable and use this information to build relevant ecological models (Cottingham et al., 2005).

In Chapter 3 we were able to demonstrate that dilbit's "time to submergence" increased with increasing spill volume, thus the more dilbit that is spilled, the longer it takes to submerge. This provides invaluable information that can be used to predict the submergence times of future dilbit spills under similar environmental conditions.

In Chapter 5, we were able to demonstrate that the concentration of PAHs in the water column was proportional to the oil:water ratio resulting from a dilbit spill. By incorporating the oil:water ratio of each individual spill as the independent variable in the regressions, we were able to provide quantitative information that can be used to inform future models. Specifically, the generated linear models in Chapter 5 can be used to predict PAH contamination at different volumetric scales of dilbit spills that occur in

boreal lakes under similar environmental conditions as the present study, something that wouldn't be possible with an ANOVA design.

Sunken dilbit poses the greatest toxicological threat following dilbit spills in freshwater

There is a growing interest in the potential for toxicity associated with water-borne PAHs stemming from dilbit spills (Alderman et al., 2017; Barron et al., 2018; Madison et al., 2017; Philibert et al., 2016). In Chapter 2, our tank based study produced ΣPAH concentrations in the water column of the 1.6 L treatment (oil:water of 1:800) that exceeded the 17 d EC_{50} values for embryotoxicity in Japanese medaka (Madison et al., 2017) and exceeded the NOEC for a variety of standard aquatic test species (Barron et al., 2018), suggesting the potential for toxicity. However, since we did not perform any formal toxicity tests, we can only compare concentrations, and cannot accurately comment on the toxicity of the water columns. In Chapter 4, none of the treatments produced ΣPAH concentrations in the water column that approached the toxicity thresholds outlined above. Therefore, we conclude that there is limited evidence to support he potential for water column toxicity under the more natural spill scenarios and calm conditions observed in Chapter 5.

The same was true for our temporal sediment samples. However, the potential for submergence adds another degree of complexity to dilbit spills. Our results from Chapter 5 suggest sediments that have come into contact with sunken dilbit can produce ΣPAH concentrations well above thresholds for toxicity to benthic organisms outlined in the literature (Barron et al., 2020). This thesis therefore stresses the

importance of recovering spilled dilbit before submergence occurs as a way to mitigate any long-lasting toxic effects to benthic dwelling organisms.

Mass transfer model can predict monocyclic dynamics following dilbit spill

Oil spill models that can accurately predict the distribution of oil-derived contaminants in the environment are an invaluable tool in oil spill related risk assessment. We thus adapted a mass transfer modelling approach that has been previously applied to oil spill scenarios under marine settings (Arey et al., 2007; Gros et al., 2014; Lemkau, 2012). In Chapter 6, we were able to adapt a mass transfer model to our specific spill scenarios to predict the distribution of the highly volatile and water-soluble BTEX compounds in the water columns of each of our individual dilbit treatments. We found that the parameter with the greatest uncertainty and the greatest influence on the overall model was oil slick thickness. Slick thickness has been well documented as an important predictor of weathering rates, but also one of the most challenging properties to accurately estimate. Therefore, future field studies such as this should place greater emphasis on accurately estimating slick thickness in order to better inform these models.

FUTURE DIRECTIONS

This work has demonstrated the value of a large scale *in-situ* limnocorral approach in addressing important knowledge gaps surrounding dilbit spills in boreal lakes. Throughout this thesis, our results have in some cases substantiated the findings from laboratory studies and in other cases contrasted them. This highlights the importance of studies conducted under realistic temporal scales and environmentally

relevant conditions. As often advocated by the late and iconic freshwater scientist David Schindler, realism should not be sacrificed for replication (Schindler, 1998). Laboratory-scale experiments, while easily replicated, often provide spurious results. Even at the scale our study was conducted, we are likely still missing some key environmental attributes only possible to achieve in the full-lake environment. While conceivably the next steps in the progression of this work would include conducting a similar study at a whole-lake scale, the specific oil-spill related risks associated with this approach likely outweigh the added value of scaling upwards. More controlled limnocorral-type oil spill studies should therefore be conducted, targeting a wider range of endpoints.

Furthermore, in future oil related large-scale experiments such as the limnocorral approach detailed in this thesis, researchers should be cautious to not attempt to describe everything, but instead focus on a set of key outcomes. Trying to cover all aspects in a single study and examine multiple different aspects is tantamount to "spreading yourself too thin". Balancing logistical aspects such as workforce, scheduling, sampling capacity, and analytical budgets is paramount to a project's success. Future studies at this scale should understand that you cannot track everything and that it is better to select a manageable number of key impacts and study them to a depth that will provide meaningful and useful insights with wide reaching applications.

While we used limnocorrals to study the behaviour of dilbit, the environmentally relevant conditions of these systems suggest they could also be used to study the efficacy of different clean up techniques as well. Specifically, options for the recovery of submerged dilbit, which was proven to be a challenge in the 2010 Kalamazoo River

spill, could be explored in detail through simulated spills such as those carried out in this thesis. Furthermore, while we were able to document submergence events at a variety of different spill sizes, future research should focus on better characterizing the dynamics of dilbit submergence, capturing these important sinking events at a higher resolution. This would allow the derivation of sinking rates, which would help inform future dilbit spill models.

The ability to accurately forecast the behaviour of some of dilbit's more harmful constituents, such as BTEX, is an invaluable tool in the field of oil spill response and planning. While our mass transfer model produced outputs that were in good agreement with our observed water column results, we only considered diffusion through the air and water films and did not consider any diffusion through the dilbit slick itself. Arey et al. (2007) adapted the Stokes – Einstein relationship (Schwarzenbach et al., 2003) which implies that as the viscosity of oil increases, the diffusion of compounds through the oil slick itself is likely to become a limiting factor. This is even more important for heavy oils, such as dilbit, whose viscosity can increase >27 000X over 70 d as seen in Chapter 3. Though the authors note that the assumptions involved in this approach are rudimentary and may overcomplicate the results, it is still a valuable tool to describe whether or not oil diffusion-limited transport is important. Therefore future mass transfer models involving dilbit should include a third diffusion term, $D_{i,oil}$, especially if the model intends to simulate over longer periods. Finally, the mass transfer model approach should be applied and parametrized to a wider range of dilbit-derived hydrocarbon compounds. In this thesis we only focus on a small subset (BTEX), therefore expanding the approach to PAHs and *n*-alkanes would be highly informative.

CLOSING STATEMENT

In summary, our work has yielded valuable insights into the physical and chemical fate of diluted bitumen following spills in freshwater. This thesis has provided accessible *a priori* knowledge that can enable efficient evidence-based management and mitigation decisions should a dilbit spill in the Boreal region of Canada occur in the future. We demonstrated that our regression based limnocorral approach was a powerful tool allowing one to capture and analyze a broad range of oil spill features. This thesis served to improve our understanding of dilbit's fate and behaviour in the freshwater environment and to provide future researchers with new tools and methods to continue to address important knowledge gaps in the field of oil spill study.

REFERENCES

Alderman, S.L., Lin, F., Farrell, A.P., Kennedy, C.J., Gillis, T.E., 2017. Effects of diluted bitumen exposure on juvenile sockeye salmon: from cells to performance. Environ. Toxicol. Chem. 36, 354–360.

Arey, J.S., Nelson, R.K., Plata, D.L., Reddy, C.M., 2007. Disentangling oil weathering using GCxGC. 2. Mass transfer calculations. Environ. Sci. Technol. 41, 5747–5755.

Atlas, R.M., 1981. Microbial degradation of petroleum hydrocarbons: an environmental perspective. Microbiol. Rev. 45, 180.

Barron, M.G., Conmy, R.N., Holder, E.L., Meyer, P., Wilson, G.J., Principe, V.E., Willming, M.M., 2018. Toxicity of Cold Lake Blend and Western Canadian Select dilbits to standard aquatic test species. Chemosphere 191, 1–6.

Barron, M.G., Moso, E.M., Conmy, R.N., Meyer, P., Sundaravadivelu, D., 2020. Toxicity of sediment oiled with diluted bitumens to freshwater and estuarine amphipods. Mar. Pollut. Bull. 163, 111941.

Cottingham, K.L., Lennon, J.T., Brown, B.L., 2005. Knowing when to draw the line: designing more informative ecological experiments. Front. Ecol. Environ. 3, 145–152.

Crosby, S., Fay, R., Groark, C., Smith, J.R., Sullivan, T., Pavia, R., Shigenaka, G., 2013. Transporting Alberta oil sands products: defining the issues and assessing the risks (No. NOAA Technical Memorandum NOS OR&R 43). U.S. Dept. of Commerce, Seattle, WA: Emergency Response Division, NOAA.

Crossland, N.O., Wolff, C.J.M., 1985. Fate and biological effects of pentachlorophenol in outdoor ponds. Environ. Toxicol. Chem. Int. J. 4, 73–86.

Dewey, S.L., 1986. Effects of the herbicide atrazine on aquatic insect community structure and emergence. Ecology 67, 148–162.

Fitzpatrick, F.A., Boufadel, M.C., Johnson, R., Lee, K.W., Graan, T.P., Bejarano, A.C., Zhu, Z., Waterman, D., Capone, D.M., Hayter, E., 2015. Oil-particle interactions and submergence from crude oil spills in marine and freshwater environments: Review of the science and future research needs (No. 2015–1076). US Geological Survey.

Giddings, J.M., Franco, P.J., Cushman, R.M., Hook, L.A., Southworth, G.R., Stewart, A.J., 1984. Effects of chronic exposure to coal-derived oil on freshwater ecosystems: II. Experimental ponds. Environ. Toxicol. Chem. Int. J. 3, 465–488.

Gros, J., Nabi, D., Würz, B., Wick, L.Y., Brussaard, C.P., Huisman, J., van der Meer, J.R., Reddy, C.M., Arey, J.S., 2014. First day of an oil spill on the open sea: Early mass transfers of hydrocarbons to air and water. Environ. Sci. Technol. 48, 9400–9411. https://doi.org/10.1021/es502437e

Hua, Y., Mirnaghi, F.S., Yang, Z., Hollebone, B.P., Brown, C.E., 2018. Effect of evaporative weathering and oil-sediment interactions on the fate and behavior of diluted bitumen in marine environments. Part 1. Spill-related properties, oil buoyancy, and oil-particulate aggregates characterization. Chemosphere 191, 1038–1047. https://doi.org/10.1016/j.chemosphere.2017.10.156

Kaushik, N.K., Stephenson, G.L., Solomon, K.R., Day, K.E., 1985. Impact of permethrin on zooplankton communities in limnocorrals. Can. J. Fish. Aquat. Sci. 42, 77–85.

Lee, K., Boufadel, M., Chen, B., Foght, J., Hodson, P., Swanson, S., Venosa, A., 2015. Expert Panel Report on the Behaviour and Environmental Impacts of Crude Oil Released into Aqueous Environments (No. ISBN: 978-1-928140-02-3). Royal Society of Canada, Ottawa, ON, Canada.

Lemkau, K.L., 2012. Comprehensive study of a heavy fuel oil spill: Modeling and analytical approaches to understanding environmental weathering (PhD Thesis). Massachusetts Institute of Technology.

Liber, K., Kaushik, N.K., Solomon, K.R., Carey, J.H., 1992. Experimental designs for aquatic mesocosm studies: a comparison of the “anova” and “regression” design for assessing the impact of tetrachlorophenol on zooplankton populations in limnocorrals. Environ. Toxicol. Chem. Int. J. 11, 61–77.

Madison, B.N., Hodson, P.V., Langlois, V.S., 2017. Cold Lake Blend diluted bitumen toxicity to the early development of Japanese medaka. Environ. Pollut. 225, 579–586.

Philibert, D.A., Philibert, C.P., Lewis, C., Tierney, K.B., 2016. Comparison of diluted bitumen (dilbit) and conventional crude oil toxicity to developing zebrafish. Environ. Sci. Technol. 50, 6091–6098.

Ron, E.Z., Rosenberg, E., 2014. Enhanced bioremediation of oil spills in the sea. Curr. Opin. Biotechnol. 27, 191–194.

Schindler, D.W., 1998. Whole-ecosystem experiments: replication versus realism: the need for ecosystem-scale experiments. Ecosystems 1, 323–334.

Schwarzenbach, R.P., Gschwend, P.M., Imboden, D.M., 2003. Environmental Organic Chemistry, 2nd ed. ed. John Wiley & Sons.

Stephenson, G.L., Kaushik, N.K., Solomon, K.R., Day, K., 1986. Impact of methoxychlor on freshwater communities of plankton in limnocorrals. Environ. Toxicol. Chem. Int. J. 5, 587–603.

Waterman, D.M., Garcia, M.H., 2015. Laboratory Tests of Oil-Particle Interactions in a Freshwater Riverine Environment with Cold Lake Blend Weathered Bitumen. Ven Te Chow Hydrosystems Lab. Univ. Ill.

APPENDIX A: DILBIT MASS BALANCE ESTIMATES

1.0 Estimating mass lost to evaporation

We used simple mass balance calculations to estimate the inputs and outputs of dilbit to and from our limnocorrals. The model assumes steady state over the 70-day study period, requiring that dilbit masses added to the water's surface of the limnocorrals (M_{in}) are balanced by outputs (M_{out}):

$$M_{d,In} = M_{d,Out} \quad (A.1)$$

Where $M_{d,In}$ is the mass of dilbit added at time 0 (Kg) and $M_{d,Out}$ is represented by:

$$M_{d,Out} = (M_{d,air} + M_{d,sediments}) - M_{d,surface\ slick} \quad (A.2)$$

Where $M_{d,surface\ slick}$ is the mass of dilbit floating on the water's surface (Kg), $M_{d,air}$ is the mass of dilbit in the air column (Kg), and $M_{d,sediments}$ is the mass of dilbit that has sank down to the sediment bottom (Kg). Accumulation in the water column is assumed negligible on a mass balance basis since it is estimated that <1% of dilbit actually enters the water column through dissolution and does not measurably affect the mass balance of the dilbit (Fingas, 2015).

Since we could not directly measure bulk dilbit loss to evaporation, we estimated this using a weathering index (WI) originally described by Wang et al. (1995). The weathering index is defined as the concentration sum of the lower molecular weight *n*-alkanes (nC$_9$ – nC$_{16}$) divided by the sum of the higher molecular weight *n*-alkanes (nC$_{22}$ – nC$_{40}$).

$$WI = \frac{\Sigma \mathrm{nC_9} - \mathrm{nC_{16}}}{\Sigma \mathrm{nC_{22}} - \mathrm{nC_{40}}} \quad (A.3)$$

This method involves creating a calibration curve from dilbit samples evaporated in the laboratory by plotting the relationship between percentage of mass loss and weathering index. This curve is then used to estimate the percentage of dilbit evaporated in field collected samples. Briefly, environmental weathering of CLWB dilbit was simulated in the laboratory using rotary evaporation to produce 3 weathered fractions characterized by percentage of mass lost to evaporation. Each fraction was then analyzed by GC-MS to quantify the concentration of individual *n*-alkanes. With these data in hand, we were able to calculate the weathering index value using equation A.3 for each fraction (Table a1.1) and develop a calibration curve (Figure A1.1A).

Table A1.1. Fractions of CLWB dilbit produced from simulated evaporation using laboratory roto-evaporation and the measured weathering index (WI) value of each fraction.

Fraction	Mass Loss (%)	WI
Fresh	0	5.47
F1	7.49	5.24
F2	15.3	4.34
F3	23.1	1.32

The regression line in figure A1.1A is described by the following equation:

$$WI = -0.17 \times D_{\%,evaporated}(t) + 6.1 \quad \text{(A.4)}$$

Where $D_{\%,evaporated}(t)$ is the percent of dilbit that evaporated over time *t.* Rearranging equation A.4 to solve for $O_{\%,evaporated}(t)$ gives:

$$O_{\%,evaporated}(t) = -4.7 \times WI + 30.720 \quad \text{(A.5)}$$

We can then substitute the WI values from our time series environmental dilbit samples into equation A.5 in order to estimate the amount of mass that has been lost to evaporation (Figure A1.1B). The percentage of dilbit lost to evaporation was assumed to be equal to the percentage of dilbit entering the air column.

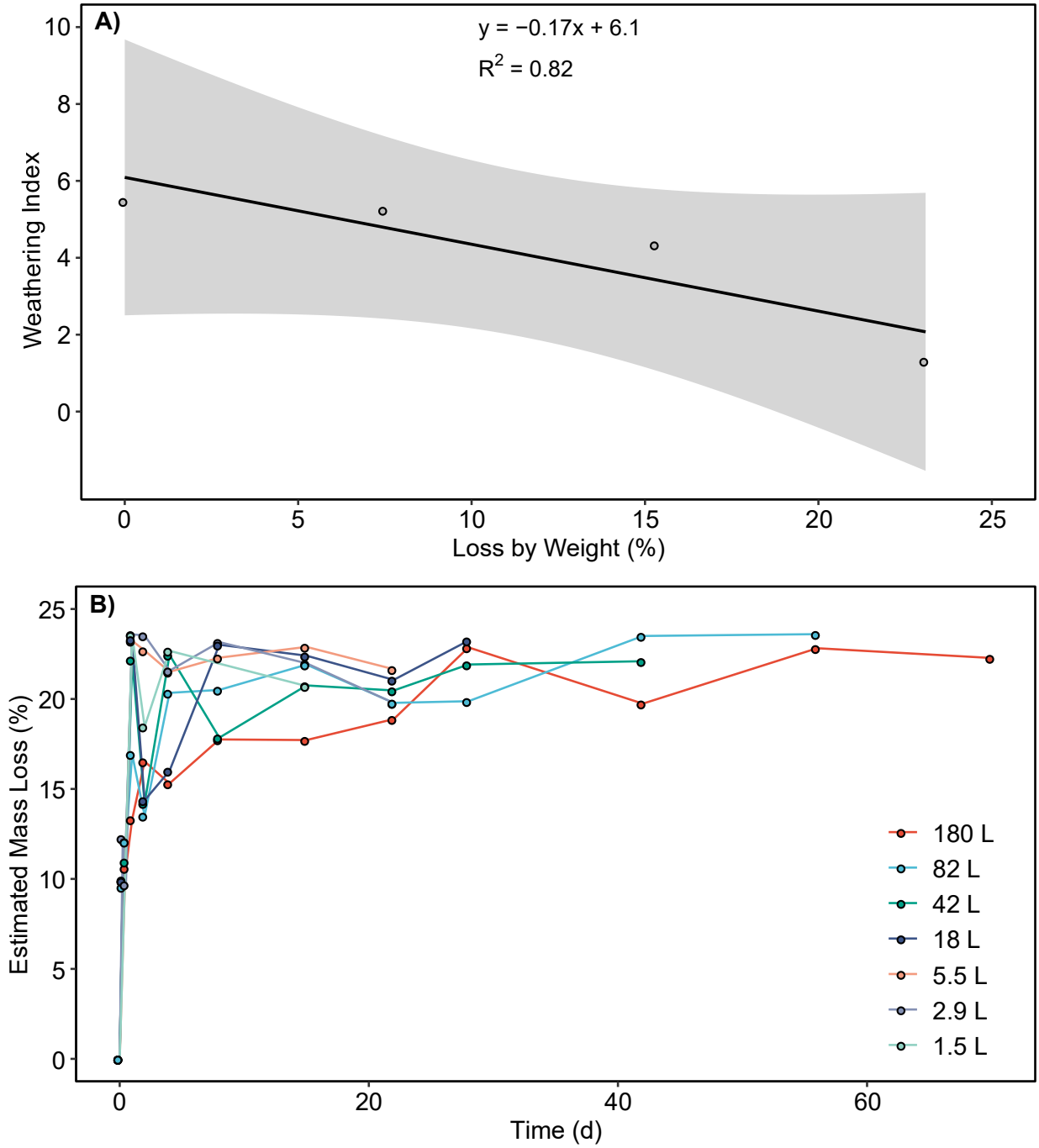

Figure A1.1. The relationship between the weathering index (WI) and the percentage of mass loss (%) in laboratory samples of 2018 CLWB following rotary evaporation (A) and the application of the weathering index to environmental samples to estimate mass loss (B).

2.0 Estimating mass lost to submergence

The onset of submergence ranged from day 13 – 31 depending on the treatment. We estimated the mass of dilbit remaining at the time of submergence based on the weathering index data. From this, we were able to determine a sinking rate, assuming the sinking was constant from the onset to completion (Table A1.2).

Table A1.2. Estimated sinking rate calculations for each dilbit amended treatment

Treatment	Sinking Onset (d)	Sinking Completion (d)	Delta sink (d)	Estimated mass at time of sinking (Kg)	Estimated Sinking Rate (Kg d^{-1})
1.5 L	12	19	7	1.06	0.15
2.9 L	14	22	8	2.10	0.26
5.5 L	15	25	10	3.95	0.40
18 L	14	28	14	13.0	0.93
42 L	15	43	28	30.7	1.10
82 L	22	61	39	59.1	1.51
180 L	31	77	46	130.0	2.83

Prior to the onset of submergence, the overall dilbit mass balance is only affected by evaporation:

$$M_{d,spilled} = M_{d,surface\ slick} + M_{d,air} \qquad (A.6)$$

However, after the onset of submergence, an additional $M_{d,sediments}$ term representing the mass of dilbit on the sediments is introduced:

$$M_{d,spilled} = M_{d,surface\ slick} + M_{d,air} + M_{d,sediments} \qquad (A.7)$$

After this point, submergence in each treatment is assumed to proceed at the rates described in table A1.2 for the remainder of the study period until no dilbit remains on the water's surface.

APPENDIX A REFERENCES

Fingas, M., 2015. Review of The Properties and Behaviour of Diluted Bitumen, in: Proceeding of the 39th Arctic and Marine Oil-Spill Program Technical Seminar. Environment and Climate Change Canada, Vancouver, B.C., Canada, pp. 470–494.

Wang, Z., Fingas, M., 1995. Study of the effects of weathering on the chemical composition of a light crude oil using GC/MS GC/FID. J. Microcolumn Sep. 7, 617–639.